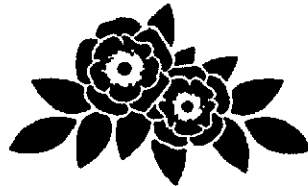


The Sliding Friction of Bonded Solid Lubricants.

David Burke

**UNIVERSITY
— OF CENTRAL —
LANCASHIRE**



**JOST INSTITUTE FOR TRIBOTECHNOLOGY
UNIVERSITY OF CENTRAL LANCASHIRE**

in collaboration with

Breed (UK) Ltd. and University of Central England.

**Submitted in partial fulfilment of
the requirements for the degree of**

DOCTOR OF PHILOSOPHY

May 2005

DECLARATION

The work presented in this thesis was carried out in the Jost Institute for Tribotechnology, Department of Technology, University of Central Lancashire, Breed (UK) Ltd. and the Technology Innovation Centre, University of Central England. Unless otherwise stated it is the original work of the author.

While registered for the degree of Doctor of Philosophy, the author has not been a registered candidate for another award of the University. This thesis has not been submitted in whole or in part for any other degree.

David Burke

May 2005

ABSTRACT.

The tribological study of Bonded Solid Lubricants, BSLs is reviewed, this includes a review of the constituent components of a BSL including a table of publications which presents a list of papers containing detailed data about the friction and wear of BSL coatings. The general theories of friction for metals in sliding contact and the friction theory applied to solid film lubrication are reviewed. A section is also included on Herzian contact theory and its application to solid films.

A screening test is described for 12 BSLs applied to commercial components. This programme provided information on the friction coefficient and allowed the selection of one of these finishes for a further more in depth study. In general the friction coefficients obtained were higher than those quoted by the material manufacturers, it was presumed that this was due as the consequence of differences in test methods.

Three test programmes are described that were conducted on a new pin on disc facility, a major programme to study the performance under various conditions at pressures above the yield pressure of the film. The information was used in the formulation of an empirical equation that can be used to predict the friction coefficient. This programme also demonstrated: that there were three distinct phases of performance, contact life increased with high loads and increased velocity, the friction coefficient in the steady state phase was between 0.18 and 0.22.

The second programme examined the evolution of the wear scar on the ball and wear track on the disc. The programme illustrated the development of a transfer film on the ball and the steady increase in friction coefficient to a point where it became stable and the wear scar on the ball changed to a circular flat.

The third programme investigated the friction coefficient at very low loads that produced pressures below or close to the yield pressure of the film. The results from this programme demonstrate that as the load increases, the friction coefficient decreases, this can be attributed to the Hertzian contact area being proportional to the load^{2/3} and the friction force is proportional to the area, then the friction coefficient F/W is proportional to the load $W^{-1/3}$.

In the penultimate chapter theoretical predictions for the friction coefficient under various contact conditions are compared with the experimental results obtained, in general the calculated results are higher and some possible causes are given for the discrepancies.

CONTENTS.

Front sheet.	i
Declaration	ii
Abstract.	iii
Contents.	iv
Nomenclature	ix
Acknowledgements.	x

Chapter	Page
---------	------

1. INTRODUCTION.

1.1 Solid Lubricants and the reasons for the research.	1-2
1.1.2 Methods of application.	1-3
1.2 Bonded Solid Lubricants.	1-4
1.3 Extreme examples of the uses of BSLs.	1-5
1.4 Summary.	1-9

2. LITERATURE SURVEY

The use of Graphite, Molybdenum Disulphide and Polytetrafluoroethylene as solid lubricants. A Review.

2.1 Graphite.	2-2
2.1.1 Uses and Applications.	2-5
2.2 Molybdenum Disulphide.	2-8
2.2.1 Uses and Applications.	2-12
2.3 Polytetrafluoroethylene.	2-14
2.3.1 Mechanism of Lubrication.	2-15
2.3.2 Uses and applications.	2-17

2.4 Bonding Agents	2-18
2.4.1. Epoxy and Phenolic Resins.	2.18
2.4.2. Polyamide-imide Resins.	2-19
2.4.3. Sodium and Sodium Silicate.	2-19
2.5 Pre treatment Techniques.	2-19
2.5.1. Grit Blasting.	2-19
2.5.2. Phosphating.	2.20
2.6 Application of BSLs to substrates.	2-23
2.7 Testing of BSLs.	2-24
2.8 Summary.	2-38

3. LITERATURE SURVEY

Models of Friction and theories of surface contact. A Review.

3. Introduction	3.2
3.1. General theories of friction.	3-4
3.2. Friction of Solid Lubricants.	3-4
3.3. Hertzian Contact theory.	3-11
3.4. Friction theory for spherical contacts and solid films.	3-12
3.5. Summary.	3-14

4. INITIAL PERFORMANCE COMPARISON AND NEW MACHINE DESIGN.

4.1. Initial Performance Comparison.	4-2
4.1.1. Introduction.	4-2
4.1.2. Test Equipment.	4-3
4.1.3. Materials and Methods.	4-8
4.1.4. Results.	4-9
4.1.5. Discussion.	4-11
4.1.6. Summary.	4-16
4.2. New Machine Design.	4-32
4.2.1. Introduction.	4.32
4.2.2. Main Bearings.	4-35

4.2.3. Top Carriage Assembly.	4-38
4.2.4. Base Plate and Main Support Frame Assembly.	4-40
4.2.5. Motor Specification.	4-41
4.2.6. Electronic Control System.	4-44
4.2.7. Load Transducers.	4-45
4.2.8. Temperature and Humidity Transducers.	4-46
4.2.9. Power Supply.	4-47
4.2.10. Data Recording Interface.	4-47
4.2.11. Commissioning and Calibration.	4-52
4.2.12. Summary.	4-58
 5. DETAILS OF FRICTION MEASUREMENTS ON A BONDED SOLID LUBRICANT FILM ABOVE THE YIELD PRESSURE.	
5.1 Test Programme	5-2
5.1.1. Introduction.	5-2
5.1.2. Test Specimens.	5-3
5.1.3. Test Conditions.	5-7
5.1.4. Test Procedure.	5-9
5.2. Results and Discussion	5-11
5.2.1. Results	5-11
5.2.2. Discussion of Results.	5-21
5.3. Summary.	5-23
 6. OPTICAL EXAMINATION OF TEST SAMPLES AND WEAR SCAR GENERATION UNDER DIFFERENT REGIMES OF DRY SLIDING CONTACT.	
6.1. Optical Examination of Test samples.	6-2
6.1.1. Introduction	6-2
6.2. A Study of the Contact Evolution During the Early Stages of Sliding.	6-7
6.2.1. Materials and methods.	6-7
6.2.2. Observation of Results.	6-17
6.3. Friction Measurement Close to the Yield Pressure.	6-19
6.3.1. Introduction.	6-19
6.3.2. Test Specimens.	6-21
6.4. Test Conditions.	6-21
6.4.1. Apparatus.	6-21
6-4-2. Test Procedures.	6-23
6.5. Results.	6-24
6.6. Discussion of Results.	6-25
6.7. Optical Examination of the Counterface and Wear Track.	6-29

6.7.1. Introduction.	6-29
6.7.2. Observation of Results.	6-42
6.8. Contact Spot Generation above the Yield Pressure of the Coating.	6-43
6.9. Calculation of the Predicted Contact Spot from Hertzian Contact Mechanics.	6-46
6.10. Discussion.	6-48
6.11. Summary.	6-48
7. COMPARISON OF THEORETICAL AND EXPERIMENTAL RESULTS.	
7.1. Empirical Model of Time Dependant Friction.	7-2
7.1.1. Generalised Performance Phases.	7-2
7.1.2. Modelling of the First Phase.	7-3
7.1.3. Discussion.	7-6
7.2. Models Dependant on Contact Geometry.	7-6
7.2.1. Elastic Contact Model.	7-7
7.2.2. Contact Spot Dimensions.	7-13
7.2.3. Models with Simple Elastic/Plastic Contact.	7-16
7.3. Real Area of Contact.	7-22
7.3.1. Area Generated at Various Stages of Sliding 10N Load.	7-22
7.4. Tangential Force Effects and Coated Surfaces above the Film Yield Pressure.	7-27
7.4.1. Tangential Force. (Side Load)	7-27
7.4.2. Contaminated Surfaces.	7-32
7.5. Hertzian Contact with Pressures above the Yield Point.	7-36
7.6. Friction due to Sliding taking place Between a Thin Film and Wear Scar.	7-41
7.7. Friction Calculators.	7-47
7.8. Summary.	7-56
8. CONCLUSION AND FURTHER WORK.	
8.1 Conclusion.	8.2
8.2 Further Work.	

9. APPENDICES

A1. Early test machine modifications.

A2. New machine bearing details.

A3. Motor wiring diagram and force sensor switch.

A4. Force sensors, temperature and humidity sensor.

A5. Publications.

NOMENCLATURE

Unless otherwise stated in the text the following abbreviations and symbols are used throughout this work.

W	applied load
F	friction force
A	real area of contact
s	bulk shear stress
τ	shear strength
μ	coefficient of friction
R or r	radius
D or d	diameter
h	film thickness
α	constant
E	elastic modulus
ν	poissons ratio
p	pressure
p_0	yield pressure
a	Hertzian contact radius
Y	tensile yield strength
H	hardness of material
kg	kilogram
km	kilometre

ACKNOWLEDGEMENTS

The author wishes to express his sincere thanks and gratitude to all those who have helped with the preparation and execution of this work, in particular the following:

Professor Ian Sherrington who's perseverance, patience and guidance over the last six and a half years has been invaluable.

My supervisors Dr E W Roberts (AEA Technology) and Dr David Ashman (tic).

Professor R Derek Arnell for his advice on surface contacts and Dr Nathalie Renevier for her advice on surface hardness of films.

The technicians at the University of Central Lancashire, Mr Michael Watson, Mr Frank Wadmore, Mr Ken Day and Mr Duncan Taylor.

The Technology Innovation Centre (UCE) Birmingham, for its sponsorship and provision of facilities.

The staff and technicians at the Technology Innovation Centre. In particular Dr Tim Burden for his understanding and encouragement and Mr Michael Conboy for his assistance with the digital photography.

Mr Martyn Crowther at Armourcote Surface Treatments Ltd. for providing the samples.

Breed (UK) Ltd. for their early contributions.

Finally to my wife Pauline for her understanding, encouragement and proof reading of the text.

CHAPTER 1
SOLID LUBRICANTS
An Introduction.

1. INTRODUCTION.

1.1 Solid lubricants and the reason for the research.

The lubrication of sliding surfaces by films or coatings made from solid materials is now commonplace. Solid lubricants are needed and used for automotive, aerospace and industrial applications in various forms, as burnished films, mixed with a resin matrix to form a bonded solid lubricant, as an additive to conventional lubricants such as oil and grease and as very thin films (in the region of 1 μ m thick) deposited by vapour deposition techniques. Bonded Solid Lubricants (BSLs) have been in use since the early 1950s and are of particular interest to the author due to their use and specification over a period of years on components used for automobile safety restraints, in particular the quick release mechanism in seat belt buckles.

The impetus for this research was initiated with the requirement to improve the performance characteristics of one of these buckle mechanisms. Although the particular mechanism had been in existence for over 15 years only changing cosmetically to suit the individual customer package, it was still deemed to be a viable cost effective solution for many applications. Over this lifetime international and customer specifications had become more stringent and with the emphasis on safety being a major selling attribute for vehicles, novel mechanisms were being introduced which placed even more performance criteria on the buckle. For example the introduction by Renault and Opel of seat belt pre-tensioners to remove slack from the seat belt system on impact, these devices, either mechanical or pyrotechnic, placed severe requirements on the buckle, firstly for it not to release on initiation of the device and secondly to release when required, under much higher loading. The aims of the project were to develop an in depth understanding of the performance of these materials and develop empirical models of the frictional characteristics that would allow the selection and specification of these materials in specific applications.

1.1.2 Methods of application.

The major uses of solid lubricants in their 'dry' form fall into three categories and are described here in order of their technological complexity.

Physical Vapour Deposition applied films, also referred to as sputtered films are applied by vaporising the material to be deposited in a vacuum chamber, The process is performed by applying a high voltage across a low pressure gas, normally argon at a pressure of 5 millitorr, to create a plasma which consists of electrons and gas ions in a high energy state. These energised plasma ions strike a target consisting of the desired coating material and cause molecules to be ejected from the target that contain enough energy to travel to, and bond with, the substrate of the material to be coated, figure 1.1. Coatings applied by this method are usually less than $2\mu\text{m}$ in thickness and have an extremely good bond to the substrate due to the bonding atom level.

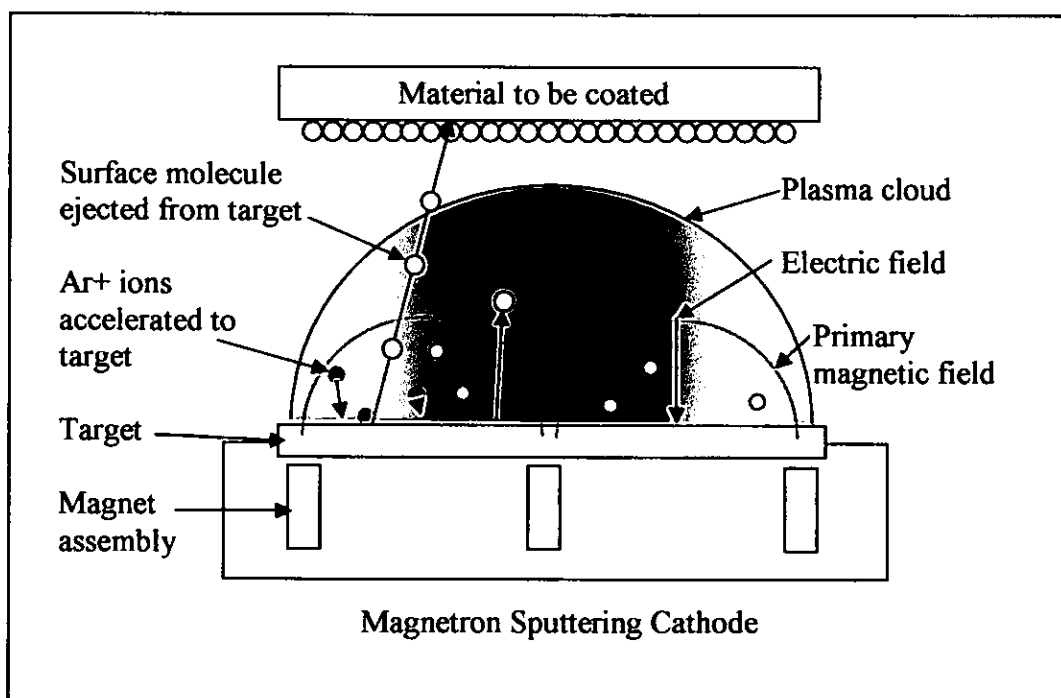


Figure 1.1 Schematic of PVD process (Sputtering).

Bonded solid lubricants are basically paints with high solid contents, the majority of this solid being either a single lubricant or a mixture of one or more lubricants in fine powder form. They can contain volatile solvents or be water

based or a mixture of both and subsequently be air curing at room temperature or oven cured at temperatures up to 180 degrees Celsius. Like paints they can be applied by brushing, spraying or dipping to the whole component to be coated or to a specific area. These films are much thicker than PVD films and are usually in the order of 10 to 25 μm level, although in some extreme cases they have been applied at much thicker levels, e.g. Space Shuttle ball joints. It is these films of 10 to 25 μm thickness that are of interest and form the basis for this report.

Burnished films are the simplest of all to apply, this process generally consists of rubbing the dry lubricant powder into the surfaces requiring lubrication, producing a very thin film up to 1 μm thick. These films are useful for fitting closely toleranced components together to prevent “galling” and in fine instruments for pivots etc.

1.2 Bonded Solid Lubricants.

There are literally hundreds of BSLs available to engineers and designers today. The most widely used in the manufacturing industry consist of a solid lubricant such as PTFE, Graphite or Molybdenum Disulphide (MoS_2) in powder form, mixed in a combination of one or more with a binder. This binder can be organic or inorganic in form. Organic binders include Polyamide-imide, Epoxy and Epoxy Phenolic Resins, inorganic binders include Silicone and Sodium Silicate. Of these binders the polyamide and epoxy resins account for the majority of BSLs in general use today and it is these that are of particular interest in this study.

The structure and mechanism of lubrication of graphite and MoS_2 is well documented in the literature and is described later, as is that of PTFE except that mechanism of lubrication is not completely fully understood. The effect on their properties when these lubricants are mixed with a binder is even less understood with very little information available in the public domain see Burke and Sherrington 2001 [1.1]. General guidelines are presented by the manufacturers but due to the number of variables affecting the performance of these materials,

see table 1, it is advisable to test them in a situation as close as possible to the application, this can be extremely expensive in some cases.

A variety of tribometers have been developed over the years for testing conventional lubricants such as oils and greases and have been adapted to test BSLs. However, in some cases the contact/sliding regime is not particularly representative of any practical application and therefore the relevance of the test is questionable. The most common of these tribometers is the pin on disk or pin on plate configuration, used either in continuous or reciprocating motion.

operating temperature,	relative speeds,
operating environment,	surface finish,
counterface material,	component size and shape,
substrate material,	coating thickness,
substrate hardness,	coating uniformity,
contact pressure,	quantity of parts,
contact geometry,	economics, including versatility.
relative motion type,	

Table 1. Parameters affecting performance.

1.3 Extreme examples of the uses of BSLs.

The following examples illustrate the versatility and extent of use of BSLs:

i) 10m diameter ball joint for the storm surge barrier near the Hook of Holland. Designed to withstand tidal surges and transmit maximum calculated tidal forces of 35000 tonne and yet allow the barrier to be opened to its standby position at a velocity of 5mm s^{-1} as well as accommodating the rolling and pitching due to wave action during opening and closing. After several simulations with conventional lubricants, grease, oil and self lubricating plastics had failed testing due to either mechanical failure or cost constraints a BSL containing PTFE /

MoS₂ with a resin binder at a thickness of 20 to 30µm was selected and met all the requirements during simulation testing. [1.2]

ii) Seat Belt Buckle locking mechanism. Designed to operate under varying loading conditions experienced during the motor vehicle life of up to 15 years the single plate locking member was expected to withstand loads of between 10 to 1000N under normal driving conditions and up to 24KN under crash conditions, then release with a force less than 60N with a traction load of 300N. The buckle also had to withstand rigorous cycling tests of 25000 cycles, one cycle consisting of connector insertion and release with a load of 10N applied to the connector. Various combinations of BSLs were tried and tested both as part of the actual assembly and as described in Chapter 4.1. The final selection being a BSL comprising PTFE and Graphite in a polyamide-imide resin binder 20 to 25µm thick.

iii) Automobile Windscreen Wiper Blade. The modern synthetic rubbers available today are more cost effective and produce better engineering solutions than natural rubbers for the small precision components used in the automotive sector, a major disadvantage with the 'softer' of these materials especially on smooth surfaces such as glass, is their inherent 'tackiness'. BSLs containing graphite in an air cured polyamide-imide resin binder have been used successfully to alleviate the effect of this 'tackiness' on windscreen wiper blades, a thin stripe of the BSL being applied to each side of the blade by spraying. A further application using the low friction and non stick properties of PTFE again with an air curing polyamide binder is the coating of 'O' rings used in hydraulic and pneumatic applications, this coating facilitates ease of assembly and provides the initial lubrication requirements of the assembly.

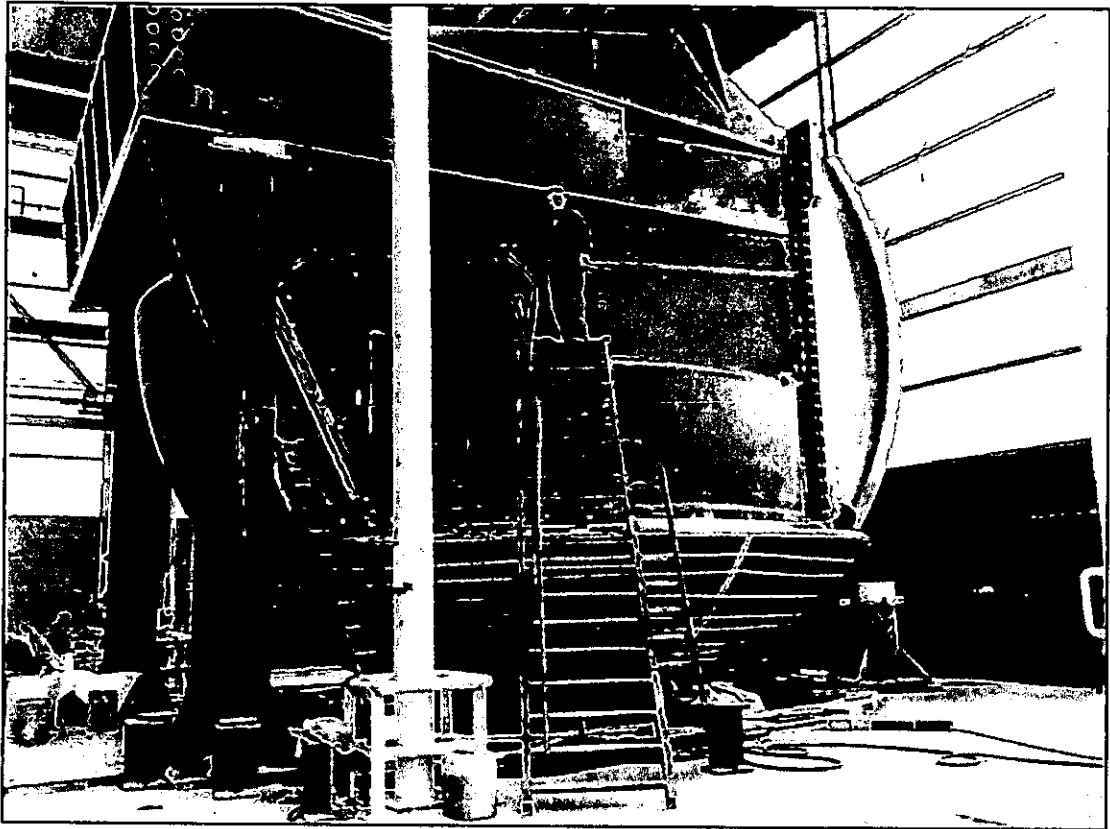


Figure 1.2 Ball joint during construction.

(Photograph by Ministerie van Verkeer en Waterstaat, NL)

Adapted from The Lubrication Carries the Complete Load. [1.1]

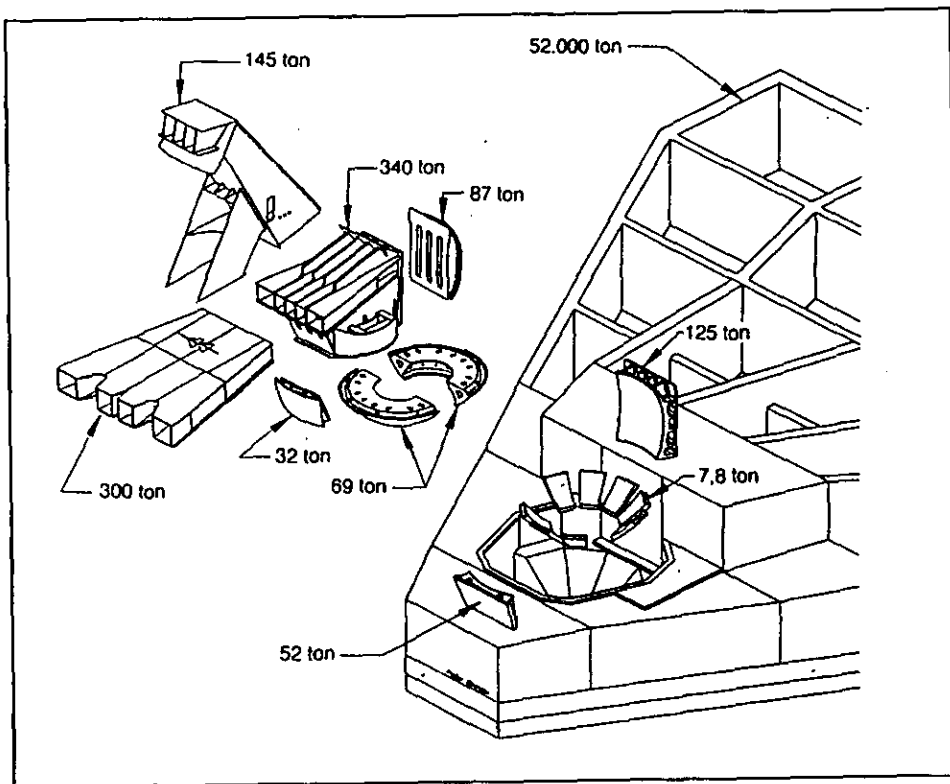


Figure 1.3 Exploded view of ball joint and massive foundation block.

Adapted from *The Lubrication Carries the Complete Load*. [1.1]

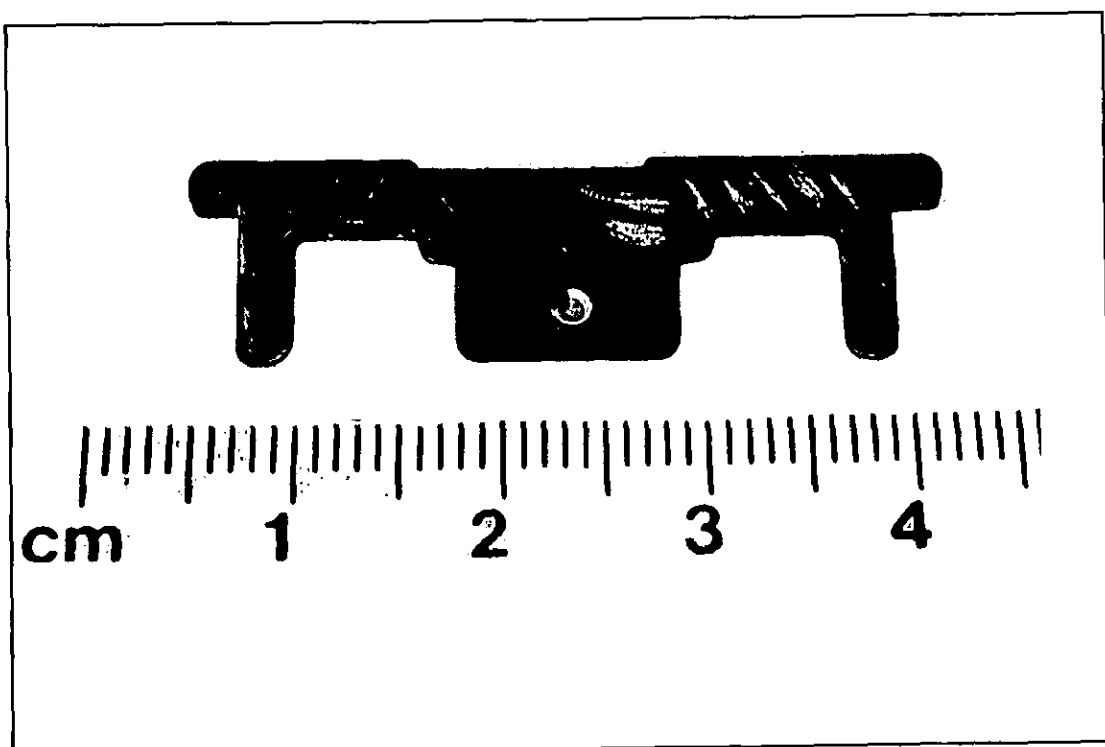


Figure 1.4 Seat belt buckle locking member.

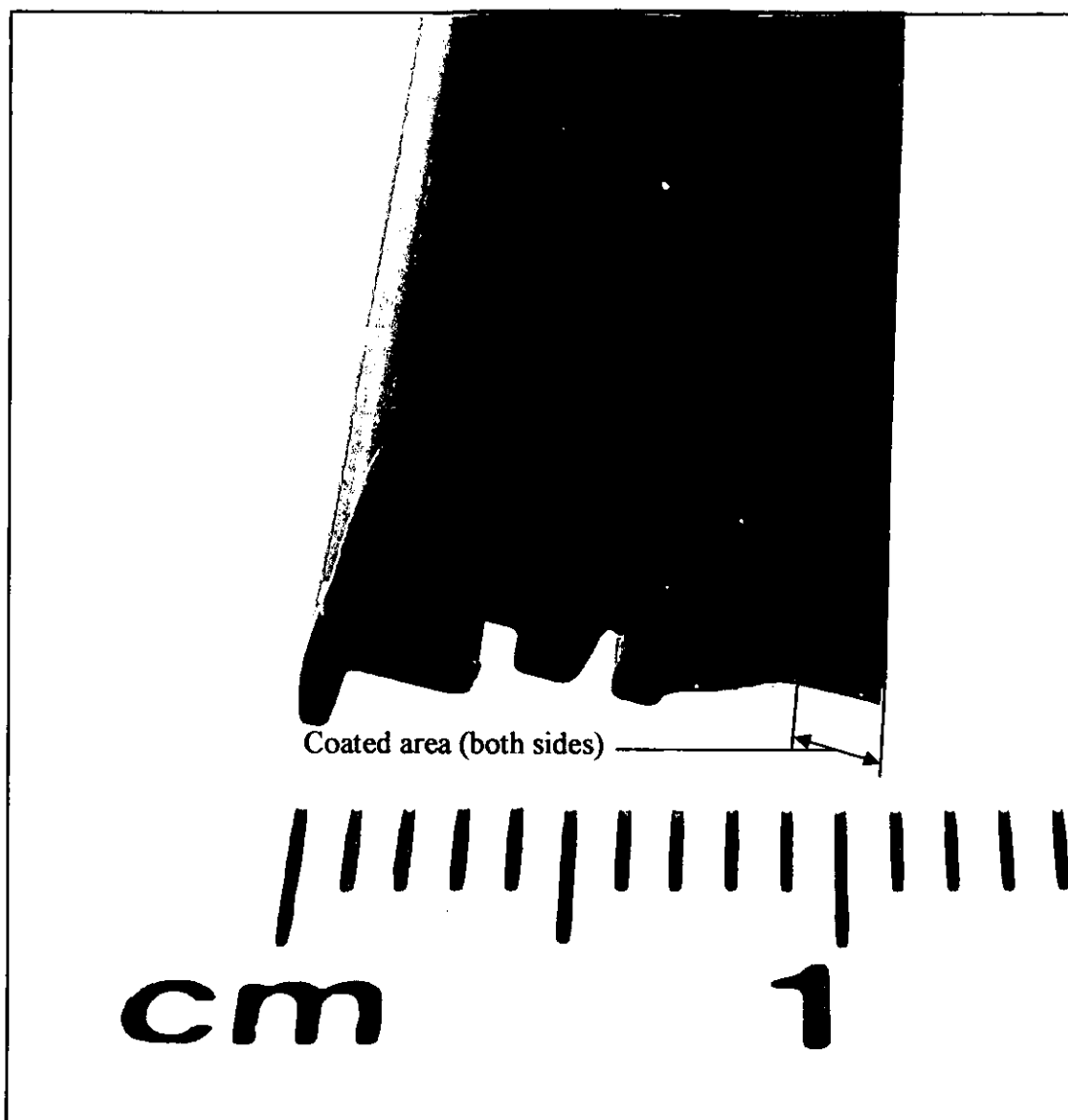


Figure 1.5 Windscreen wiper blade.

1.4 Summary.

Solid lubricant types are discussed along with their method of application, a table of parameters that affect their friction and wear performance is included. The initial impetus for the research is described and extreme examples of practical applications are given.

The following chapters describe the scientific study of solid lubrication as far back as the early 20th century and even further back in time to the mechanisms of friction described by Leonardo da Vinci are discussed.

A screening programme is described for 12 bonded solid lubricants and the results discussed, the shortcomings of the initial test facility are reviewed. A detailed description of the design of a new test apparatus is given and several test programmes conducted on this apparatus are described and discussed. The results from these programmes are given and comparison is made with theoretical models.

REFERENCES.

1.1] Burke, D. Sherrington, I. Roberts, E. W., The influence of counter-face surface finish on the performance of bonded solid lubricant films. Proceedings of the 2nd World Tribology Congress. Sept 2001.

1.2] Glusing. H. The lubricant carries the complete load. NORDTRIB '98 Proceedings of the 8th International conference on Tribology. 7-10 June 1998 Denmark. 27-35.

CHAPTER 2

LITERATURE SURVEY

The use of Graphite, Molybdenum Disulphide and Polytetrafluoroethylene as solid lubricants.

A Review.

In this chapter the tribological study of the constituent components of bonded solid lubricants i.e. Graphite, Molybdenum Disulphide, PTFE, Epoxy and Polyamide-imide resins is examined over a period from 1935 to date. The general uses and applications of these materials in sliding and rolling contacts are described and the mechanism of failure commented upon. The pre-treatment techniques required to ensure adequate adhesion of the BSL to the load bearing substrate are explored and tables included as a guide for various substrate materials.

Comparatively little information is available in the public domain for BSLs and this is one of the reasons for conducting this research. A table summarising tribotesting of these materials conducted since 1965 and involving BSLs in six distinct categories is included for reference.

2. LITERATURE SURVEY.

The use of Graphite, Molybdenum Disulphide and Polytetrafluoroethylene as solid lubricants. A Review.

In order to understand the lubricating properties of a bonded solid lubricant it is necessary to understand the properties/lubricating mechanism of the constituent components: Graphite, Molybdenum Disulphide, PTFE, Epoxy Resins and Polyamide – imide resins. The tribological study of these materials goes back to the early 20th century.

2.1 Graphite.

Graphite is one of the two naturally occurring crystalline forms of carbon, the other being diamond. This soft black material is composed of a series of parallel layers of carbon atoms, in regular hexagonal arrays with covalent bonds, illustrated in figure 2.1 and 2.2. As each carbon atom is bonded to only three others, not the four that would satisfy all the valence bonds, electrons can move freely throughout the graphite crystal, making it a good conductor of heat and electricity. The inter-planar bonding is primarily from van der Waals forces with a weak covalent contribution resulting from interaction between the pi-electron of the carbon atoms [2.1]. This inter planar bond has a strength about one tenth to one hundredth of that between the atoms within the layers. This sheet like structure, which is strong in compression with a low value of interfacial shear strength, in part accounts for the material's value as a lubricant.

In 1935 Dobson [2.2] observed that in certain environmental conditions rapid wear and high friction occurred. This phenomenon assumed practical significance in the early 1940's with the carbon brushes of the generators of high flying aircraft [2.3]. The early work of Van Brunt [2.4] and Savage [2.5] demonstrated that in ordinary atmospheric conditions the rapid wear and high friction of graphite was inhibited by the presence of water vapour, demonstrating that the presence of water vapour enhanced the lubricating properties of graphite. Early research into this phenomenon was hampered by the absence of reliable vacuum pumps and chambers, this was

overcome in the mid fifties and a further paper by Savage [2.6] demonstrated the effects of water and other condensable vapours on wear rate, (see figure 2.3.)

The role of these adsorbed vapours and gasses was the subject of a number of investigations throughout the early 60's and 70's. Work by Bryant [2.7] demonstrated directly that the inter lamellar binding energy of graphite is much higher in vacuum than when oxygen and water vapour are present, suggesting that these vapours could reduce the binding energy of the pi-electrons during cleavage.

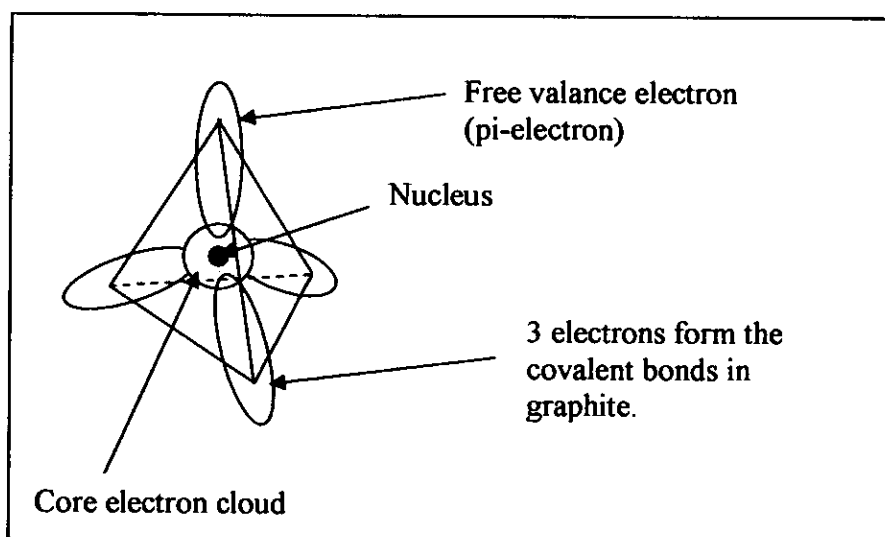


Figure 2.1. Hybridized Carbon atom showing four sp^3 hybrid orbitals in tetrahedral geometry.

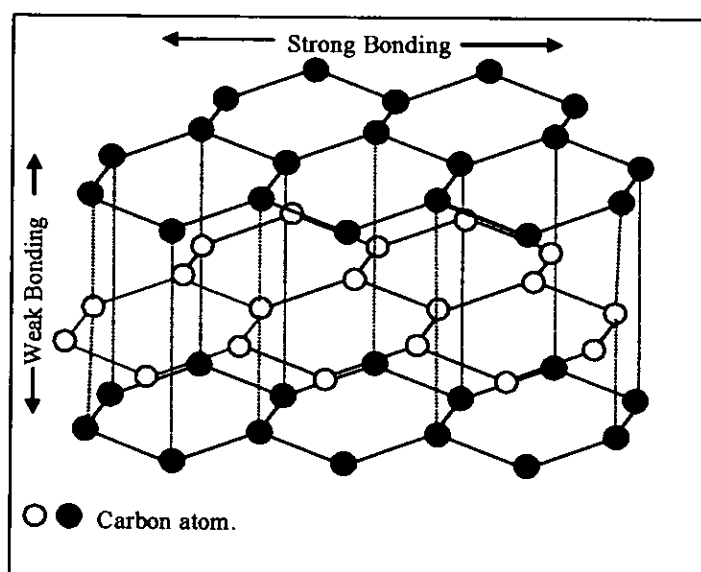


Figure 2.2. Graphite lattice.

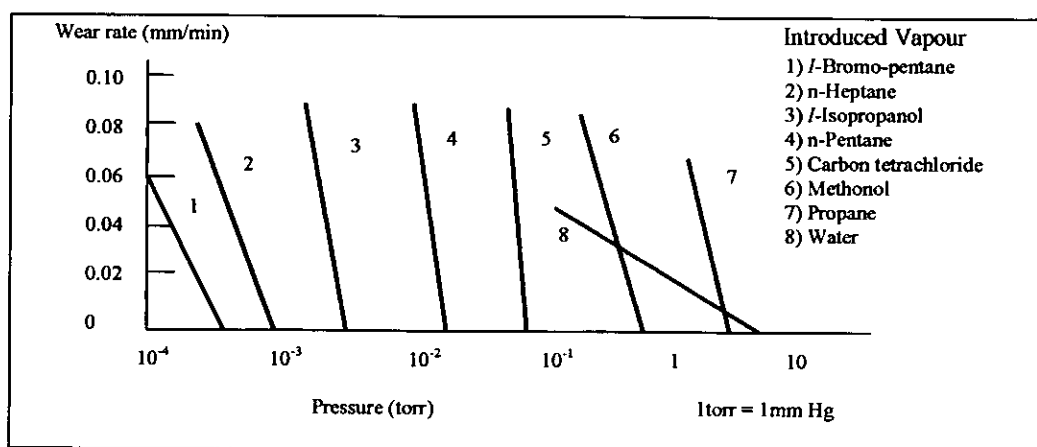


Figure 2.3. Wear rate of graphite sliding on copper under different partial pressures of various vapours.

Adapted from R H Savage & D L Schaefer et al [2.6]

In contrast Rowe [2.8], proposed that oxygen and water might intercalate between basal plane lamellae and therefore reduce the pi-electron bonding, but a study by Arnell and Teer [2.9] using X-ray diffraction failed to show any increase in interlamellar spacing which would be necessary for intercalation. Roselman and Tabor [2.10] proposed that adhesion and friction between the basal planes of graphite remained low even in vacuum due to them being low energy surfaces, until they become damaged, leading to the production of edge sites. The shear strength of the edge site interactions would be 10-100 times greater than that between basal planes [2.11] making these sites almost as strong as the bonding within the planes, giving rise to high friction and high wear rates or “dusting”. Some support for this is given in Savage’s original observations [2.6] in that only about a 10% monolayer coverage of water vapour over the whole surface was necessary to prevent severe wear, inferring selective adsorption on preferred sites.

In 1981 Lancaster and Pritchard [2.12] demonstrated the effect of temperature at the contacting asperities to be critical to the onset of severe wear or dusting in the presence of a variety of vapours and gasses. Load, speed and ambient temperature only being important so far as they influenced this temperature. The magnitude of this critical temperature (temperature at the onset of severe wear) was dependent on the type of vapour and its partial pressure, it was also suggested that adsorbed vapours on the basal planes functioned as reservoirs from which molecules migrated to neutralise freshly exposed edge sites, and that the onset of dusting occurs when

the basal plane coverage falls below some critical value. This work also confirmed some of the earlier work of Savage.

To summarise, graphite is not intrinsically a solid lubricant, it lubricates in normal air atmosphere, but fails at high altitudes or in vacuum. (It can be modified by adding adjuncts such as barium fluoride or molybdenum disulphide for example to improve performance at altitude.) The lubricating mechanism is due to several factors: lamella structure, adsorption of condensable vapours, possibly intercalation of these vapours and other elements, some of these vapours being much more effective than water, its ability to form layers or transfer films that adhere strongly to metal surfaces.

2.1.1 Uses and Applications.

By far the greatest use of graphite is in carbon brushes for electrical equipment such as electric motors and generators. In a fine powder form it is added to lubricating oils to supplement the properties of the oil and provide protection during boundary lubrication regimes such as those found on start up. In this form it can also be used solely as a solid lubricant for fine instruments. Applied as a burnished film to a polished substrate it can provide, in atmosphere, a lubricant with a coefficient of friction as low as 0.07. Unfortunately, because of the very thin layer produced, in most cases less than 1 μ m, the wear life of this type of film is short and is largely dependent on the surface topography of the base material. The life of burnished films can be extended by careful finishing of the base material by mechanical i.e.: grit blasting, or chemical treatment such as zinc phosphating. In 1984 Fusaro [2.13] conducted a study on various surface finish pre-treatments for burnished films of graphite, these experiments were performed on a pin and disc apparatus. Table 2.1 gives the surface finish details before and after pre-treatment.

Disk surface Treatment	Rockwell Hardness HRC		Surface roughness of disk, $R_a \mu m$	
	Pin	Disk (after treatment)	Before coating	After coating
Sandblasting	8.90	28	1.1-1.2	0.85-1
Gas-nitriding	8.9	57	0.45-0.7	0.45-0.6
Zn Phosphate	8.9	26	3.2-3.8	1.5-1.8
Salt nitride smooth	8.9	29	0.32-0.39	0.27-0.34
Salt nitride rough	8.9	29	1.2-1.4	1.1-1.2
Sulfo nitride	8.9	27	1.3-2.5	1.0-1.5

Table 2.1. Summary of material properties and finish.

Adapted from Fusaro [2.13]

Those surfaces treated by sand blasting and phosphating provided the longest service life. The long service provided by the phosphate was thought to be due to the graphite mixing with the phosphate to provide a thin, plastically flowing surface layer. The phosphate did not appear to increase the adhesion of the graphite to the surface, failure occurred when the phosphate layer was depleted. With sand blasting the roughened surface provided a good interface for the graphite to adhere to, with pockets in the surface providing reservoirs of lubricant, this also occurred with the surface of the phosphated samples. Table 2.2. shows a summary of the results.

Disk surface Treatment	Test	Friction coefficient	Endurance to $\mu=0.25$ Disk rev's x 1000	Pin wear m^3/m rate $\times 10^{-18}$		
				0-1km	1-3km	1km to fail
Sand blasted	1	0.11	167	530	-----	80
	2	0.15	176	320	-----	44
	3	0.13	179	630	20	70
Gas nitrided	1	0.12	99	1200	-----	570
	2	0.14	112	1700	-----	530
	3	0.16	78	1300	120	910
Zn phosphate	1	0.12	412	270	-----	6.8
	2	0.13	507	210	-----	7.7
	3	0.13	470	280	5	10
Salt nitrided smooth	1	0.19	150	540	-----	280
	2	0.18	155	490	20	148
Salt nitrided rough	1	0.15	30	7200	-----	1100
	2	0.14	31	6300	3900	3900
Sulpho nitrided	1	0.11	46	9900	-----	1640
	2	0.12	33	11000	-----	4700
	3	0.14	20	6800	-----	5200

Table 2.2. Summary of test results.

Adapted from Fusaro [2.13]

Graphite in powder form is also mixed with resin to form a bonded solid lubricant. This mixture, in the form of a liquid, is applied to a surface by dipping, spraying or brushing. It is then cured at a temperature dependent on the type of resin used. Typical resin binders are: Epoxy, Phenolic, Polyimide, Polyamide-imide, Silicone and Sodium Silicate, each resin imparting its own particular properties to the film. For optimum performance film thicknesses of between 5 and 20 μ m are recommended by the manufacturers as a general guide, but testing may be required to determine optimum thicknesses for specific applications. These bonded films offer much longer service life than burnished films with the addition of providing a

barrier to corrosion products for the base material due to the resin binder. Their performance is still dependent on atmospheric effects, as for pure graphite, but careful selection of the binder to the application can optimise the lubrication properties of these materials. Very little information is available in the public domain for bonded graphite films and their use is fairly limited, normally graphite is found in bonded films in combination with molybdenum disulphide or PTFE or its intercalated compound graphite fluoride [2.14].

With bonded lubricants the surface finish of the substrate is more critical than with burnished films, some sort of “key” must be provided for the film to have good adhesion to the surface. This is normally provided by pre-treating the surface to be coated mechanically or chemically, i.e. grit blasting or phosphating.

2.2. Molybdenum Disulphide.

Molybdenum disulphide (MoS_2) is similar in appearance to graphite, and is often confused with it, both being dark grey to black in colour, although graphite appears more shiny when burnished. The crystal structure of MoS_2 is laminar and similar to that of graphite. The structure consists of planes of Molybdenum atoms in hexagonal formation sandwiched between layers of sulphur atoms with each atom of molybdenum equidistant from six atoms of sulphur placed at the corners of a triangular prism figure 2.4. Strong covalent bonds hold the atoms of molybdenum and sulphur together. The spacing between the sulphur atoms is relatively large and the van der Waals bonding between them weak so that cleavage between the basal planes occurs easily [2.15].

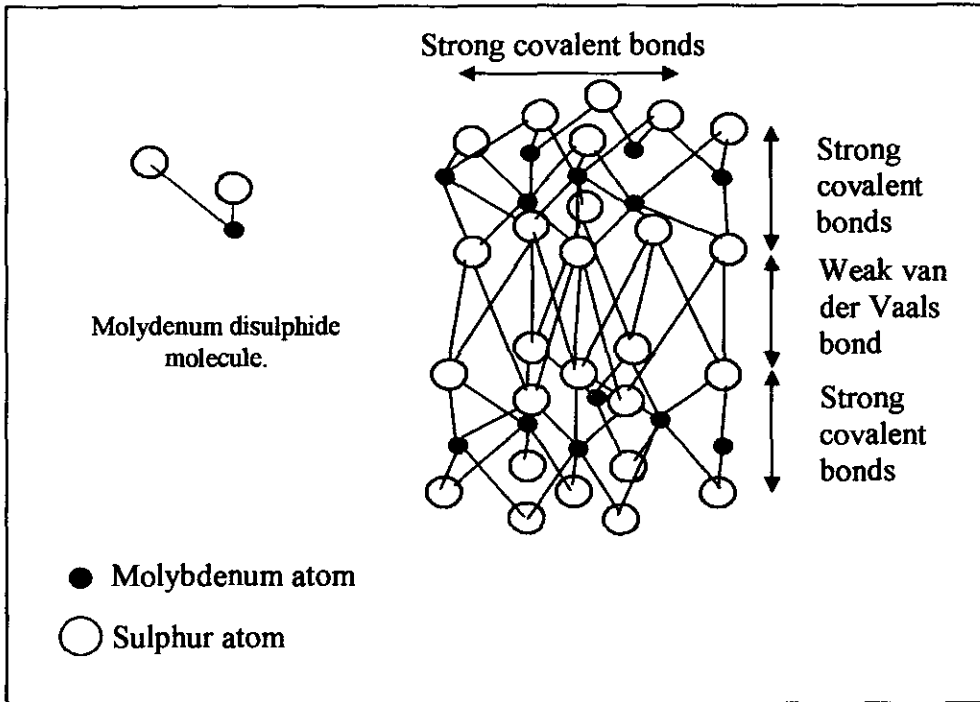


Figure 2.4. Crystal structure of MoS₂.

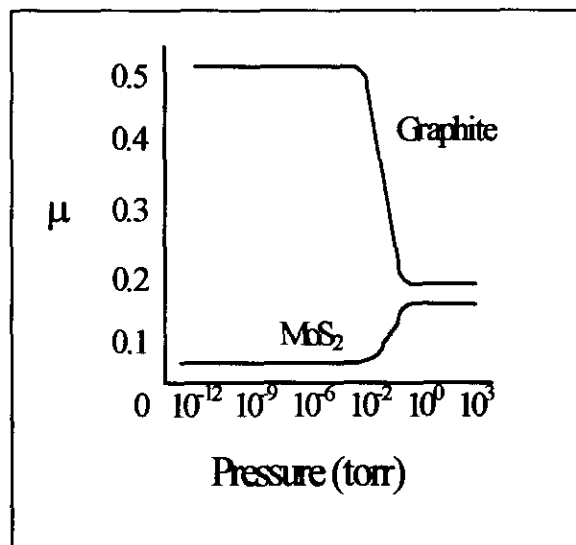


Figure 2.5. Effect of vacuum on friction coefficient

Adapted from D H Buckley Surface Effects [2.16].

Unlike graphite, MoS₂ maintains its lubricating properties in vacuum, in fact its coefficient of friction decreases in vacuum [2.16] figure 2.5. It should be borne in mind for both graphite and MoS₂ and any other layer lattice structure with good

lubricating properties, that the ideal lattice structure is maintained only over a very small region of the individual particle, these regions being separated by gross discontinuities. During sliding, compaction of the film and the mechanical interactions involve re-alignment of the structure at the surface so that the basal planes of the lattice are parallel to the direction of sliding [2.17]. In this early sliding process, or running in, continuous layers of oriented MoS₂ are built up between the substrate and counterface. During this running in phase the coefficient of friction decreases until it reaches a steady state, this steady state continues depending on the effects of atmosphere, temperature, film thickness, substrate pre-treatment and surface finish. Eventually breakdown of the lubricating film occurs with a corresponding increase in friction. It is this mechanism of breakdown of the lubricating film that has been studied in great detail, for almost all conditions imaginable, over the past fifty years.

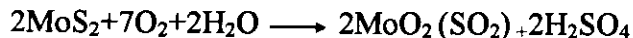
Using a LFW-1 (block on ring) and pin on disk apparatus, Salomon, in 1964 [2.18], studied the mechano-chemical reaction of burnished powder films of MoS₂ with water vapour and with oxygen, finding that in a neutral dry atmosphere of argon with 0.05% oxygen the endurance limit was raised to 150 hours, see Table 2.3. He summarised that *ageing* of the MoS₂ film was initiated via the blocking of slip planes by the inclusion of oxidized areas in the crystalline friction film, this giving rise to the nucleation of blisters in this dense film due to shear compression and oxidation in situ of reactive sites. He also observed that a small quantity of water vapour had a beneficial effect on endurance albeit with a slight increase in friction, yet high humidity led to large scale chemical decomposition of MoS₂ and hence a considerable reduction in life expectancy of the film. The experimental results of this work were similar to those found by Palmer [2.19] for resin bonded films, also work by Sonntag [2.20] again with bonded films and block on ring apparatus, demonstrating the effect on film life as a function of the surface roughness i.e. very fine finishes covered with MoS₂ only lasted a matter of minutes, whereas sand blasted surfaces lasted on average some 13 hours.

Gas	Time to onset of stick slip (hours)
Oxygen	2-4
Air	6-9
Argon containing 0.05% oxygen	>150

Table 2.3. Influence of oxygen on endurance limit of MoS₂ film.

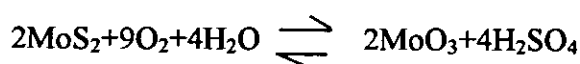
Adapted from Salomon G. De Gee AWJ. and Zaat JH. et al [2.18]

This work was extended in 1965 by De Gee, Salomon and Zaat, [2.21] who found that during the friction process, high levels of humidity, 90% at 25° C in a nitrogen or argon atmosphere, promoted molybdenum oxides and oxide hydrates, with the simultaneous evolution of H₂S being formed. In air, however, rapid formation of molybdenum oxides were observed but H₂S was not found, instead the principle oxidation product being SO₂ being dependent upon the ratio of water vapour to oxygen. Also in 1965 in a separate paper Kay [2.22] reported the corrosive effect of MoS₂ on metallic surfaces in humid atmospheres in the presence of oxygen due to the formation of H₂SO₄ by the following reaction:



The implication of this for bonded films on steel substrates in humid atmospheres would be the breakdown of the lubricant film due to the corrosive effects on the substrate from the acid produced. Thus the use of MoS₂ in high humidity environments is not recommended.

Holinski and Gansheimer [2.23] in 1972 concluded that during running in, adsorbed water vapour bonds simultaneously to two polarised sulphur-atoms therefore increasing the coefficient of friction across the basal planes, whereas Roberts [2.24] attributed the increase in friction due to the humidity, to the adsorption of water molecules at two different sites, edge sites and intercalation sites, from which the water molecules could penetrate between the layers. Panitz [2.25] suggested that water and oxygen chemically react with MoS₂ as follows:



and that the MoO_3 increases the friction between the MoS_2 layers.

2.2.1. Uses and Application.

MoS_2 can be applied as a burnished film, bonded lubricant or by Physical Vapour Deposition, PVD. Burnished films are normally only used for very limited life applications e.g. as an assembly aid for close toleranced components to allow alignment on assembly, this type of film is applied in powder form and burnished into the surfaces with a medium hard “sponge”. It can also be applied by aerosol, where the propellant carries the fine powder to the surface and then evaporates. Surfaces to be treated in this manner must be free from oil or grease but normally no special treatment is required. Film thickness can be up to $1\mu\text{m}$ thick but it varies considerably dependent on the surface finish of the component.

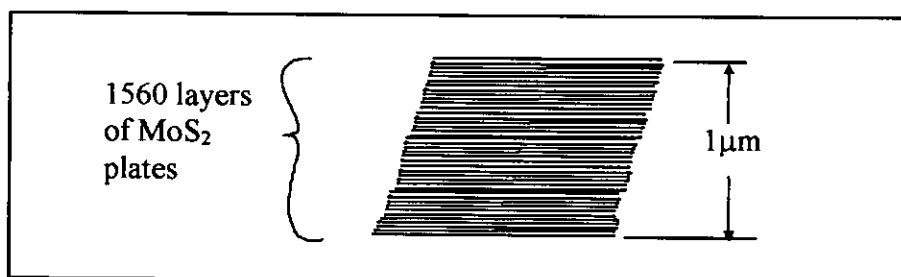


Figure 2.6. Example of thickness of MoS_2 layers

If a perfect structure of MoS_2 could be formed into layers of parallel plates then, from the sandwich size plus the basal plane gap, $3.16\text{\AA} + 3.49\text{\AA} = 6.65\text{\AA}$, theoretically there would be about 1560 layers in $1\mu\text{m}$ figure 2.6. Similarly for graphite with a basal plane gap of 3.4\AA there would be about 3000 layers in $1\mu\text{m}$, these layers are very thin if compared to the average length of an oil molecule at about $0.2\mu\text{m}$.

Bonded films contain a mixture of MoS_2 powder and other fillers in a resin matrix with a volatile thinner to facilitate application. The resin types available are as those previously quoted for graphite in section 2.1.1. These bonded films are by far the most widely used in industry and are available in bulk for application by dipping, brushing and spraying, they are also available in aerosol form. Surfaces to be treated with a bonded lubricant must be free of contamination by oil, grease and water and corrosion products and therefore, require treatment by mechanical or

chemical means before application of the film, this is normally, for steel substrates, either grit blasting or some form of phosphating or a combination of both. Film thickness is dependent on application method, surface pre-treatment and part geometry but is normally quoted for optimum performance at 10-20 μ m.

Physical Vapour Deposition (PVD) applied films, also known as sputtered films, are used mainly in aerospace applications where the thin, oriented uniform film can be applied to very close tolerance parts with very fine surface finishes usually in the order of 0.04 to 0.3 μ m R_a with film thickness in the order of 1- 2 μ m. A study by Cunningham [2.26] on surface roughness and film thickness demonstrated the effects of various surface finishes on the coefficient of friction. Surface preparation of PVD film is extremely critical, as is the preparation of the MoS₂ source if the sample is required for vacuum applications, adsorbed water and oxygen must be excluded and the finished components stored appropriately. Normally the components would first be polished to the required finish then ultrasonically degreased and finally, but not always, cleaning in vacuum by sputtering prior to application of the desired film.

It can be seen from the above that surface finish of the film substrate plays an increasingly important role in the performance of the film produced, as does the method of application and size of the powder used, in the case of burnished and bonded films, and the purity of the MoS₂ material itself.

In air the same mechanism of failure, generation of SO₂, H₂SO₄, MoO, MoO₃ at the sliding interface due to thermal, mechanical and chemical interaction will apply to all three methods of coating, as well as the added complication of the breakdown of the resin binder in bonded films. Although some protection is afforded by the resin matrix for the MoS₂ against the reactions of water and oxygen, the reaction only takes place at the surface of the sliding interface, new material being fed to this interface as wear takes place from the matrix of the coating, thus the life and performance of the film will depend on the characteristics of its operational environment i.e.: humidity, sliding velocity, temperature, load, oxygen content, atmospheric pressure, film type and thickness, etc.,

2.3. Polytetrafluoroethylene.

Polytetrafluoroethylene (PTFE) is probably the most well known of the fluorocarbon range of fluoropolymers. Discovered by chance in 1938, it is a white, waxy solid. The polymer consists of a helical chain of carbon atoms in a zigzag pattern with two fluorine atoms with covalent bonds to each carbon atom. These covalent bonds are extremely strong, the helical form of the carbon backbone is caused by the repulsion between fluorine atoms due to the molecule being so compact, the helix completes one full 360 deg twist in 33.6Å, 13 zigzags or 26 chain atoms figure 2.7 [2.27]. The fluorine atoms form an almost impenetrable sheath that gives protection from chemical attack for the carbon backbone, hence the material is almost completely inert.

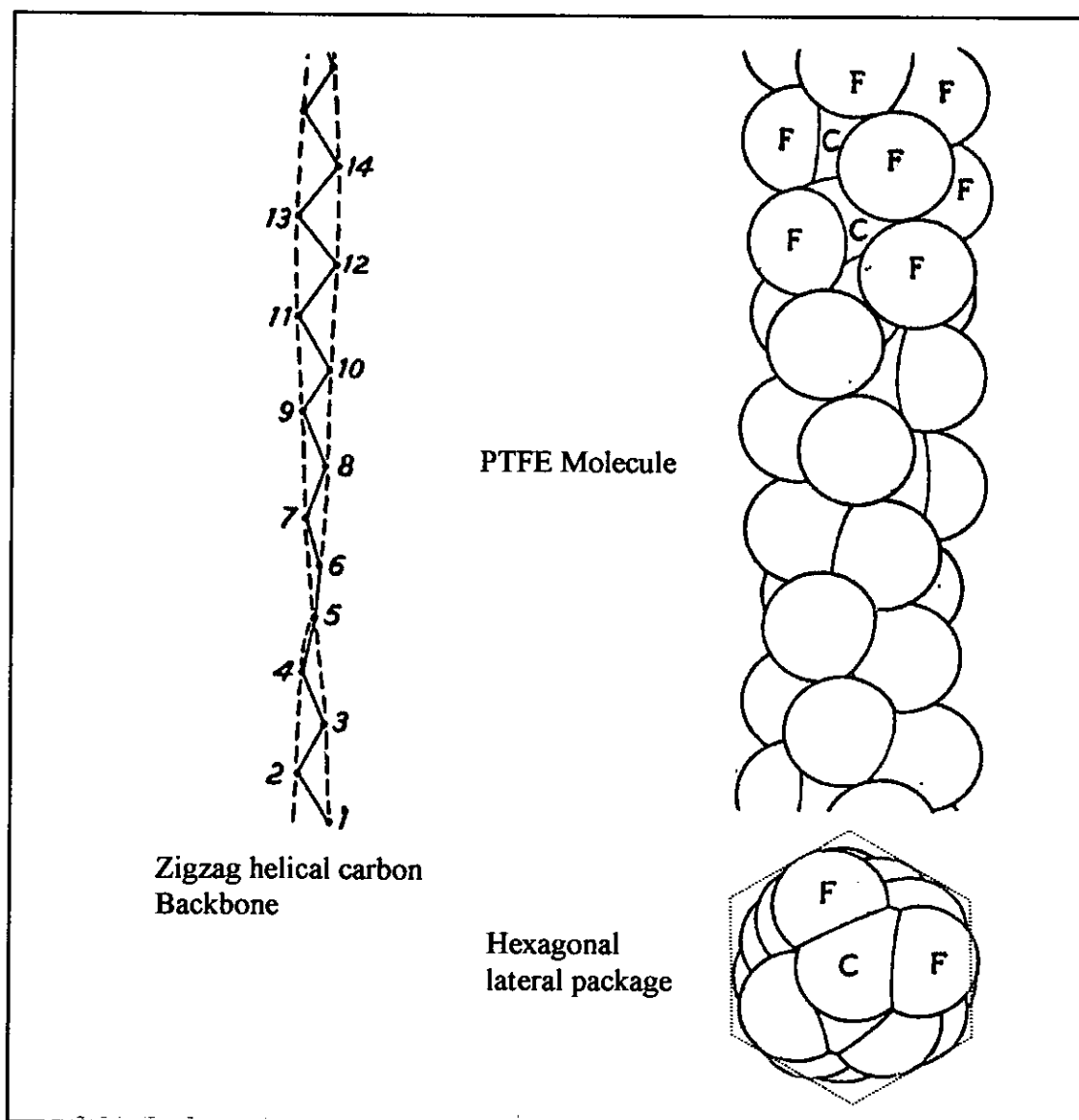


Figure 2.7. PTFE Molecular Structure.

Adapted from Bunn & Howells, et al [2.27]

The lateral package of these rod like molecules is hexagonally shaped with $a_0 = 0.562\text{nm}$. These molecules form thin crystalline bands separated by amorphous or disordered regions. Its melting point - the transition from partly crystalline to a completely amorphous structure is about 330 degrees C, very much higher than that of corresponding hydrocarbons.

2.3.1. Mechanism of Lubrication.

PTFE has a working temperature range from 250 deg C down to -196 deg C, the temperature of liquid nitrogen. It is non flammable, not wetted by water and does not absorb water and is an efficient electrical insulator. The coefficients of static and dynamic friction are quoted as being numerically equal. A value of 0.04 is usual for its coefficient against steel, and values as low as 0.016 have been reported for very high loads, high loads and slow sliding speeds normally produce the lowest coefficients of friction [2.28] see figure 2.8.

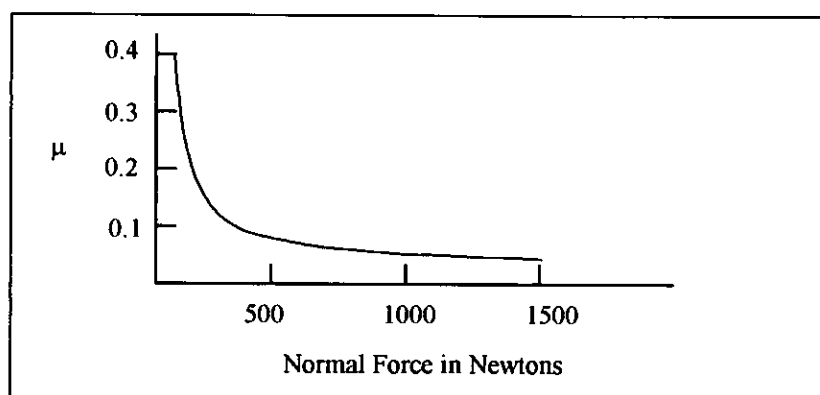


Figure 2.8. Effect of load on friction coefficient of PTFE.

"Adapted from Soc of Plast Eng. 16, 1960 943-948."

Although there are numerous descriptions in the literature on the mechanism of lubrication [2.27] [2.29] it is now widely accepted that the low friction properties of PTFE are due to the smooth rod like molecules being able to slide over each other with relative ease and form a highly oriented transfer film on the sliding counterface, so eventually the sliding occurs between this transfer film and the bulk of the material. Unfortunately PTFE on its own has a high wear rate, does not conduct heat very well and thus is unpredictable at high speeds with medium to high loading. A study by Uchiyama and Tanaka [2.30] in 1979 into the effects of sliding speed,

contact pressure and surface temperature demonstrated the interaction between these parameters as well as the existence of a wear law related to the viscoelastic nature of PTFE the linear wear rate at temperature T and contact pressure p, it is given by:

$$\alpha = \frac{k_0(a_T V) \left(\frac{p}{p_0} \right)^n}{b_s}$$

Where: α is linear wear rate (wear depth per unit sliding distance), n is a constant greater than unity, a_T and b_s are shift factors that vary towards the speed axis and wear rate axis respectively, p_0 is the contact pressure and k_0 is a constant that varies with sliding speed at temperature T_0 .

Lancaster [2.31] in 1982 studied the effect of oscillating sliding on woven PTFE/glass fibre composites used in aerospace dry bearings demonstrating a coefficient of friction lower than that for unidirectional sliding, also observed and analysed the third bodies generated during the wear process. Ratner in 1967 [2.32] developed a model (often referred to as the Ratner correlation) for describing the abrasive wear of organic polymers in terms of their toughness by the correlation of their wear rate with $(\sigma\epsilon)^{-1}$, where σ and ϵ are the stress and strain to rupture an asperity in tension respectively. Briscoe in 1988 [2.33] examined the Ratner correlation with respect to the abrasive wear of PTFE concluding that within the limits of the original wear experiments, that the principles were basically sound i.e. work is done and damage produced is inversely proportional to the tensile toughness. However with the PTFE wear experiments the model failed to predict accurately due to three main reasons:

1. debris accumulates at the contact,
2. the effective roughness decreases and this is a function of many variables, in particular the rate of wear,
3. the adoption of the total toughness as the material damage criterion.

The work developed modifications which produced a sensible correlation for the polymer system under test but severely undermined the simplicity of the original equations.

2.3.2 Uses and Application.

The main limitation of PTFE is that it cannot be converted into useful forms by rapid means; when heated above its melting point it becomes an amorphous transparent gel that is mechanically weak and will not flow without fracture, therefore it cannot be moulded by standard moulding and extrusion processes. It can be cold formed then sintered at 350 - 400 degrees C similar to processes used in powder metallurgy, in fact this property has been exploited in the production of sintered bronze bushes containing PTFE. There are a myriad of products containing PTFE now on the market from non stick pans to high tech bearings for aircraft and aerospace applications, the following list gives a few examples but is by no means exhaustive:

Expansion joints.	Gaskets.	Packing tape (plumbers)
Electrical cables.	Valves.	Sintered bushes
Bakery machinery Rollers.	Tubes.	Bowden cable liners
Artificial hip joints.	Paint.	Cookware.(domestic)
Food Machinery comp'nts.	Seat belt Comp'nts.	Engine piston skirts.
Power tool accessories.	Automobile carburettor.	
Camera components.	Work surfaces (food preparation)	

In tribological applications PTFE is found generally in one of three forms, as part of a sintered type bushing, a bonded lubricant applied to the sliding surface or more rarely a PVD film applied to a sliding surface. Sintered bushings are used in both dry lubrication regimes, such as required in the food industry, as well as conventionally oil or grease lubricated applications to afford protection during cold starts or where mechanisms undergo continuous start stop sequences. Bonded lubricants can be of PTFE powder on its own in one of the binding agents already mentioned for graphite, or a combination of PTFE, graphite and MoS₂. The condition of the surface topography and preparation of the surface is equally as important to this material as for graphite and MoS₂, the same mechanical and chemical treatment processes being used. One particular use of this type of material, applied by electrophoresis, is to the foot of a "handyman's" jigsaw where on first impressions it would appear purely decorative and a corrosion protector, but the non-stick properties and low friction are used to enhance the performance of this tool by almost eliminating "stick slip" as it runs over the surface of a variety of timber,

plastic and even metal surfaces during its lifetime, this type of coating is now being used in large quantities in place of conventional surface treatment such as chromium and zinc plating due to its relatively low cost, aesthetic appearance, no apparent environmental hazardous by-products and much superior friction properties.

Sputtered films of PTFE deposited by RF or DC diode sputtering in an argon atmosphere have been used on complex surfaces such as gears, ball bearings and surgical needles, the components being conventionally cleaned by degreasing etc., then sputter etched immediately prior to deposition of the required film, these films are not limited to use on metal substrates, but can be applied equally as well to wood, paper, plastics and glass surfaces. The properties of sputtered films are as those generally accepted for PTFE in that the coefficient of is in the order of 0.08 to 0.2 and decreases markedly with load for any given film thickness [2.34]. There appears to be very little information available in the literature on sputtered films of PTFE other than that already mentioned and several papers by Spalvins [2.35] in the early to mid seventies. PTFE is also available in aerosol sprays, hypodermic type oilers containing a suspension of PTFE in silicon or conventional oil and in bulk or sachet form, for application to replacement camshafts to help in "running in".

2.4 Bonding Agents.

Organic resins are used in conjunction with a volatile solvent and other components such as stabilisers, pigments, fillers etc., as well as the solid lubricant to form a "paint" like liquid (the solid contents of these liquids being much higher than that of conventional paints, up to 80% in some cases). By far the most common in use in general engineering today are those based on Epoxy and Polyamide-imide resins.

2.4.1 Epoxy and Epoxy Phenolic Resins.

These resins provide films with high impact resistance and elasticity with surface hardness that are resistant to water, aqueous chemicals and a long list of synthetic solvents. They provide better corrosion protection than polyamide-imide and other resin binders and their adhesion to metal substrates enhances this property. These bonding agents are generally designed to be cured by stoving at elevated temperatures usually in the order of 200°C - 250°C for 30 to 40 minutes. Some systems can be cured as low as 160°C but the time required becomes prohibitive and

these are only used when the higher temperature would cause problems, for example with zinc die castings. As these materials are thermosets they can only be removed by mechanical means after curing. In recent years the drive for more environmentally friendly materials has made manufacturers produce resin systems that are predominantly water based, the use of these systems is growing due to health and safety and environmental pressures.

2.4.2 Polyamide – imide Resins.

These resins have resistance to elevated temperatures and are capable of performing continuously up to 260°C (Epoxyes are limited to 204°C). The Amide groups in these resins impart flexibility and elasticity to form a film of exceptional toughness. They also have very low coefficients of thermal expansion and high creep resistance. At room temperature the bond strength to the substrate is less than that of epoxy phenolic resins, but unlike epoxyes does not deteriorate with increase in temperature and time, hence for room temperature applications these materials do not provide quite as good protection against corrosion. They are also less costly than epoxyes and generally have curing temperatures in the order of 140°C - 170°C.

2.4.3 Silicone and Sodium Silicate.

The inorganic binders silicone and sodium silicate are used only for specialist applications requiring high temperature performance. Due to their lack of use in industrial applications are not detailed in this chapter.

2.5 Pre-treatment Techniques.

It has already been stated that the surface finish of the part to be coated can have a major effect on the finished lubricant film performance. For bonded films applied to steel substrates this finishing is accomplished by either mechanical or chemical means or a combination of both, as follows.

2.5.1 Grit Blasting.

Grit blasting cleans a surface by bombarding it with small carborundum grit particles. The grit is delivered in a stream of high pressure compressed air, which is directed onto the work piece via a hose connected to a nozzle. The action of these

high velocity grit particles is to remove contamination, oxide layers and small particles of metal from the surface being treated, leaving the surface in a reactive state. Components cleaned by this method should be coated quickly to reduce the reformation of oxide films. Several types of facilities are commercially available for performing this type of operation. They range from large cabinets in which the operator wears a full protective suit and breathing apparatus; to small cabinets which isolate the operator from the delivery system and the work. In the latter case, work is conducted by operating the delivery nozzle in the cabinet using integral gloves and viewing the activity through a transparent inlay. Other types of machine are also available for treating small components in bulk.

2.5.2 Phosphating.

The application of phosphate in conjunction with oil or wax was originally employed to provide corrosion protection for steel. Crystalline phosphate coatings provide a porous surface that can absorb oil and this is valuable in improving the tribological characteristics of a surface for some applications. This feature was first used to great effectiveness on the bearings and cam faces of early Singer sewing machines and is still used in similar applications today [2.36]. An absorbent phosphate surface also provides an excellent “key” for paint systems. For example, it is widely employed in the preparation of automotive vehicle bodies prior to painting. In general there are three types of phosphate in common usage:

- Zinc phosphate, for general usage to promote better adhesion and increase corrosion resistance and chemical protection.
- Iron Phosphate, tends to be less expensive than zinc but does not offer as good corrosion resistance.
- Manganese phosphate, offers the best corrosion resistance but it is advisable to use a grain refining wash prior to application otherwise a thicker coating will be required to cover the coarser crystalline structure.

The absorbency of a phosphated surface makes it an ideal preparation process prior to coating with BSLs. It may also be beneficial from a tribological point of view, as has been demonstrated by Fusaro [2.13], and described earlier in this chapter. (He

showed that phosphate has a synergistic effect with burnished films when it becomes mixed with the solid lubricant, extending the life of the component.) A more detailed description of the different types of phosphate coatings, uses and their application process can be found in the ASM Handbook Volume 5 [2.37].

Table 2.4 provides suggestions for pre-treatment for a variety of materials in general friction/wear applications. For more severe regimes or specialist applications a combination of mechanical and chemical treatment may be required and in some cases a primer may be used prior to application of the final coating, a few suggestions for these are shown in Table 2.5.

Substrate	Pre-treatment	Comments
Steel (carbon and alloy)	Degrease, grit blast to 2.5µm.	Coat within 2 hours or phosphate where corrosion protection is required.
Steel (Stainless)	Degrease, grit blast to 2.5µm.	
Aluminium (Wrought)	Degrease or alkaline wash, grit blast to 2-3µm.	Light phosphate may be applied for increased adhesion.
Aluminium (Cast)	Degrease or alkaline wash, grit blast to 1µm.	Light phosphate may be applied for increased adhesion.
Aluminium (Anodised)	Degrease or alkaline wash.	
Zinc (Die cast)	Degrease, grit blast to 1-1.5µm.	
Sintered metal.	Bake to 260°C, degrease or alkaline wash.	Baking will bring the resins and oils that are used in the process, to the surface.
Cast Iron	Degrease, grit blast to 1.5µm.	Phosphate where corrosion protection is required.
Non-metallic	Clean with suitable solvent or detergent.	

Table 2.4 Guide to surface preparation for various substrates.

Adapted from Whitworth Plastics Ltd Design Guide.¹

¹Whitworth Plastics Ltd. 10 Christleton Court, Runcorn, Cheshire. UK WA7 1ST

Application	Substrate	Pre-treatment
Fasteners (screw threads)	Steel (carbon & alloy)	Grit Blast to 3µm degrease and phosphate, apply primer if required.
Other. (Valves, slides, automotive applications, marine applications.)	Cast Iron	Grit Blast to 3µm degrease and phosphate, apply primer if required.
	Aluminium (Cast & Wrought)	Alkaline wash, grit Blast to 3µm anodise if practical, apply primer if required.
	Brass & Bronze.	Degrease, Grit Blast to 3µm degrease, apply primer if required

Table 2.5 Specific applications requiring better overall adhesion and corrosion protection.

Adapted from Whitworth Plastics Ltd Design Guide.¹

2.6 Application of BSLs to substrates

After surface preparation, the chosen lubricant can be applied by brushing, dipping or spraying. The desired thickness of coating is determined by the number of coats applied. In general, a film thickness of between 10µm and 20µm is usually specified by the manufacturers as being appropriate for optimum performance.

Coating thickness is a function of many parameters of the coating process. These include the viscosity of the resin/lubricant/solvent mixture, the resin and solvent type, spin time (in dip spin processes) nozzle/pin/air pressure relationship (in spray processes) and the number and shape of components loaded into the coating machine. Consequently, careful control/monitoring of these parameters during coating is required to obtain a specific and reliable coating thickness.

Components coated with BSLs should be free from sharp edges, as films will not adhere well to sharp edges. Additionally as the coatings are soft the removal of sharp edges on components will help reduce scratching in manufacture and assembly operations. Tolerances on the size of coated components should be considered at the design stage. If a BSL film in the order of $20\mu\text{m} \pm 5\mu\text{m}$ thick is to be applied to a component, component design should take into account whether it is double sided and/or if it is running in a slot or bore. This may seem obvious, but if not accounted for it could be an expensive oversight. For economy, only one friction surface requires coating, normally the one with the largest surface, for example the piston rod in a gas spring, the rod is coated not the guide bush. However this may depend on component size and process choice/availability. When coating small components, it is more economical to coat the whole component to avoid expensive masking and jiggling.

2.7 Testing of BSLs.

A great deal of published data is available on the structure, mechanism of lubrication and performance of solid lubricants laid down by relatively high cost processes such as sputtering. However, published data relating to the performance of the much more widely used bonded solid lubricants is less common. To assist potential users of BSLs to gain access to the relatively limited public domain data on these lubricants, an extensive review of the papers and other documentary material published on the performance of BSLs has been undertaken. The majority of the literature published since 1965 directly involving testing of bonded solid lubricants falls into six categories of experimental testing:

- a) Pin on Plate
- b) Pin on Disk
- c) Block on Ring
- d) Falex
- e) 4 Ball
- f) Special or specific application.

The first 3 categories can also be split into continuous motion (C) and reciprocating motion (R). The product of the review of academic papers is summarised by table

2.6. The table is intended to provide a single summary which presents a list of papers containing detailed data about the friction and wear of BSL coatings along with a brief outline of the experimental work conducted. The lubricant materials discussed by the papers listed in table 2.6 include graphite, PTFE and MoS₂ as well as graphite fluoride and mixtures of these materials. Papers discussing metallic coatings such as cadmium, lead, tin and indium can also be found. The range of binders covered include epoxies, polyamide-imide, polyimide, polybutyl-titanate, sodium silicate, silicon and synthetic mica. The papers themselves give results which are too detailed and complex to include in the table in this chapter, therefore, only brief comments are given to highlight what was tested, the specific data available and the themes of the data produced.

The details of friction and wear results that are in the papers demonstrate considerable variation in the values for wear and friction coefficients. It is extremely difficult to compare specific data due to differences in test type, material combination, speed, load, etc., However some clear observations can be drawn from reference to the papers these being:

- Graphite, for most practical purposes, is useless as a lubricant in vacuum applications. However, it is effective in conventional air/nitrogen atmospheres containing vapours and at elevated temperatures. It is also stable in radioactive environments.
- MoS₂ is an effective general purpose lubricant especially in vacuum and under high loading conditions; but, it is generally a poor lubricant if humidity levels are high.
- PTFE is the most commonly specified BSL and is an effective lubricant under low to medium load applications. It can provide a very low coefficient of friction and when combined with the correct binder, it also offers extremely good corrosion protection.
- In practice it is often worthwhile to use a combination of two or more materials as a composite lubricant to extend the range of useful engineering applications. For example the addition of graphite to PTFE can improve the load carrying capacity and wear life in certain regimes.

Table 2.6 Tribological test data for bonded solid lubricants.

a) Pin on Plate

No	Year	Authors	Speed/motion	Load Kg	Lubricant coating	Bonding Agent	Results
2.38	1999	Jen Fin Lin Yeong Yan Guu	0.3m/s (C)	3 5 10 15	PTFE, MoS ₂ , MoS ₂ + Graphite	Resin (Not specific)	Friction v Load Graphs Friction v Load v Thickness Graphs Wear Coefficients
2.39	1998	D Burke I Sherrington	0.8Hz (R)	1 10	Graphite, MoS ₂ , PTFE	Epoxy, Polyamide-imide	Friction v cycles graphs Images of coatings before and after testing Images of counterface showing transfer films
2.40	1998	W Scheerer F Durr	10mm/s 5mm stroke 0.1Hz (R)	1170N/mm ²	PTFE MoS ₂		Friction v Time & Wear v Time Graphs REM micrographs of finishes and base coating (In German)

No	Year	Authors	Speed/motion	Load Kg	Lubricant coating	Bonding Agent	Results
2.41	1996	J F Carton A B Vannes G Zambelli L Vincent	1 or 5Hz Amplitude $\pm 5\mu\text{m}$ and $\pm 100\mu\text{m}$ (R)	30 to 90	Cadmium PTFE PTFE	None Epoxy Polyimide	Scratch test results Fretting tests of three coatings Polar diagrammes of coating behaviour
2.42	1995	T Shimizu A Iwabuchi H Mifune K Kishi M Arita	25Hz Amplitude 20, 40 & $80\mu\text{m}$ (R)	10^5 Pa 10^{-1} Pa 10^{-5} Pa	$\text{MoS}_2 + \text{Sb}_2\text{O}_3$	Polyamide-imide	Study of film behaviour
2.43	1984	M Kawamura I Aoki K Yoshida	(R)		Graphite	Organic Polymer	Effect of surface finish on camera shutter.
2.44	1977	V Hopkins M Campbell	0.061-0.183m/s (C)	10.34- 41.37MPa	$\text{MoS}_2 + \text{Metal}$ Oxide	PPS	Effects of thickness on wear life of film

b) Pin on Disk

No	Year	Authors	Speed/motion	Load Kg	Lubricant coating	Bonding Agent	Results
2.45	2001	D Burke I Sherrington	0.1, 0.5, 1.0m/s (C)	1 & 10	PTFE + Graphite	Poly amide- imide	Graphs of Friction Coefficient v distance travelled.
2.46	1992	T A Blanchet F E Kennedy	0.2m/s (C)	5.24	PTFE filled and unfilled	None	Friction and wear Graphs for four materials
2.47		R L Fusaro	(C)				Introduction to pin on disk tribometers with instructions for application of solid lubricant films
2.48	1984	M El-Sherbiny			Lead & tin	None	Generation of friction model for solid lubricants including bonded and naturally formed films
2.49	1981	R L Fusaro	1000RPM (2.6m/s) (C)	0.25 to 5.88	Graphite Fluoride	Polyimide	Surface profiles of wear tracks Photomicrographs of rider contact area and disk wear track

No	Year	Authors	Speed/motion	Load Kg	Lubricant coating	Bonding Agent	Results
2.50	1978	Matveesky Lasovaskaya Popov	0.1m/s (C)	0.5	MoS ₂	Polyimide and Silicon	Friction coefficient v cycles
2.51	1978	E Rabinowicz D M Boyd N Ohmae	40RPM (C)	5	MoS ₂ PTFE	Resin	Friction coefficients
2.52	1973	R L Fusaro H E Sliney	2.6m/s (C)	1	Graphite Fluoride MoS ₂ MoS ₂ + Graphite	Polyimide Polyimide Sodium Silicate	Friction Coefficients over a range of temperatures in various atmospheres. Evaluation of polyimide as a stand alone lubricant
2.53	1971	H Gisser M Petronio A Shapiro	1200RPM (C)		Graphite Fluoride Graphite	Silicate Epoxy Phenolic	Variety of test and test regimes
2.54	1969	V Hopkins	0.51m/s (C)	0.6	MoS ₂ + Sb ₂ O ₃	Polyimide	Friction Coefficients

No	Year	Authors	Speed/motion	Load Kg	Lubricant coating	Bonding Agent	Results
2.55	1967	E Rabinowicz	4 – 250RPM (C)	0.1 0.5 1 10	Lead Indium MoS ₂	 Epoxy	Graphs of friction coefficients. Friction coefficient v film thickness for MoS ₂ and Lead film

c) Block on Ring (including LFW 1 and block on shaft testing)

No	Year	Authors	Speed/motion	Load Kg	Lubricant coating	Bonding Agent	Results
2.56	1991	W J Bartz J Xu	500, 1000, 1500, 2000RPM (C)	61.2, 98, 147, 196	MoS ₂ + Graphite + Sb(SbS ₄)	Polybutyl- titanate	Mathematical function for wear behaviour of bonded solid lubricants in the region of stable friction
2.57	1987	W J Bartz J Xu	500, 1000, 1500, 2000RPM (C)	61.2, 98, 147, 196	MoS ₂ + Graphite + Sb(SbS ₄)	Polybutyl- titanate	Detailed friction coefficients and wear life graphs
2.58	1986	W J Bartz J Xu	500, 1000, 1500, 2000RPM (C)	61.2, 98, 147, 196	MoS ₂ + Graphite + Sb(SbS ₄)	Polybutyl- titanate	Stable friction coefficients tabulated
2.43	1984	M Kawamura I Aoki K Yoshida	100 cycles/min (R)	3	PTFE	Polyamide- imide	Effect on wear life of substrate pre- treatment for a carburettor shaft

No	Year	Authors	Speed/motion	Load Kg	Lubricant coating	Bonding Agent	Results
2.59	1984	W J Bartz R Holinski J Xu	500, 1000, 1500, 2000RPM (C)	0 to 150	MoS ₂ + graphite + antimony thioantimonate	Polybutyl- titanate	Graphs of wear life data and thickness v duration
2.60	1978	Y Tsuya M Kitamura	1000RPM (C)	8.9 – 44.5	MoS ₂	Epoxy Resin	Graphs of wear rate, friction coefficient and temperature v contact pressure
2.61	1972	J T Martin C H Baster F Abdulhadi	11m/min, 66m/min, 144m/min (C)	2.27, 4.55, 9, 13.55	MoS ₂ + antimony trioxide Graphite	Epoxy	Shear modulus and wear life data
2.62	1971	R J Benzing V Hopkins M Petronio	72RPM (C)	13.6 - 286	MoS ₂ + Sb ₂ O ₃	Resin	Optimisation study of binder/lubricant/lubricant ratios and thicknesses
2.63	1969	C J Bahun J R Jones	20 – 95 cycles/min 60deg amplitude (R)	1.82 – 9.55	MoS ₂ + Graphite	Phenolic	Latin square approach to statistical analysis of test programme with load, speed and film thickness as variables

d) Falex

No	Year	Authors	Speed/motion	Load Kg	Lubricant coating	Bonding Agent	Results
2.60	1978	Y Tsuya M Kitamura	297RPM	22 - 444	MoS ₂	Sodium silicate + Synthetic mica	Graphs of wear rate, friction coefficient and temperature v sliding velocity
2.44	1977	V Hopkins M Campbell	0.0066 – 0.096m/s	2.22 – 4.44KN	MoS ₂ + Metal Oxide	PPS	Wear life of film to 700 deg K
2.64	1977	B D McConnell C E Snyder J R Strang	290RPM	455	Graphite Fluoride MoS ₂ MoS ₂ + Sb ₂ O ₃	PBI Polyimide Epoxy Phenolic	Comprehensive study of three lubricants in three binders at various mixture ratios. Tables of wear life v film thickness
2.65	1975	M T Lavik R B Hubbell B D McConnell	290RPM	455	MoS ₂ MoS ₂ + Sb ₂ O ₃ or Sb ₂ S ₃	PBI	Graphs of wear life and friction coefficients for each material tested. Some friction data at elevated temperature

No	Year	Authors	Speed/motion	Load Kg	Lubricant coating	Bonding Agent	Results
2.53	1971	H Gisser M Petronio A Shapiro	1200RPM	0 - 456	Graphite Fluoride Graphite	Silicate Epoxy Phenolic	Variety of test and test regimes including grease and additives
2.62	1971	R J Benzing V Hopkins M Petronio		136 - 455	MoS ₂ + Sb ₂ O ₃	Resin	Optimisation study of binder/lubricant/lubricant ratios and thickness
2.54	1969	V Hopkins	0.1m/s	455	MoS ₂ + Sb ₂ O ₃	Polyimide	Friction Coefficients and wear life at various thicknesses. Contact zone stresses
2.66	1967	M Campbell V Hopkins	100RPM	364 455	MoS ₂ + Sb ₂ O ₃	Polyimide	Comparison of 4 blends of lubricant ratio and binder – wear lives for each type at various temperatures.
2.67	1965	S F Calhoun F S Meade G Murphy R L Young			MoS ₂ Graphite Various combinations of above + ten additives	18 resins or resin combinations	Summary of work done over a 12 year period. Tables of friction coefficients failure loads and wear life

e) 4 Ball Tests.

No	Year	Authors	Speed/motion	Load Kg	Lubricant coating	Bonding Agent	Results
2.51	1978	E Rabinowicz D M Boyd N Ohmae	40RPM	5	MoS ₂ PTFE	Resin	Friction coefficients
2.53	1971	H Gisser M Petronio A Shapiro	1200RPM	0 - 456	Graphite Fluoride Graphite	Silicate Epoxy Phenolic	Variety of test and test regimes including grease and additives
2.67	1965	S F Calhoun F S Meade G Murphy R L Young			MoS ₂ Graphite Various combinations of above + ten additives	18 resins or resin combinations	Summary of work done over a 12 year period. Tables of friction coefficients failure loads and wear life

f) Special or Specific application.

No	Year	Authors	Speed/motion	Load Kg	Lubricant coating	Bonding Agent	Results
2.68	1995	T Endo T Iijima Y Kaneko Y Miyakawa M Nishimura	998RPM	10	MoS ₂ + Sb ₂ O ₃ MoS ₂	Polyamide-imide Sodium Silicate	Two roller tests. Graphs of wear life v slip ratio. Friction coefficient v slip ratio
2.69	1978	J N Drozdov V N Puchkov	0.05mm/s	0 to 400	MoS ₂	Epoxy	Reciprocating steel ball on conical or cylindrical mandrel. Determination of bearing capacity of solid lubricant
2.70	1972	V Hopkins H E Sliney	20, 60, 100RPM		Mil-L-8937		MRI journal bearing. Development of predictive model for wear life of film
2.71	2001	M H Zhu Z R Zhou	Amplitudes of ± 2 , 5 and 60 μ m @ 5Hz	30	MoS ₂	Epoxy	Fretting wear tests. Friction coefficient v cycle graphs and fretting logs.
2.72	2003	J Xu M H Zhu Z R Zhou Ph. Kapsa L Vincent	Amplitudes of \pm 10, 20 and 40 μ m @ 10Hz	60	MoS ₂ six types	Epoxy	Fretting wear tests. Friction coefficient v cycle graphs and fretting logs. Effect of substrate and coating thickness.

No	Year	Authors	Speed/motion	Load Kg	Lubricant coating	Bonding Agent	Results
2.73	2003	V Fridrici S Fouvry P Kapsa P Perruchaut	Amplitudes between ± 15 and $\pm 75\mu\text{m}$ @ 5Hz	200 or 300	MoS ₂	Phenolic	Fretting logs. Lifetime prediction by dissipated energy approach.

See also:

No	Year	Test description	Results
2.60	1978	Timkem EFM-111	Wear rates coefficients of friction for MoS ₂ in different binders
2.44	1977	Journal Bearing	MoS ₂ + Metal Oxide tests comparing two other solid lubricants
2.65	1975	Pallet Tester Dual Rub Shoe	Wear life and friction coefficients
2.66	1967	Dual Rub Shoe x 2 (Hohman A-3 & MarkV)	Comparison of 4 blends of lubricant ratio and binder – wear lives for each type at various temperatures.

2.8 Summary.

Table 2.6 demonstrates the complexity of the lubricating performance of solid lubricants, in most of the papers reviewed, the work was undertaken to investigate specific problems with the material or sliding regime. The fact that there is no accurate model for BSLs that can predict the friction coefficient and wear life, compounded with the lack of detailed information that is available in the public domain (40-50 scientific papers over a period of almost 40 years) and the reluctance of the lubricant manufacturers to divulge detailed information about their products reinforced the initial impetus to undertake this project.

The review has provided an insight into the performance of solid lubricant materials and where their use is appropriate i.e. graphite is useless as a lubricant in vacuum and MoS_2 should not be used on metals in humid atmospheres. An understanding of the surface finish and pre-treatment requirements for BSLs and their effect on performance has also been gained. This background information is also necessary to inform the requirements for future test programmes to be undertaken. E.g. have the materials to be investigated been tested before and if so is that test regime relevant to the proposed programme?

With very thin films such as those applied by PVD the coating thickness is ignored and the mechanical properties of the base material and counterface used when modelling the contact geometry to determine friction and wear characteristics. This approach has also been used to predict a friction model for BSLs, this is discussed in the next chapter, and apart from the shear strength of the film the material properties of the lubricant are ignored. With these relatively thick films it is possible that the contact may operate above and/or below the yield pressure of the coating material. The thickness of the film may also have significant effect on the performance, depending on the operating contact of the tribosystem. The literature survey continues in the next chapter where the existing knowledge of models for friction is reviewed.

REFERENCES

- [2.1] "Solid Lubricants". Industrial Lubrication and Tribology. Vol. 47, No 6, 1995, pp.7-18.
- [2.2] Dobson, J. V., "The effect of humidity on brush operation." Elec j. 32, 1935, pp.527-8.
- [2.3] Ramadanoff, D., and Glass, S. W., "High altitude brush problem." Trans of AIEE, 63, 1944, pp.825-9.
- [2.4] Van Brunt, C., and Savage, R. H., "Carbon brush contact films: Part 1." General Electric Review. 47, 1944, pp.16-19.
- [2.5] Savage, R. H., "Graphite lubrication." J. appl. phys, 19, No 1, 1948, pp.1-10.
- [2.6] Savage, R. H., and Schaeffer, D. L., "Vapour lubrication of graphite sliding contacts." J. appl. phys, 27, No 2, 1956 pp.136-8.
- [2.7] Bryant, P. J., Gutsall, P. L., and Taylor, L. H., "Mechanisms of Solid Friction", Elsevier Press. 1964, pp.118-126.
- [2.8] Rowe, G. W., "The friction and strength of clean graphite at high temperatures." Wear, 3, 1960, pp.454-462.
- [2.9] Arnell, R. D., and Teer, D. G., "Lattice parameters of graphite in relation to friction and wear." Nature, 218, 1968, pp.1155-6.
- [2.10] Roselman, I. C., and Tabor, D., "The friction of carbon fibres." J. Phys, D: Appl Phys. 9, 1976, pp.2517-32.
- [2.11] Skinner, J. Ph.D., University of Cambridge, 1971.
- [2.12] Lancaster, J. K., and Pritchard, J. R., "The influence of environment and pressure on the transition to dusting wear of graphite." J. Phys. D Appl Phys, 14, 1981 pp.747-62.
- [2.13] Fusaro, R. L., "Effect of substrate chemical pre-treatment on the tribological properties of graphite films". ASLE 3rd International conf on solid lubrication. pp.1-11. 1984
- [2.14] ASM Handbook, Vol. 18, "Solid Lubricants." 1992, pp.113-122.
- [2.15] Molykote. Dow Corning. 1991.
- [2.16] Buckley, D. H., "Surface effects in adhesion, friction, wear and lubrication." Elsevier, 1981.

- [2.17] Farr, J. P. G., "Molybdenum disulphide in lubrication: A review." *Wear*, 35, 1975, pp.1-22.
- [2.18] Salomon, G., De Gee, A. W. J., Zaat, J. H., "Mechano-chemical factors in MoS₂-lubrication." *Wear*, 7, 1964, pp.87-101.
- [2.19] Palmer, E. B., "Solid film molybdenum disulphide lubricant." *Mater, Design Engineer*, August 1961, pp.122.
- [2.20] Sonntag, A., "The significance of surface finish on friction, wear and lubrication." *Lucerne*, Sept. 1969.
- [2.21] De Gee, A. W. J., Salomon, G., Zaat, J. H., "On the mechanism of MoS₂ film failure in sliding friction." *ASLE trans*, 8, 1965, pp.156-163.
- [2.22] Kay, E., Tech report No 65219, Royal Aircraft Establishment, Oct. 1965.
- [2.23] Holinski, R., and Gansheimer, J., "A study of the lubricating mechanism of Molybdenum disulphide." *Wear*, 19, 1972, pp.329-42.
- [2.24] Roberts, E. W., "Towards an optimised sputtered MoS₂ lubricant film." 20th AMS, NASA conf pub, 2423, 1986, pp.103-119.
- [2.25] Panitz, J. K. G., Pope, L. E., Lyons, J. E., Staley, D. J., "The tribological properties of MoS₂ coatings in vacuum, low relative humidity and high relative humidity environments." *J. Vac. sci. technol. A6* (3) 1988, pp.1166-70.
- [2.26] Cunningham, J. M., Ford, I. J., Ogilvy, J. A., Roberts, E. W., "Interpretation of friction and wear properties of MoS₂ coated steel substrates." *Wear*, 177, 1994, pp.93-100.
- [2.27] Banks, R. E., "Fluorocarbons and their derivatives". Oldbourne Press, London, 1964.
- [2.28] Clauss, F. J., "Solid Lubricants & Self Lubricating Solids." Academic Press, 1972.
- [2.29] Hutchings, I. M., Tribology, "Friction and Wear of Materials." Arnold 1992.
- [2.30] Uchiyama, Y., and Tanaka, K., "Wear laws for Polytetrafluoroethylene." *wear*, 58, 1980, pp.232-235.
- [2.31] Lancaster, J. K., Bramham, R. W., Play, D., Waghorne, R., "Effects of amplitude of oscillation on the wear of dry bearings containing PTFE." *J. of lubrication technology*. Vol. 104, 1982, pp.559-67.
- [2.32] Ratner, S. B., Farberova, I. I., Radyukavich, O. V., Lur'e, E. G., James D. I.,(Ed) "Abrasion of Rubber". McClaren, London, 1967, pp.145.

- [2.33] Briscoe, B. J., Evans, P. D., Lancaster, J. K., "The influence of debris inclusion on abrasive wear relationships of PTFE." *wear*, Vol. 124, No 2, 1988, pp.177-194.
- [2.34] Harrop, R., *Thin Solid Films*, 3 1969 pp109.
- [2.35] Spalvins, T., "Coatings for wear and lubrication." *Thin Solid Films*, 53, 1978, pp.285-300.
- [2.36] *Phosphating and Metal Pre-treatment*. Freeman, D. B., Pub. Woodhead-Faulkner. Cambridge, 1986.
- [2.37] *ASM Handbook. Volume 5. Surface Cleaning, Finishing and Coating*. ASM International. 1994.
- [2.38]. Lin, J.F., and Guu, Y.Y., "Factors affecting the tribological performance of three resin bonded solid film lubricants." *Tribology Transactions*. 42 (3). 1999, pp.601-609.
- [2.39]. Burke, D., Sherrington, I., "Evolution of the Frictional Characteristics of Commercially Available Bonded Solid Lubricants." *Nordtrib '98. Proceedings of the 8th International Conference on Tribology*. pp.383-393.
- [2.40]. Scheerer, W., and Durr, F., *Tribologie von Gleitlacken*. MO "Metalloberfläche Beschichten von Metall und Kunststoff." 52 (8) 1998, pp.640-645. (In German)
- [2.41]. Carton, J. F., Vannes, A. B., Zambelli, G., and Vincent, L., "An investigation of the fretting behaviour of low friction coatings on steel." *Tribology International*. 29(6) 1996, pp.445-455.
- [2.42]. Shimizu, T., Iwabuchi, A., Mifune, H., Kishi, K., and Arita, M., "The frictional properties of spray-bonded $\text{MoS}_2/\text{Sb}_2\text{O}_3$ film under the fretting in vacuum." *Lubrication Engineering*. 51(12) 1995, pp.943-949.
- [2.43]. Kawamura, M., Aoki, I., and Yoshida, K., "Practical applications of bonded solid film lubricants in the commercial field." *ASLE SP 14*, 1984, pp. 114-122.

- [2.44]. Hopkins, V., and Campbell, M. A., "Composite-like solid film lubricant." *Lubrication Engineering* 33(5) 1977, pp.252-257.
- [2.45] Burke, D. Sherrington, I. Roberts, E. W., The influence of counter-face surface finish on the performance of bonded solid lubricant films. *Proceedings of the 2nd World Tribology Congress*. Sept 2001.
- [2.46]. Blanchet, T. A., and Kennedy, F. E., "Sliding wear mechanism of polytetrafluoroethylene (PTFE) and PTFE composites." *Wear* 153 1992, pp.229-243.
- [2.47]. Fusaro, R. L., "How to evaluate solid-lubricant films using a pin-on-disk tribometer." *Lubrication Engineering*. 43(5) 1987, pp.330-338.
- [2.48]. El-Sherbiny, M., "The friction of solid film lubricants: A theoretical approach." *Proceedings of the 3rd international conference on solid lubricants*. ASLE SP 14. 1984, pp.39-48.
- [2.49]. Fusaro, R. L., "Effect of load, area of contact and contact stress on the tribological properties of polyimide bonded graphite fluoride films." *ASME Proceedings of the International conference on wear of materials*. 1981, pp.625-636.
- [2.50]. Matveevsky, R. M., Lazovskaya, O. V., and Popov, S. A., "Temperature stability of Molybdenum disulphide solid lubricant coatings in vacuum." *Proceedings of the 2nd international conference on solid lubricants*. ASLE SP 6 1978, pp.41-44.
- [2.51]. Rabinowicz, E., Boyd, D. M., and Ohmae, N., "Use of Exoelectron emission in the study of solid lubricant failure." *Proceedings of the 2nd international conference on solid lubricants*. ASLE SP 6 1978, pp.9-13.

- [2.52]. Fusaro R L and Sliney H E. "Lubricating characteristics of polyimide bonded graphite fluoride and polyimide thin films." ASLE Transactions. 16(3) 1973, pp.189-196.
- [2.53]. Gisser, H., Petronio, M., and Shapiro, A., "Graphite fluoride as a solid lubricant." Proceedings of the First international conference on solid lubricants ASLE 1971, pp.217-221.
- [2.54]. Hopkins, V., and Campbell, M., "Film thickness effect on the wear life of a bonded solid lubricant film." Lubrication Engineering. 25(15) 1969, pp.15-24.
- [2.55]. Rabinowicz, E., "Variation of friction and wear of solid lubricant films with film thickness." ASLE Transactions 10 1967, pp.1-9.
- [2.56]. Bartz, W. J. and Xu, J., "Wear behaviour and failure mechanism of bonded solid lubricants." Wear. 150 1991, pp.231-246.
- [2.57]. Bartz, W. J., Holinski, R., and Xu, J., "Tribological behaviour of two and three-component bonded solid lubricants." Wear 115 1987, pp.167-184.
- [2.58]. Bartz, W. J., Holinski, R., and Xu, J., "Wear life and frictional behaviour of bonded solid lubricants." Lubrication Engineering. 42(12) 1986, pp.762-769.
- [2.59]. Bartz, W. J., Holinski, R., and Xu, J., "A study on the behaviour of bonded lubricating films containing molybdenum disulphide (MoS_2), graphite and antimony thioantimonate ($\text{Sb}(\text{SbS}_4)$)." Proceedings of the 3rd international conference on solid lubricants. ASLE SP 14. 1984, pp.88-96.
- [2.60]. Tsuya, Y., and Kitamura, M., "Effect of sliding conditions on the wear rate of organic and inorganic bonded solid lubricant films." Proceedings of the 2nd international conference on solid lubricants. ASLE SP 6 1978, pp.85-94.

- [2.61]. Martin, J. T., Balster, C. H., and Abdulhadi, F., "Measurement of shear modulus for solid lubricants: Wear life coefficients for MoS₂ in epoxy resin." Lubrication Engineering. 28 1972, pp.43-47.
- [2.62]. Benzing, R. J., Hopkins, V., and Petronio, M., "Bench test versus machine element test in optimising a solid lubricant film." Proceedings of the First international conference on solid lubricants ASLE (1971) pp.103-115
- [2.63]. Buhan, C. J., and Jones, J. R., "Influence of load, speed, and coating thickness on the wear life of a bonded solid lubricant." Lubrication Engineering. 25(9) 1969, pp.351-355.
- [2.64]. McConnell, B. D., Snyder, C. E., and Strang, J. R., "Analytical evaluation of graphite fluoride and its lubrication performance under heavy loads." Lubrication Engineering 33(4) 1977, pp.184-190.
- [2.65]. Lavik, M. T., Hubbell, R. D., McConnell, B. D., "Oxide interaction-a concept for improved performance with molybdenum disulphide." Lubrication Engineering 31(1) 1975, pp.20-27.
- [2.66]. Campbell, M., and Hopkins, V., "Polyimide bonded solid lubricants." Lubrication Engineering 23(7) 1967, pp.288-294.
- [2.67]. Calhoun, S. F., Meade, F. S., Murphy, G. P., and Young, R. L., "Factors affecting the performance of resin bonded solid film lubricants." Lubrication Engineering 21(3) 1965, pp.97-103.
- [2.68]. Endo, T., Iijima, T., Kaneko, Y., Miyakawa, Y., Nishimura, M., "Tribological characteristics of bonded MoS₂ films in rolling-sliding contact in vacuum." Wear 190, 1995, pp.219-225.

- [2.69]. Drozdov, J. N., and Puchkov, V. N., "The bearing capacity of solid lubricating coatings." Proceedings of the 2nd international conference on solid lubricants. ASLE SP 6, 1978, pp.95-100.
- [2.70]. Hopkins, V., and Lavik, M. T., "Accelerated testing of solid film lubricants. Lubrication Engineering." 28(10) 1972, pp.365-372.
- [2.71]. Zhu, M. H., and Zhou Z. R., "An investigation of molybdenum disulphide bonded solid lubricant coatings in fretting conditions." Surface & Coatings Technology 141, 2001, pp.240-245.
- [2.72]. Xu, J., Zhu, M. H., Zhou, Z. R., Kapsa, Ph., Vincent, L., "An investigation on fretting wear life of bonded solid lubricant coatings in complex conditions." Wear 255, 2003, pp.253-258.
- [2.73]. Fridrici, V., Fouvry, S., Kapsa, P., Perruchaut, P., "Impact of contact size and geometry on the lifetime of a solid lubricant." Wear 255, 2003, pp.875-882.

CHAPTER 3 LITERATURE SURVEY

Models of Friction and theories of surface contact.

A Review.

In this chapter the historical background to the development of theories and models of friction are explored. The modern theories of friction for metals and polymers in contact are well documented in the literature and are not reproduced here, however references are given for the more notable works. Finally the application of these theories to bonded solid lubricants is discussed.

3. Introduction.

Over 500 years ago Leonardo da Vinci (1452-1519) was the first to recognise that the friction force was proportional to the applied load and independent of the nominal area of contact [3.1]. However almost 200 years were to pass before these two laws were proposed by Amontons in 1699 independently of Leonardo da Vinci and it is Amontons who is usually credited with their discovery [3.2]. In 1780 Coulomb added a third law suggesting that friction was independent of velocity [3.3].

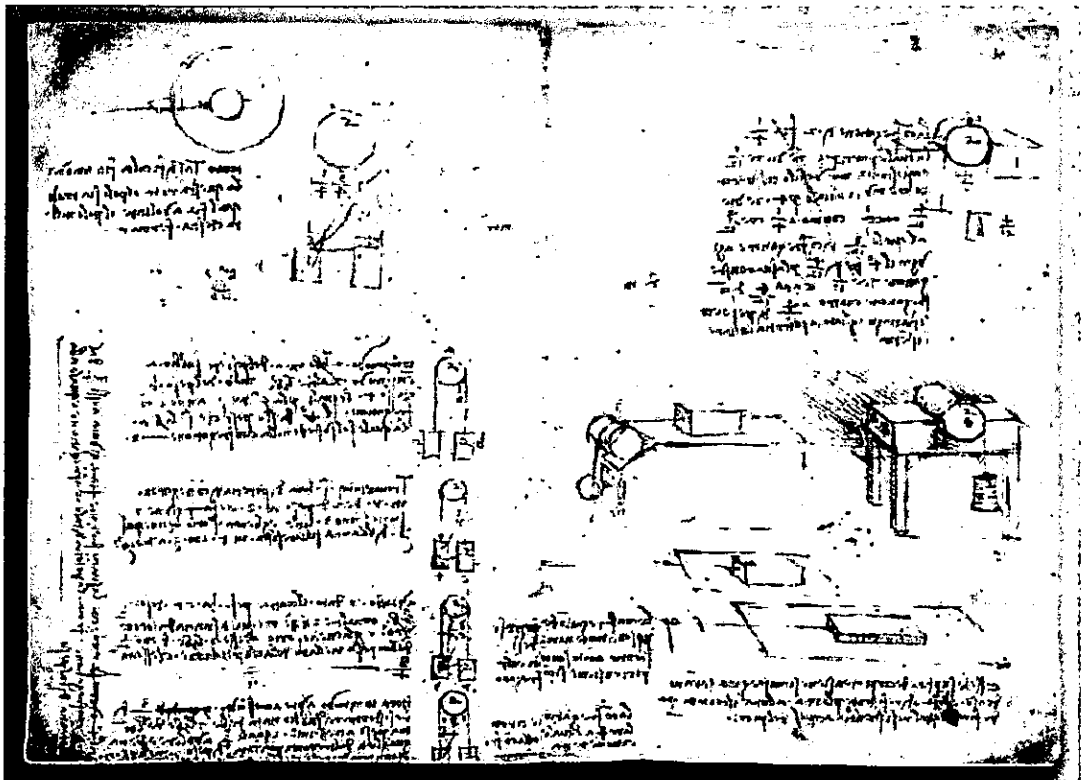


Figure 3.1 Pages from Leonardo da Vinci's notebook, Study of Weights and Friction.

Source – The British Library. www.bl.uk Something for everyone – turn the pages of our great books.

Any study of tribology requires a detailed understanding of the nature of solid surfaces and their contact mechanics, what appears at the macro level to be a single point contact may in real terms have multiple point contacts on the micro scale and indeed very complex multi point contacts on the nano and molecular level. It is the effect of normal and tangential loads on these real areas of contact that we must consider when we study the mechanisms of sliding friction.

When two apparently flat surfaces are brought together under load, some parts of the contact can adhere to each other, this adhesion is one form of surface interaction causing friction. If no adhesion takes place then the alternative interaction which results in resisting motion is one where material must be deformed and displaced.

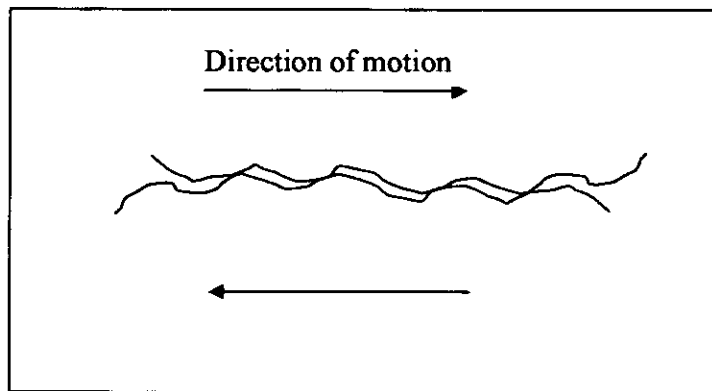


Figure 3.2 Asperity interlocking.

Two types of interaction need to be considered for relative motion to take place, the first shown in figure 3.2 asperity interlocking and in figure 3.3 an example of a displacement type of interaction where a relatively hard sphere is loaded against a soft flat surface. For relative motion to take place some of the material in the soft flat surface must be displaced.

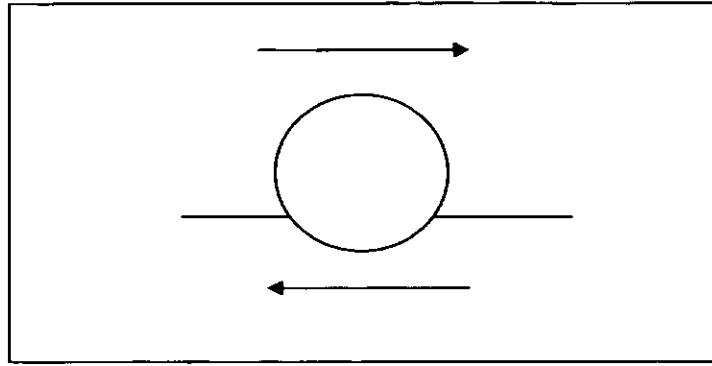


Figure 3.3 Macro displacement.

3.1 General Theories of Friction.

When two surfaces in contact with each other under an applied load slide together with relative motion, energy is lost due to friction, this energy loss can be due to three mechanisms:

- deformation either by plastic deformation or elastic deformation,
- the material may fracture,
- the asperities of the surface and counterface interlock,

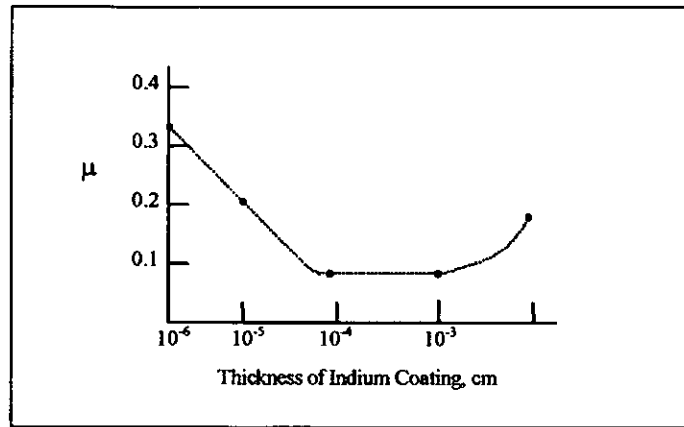
The major component of friction is given by plastic deformation, fracture can occur when adhesion takes place and also when asperities interlock. When elastic deformation takes place in general most of the energy is recoverable. The theories and mechanisms that model these phenomena are well documented in the literature by: Bowden and Tabor [3.4], Buckley [3.5], Halling [3.6], Greene [3.7], Edwards and Halling [3.8], Hutchings [3.9], Black [3.10]

3.2 Friction of Solid Lubricants.

Several attempts have been made to model the frictional behaviour of a soft solid film on a hard substrate during the last fifty or so years with varying amounts of success, it can be seen from the previous sections that the subject is an extremely complex one involving a host of complex interactions caused by the effects of such

parameters as: atmosphere, temperature, surface topography and type of lubricant, to mention but a few.

Some of the early pioneering work of Bowden and Tabor in 1942 [3.11] was with thin metallic films on hard substrates, using electroplated films of indium and lead on hard metals such as tool steel and silver they observed low friction in the film thickness range 10^{-4} to 10^{-3} cm, Figure 3.4.



**Figure 3.4 Friction of steel rider on Indium coated tool steel
flat, Load 4kg, rider dia 0.6cm.**

Adapted from Bowden and Tabor et al [3.11]

This low friction was explained by the expression for the coefficient of friction f ,

$$f = s/p,$$

where s is the shear strength of the material at the interface, and p is the flow pressure of the contacting material next to the interface. For a thin soft film on a hard substrate, s is determined by the soft material and p by the hard material. Rabinowicz in 1967 [3.12] linked the variation in friction and wear of solid lubricant films with film thickness, concentrating on the increase in friction with increase in thickness. Building on Bowden and Tabor's original equation, he developed the following equations:

$$f_{min} = s_s/p_h \quad (1)$$

$$f_{\max} = s_s/p_h \quad (2)$$

where f_{\min} is the low friction coefficient, s_s refers to the shear strength of the soft material and p_h the flow pressure relating to the hard material. The actual friction coefficient f attributed to a junction is given by the linear relationship.

$$f = \frac{\Delta W_{\text{sub}}}{\Delta W} \cdot f_{\min} + \frac{\Delta W_{\text{film}}}{\Delta W} \cdot f_{\max} \quad (3)$$

A typical junction of diameter d_j can be split up into its two components Figure 3.5.

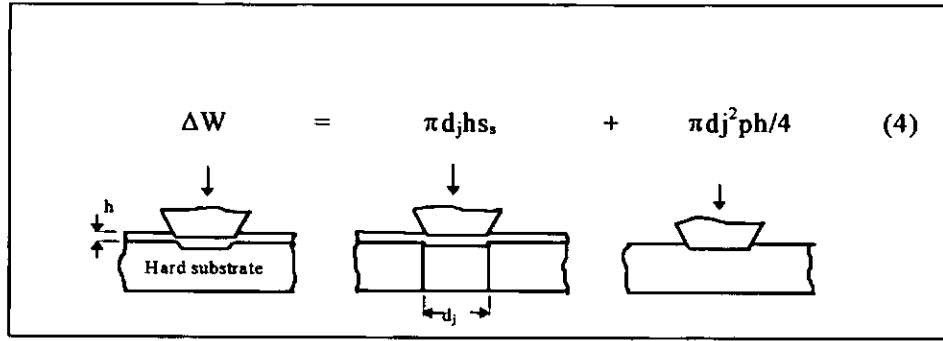


Figure 3.5. Hypothetical model of a junction.

Adapted from Rabinowicz et al [3.12]

In Figure 3.5 $\pi d_j h s_s$ corresponds to ΔW_{film} , and $\pi d_j^2 p_h / 4$ being ΔW_{sub} , then substituting into (3) the following relationship is obtained:

$$f = f_{\min} \frac{1 + 4 f_{\max} \frac{h}{d_j}}{1 + 4 f_{\min} \frac{h}{d_j}} \quad (5)$$

If the junctions in equation (4) cover a range of sizes, then d_j represents a mean value of junction diameter. Equation (5) is plotted in figure 3.9 for a typical case when $f_{\max} = 1$ and $f_{\min} = 0.2$, giving $f = f_{\min}$, when $h = 0$, and $f = f_{\max}$ when $h = 8$. For convenience of comparison between theory and experiment a single point is considered in Figure 3.12, a

particularly simple point is where f is half way between its extreme values, this friction coefficient value is derived from:

$$f_{1/2} = 1/2. (f_{\min} + f_{\max})$$

which if substituted into equation (5) gives the film thickness $h_{1/2}$ for a coefficient of $f_{1/2}$:

$$h_{1/2} = d_j / 4f_{\min}$$

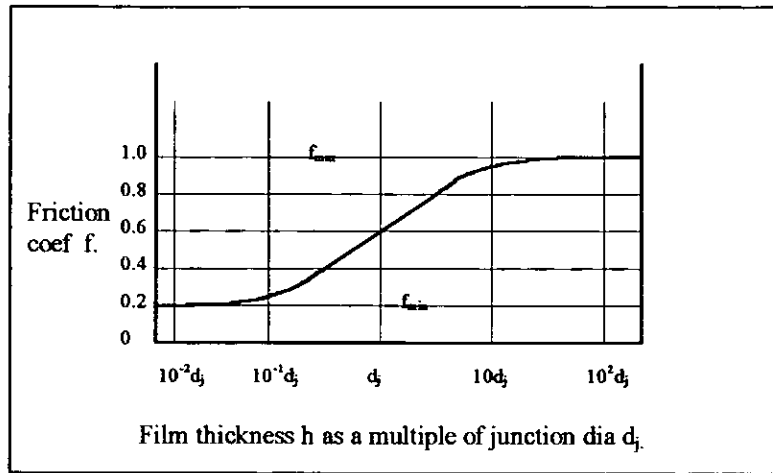


Figure 3.6. Plot of equation (4) for $f_{\max}=1.0$ to $f_{\min}=0.2$.

Adapted from Rabinowicz [3.13]

Rabinowicz also postulated that there is a distinct film thickness above which the film life deteriorates and related this phenomenon to the process of wear particle formation and derived the equation: $h_c = d_L / 3 = 20000W_{ab}/p$ from the general wear particle equation $d_L = 60000W_{ab}/p$ where d_L is the characteristic wear particle diameter, W_{ab} the energy of adhesion between the surfaces, h_c the critical film thickness.

An experimental programme was run using a simple pin on disc machine on several types of lubricant films including MoS_2 bonded in epoxy resin. The findings of this programme were compared, and in general, agreed reasonably well with the theoretical predictions based on the concepts of characteristic junction size and wear particle size.

In a similar paper in 1969, Finkin [3.13] reviewed the effect of film thickness on friction and put forward a theory for the contact situation corresponding to a model of an elastic layer of much less rigidity than the substrate and indenter, corresponding to all naturally occurring and bonded nonmetallic solid lubricant films. He showed that the coefficient of friction f , obeys the relationship:

$$f \propto \sqrt{1/P}$$

for a variable load P and a constant thickness h ,

$$f \propto \sqrt{h}$$

for constant load and variable film thickness, and

$$f \propto \sqrt{h/P}$$

for the general case.

He verified these expressions using data derived from pin on disk tests, Falix tests, 4 Ball tests, modified Macmillan tests, and others, with the materials:

- naturally formed graphite on diamond,
- SiO_2 bonded PbO on stainless steel,
- Phenolic bonded MoS_2 - graphite films on steel and aluminium.

El-Sherbiny in 1984 [3.14] building on the work of Bowden and Tabor, Finkin and Halling [3.15], developed a mathematical model to take account of the effects of film thickness, surface roughness and the material properties of both the film and substrate.

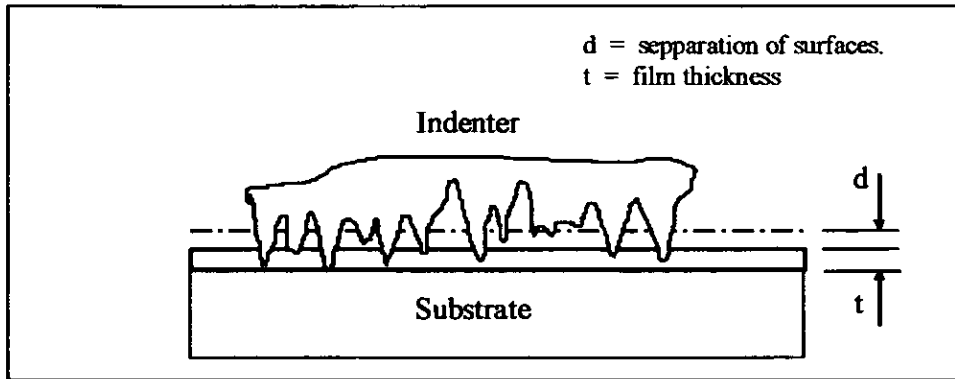


Figure 3.7 Idealized contact model.

Adapted from El-Sherbiny et al [3.14]

The coefficient of friction for the system is expressed as:

$$\mu = \frac{1}{\alpha} \frac{\bar{\lambda} \bar{H} \bar{A} f_s + f_f}{\bar{\lambda} \bar{H} \bar{A} (1 - 2f_s^2)^{\frac{1}{2}} + (p_e^{-2} - f_f^2)^{\frac{1}{2}}}$$

where:- $\bar{\lambda}$ is the dimensionless constant = λ_s/λ_o .

λ is the constant defining deformation mode.

\bar{H} is hardness ratio H_s/H_f .

\bar{A} is the area ratio A_s/A_f .

f is the constant defining shear strength $0 < f < 1$

α is the constant in contact stress.

p_e the mean effective pressure.

Subscripts.

f film.

s substrate.

c film/substrate composite.

An experimental programme was conducted on tin, indium and lead films, formed by ion plating, giving results in agreement with the theoretical predictions. El-Sherbiny also adapted the above theory to give a model for wear of thin films [3.16]. Shou and Arnell

[3.17] in 1987 used a similar model to El-Sherbiny but measured experimentally the shear strength τ , the constant λ where, for purely elastic behavior $\lambda = 1$ and for plastic behavior $\lambda = 2$, and determined the empirical constant K . This information was then used to determine the coefficient of friction and verify the theoretical predictions from the following.

The normal load given by:- $W + A_f H_e + A_f' H_e + A_s H_s$

where the first and second terms represent the loads supported by film in A type and B type contacts, A type contacts being those where the load is carried entirely within the surface film and B type contacts where the load is shared between the surface film and the substrate. The coefficient of friction being given by:

$$\mu = \frac{F_a + F_b}{W}$$

where W = the normal load.
 A = area of contact.
 H = hardness.
 H_e the effective hardness given by $H_e = H_f + (H_s - H_f) \exp(-Kt/\beta)$
 t = film thickness.
 F = friction force

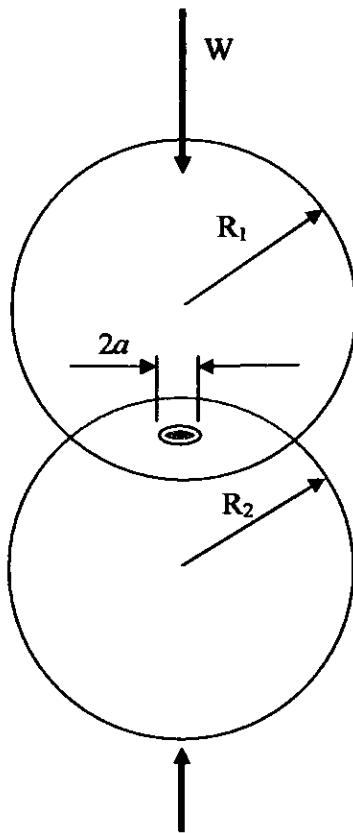
Subscripts

a for A type contacts.
b for B type contacts.
f for film.
s for substrate.

Both soft films on hard substrate and hard films on soft substrate were used in the experimental study correlating with the theoretical predictions, the actual films being lead on mild steel and mild steel on lead.

3.3 Hertzian Contact Theory.

When two spheres are brought gently together, contact will occur initially at only a few points (asperities). As the normal load is increased, the surfaces will move closer together and a larger number of asperities will come together to form a larger area of contact, it is this real area of contact that will support the normal load and be responsible for any frictional forces generated between the two spheres when movement occurs between them. In the case of two spheres a circular area of radius a is given by the elastic contact theory developed by Heinrich Hertz [3.18] in 1882. Where:



$$\text{Contact radius } a = \left(\frac{3WR}{4E^*} \right)^{\frac{1}{3}}$$

Effective curvature

$$\frac{1}{R} = \frac{1}{R_1} + \frac{1}{R_2}$$

Contact Modulus

$$\frac{1}{E^*} = \frac{1-\nu_1^2}{E_1} + \frac{1-\nu_2^2}{E_2}$$

Maximum pressure (Hertz pressure)

$$P_0 = \left(\frac{6WE^*}{\pi^3 R^2} \right)^{\frac{1}{3}}$$

Mean pressure

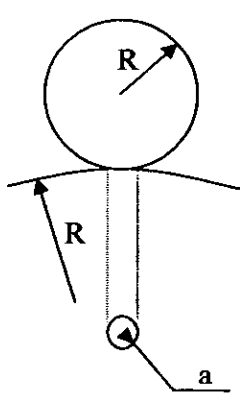
$$P_m = 0.33P_0$$

Where W is the normal load, ν is Poisson's ratio and E^* is the combined elastic modulus of the two materials.

In the case of a sphere in contact with a plane surface i.e. R_2 approaches infinity then $R \approx R_1$.

3.4 Friction theory for spherical contacts and solid films.

BSLs are normally applied to hard substrates and due to the relatively soft nature of these films the contact mechanics at the interface is fairly complex. With very thin films for example less than $2\mu\text{m}$, if the compliance of the film is ignored, then the contact can be modelled as a sphere on a flat plate which has a contact pressure distribution described by Hertzian contact theory. The radius of the contact spot can be calculated from:



$$a = \left(\frac{3WR}{4E^*} \right)^{\frac{1}{3}} \quad (1)$$

$$\text{where } \frac{1}{R} = \frac{1}{R_a} + \frac{1}{R_b}$$

(where a sphere is in contact with a flat surface $R_b = \infty$)

$$\text{and } \frac{1}{E^*} = \frac{(1-\nu^2)}{E_1} + \frac{(1-\nu^2)}{E_2}$$

It is generally accepted for very thin/low shear solid films on hard substrates that the friction coefficient for ball on plate contact follows the equation derived from the above contact theory.

$$F = \mu W \quad (2)$$

$$\text{And } sA_r = \mu W \quad (3)$$

$$\text{Therefore } \mu = \frac{sA_r}{W} \quad (4)$$

Where A_r = the real contact area determined by (1) above.

Substituting for A_r in (4)

$$\mu = \frac{s\pi a^2}{W}$$

$$\mu = \frac{s \left[\pi \left\{ \left(\frac{3WR}{4E^*} \right)^{\frac{1}{3}} \right\}^2 \right]}{W} \quad (5)$$

$$= \frac{s\pi \left(\frac{9W^2 R^2}{16E^{*2}} \right)^{\frac{1}{3}}}{W} = \frac{s\pi \left(\frac{9W^{\frac{2}{3}} R^{\frac{2}{3}}}{16E^{*\frac{2}{3}}} \right)}{W}$$

$$\mu = \frac{s\pi 3R^{\frac{2}{3}}}{W^{\frac{1}{3}} 4E^{*\frac{2}{3}}} \quad (6)$$

where s = shear strength of the softer material, s will be fixed for a particular type of coating material and is determined experimentally or by approximating the combination of the bulk material shear strengths. Singer in 1990 [3.19] demonstrated for thin films of MoS_2 , $\sim 1\mu\text{m}$ thick, that the friction coefficient under elastic contact conditions is controlled by the mechanical contact conditions given by the Hertzian contact pressure and the shear strength of the interface.

3.5 Summary.

Models for friction for coating films from 1942 to 1987 have been reviewed and the Hertzian contact theory and its application to thin coatings explored. With relatively thick coatings, greater than 10 μ m such as bonded solid lubricants the effect of these mechanisms are more complex, asperities on the counterface are initially unable to contact the metal substrate due to the coating, this will depend on the applied load and hence the contact pressure, under these circumstances asperity welding cannot occur and at the onset of sliding the friction will be dependant on the shear strength of the film, the counterface ploughing through the film. A tendency of the solid lubricants in these films to form very strong transfer films ensures that as movement continues sliding occurs between the transfer film and the bulk coating material. At some point in time, this will depend on the contact pressure, metal to metal contact will occur and a wear scar will begin to form on the contact counterface. It is this phenomenon which is explored experimentally in the following chapters:

- Tests will be conducted above and below the yield pressure of the film.
- Empirical models will be developed to describe friction above the yield pressure.
- The mechanism of friction for a sphere sliding on a flat plate will be described in detail.
- The relationship of the Hertzian contact analysis will be established above and below the yield pressure.

Reference

- [3.1] Leonardo da Vinci, Notebooks, Johnathon Cape London 1938.
- [3.2] G Amontons, Hist, Acad. Roy. Sci.(Paris), 1699.
- [3.3] C A Coulomb, Mem. Math. Phys. R.S., 1785
- [3.4] Bowden, F. P. Tabor, D. "The Friction and Lubrication of Solids." Pt II Oxford University Press, 1964.
- [3.5] Buckley, D. H., "Friction, Wear and Lubrication in vacuum." NASA SP-277, 1971.
- [3.6] Halling, J. "Principles of Tribology." Macmillan, 1975.
- [3.7] Greene, A. P. "Friction between unlubricated metals, a theoretical analysis of the junction model". Proc. R. Soc., 228, A, 1955, pp.191
- [3.8] Edwards, C. M., Halling, J., "An analysis of the plastic interaction of surface asperities and its relevance to the value of the coefficient of friction". J. Mech. EGINEERING Sci., 10. 1968, pp.101
- [3.9] I M Hutchings, Tribology. Friction & Wear of Eng, Mat's, pp.25 1992. Edward Arnold.
- [3.10] A J Black Asperity Deformation Models. Proceeds of the I Mech E part C 1993 Vol 207 pp.335-353.
- [3.11] Bowden F P and Tabor D, "The Friction of Thin Films." Bull, 145, Comm. of Australia, Counc. Sci Ind Res, 1942, pp.39-59.
- [3.12] Rabinowicz E, "Variation in friction and wear of solid lubricant films with film thickness." ASLE trans, 10, 1967, pp.1-9.
- [3.13] Finkin E F, "A theory for the effects of film thickness and normal load in the friction of thin films." Trans of the ASME, series F, j. of Lubrication Technology. V91, Pt3, 1969, pp. 551-6.
- [3.14] El-Sherbiny M, " The friction of solid lubricants: A theoretical approach." ASLE, sp, 14, 1984, pp. 39-48.
- [3.15] Halling J, and El-Sherbiny M, "Friction of Soft Metallic Films", Imech E. 1978 pp. 155-158.
- [3.16] El-Sherbiny M and Salem F, " A wear equation for solid lubricant films." ASLE, sp, 14, 1984, pp. 44-49.

- [3.17] Shou F and Arnell R D, "Empirical validation of a predictive model for the friction coefficients of coated surfaces." Proc of the IMechE, 1987, Intl conf. "50 Years On" Vol. 2, C217/87, pp. 657-63.
- [3.18] Johnson, K. L. "Contact Mechanics." Cambridge University Press, 1985.
- [3.19] Singer, I.L., Bolster, R. N., Wegand, J., Fayeulle, S., Stupp, B. C., "Hertzian stress contribution to low friction behaviour of thin MoS₂ coatings." Appl. Phys. Lett. 57. (10) 1990. pp. 995-997.

CHAPTER 4.

INITIAL PERFORMANCE COMPARISON & NEW MACHINE DESIGN.

The first half of this chapter describes the modifications required to an existing reciprocating test apparatus to allow it to accommodate test samples that were produced from commercial components. It also describes the test programme for the comparison of some of the bonded solid lubricants commercially available. The performance limitations of the test apparatus are outlined and design of a new test facility is justified.

The latter half of the chapter describes in detail the design of the new test apparatus developed to overcome the limitations of the previous one. The main drive and electronic control system specification is discussed along with the data acquisition package, measurement of the friction force, temperature, humidity and the power supply arrangements to these devices also the commissioning and calibration details.

4.1. INITIAL PERFORMANCE COMPARISON.

4.1.1. *Introduction.*

Today there are many suppliers of bonded solid lubricants, each supplier having a fairly extensive product range utilising either one or more of the previously mentioned solid lubricants, on their own or in combination, using one of several binding agents. To obtain a comparison in performance between some of these commercially available materials, twelve were selected for test on a simple reciprocating apparatus. The materials tested are listed in Table 4.1. The materials were chosen because they had already been tested in a commercial product and had demonstrated variations in performance with extensive data being recorded for each. The components used for the test programme were selected from commercially produced components used in the manufacture of an automotive seat belt buckle. A reciprocating test apparatus was employed in testing as its operational action matched that of the product to be tested. The investigation also allowed familiarization with the important design and operational criteria in the use of tribological apparatus for experimentation and more importantly generated some initial information from a standardized test regime about:

- a) static coefficient of friction,
- b) dynamic coefficient of friction,
- c) electrical resistance,
- d) ambient temperature,
- e) specimen bulk temperature,
- f) humidity.

Sample	Material	Binder	μ^*
1 (I)	Mos ₂ +Graphite+ZnPh	Polyamide-imide	N/A
2 (II)	Mos ₂ +Graphite+ZnPh	Polyamide-imide	N/A
3 (III)	PTFE	Polyamide-imide	N/A
4 (IV)	PTFE	Polyamide-imide	0.06
5 (V)	PTFE	Epoxy	0.06
6 (VI)	Graphite 12 μ m	Epoxy	0.06
7 (VII)	Graphite 21 μ m	Epoxy	N/A
8 (VIII)	PTFE+ Graphite 16 μ m	Polyamide-imide	N/A
9 (IX)	PTFE+Graphite 20 μ m	Polyamide-imide	N/A
10 (X)	MoS ₂	Epoxy Phenolic	N/A
11 (XI)	Mos ₂ + Graphite	Epoxy	0.03 – 0.08
12 (XII)	Mos ₂ +Graphite	Epoxy	0.03 – 0.08

μ^* given by manufacturers. N/A none specified.

Table 4.1 Bonded Solid lubricants for comparison testing.

4.1.2 Test Equipment.

The utilisation of an existing reciprocating apparatus, with some minor modifications to the work holder and reciprocating platen, allowed the test programme to be conducted. (Modifications are detailed in Appendix A1.) The test apparatus consisted of a variable speed electric motor driving a reciprocating platform through a “Scotch Yoke” mechanism, the stroke length being adjustable by moving the driving pin and bush to a suitably positioned hole on the drive disk. The minimum stroke obtainable was 20mm and the maximum 80mm. The variable speed motor allowed speeds as low as a few cycles per minute to over 100 cycles per minute.

The measurement of the friction force and the application of the test loads was accommodated by means of a beam pivoted at the centre with a loading mechanism at one end and the work holder at the other as shown in Figure 4.1. Strain gauges were mounted midway between the pivot and the work piece holder, one gauge either side of the beam and two more gauges were mounted on a block of the same type of material as the beam, this was conveniently located on top of the pivot housing. The gauges were wired to form a full temperature compensated Wheatstone bridge circuit. The beam was calibrated by suspending weights over a pulley system attached to the upper work holder as Figure 4.3 taking readings from 0kg – 10kg and back in 1kg steps.

The specimen temperature was measured by means of two K type thermocouples one mounted in a two millimetre diameter hole in the lower specimen the other being attached to the outside of the test rig. Both thermocouple tips were electrically insulated by applying a thin coat of epoxy resin. Ambient temperature and ambient humidity were measured using the commercial temperature and humidity sensor described later in section 4.2.8 and appendix A4. Electrical resistance measurement was accomplished by the lower work holder being electrically insulated from the main frame by a PTFE plastic strip and being secured by nylon screws as shown in Figure 4.2, the upper work holder was insulated from the beam by similar means. The lower and upper work holders formed one of the resistor arms of a potential divider as shown in Figure 4.4 to allow resistance to be measured. Figure 4.5 is a digital photograph of the test rig with the main features highlighted.

During testing it was necessary to know the exact point on the counterfaces where the friction measurements were to be taken in order to provide a trigger point for the data acquisition package to start and stop recording the data, this was accomplished by the attachment of a digital linear transducer between the reciprocating platform and the main frame of the machine. Data acquisition from all the transducers was accommodated by use of a PC installed with an early version of “Lab Windows” software with the data being saved as text files. The use of the PC and installation of a low voltage mains relay in the motor power supply allowed the rig to be run automatically.

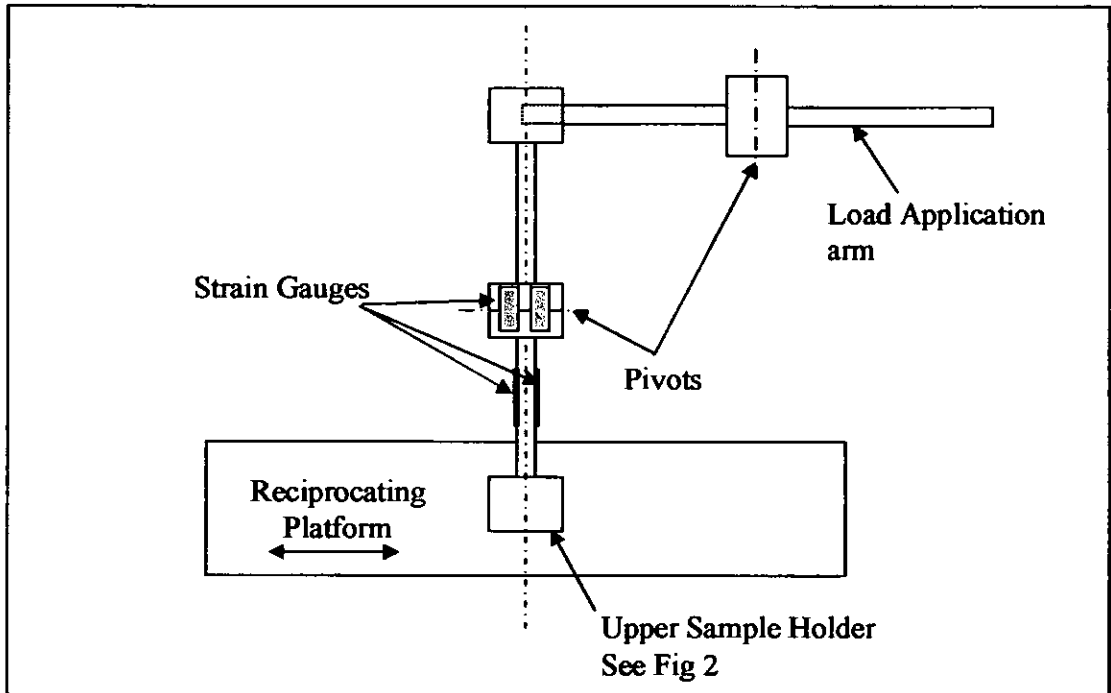


Figure 4.1. Test Apparatus Schematic.

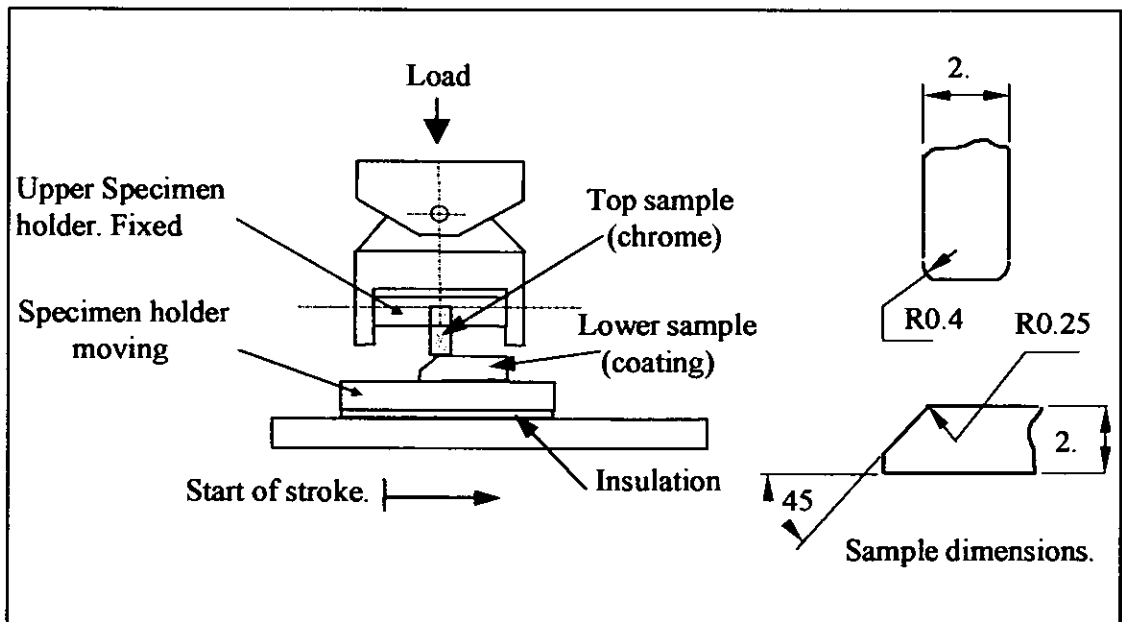


Figure 4.2. Test set up

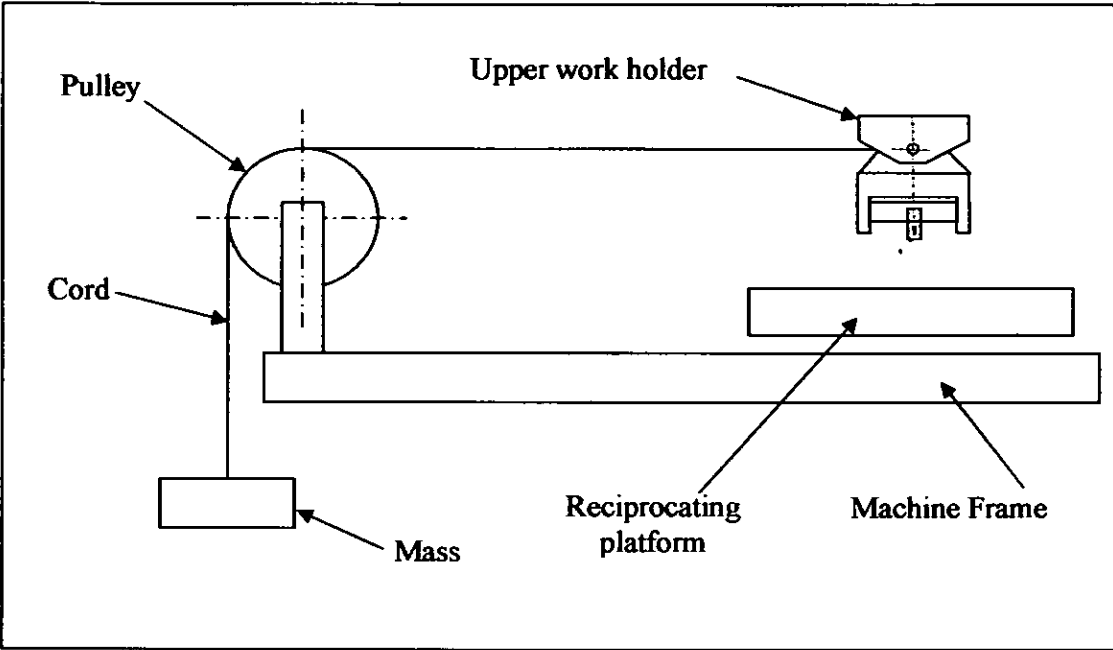


Figure 4.3. Calibration Method.

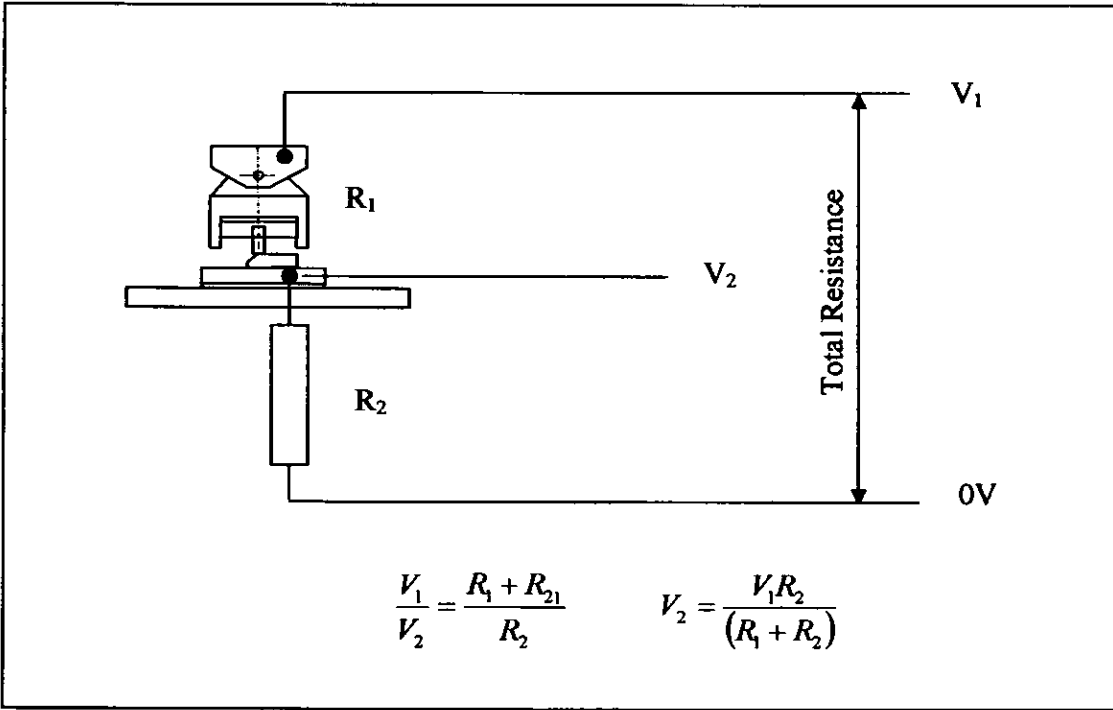


Figure 4.4. Resistance measurement schematic.

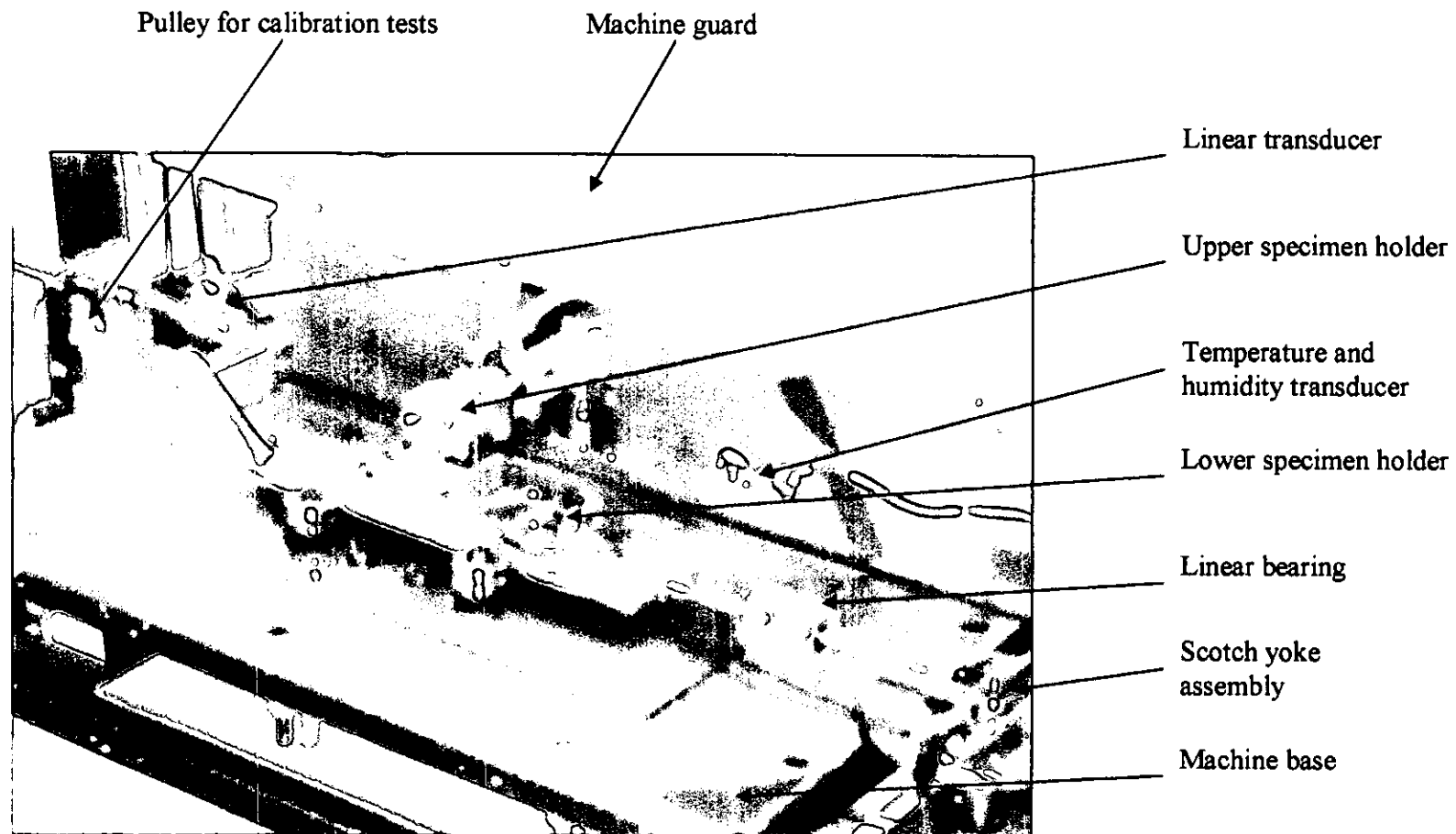


Figure 4.5. Reciprocating Test Rig.

4.1.3. Materials and Methods.

The components to be used were produced by a commercial process¹ consisting of: vapour degreasing process followed by a grain refining wash to help produce a fine uniform phosphate layer, then deposition of manganese iron phosphate² by immersion in a phosphating bath for a set period of time to provide a “Key” for the final coating of bonded lubricant³, which was applied by spraying. The component was then heated to remove most of the solvent and cured at elevated temperature. The base material of the component was CS40 steel, heat treated to 35- 45 HRC then “barrelled” with an abrasive media to remove any burrs and oxide layer. The material sliding against the bonded lubricant was again obtained from a commercial product, test pieces being cut from a specific area of the product to provide suitably sized specimens. This donor product was produced from CS60 steel, heat treated to 45-48 HRC followed by barrelling then electroplating; first with copper then by nickel and then chromium to provide a decorative finish. The material specification for both counterfaces is given in Table 4.2 and thickness of the plated layers in Table 4.3.

	C	Mn	Si	Cr	Ph	S
CS40	0.4-0.45	0.7-0.9	0.15-0.35	-	0.02max	0.01max
CS60	0.6-0.65	0.7-0.9	0.15-0.35	0.20-0.30	0.015max	0.01max

Table 4.2. Sample Materials. (% of element content in steel)

Material	Copper	Nickel	Chromium
Thickness μm	0.5 minimum	8.0 minimum	0.13 minimum

Table 4.3. Electroplating Thickness.

¹ Armourcote Surface treatments Ltd, Long Causeway, Cross Green, Leeds. LS9 0NY

² XYLAN 1053, Whitford Plastics Ltd, 10 Christleton Court, Manor Park, Runcorn, Cheshire. WA7 1ST

³ Chemetall PLC. Performance Products Division, Bletchley, Milton Keynes. MK1 1PB

A test run was conducted with the samples mounted as shown in Figure 4.2. A Piezo accelerometer was mounted on top of the upper work holder to measure the vertical acceleration. A mechanical stop was provided to prevent the beam from dropping too far down when the upper specimen was clear of the lower specimen, this was adjusted to give approximately 0.25mm interference of the upper specimen with the lower specimen in the vertical plane. Weights were applied to the load application arm to give a 10N and 100N load respectively at the upper specimen holder, this was checked with a digital force gauge by lifting the specimen holder until the specimen was just clear of the lower specimen and a reading of 10N obtained. (This was conducted before the start of each test with actual readings recorded of 9.8N for 10N loads and 99.85N for the 100N tests.) Several test runs were made at various speeds to determine the vertical acceleration and ensure that there was no vertical bounce or vibration that could affect the friction force measurement. A speed of 48 cycles per minute gave satisfactory performance.

Tests were conducted with 10N and 100N normal loads at a cycling speed of 48 cycles per minute for a duration of 50,000 cycles. Measurements were taken of: friction force, electrical resistance, ambient temperature, ambient humidity and specimen bulk temperature, every 10th cycle for the first 200 cycles then every 200th cycle thereafter.

4.1.4. Results.

During the test programme and analysis of the early results it was noticed that the load beam stiffness and damping was insufficient to prevent uncontrolled oscillation of the specimen. This was determined by producing a video of a test while running, with a high speed video camera, equivalent to 1000 frames/second, which was normally used by Breed Technology Limited for analysis of seat belt testing during simulated vehicle crash tests. This video confirmed the uncontrolled oscillation and the cause, the top specimen riding on and off the bottom specimen, it also showed that the oscillation was continuous during the whole of the testing, this oscillation corresponded to the fluctuations in the trace obtained for the friction force shown in Figure 4.6. A low pass Butterworth filter with a cut off of 30 Hz was used to filter all the friction force results. The maximum dynamic friction force as a function of number of cycles was derived from these filtered

results. (Note, the location of the friction force measurement is not necessary at a fixed point in the stroke due to the variation of the peaks of the oscillations, sometimes peaking at the end of the stroke as in Figure 4.6 sometimes towards the centre and sometimes towards the beginning.) A summary of the friction force measurements obtained for the 10N load are illustrated in Figures 4.7 & 4.8. (Note, it was not possible to determine the static coefficient of friction due to this uncontrolled oscillation of the beam. The oscillation may also have influenced the results in that it provided a more severe or different test regime than was intended the horizontal vibration reducing adhesive “sticking”).)

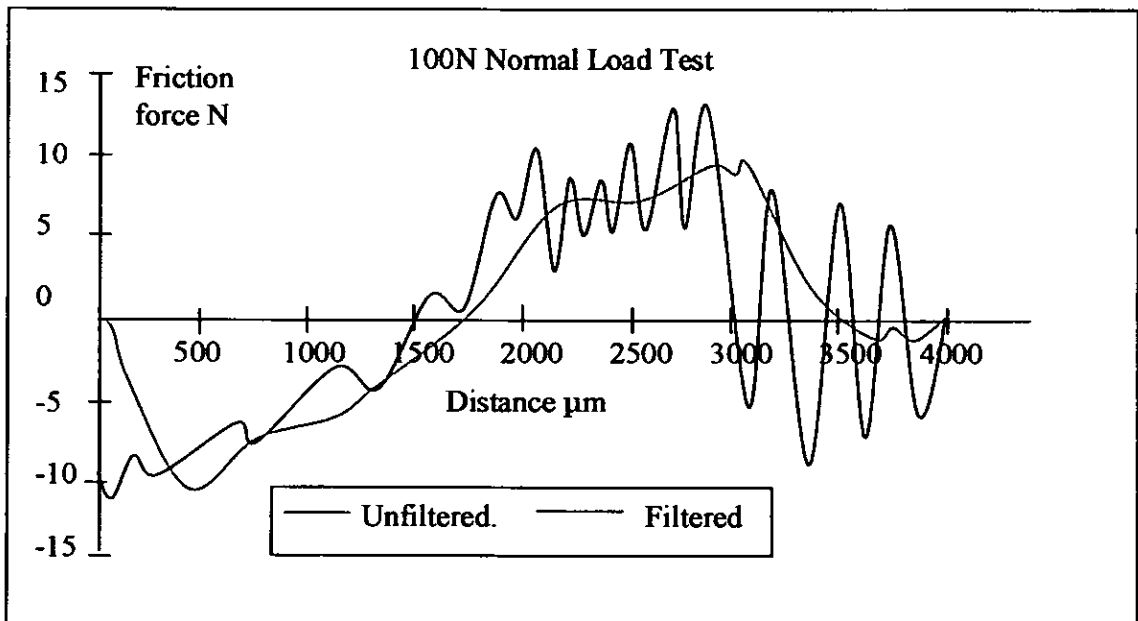


Figure 4.6. Filtered / Unfiltered Comparison.

Figures 4.9 and 4.10 illustrate the average electrical resistance between the counterfaces as a function of the number of cycles. This measurement was made over a variable length of stroke towards the zero velocity end where the stress at the contact was lower. Similar data is plotted for six of the 100N tests in Figures 4.11 and 4.12. Figure 4.13 contains the typical ambient temperature, specimen temperature and ambient humidity curves vs. number of cycles for the series of tests. No significant temperature rise was observed in the specimens during each of the tests. Two further tests were conducted

with a sample with no coating at all and a sample with only the phosphate coating. The friction curves for these two tests are shown in Figure 4.14 and the electrical resistance in Figure 4.15, a digital image of the surface is shown in Figure 4.27. Figure 4.16 shows the friction force for the second batch of 100N tests.

4.1.5. Discussion.

All the sample surfaces were examined under a microscope before and after cycling and a digitised image produced of the surfaces, these are shown in Figures 4.19, 4.20, 4.21 and 4.22 for the 10N loads and Figures 4.23, 4.24, 4.25, and 4.26 for the 100N loads. The images show (a) the unworn coatings, (b) the worn coatings and (c) the worn counterfaces. These images show that before cycling the coatings have asperities of differing sizes and texture, some appear “granular” while others appear to have “flowed” and have a “spattered” appearance. Also apparent are defects such as small cracks, probably due to the curing process. After cycling the topography of the counterface is such that it contains unidirectional scratches. Some scratching appears to be more aggressive on certain samples and some samples appear to contain craters in which wear particles accumulate. The chrome plated specimen is displayed as the far right hand illustration with the leading edge to the right. In all cases they appear to acquire a “transfer” film which rubbed off easily on samples 3 & 4 and on samples 8 & 9 appeared to be mechanically or chemically attached.

Samples 3 & 4 (PTFE/Polyamide-imide binder) in the 10N load tests exhibited the lowest coefficient of friction over the test duration, sample 5 (PTFE/Epoxy binder) was in the same range with the epoxy binder apparently having little effect on performance. Samples 8 and 9 (Graphite/PTFE polyamide-imide binder) starts with a friction coefficient of 0.06. These increase to 0.24 and 0.17 over the first 500 cycles then, for sample 8, to 0.3 over the next 2000 cycles with sample 9 showing a gradual increase to 0.22 over some 20,000 cycles. It should be noted that samples 8 and 9 are the same material the only difference being the initial coating thickness, of which the thicker sample exhibits the lower friction coefficient and more stable performance. Samples 1, 2 and 11 start with a friction coefficient of 0.05 – 0.08 and rise to their limiting coefficient.

Samples 2 and 11 over 200 cycles and sample 1 over 12000 cycles. Sample 12 “beds in” over 2000-3000 cycles then ramps up to its limiting friction coefficient. This test was stopped for a period of one hour at about 25000 cycles and on restart appeared to repeat this phenomenon. It is thought this effect could be due to water vapour from the atmosphere having an effect while the components were at rest, the phenomenon is well documented and was previously observed by Saloman, De Gee and Zaat [4.1]. Sample 10 was the only sample to contain the lubricant MoS₂ on its own and there is nothing very similar to compare its performance directly with, but against samples 1, 2, 11 and 12 it has a higher friction coefficient after 2000 cycles and is similar to sample 2. Samples 6 and 7 have similar trends but again like samples 8 and 9 the friction coefficient varies with initial film thickness, only this time the lower coefficient belonging to the thinner of the two.

Twelve of these materials were tested with a 100N normal load, in the first batch of six tests, sample 1 “bedding in” over 700 cycles then rapidly ramping up to a friction coefficient over 0.3, at which point the test was stopped. Samples 7, 9 and 11 gave the best performance with the friction coefficient ranging from 0.05 to 0.08 with little deterioration over the cycling period. Samples 4 and 10 started with a friction coefficient of 0.08 and 0.05 and gradually deteriorated to 0.2 and 0.15. During the testing of the second batch of tests, samples 2, 5, 6, and 8 exhibited evidence of the upper specimen holder having moved during testing, illustrated by the ramp up in friction force followed by a rapid fall off for sample 5, and gradual decrease for samples 2, 6 and 8, whereas sample 12 followed a similar pattern to samples 7, 9 and 11 in the previous tests. Sample 12 is probably the only test measurement at 100N in this batch that is entirely satisfactory due to the movement of the upper specimen holder. It should be noted that the test were not conducted in numerical order and it is feasible that the movement (albeit some movement occurred during all the high load tests due to the lack of rigidity of the apparatus, but after this test the upper specimen holder slipped on the clamping screws and assumed a new position,) occurred after sample 12 was tested (sample 12 being the first test in this group). Also the data for sample 3 became corrupted during processing and was subsequently lost. The movement presented the upper specimen at a more acute

angle to the lower specimen, contact in this instance being made only by the edge of the specimen opposed to the full face in the previous tests. This twist increased contact pressure and although at first it was thought that the data from these tests would be of little use in the investigation it does demonstrate that even under such an aggressive contact regime, solid lubricants can still be effective, achieving a friction coefficient approximately one third of that of samples with no lubrication. The digitised images of the surfaces obtained after testing, Figures 4.25 and 4.26, demonstrate a totally different condition from the previous images in that the lubricant has been almost totally removed from the surface with heavy scratching evident on all samples. The counterface surfaces shown on the far right again show heavy scratching with the chrome plating being worn away in the main contact area also deposits of lubricant can be seen behind this worn area.

During the 10N tests electrical resistance curves for samples 2, 6, 7, 8, 9 and 11 showed very low resistance throughout the test and this is probably indicative of the high amount of graphite present. Sample 1 and 12 start with high resistance levels but rapidly drop over 2500 cycles to a fairly stable level possibly indicating the contribution of the graphite content and metallic contact as the film begins to wear, that is, the epoxy and MoS₂ gave high electrical resistance initially but as the film began to wear the graphite and metallic contact provided a lower resistance path as it became exposed. Sample 10 is similar to 1 and 12, but its performance is more erratic towards the end of the cycling suggesting the wear debris and transfer film building up on the counterface increasing the resistance, then breaking down giving a lower resistance. Samples 3 and 5 showed high resistance at the start then fluctuated between high and low resistance, possibly as small areas of the coating were broken through allowing metallic contact and then repeatedly becoming re-covered with a transfer film. Sample 4 starts with high resistance and then after 15000 cycles gradually reduces, possible due to asperities of the metal substrate being exposed as the deep scratches developed through the coating.

It can be seen that in the low load tests none of the friction coefficients measured matched those claimed by the manufacturers, although sample 3 was very close for a

period with a coefficient of 0.075. In general, it is believed that the friction coefficients differ from those quoted because the test conditions employed by the manufacturers differ radically from those described here. (Only samples 11 and 12 have clearly defined test conditions published by the manufacturer [4.2] to the author's knowledge. In the high load tests samples 7 and 9 had friction coefficients fairly close to those quoted by the manufacturer.

Although the data collected was obtained from only one test of each material and consequently may not be fully representative of their performance, it does highlight several points for future study:

- Friction coefficients measured are in general higher than those stated by the manufacturers, possibly due to the method of test and the mode of operation i.e. the components being separated at the end of each stroke.
- On some tests the friction coefficient reduced as load increased, this is well documented in the literature for solid lubricants such as MoS₂, PTFE and Graphite.
- In severe wear regimes solid lubricants may still be effective in providing lubrication and preventing seizure of the components.
- Sample 1 and 10 in the 100N load test show a fall in resistance as friction increases, sample 1 testing was stopped at 1600 cycles due to the complete breakdown of the film.
- Apart from sample 1 and 10 there appears to be little or no correlation of the friction curves with resistance measurements, with the exception of samples 2, 6, 7, 8 and 9, all the samples, electrical resistance appears to be more related to the film wear and metallic contact being made. The digital images show little evidence of this although sample 5 shows polished metal towards the right hand side. It is possible that metallic contact was made through the deep scratches evident on most of the samples.
- Samples 2, 6, 7, 8 and 9, which all contain large proportions of graphite exhibit a very low electrical resistance throughout the tests.

The average friction coefficients are shown in figure 4.17, from this a ranking of the friction performance of the BSLs can be generated and is shown in table 4.4. Figure 4.18 shows the maximum and minimum levels of electrical resistance reached by each BSL during testing.

	10N Load Tests	100N Load tests
Lowest coefficient	3	9
	4	7
	5	5*
	12	2*
	9	11
	11	8*
	1	10
	6	6*
	8	4
	2	12
	7	1 test stopped at 1600
Highest coefficient	10	3 data lost

* data from second batch of tests.

Table 4.4 Ranking of BSLs lowest to highest friction coefficient.

In the seat belt application that this lubricant was to be used it was important to have a low friction coefficient at both high and low load conditions. For the majority of the life of the buckle it is cycled at a load of 10N, only after an impact is the buckle subjected to a high load, it is critical at this point that the friction coefficient is also as low as possible. From examination of the graphical data for the 100N tests and reference to the ranking table above, three of the lubricants tested would be suitable, samples 7, 9 and 11, 7 was discounted due to the high friction coefficient demonstrated at 10N load i.e. 0.35, leaving sample 9 and 11 with comparable performances. Sample 11 was discounted due to the possible effects that water vapour has on MoS₂ previously described in Chapter 2.

4.1.6. Summary.

The test programme produced a valuable insight into the performance of several types of bonded solid lubricants and the use of tribological test equipment. It also provided sufficient evidence to justify the change of coating used in the seat belt buckle to that used in sample 9. Subsequent testing in complete buckle assemblies demonstrated a significant improvement in the release performance (measurement of the force to release the buckle and tongue when under 300N & 500N tension) both before and after environmental testing.

During the performance of this test programme several observations were made on the performance of the test equipment being used:

- Uncontrolled oscillation of the measuring beam complicated the analysis of the results.
- The method of applying the normal load was cumbersome and it was difficult to match the desired loads due to friction losses in the pivot of the system.
- The safety guarding of the machine did not allow easy observation of the test in progress.
- The AC drive motor vibration was transmitted through the frame and although discernable to the touch was not recorded by the load measurement beam possibly due to the insensitivity of the strain gauges and data collection method.
- The design of the specimen holder clamping was not robust enough during the 100N load tests to withstand the intermittent shocks applied when the components separated and came back together. This may have added another variable to the test, the twisting of the specimen holder which eventually slipped to a position that altered the presentation angle of the upper specimen to the lower specimen.

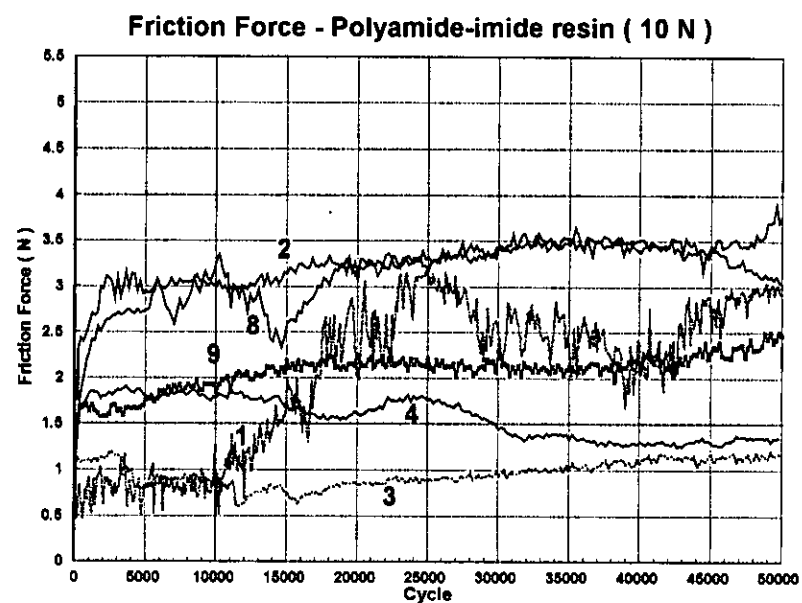
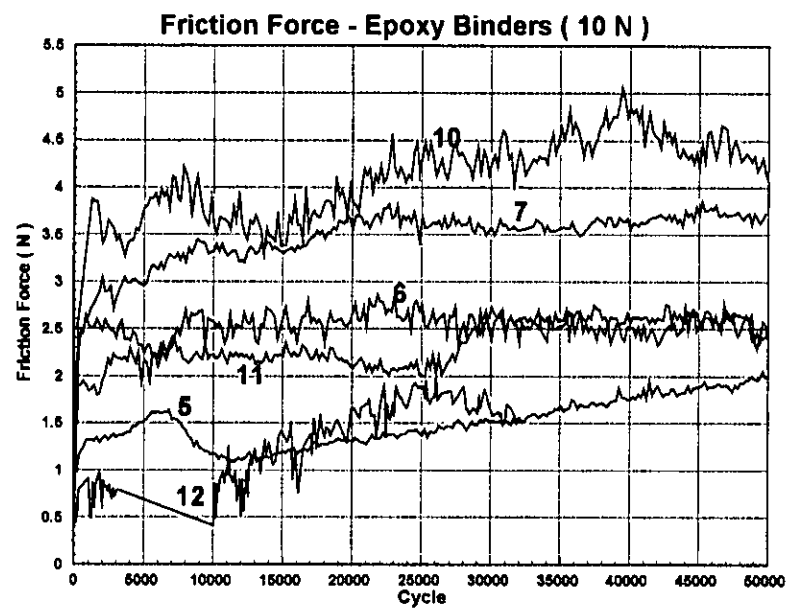


Figure 4.7 & 4.8. Friction forces 10N load tests

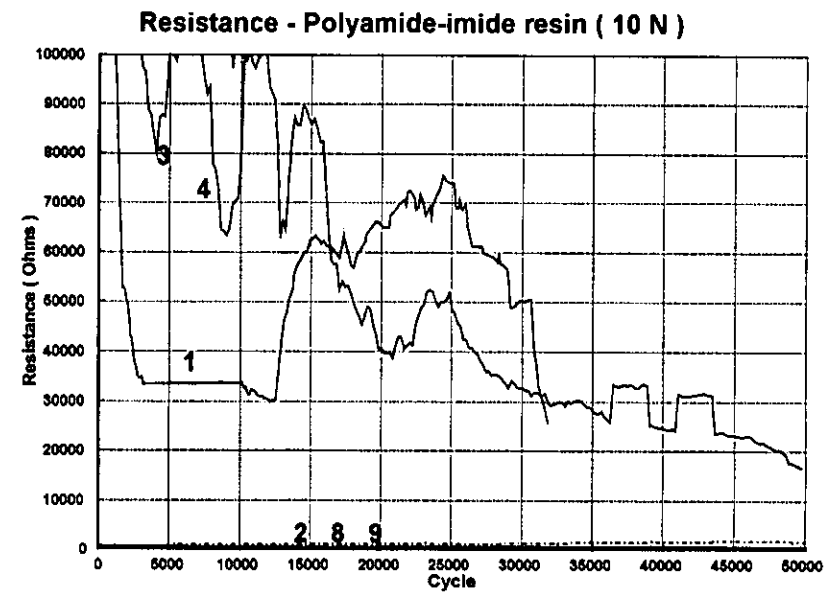
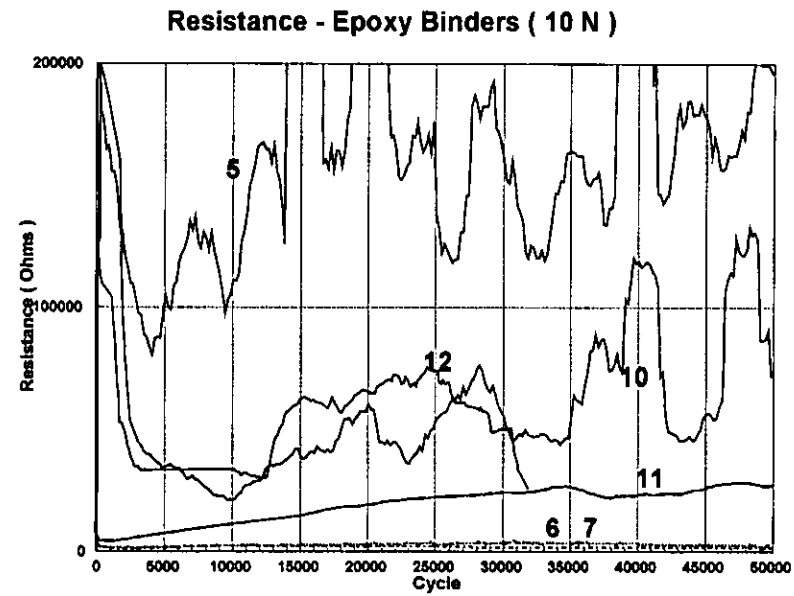


Figure 4.9 & 4.10 Electrical Resistance in 10N load tests

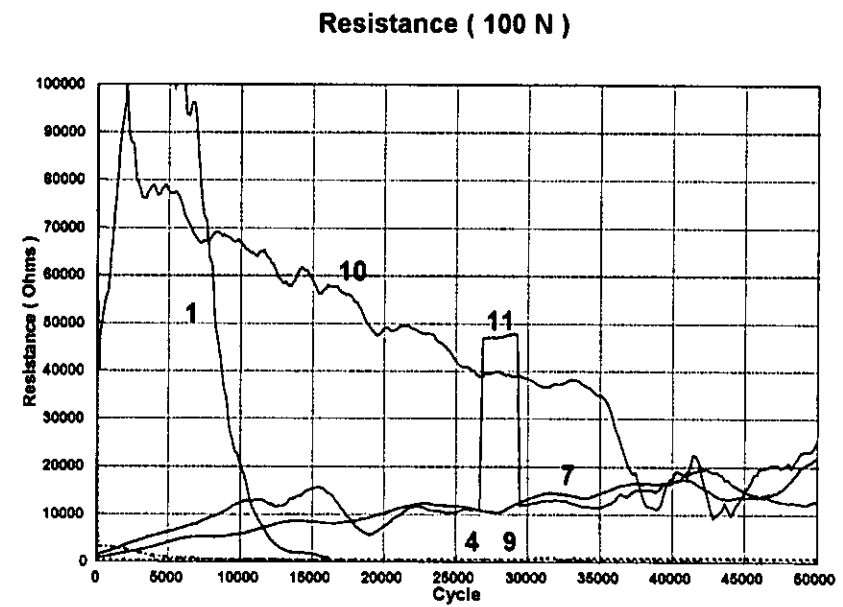
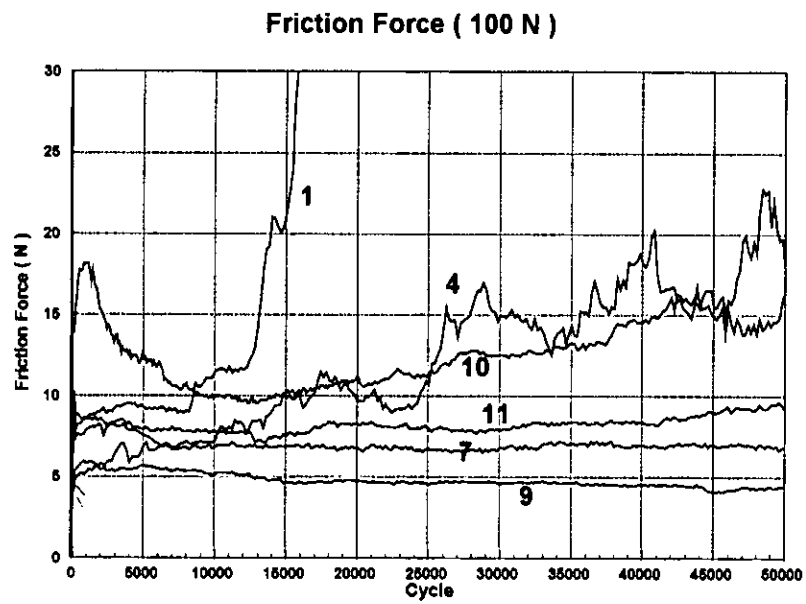


Figure 4.11 & 4.12 friction force and resistance 100N load tests (first 6 tests)

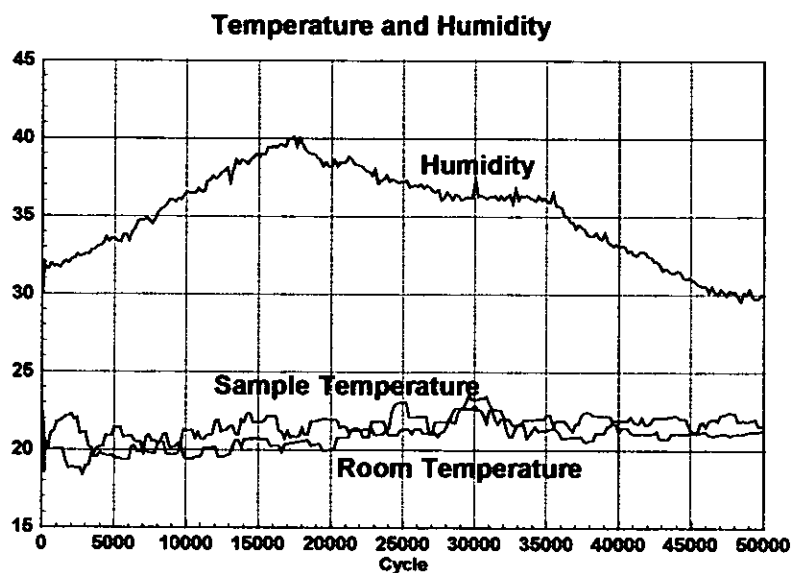


Figure 4.13 Typical temperature and humidity curves.

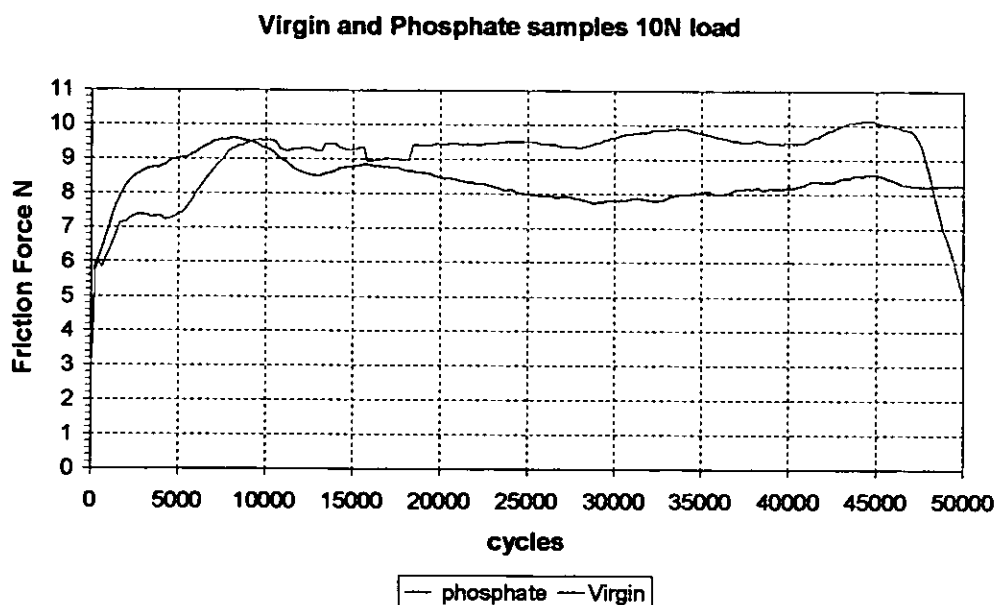


Figure 4.14 Friction forces in 10N load virgin and phosphate samples

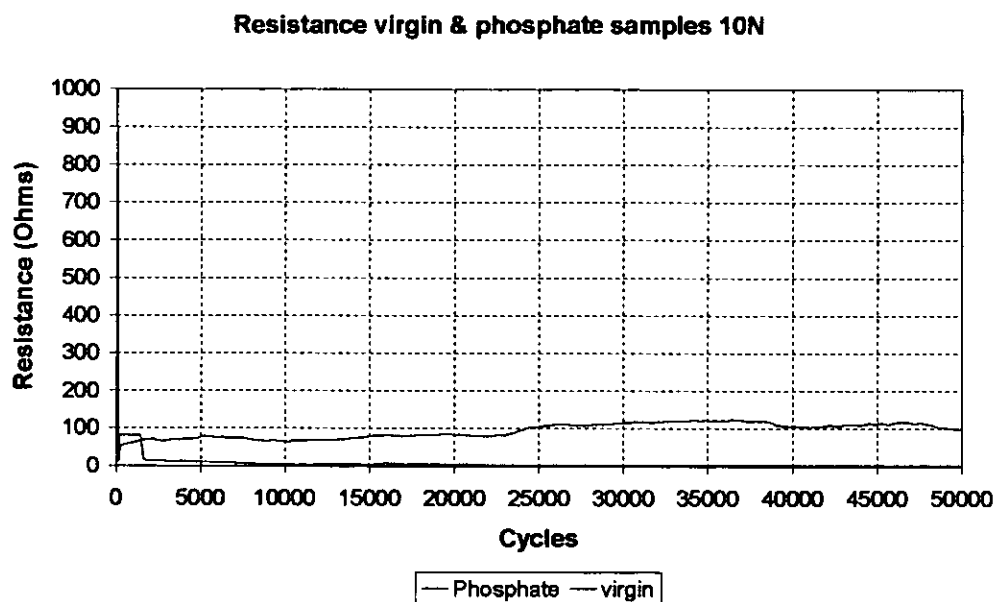


Figure 4.15 Electrical contact Resistance between virgin and Phosphate samples.

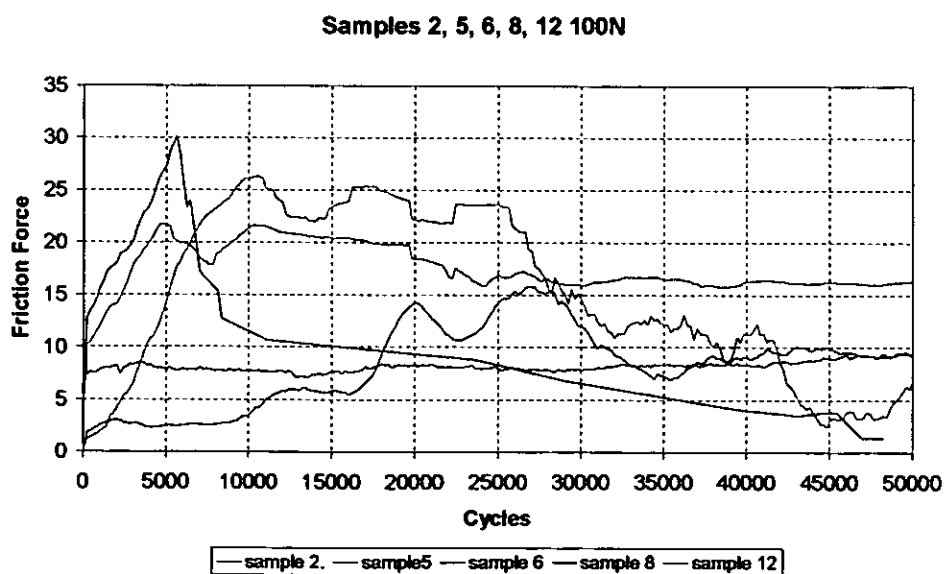


Figure 4.16. Friction force in 100N load tests (2nd six tests.)

Average friction Coefficients post 20k cycles 10N & 100N load tests.

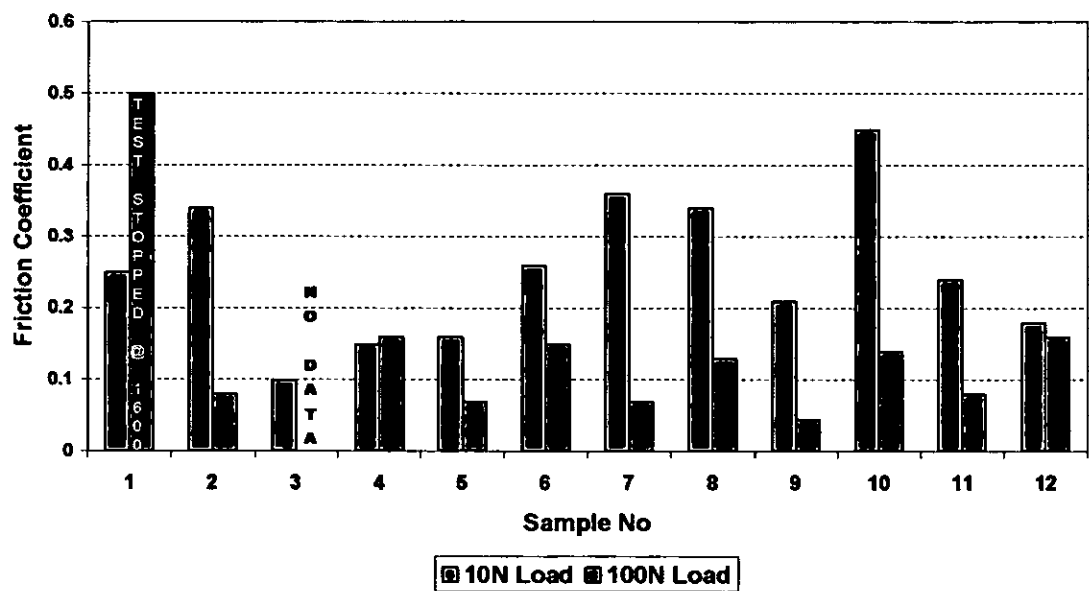


Figure 4.17 Average Friction coefficients 10N and 100N load tests.

Electrical resistance Max/Min post 5000 cycles 10N & 100N Loads

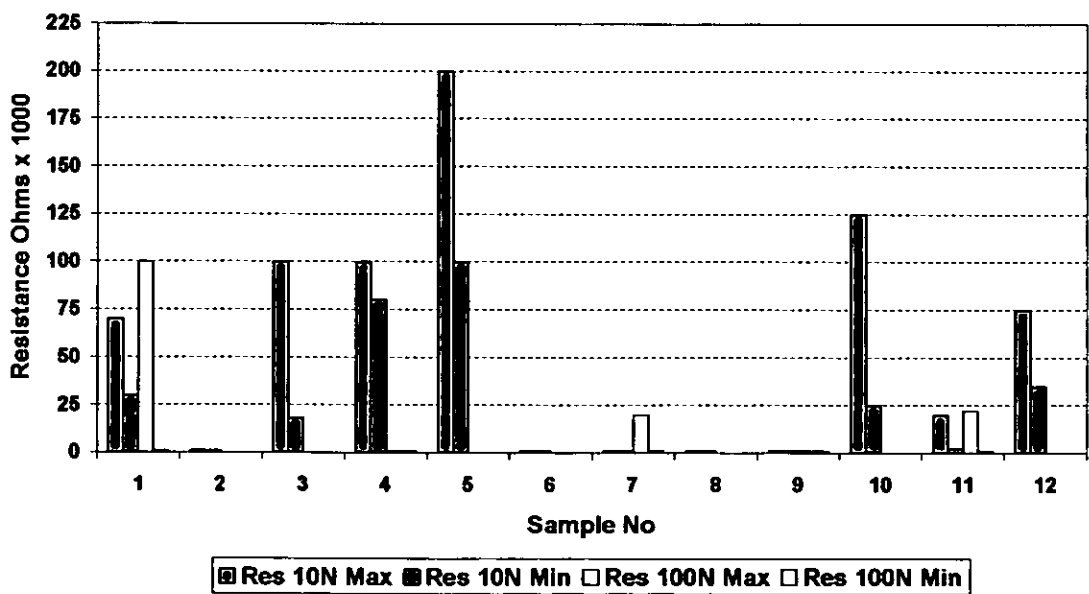


Figure 4.18 Max/Min electrical resistance 10N and 100N load tests.

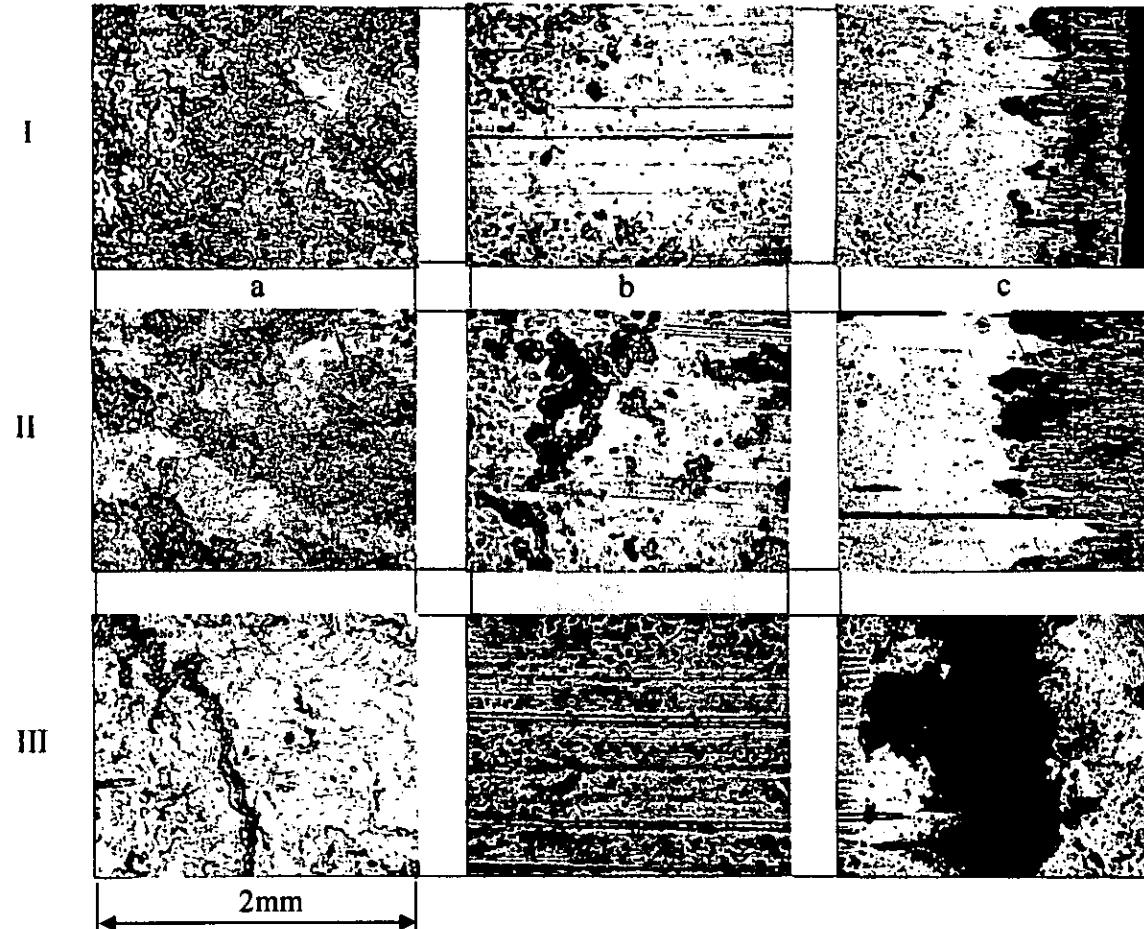


Figure 4.19. Surface images samples 1,2 & 3 10N tests.

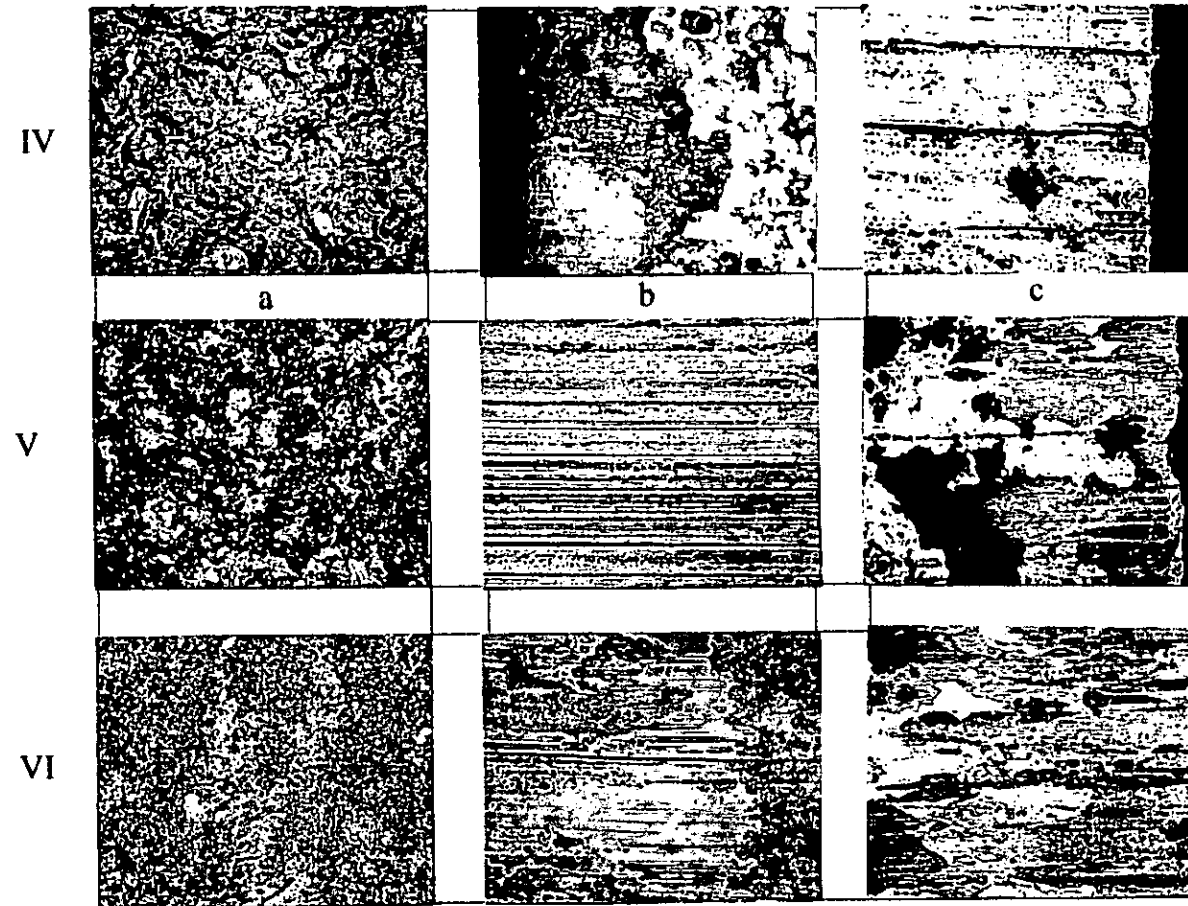


Figure 4.20. Surface images samples 4, 5 & 6 10N tests

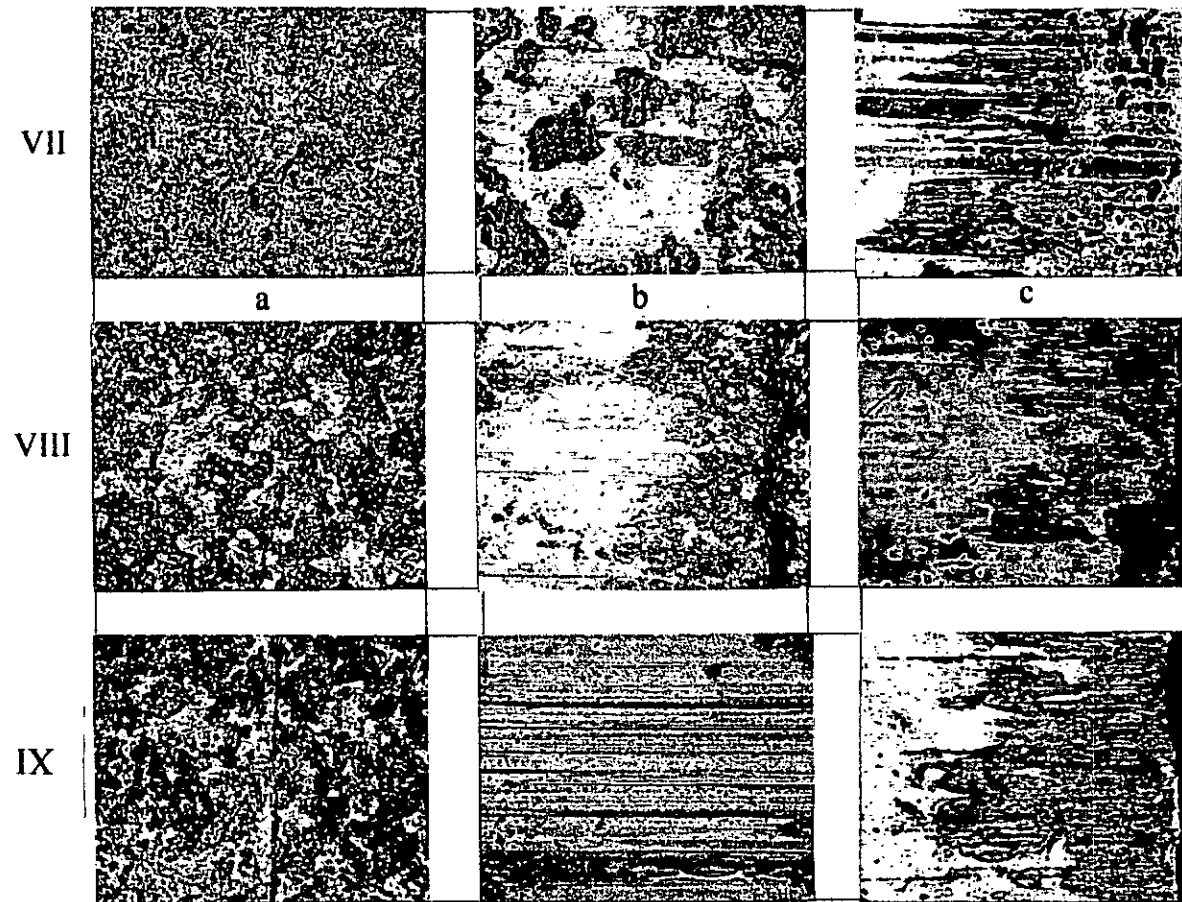


Figure 4.21. Surface images samples 7, 8 & 9 10N tests

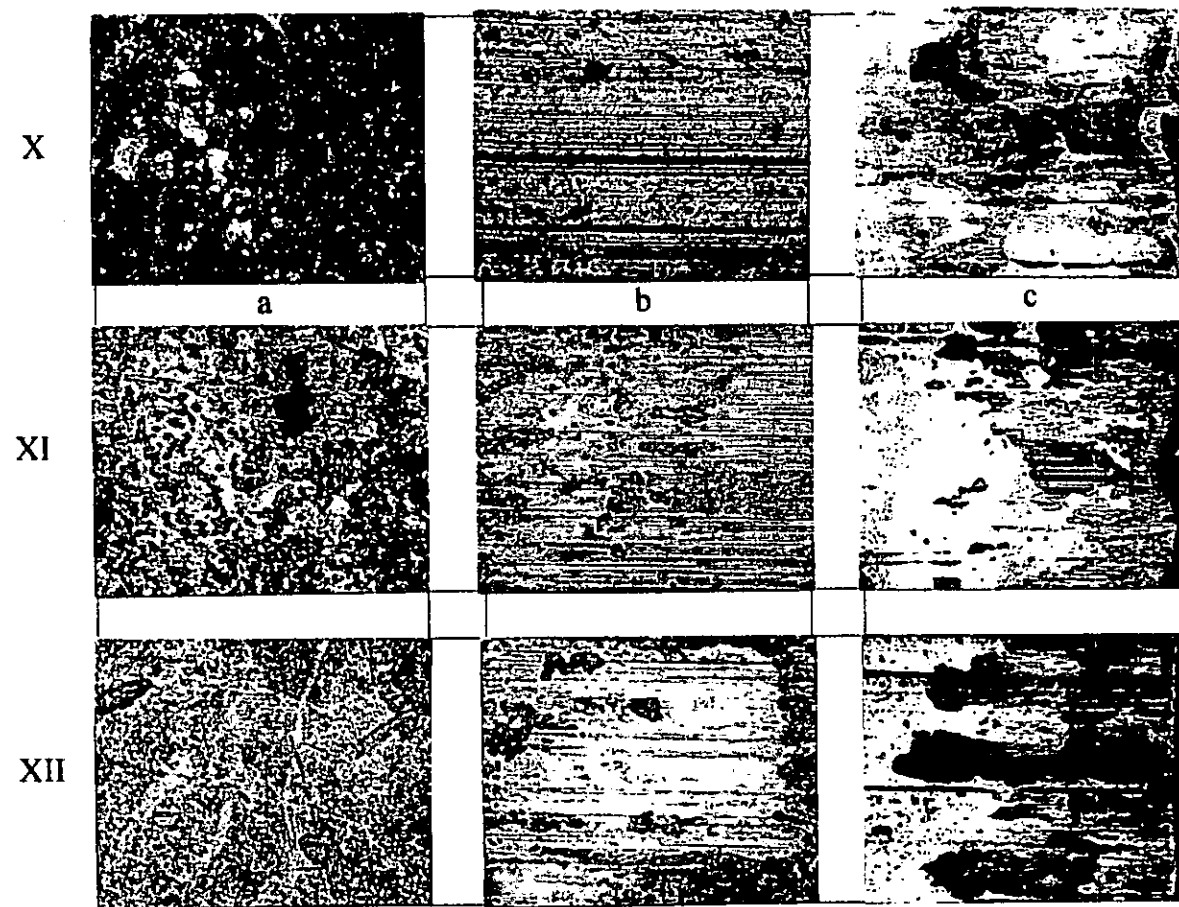


Figure 4.22. Surface images samples 10, 11 & 12 10N tests

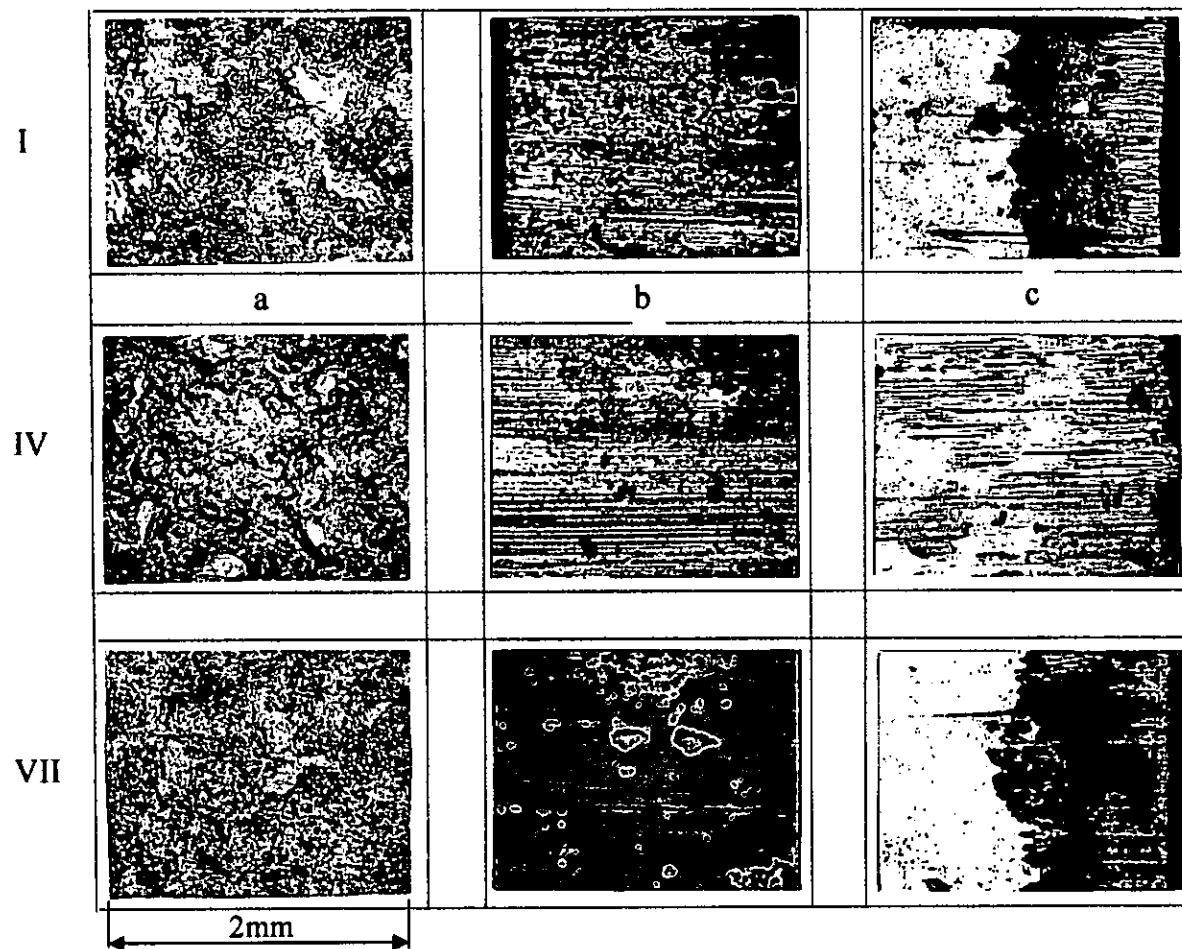


Figure 4.23. Surface images samples 1, 4 & 7. 100N tests

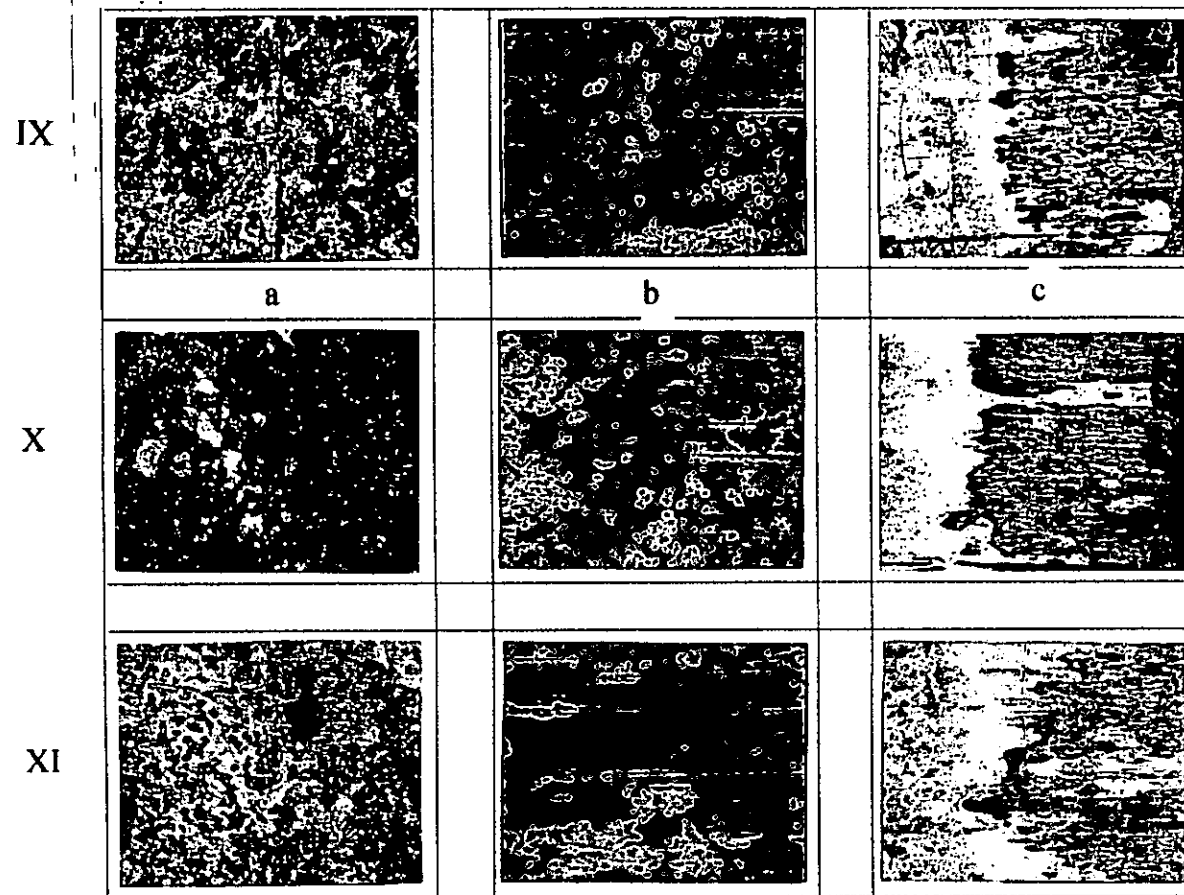


Figure 4.24. Surface images samples 9, 10 & 11. 100N tests

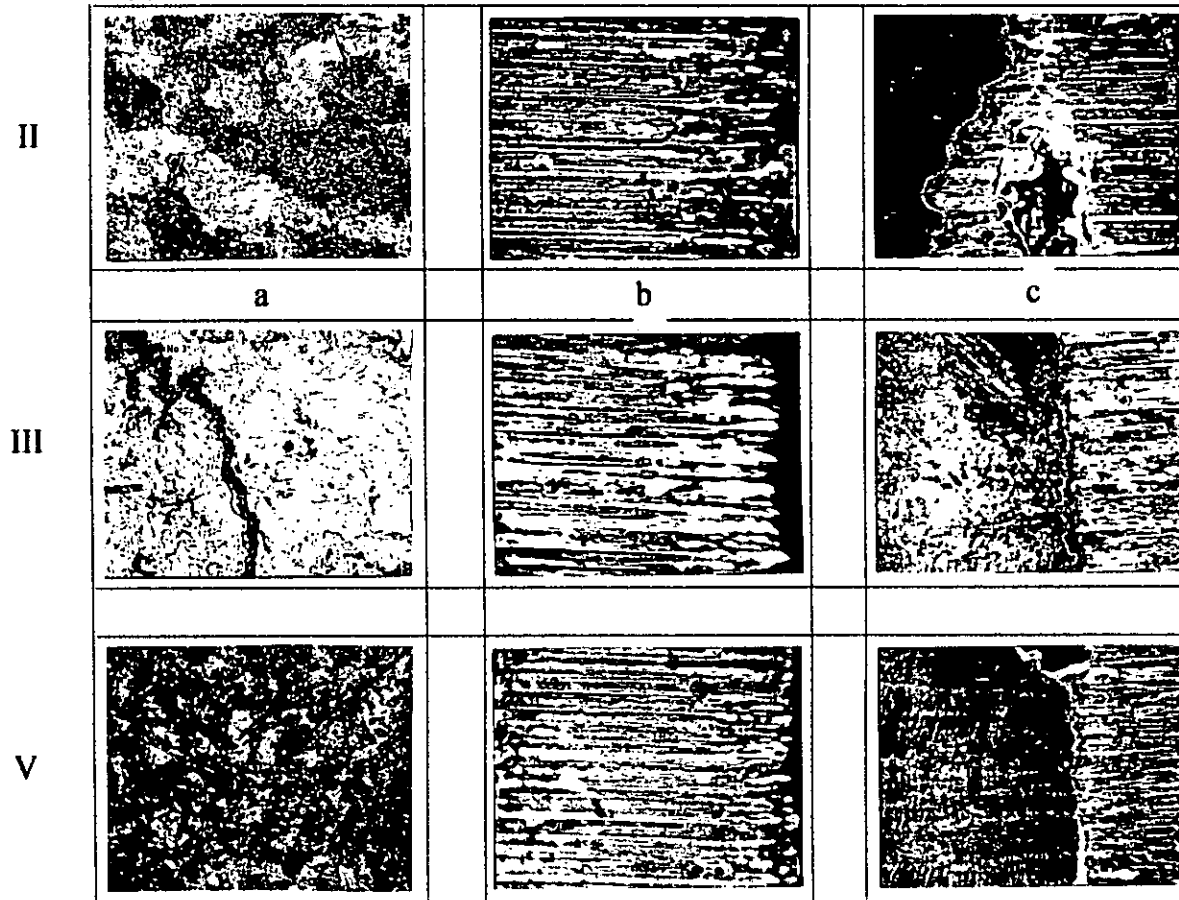


Figure 4.25. Surface images samples 2, 3 & 5. 100N tests

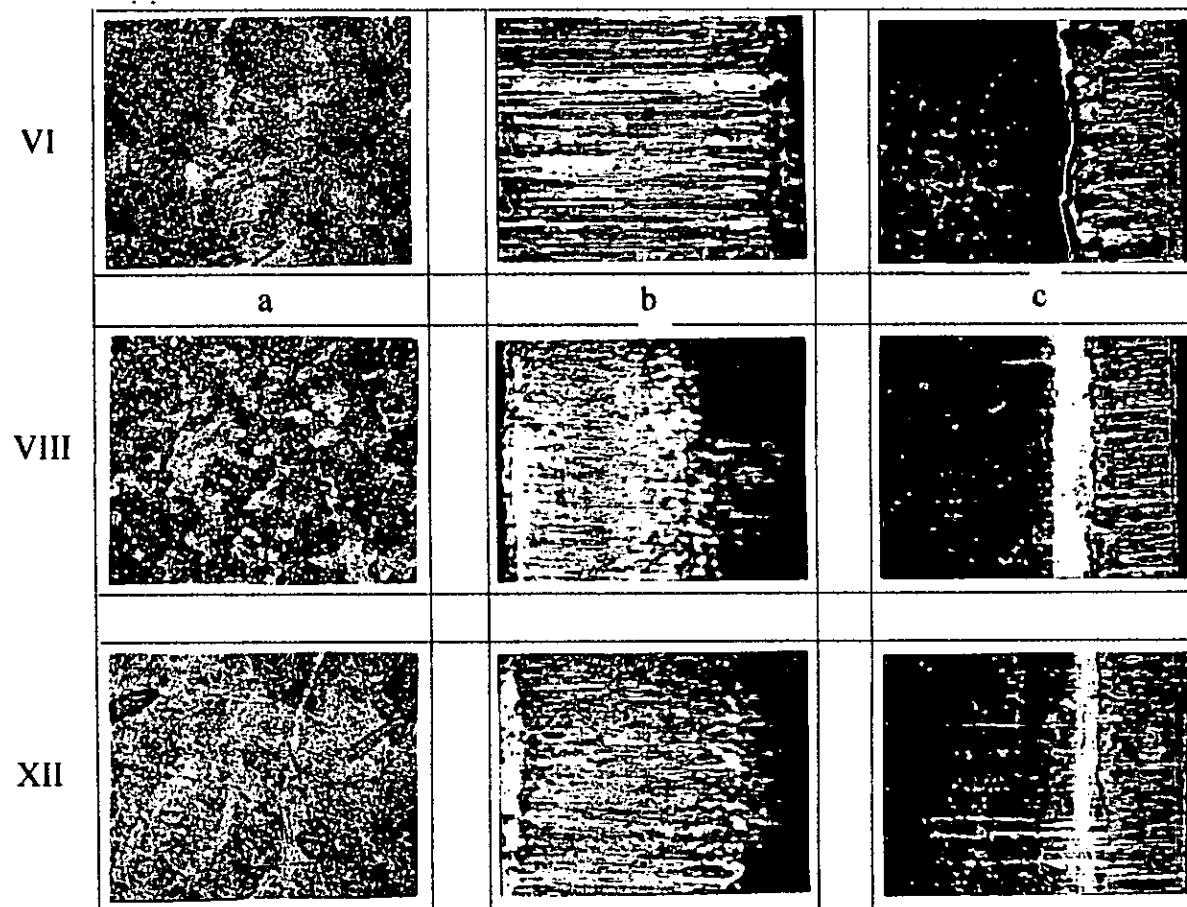


Figure 4.26. Surface images samples 6, 8 & 12. 100N test

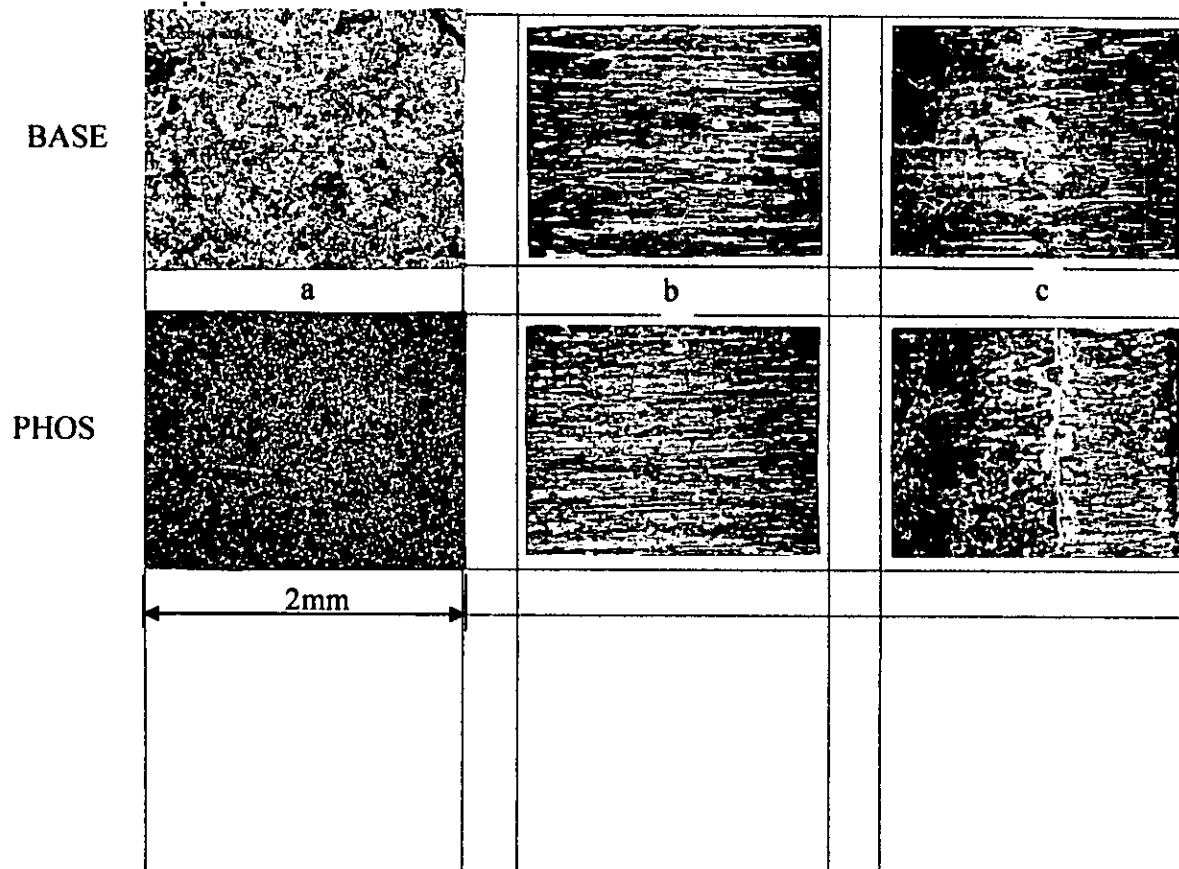


Figure 4.27. Surface images Base material and phosphated. 10N test

4.2 NEW MACHINE DESIGN.

4.2.1 Introduction

The aim of this phase of the project was to design and construct apparatus to measure the long term friction performance of Bonded Solid Lubricant materials that could be flexible enough to simulate a practical application or replicate a standard test regime (pin on disk/plate) and overcome the limitations of the previous apparatus.

There are only two recognised standards for testing bonded solid lubricants, these being: ASTM D2981-94 (Block on ring oscillating test) [4.3] and ASTM D2625-94 (Falex pin and vee method) [4.4], both these tests are line contact, being single for D2981 and multiple for D2625. The tests are mostly used for screening for load carrying capacity and wear life measurement. The information generated therefore is of limited use to engineers for BSL selection for specific applications. A pin on disk configuration would allow tests to be conducted under several configurations, for example point contact, flat on flat, line or a combination of these in continuous and reciprocating motion. Also with this type of apparatus it is quite simple to incorporate the linear reciprocating feature that is described in detail in the following sections. To this end a dual purpose test facility was designed as shown in Figure 4.28. This was accomplished by mounting a “scotch yoke” mechanism centrally on a substantial base to drive a removable linear platform, this platform was straddled by a goal post assembly that carried the load application means and friction force measurement transducers. By adjusting the pitch of the drive cam the stroke of this platform could be set between 10mm and 50mm. The use of an adapter on the driving plate after removal of the linear platform allowed the machine to be used in a pin on disk configuration.

During the design of this machine special consideration was given to the stiffness of the supporting members and drive mechanism. Test machine stiffness is known to have a significant effect in tribotesting [4.5]. A second important consideration relates to the selection of the tribo-couple for testing. Alliston-Greiner [4.6] explains that it can be misleading to attempt to define some real life conditions, such as load, and apply them to a small test piece on a test machine. During testing, energy is dissipated into the test specimen. If the energy input, or the temperature of the specimen, differs

significantly from that in the real contact, the tribological phenomena which arise may differ from those found in the real application. This results because the formation of oxides, microstructure transformations, the formation of lubricant additive products, surface micro-melting etc., may not be adequately reproduced in a test specimen as a consequence of differences in energy flux or temperature. Consideration of the Energy Pulse concept, first presented by Plint [4.7], can help to avoid misjudgements of this kind in the tribological testing of contacts.

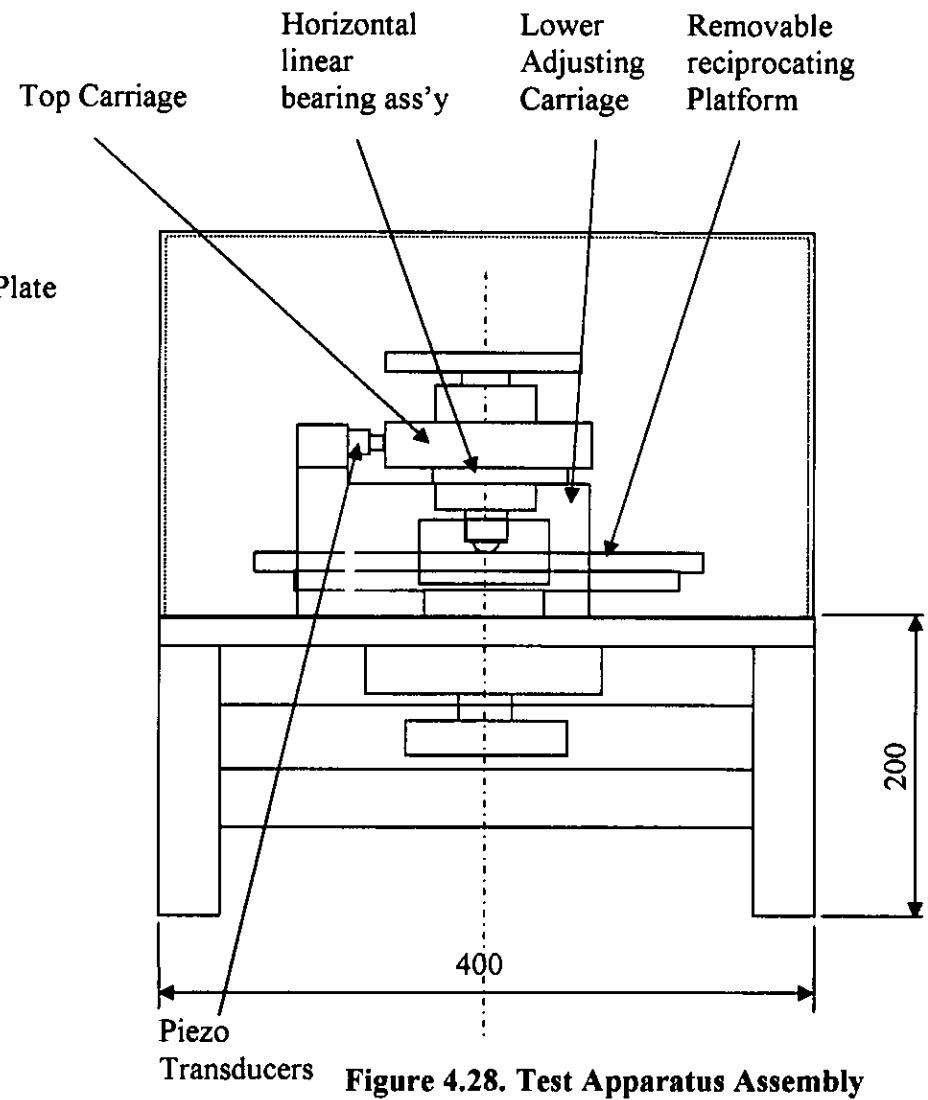
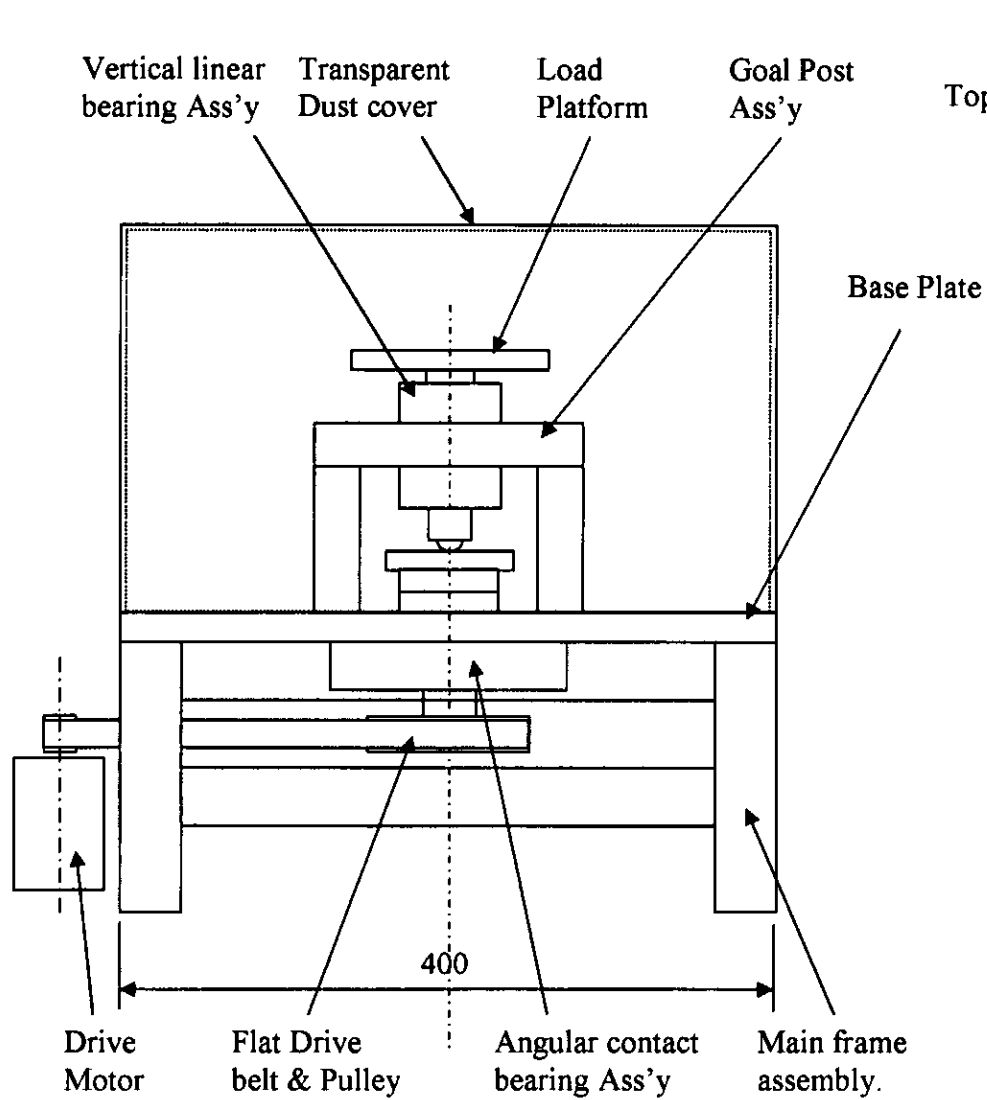


Figure 4.28. Test Apparatus Assembly

4.2.2 Main Bearings.

The main bearing and support shaft for the Pin on Disk (POD) and reciprocating configuration is based on the well proven automotive stub axle turned through 90 degrees. The design consists of the drive platform at one end and driven pulley keyed to the shaft and secured by two collar nuts at the opposite end as shown in Figure 4.29. The collar nuts are used to lock the whole assembly together and also provide adjustment for the main support bearings and eliminate any unwanted axial movement. The main bearings are a pair of angular contact bearings manufactured by NSK-RHP of the type 7205 having mechanical seals, 25mm bore 52mm outside diameter and 15mm thick. They were packed with a high performance grease prior to fitting. The loads experienced by these bearings are $1/160^{\text{th}}$ of their rated load and should therefore last the lifetime of the equipment without maintenance.

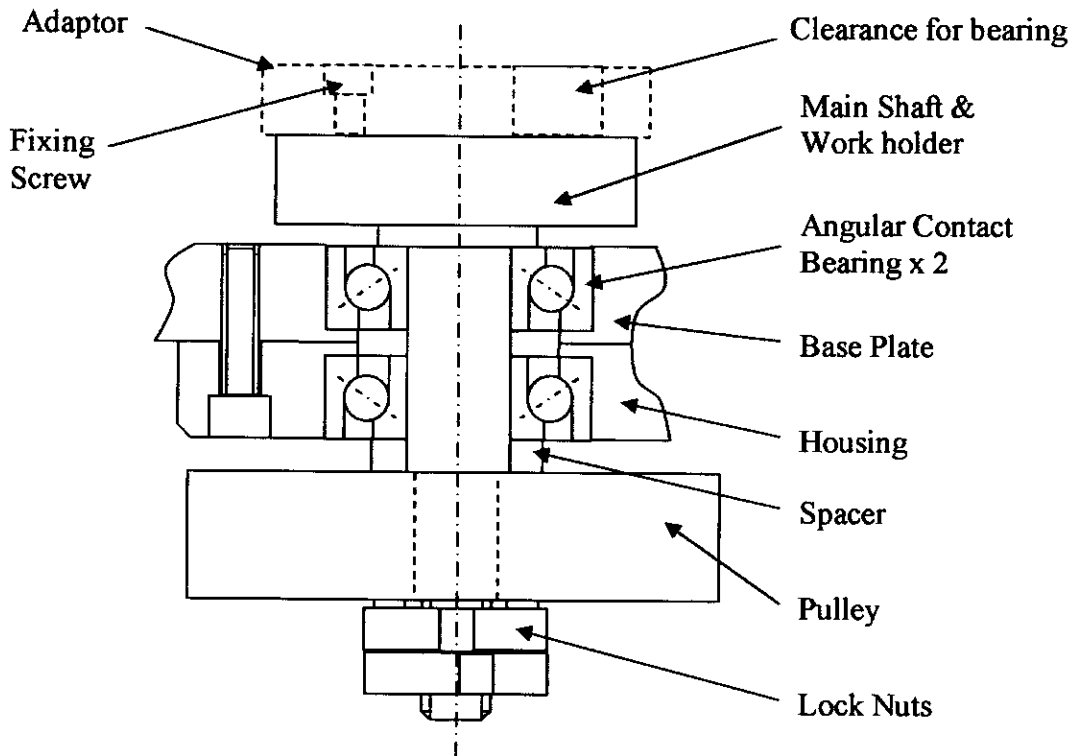


Figure 4.29. Main Bearing and Drive Assembly.

The main shaft and work holder top face contains several tapped holes to accommodate the securing of the disc adaptor for the POD mode of test Figure 4.30. These tapped holes form a spiral from the centre outwards and allow the drive bearing for the scotch yoke mechanism to be adjusted to give a stroke length from 10mm up to 50mm in increments of 10mm. The disk adaptor consists of a 65mm diameter by

20mm thick hardened steel plate tapped M8 in the centre, to accommodate the mounting of the disc specimens, with two offset holes one to accommodate fixing to the shaft and a 20mm diameter hole to accommodate the scotch yoke drive bearing. Figure 4.31.

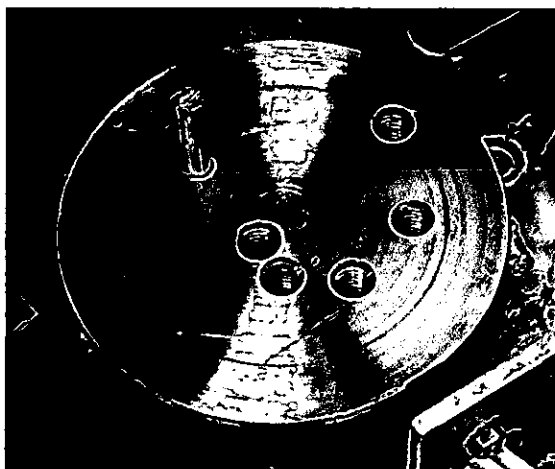


Figure 4.30. Shaft end showing fixing holes.

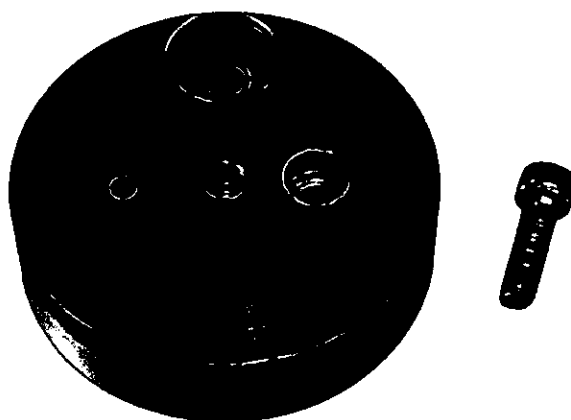


Figure 4.31. Adaptor plate.

When used in the reciprocating mode the disc adaptor can be removed and attached to the main frame cross rail for storage, the scotch yoke bearing set to the required stroke position by repositioning the bearing post in the desired tapped hole. The reciprocating platform is then lowered into position taking care to locate the bearing in the central cross slot of the scotch yoke mechanism, this platform is also located in the

V guide wheels of the Hepco linear slide system illustrated in Figure 4.32. Two of these guide wheels on one side of the reciprocating platform are mounted on eccentric adaptor bushings to provide a simple and effective means of adjusting the free play in the system. The dynamic and static radial load capacity of these guide wheels is given in Table 4.5, it can be clearly seen that the load capacity is dependant on the angular velocity of the wheel. With a reciprocating motion of 50mm stroke the angular velocity at 240 cycles per minute would equate 120 revolutions per minute giving a dynamic radial load capacity of around 200Kg per wheel, 800Kg for the total assembly, this is 80 times the envisaged maximum test load of 10Kg, additionally the normal applied load is designed to be taken by the reciprocating platform being in contact with, and supported by the main bearing shaft, and therefore the guide wheels would only act as guides. This may be considered to be excessively over designed but considering the average life expectancy of these wheels of 2500 hours at the designated ratings and the requirement to run continuously in excess of 5 weeks (840hrs) they were deemed to be adequate and due to their accessibility could be easily changed.

Size	Dynamic radial capacity kg.				Static radial capacity kg	Moment capacity kg
	33.3RPM	100RPM	500RPM	1000RPM		
2	317	218	128	101	112	17

Table 4.5. Dynamic and Static radial load capacity for Type 2 Guide Wheels.

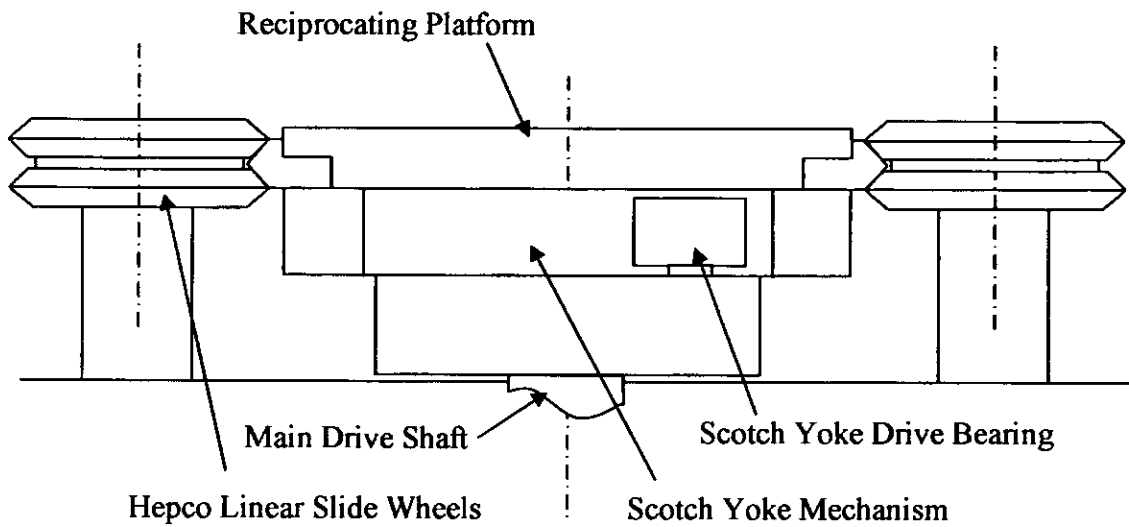


Figure 4.32. Scotch Yoke and Linear Slide assembly.

4.2.3. Top Carriage Assembly.

The friction force was measured by means of two parallel mounted piezo resistive load cells mounted on an adjustable “goalpost” structure. The top carriage of this structure housing linear bearing outside diameter 40mm, inside diameter 25mm and 58mm long and a vertically mounted shaft containing the sample holder and loading means. The underside of this plate is attached to precision ball slides 20mm wide, 10mm high and 50mm long mounted in the same axial direction as the reciprocating platform with the load transducers mounted in line of the direction of movement off these bearings. The whole of this assembly is shown in Figure 4.33 and 4.34 and the technical details of all these bearings are given in Appendix A2

The installation of these precision ball slide must allow for a small amount of adjustment to allow parallel alignment to give the best “friction free” assembly and in fact when this is achieved the whole test apparatus must be set up in a position which is perfectly level, achieved by using a precision spirit level. The manufacturers state a coefficient of friction of 0.001 for these precision re-circulating ball slides, if this compared with the expected measurements to be taken, possibly down as low as 0.02 then the effect on the measured values would be negligible. In any case this factor will be automatically taken into consideration during the calibration procedure described in section 4.2.11.

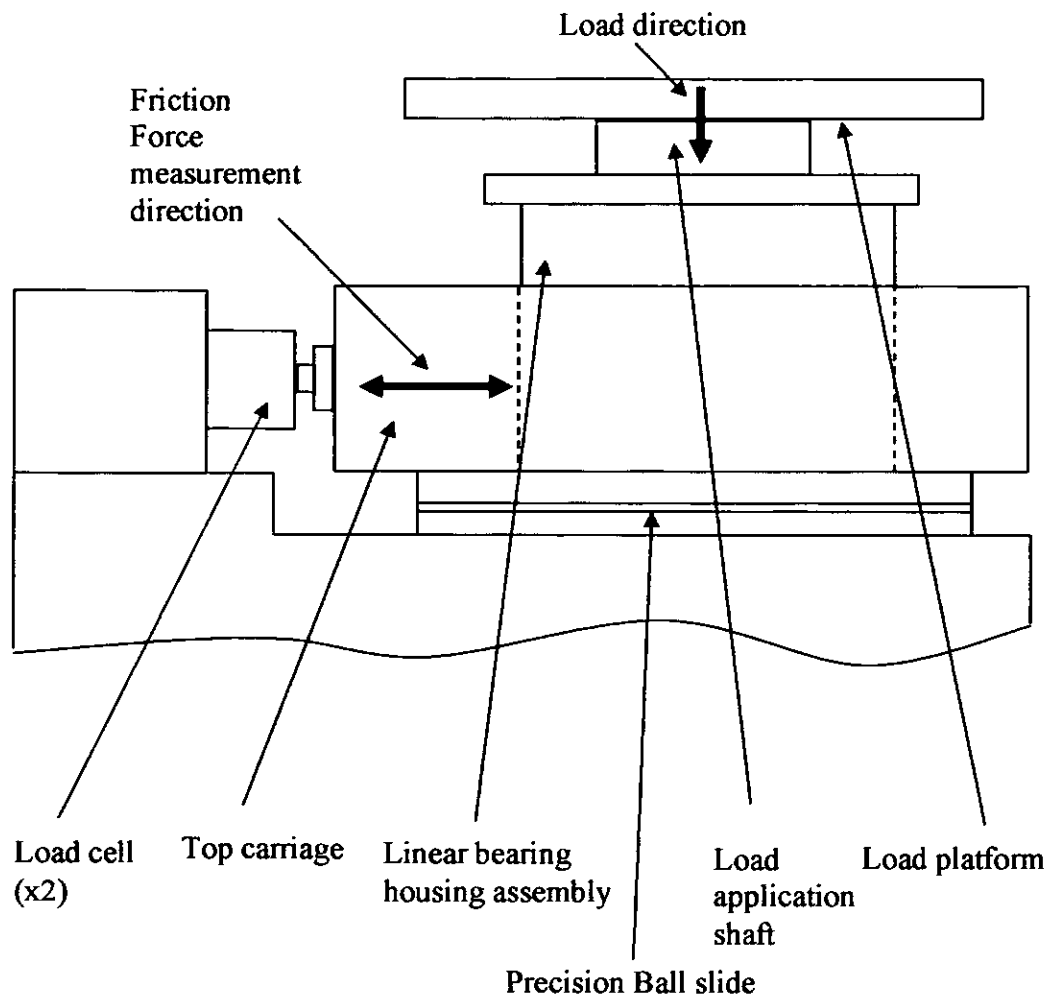


Figure 4.33. Top carriage and load cell assembly.

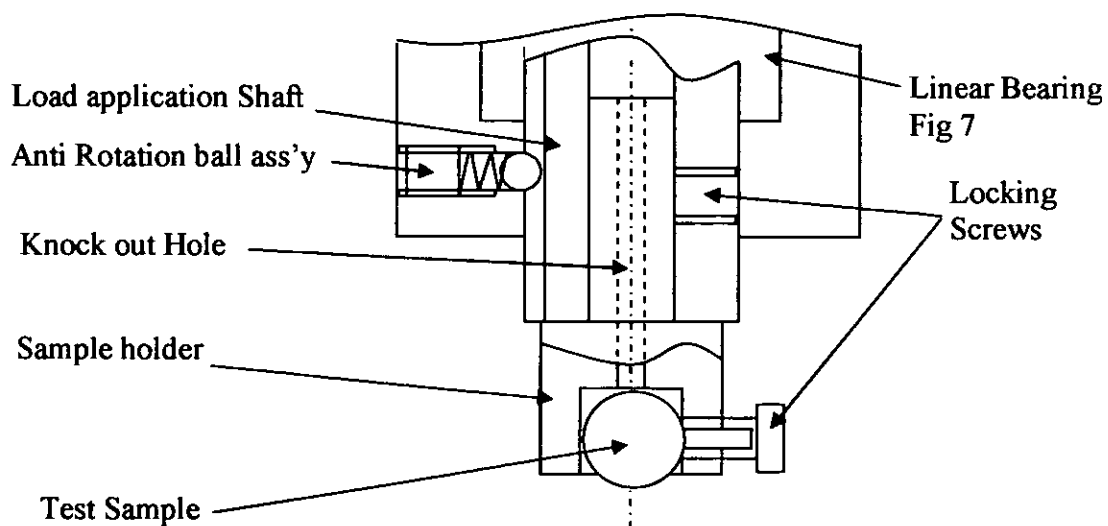


Figure 4.34. Sample holder and securing method.

4.2.4. Base plate and Main Support Frame Assembly.

The main base plate to which all the operating components were to be either attached or housed was of sufficient mass to remain stable when operating at high speeds and yet allow the whole assembly to be moved comfortably by two people. It also needed to be thick enough to house the main bearings and large enough to accommodate all the components on the top surface including the enclosure. The base size chosen 400 x 400 x 20mm thick Mild Steel plate which with a density of 7.85g/cm^3 would have a mass of 25kg, giving a total mass for the equipment of less than 40kg.

The main frame and support assembly was constructed using an Aluminium Structural System illustrated in Figure 4.35. Consisting of a modular range of standard components which can be combined to form a structure for a wide variety of applications, from workbenches and enclosures to special machine framework and guarding. The aluminium system can be assembled quickly and economically using only hand tools. The system comprises of a modular range of aluminium extruded beams together with framework connectors, feet, sliding elements and enclosure components. The T-slot nuts illustrated in Figure 4.36 and 4.37 enable additional components to be easily integrated, such as pneumatic cylinders, sensors and cable. The type used has 7.2mm wide T-slots and is available with cross sections of 30mm. x 30mm. and 30mm. x 60mm. (only the 30 x 30mm was used in this case).

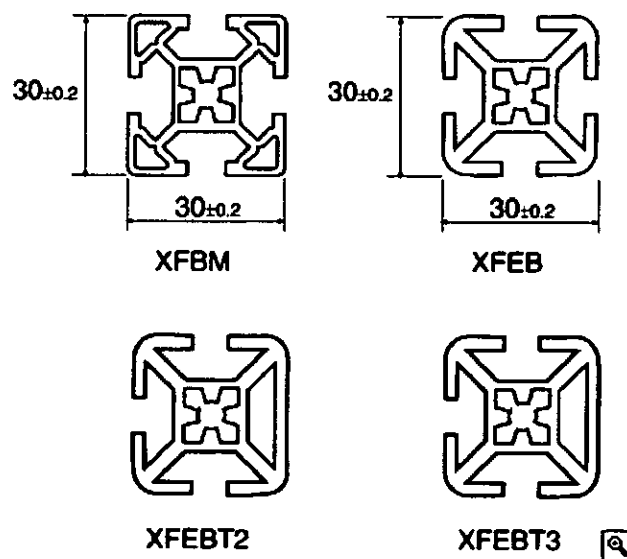


Figure 4.35. Cross section of aluminium section.

(Adapted from RS components)

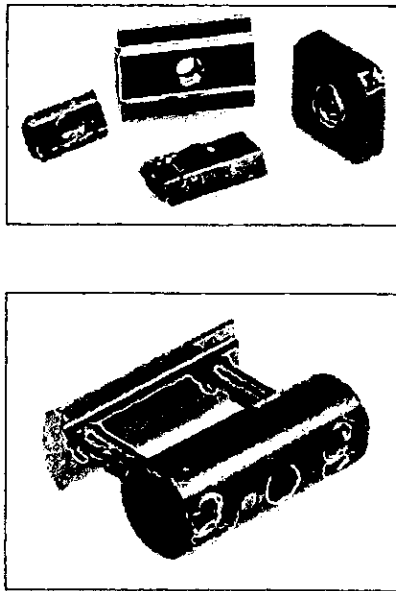


Figure 4.36. Various Fixings used to construct support frame.
(Adapted from RS components)

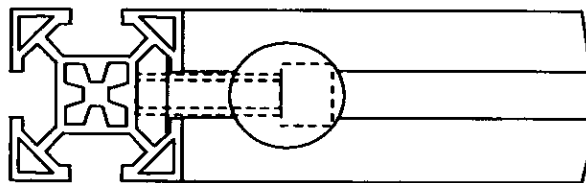


Figure 4.37. Method of fixing corner pieces with fixings shown in figure 4.36.

4.2.5. Motor Specification.

It was intended to use a similar motor to the one used on the original reciprocating apparatus, this being a variable speed AC motor with a worm drive final output, that was readily available with control system and power supply. This motor/gearbox was attached to a mounting plate with rubber insulating bushes; the plate was then fixed to the aluminium structural frame by use of the T nuts already described and the final drive accommodated by a 4:1 reduction pulley system with a 20mm wide flat belt.

The initial set up for commissioning utilised two Kistler piezo transducers fixed between the top carriage and the fixed goalpost structure. Initial tests running this motor with outputs from the transducers being displayed on an oscilloscope proved to

be problematic. The noise (vibration) generated by the motor was transmitted through the frame and detected by the transducers, this was deemed to be of a level sufficient to significantly influence the accuracy of measurements being made of the friction force between the specimens. Several attempts to eliminate this noise by use of propriety vibration damping techniques were unsuccessful. Even mounting the motor remotely on a substantial steel block was unsuccessful due to the vibration being transmitted through the belt drive. Finally this drive solution was abandoned and the following specification generated.

The main requirements for the motor specification were derived from:

- the previous experience with vibration encountered from earlier test equipment i.e. the vibration generated by the AC drive motor,
- the load cell limitation of 30N (15N per cell)
- the diameter of the test disc and desired test velocities required.

To allow tests to be conducted at various diameters on the disks, the goalpost assembly incorporated two dowel holes next to the clamping nut on one of the legs. These correspond to two rows of dowel holes at 10mm pitch offset by 5mm to facilitate the adjustment of the upper test sample position relative to the centre of the drive spindle Figure 4.38.

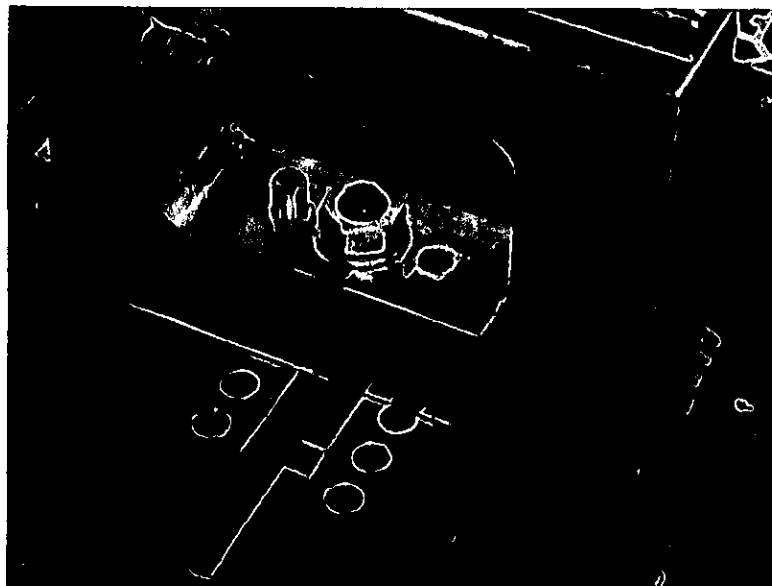


Figure 4.38. Goalpost adjustment.

This arrangement permitted tests to be performed at diameters of 30, 40, 50 & 60mm. Table 4.6. shows these test diameters and the corresponding velocity and shaft speed in rpm. The desired velocities were selected at magnitudes apart, i.e. 0.1m/s and 1m/s, and one in the centre at 0.5m/s. The reason for the magnitude spacing is because differences in tribological phenomena tend to be small with small changes in variables with magnitude changes these differences become more obvious. The centre point value is useful during analysing results and can sometimes indicate whether a relationship is linear or otherwise.

Diameter m	Circumference m	Speed RPM	Speed rev/s	Velocity m/s
0.03	0.09426	65	1.083	0.102
0.03	0.09426	130	2.167	0.204
0.03	0.09426	319	5.317	0.501
0.03	0.09426	638	10.633	1.002
0.04	0.12568	48	0.800	0.101
0.04	0.12568	96	1.600	0.201
0.04	0.12568	240	4.000	0.503
0.04	0.12568	478	7.967	1.001
0.05	0.1571	48	0.800	0.126
0.05	0.1571	78	1.300	0.204
0.05	0.1571	382	6.367	1.000
0.05	0.1571	764	12.733	2.000
0.06	0.18852	65	1.083	0.204
0.06	0.18852	130	2.167	0.408
0.06	0.18852	319	5.317	1.002
0.06	0.18852	638	10.633	2.005
Grey background = preferred test condition Blue and white background alternative test condition and additional velocities.				

Table 4.6. Velocity and Shaft speed v test track diameter.

It can be seen from the above table that a maximum speed of 638rpm would be required at the main shaft. This translates to a motor speed of 2552rpm due to the 4:1 reduction pulley system proposed. To allow an amount of flexibility 3000rpm was used for the final specification. It was considered unlikely that the 60mm diameter

would be used for the main test programme, all requirements being met by the 30, 40 and 50mm diameter test positions. The torque requirement was derived from the maximum load requirements as follows:

Test load = 100N

Friction coefficient at breakdown = 0.3 (load cell limit 30N)

Test diameter for max torque 50mm ($r = 25$)

Therefore maximum operating torque = $100 \times 0.3 \times 25 \times 10^{-3} = 0.75\text{Nm}$

The continuous running torque was expected to be lower than this and testing would be stopped when friction coefficients exceeded 0.3 (The load transducers used have an overload capability and choosing the 30N limit ensured they were kept well within this limit).

The motor would need to offer variable speed at constant torque and be completely silent during running i.e. vibration free. Advice was sought from a specialist supplier and a brushless DC servomotor and control system to the following specification purchased:

- Brushless DC Motor 3000rpm 0.74Nm torque (continuous) 1.48Nm (Peak)

To give infinite variable speed control at constant torque the control system described in the following section was recommended.

4.2.6. Electronic Control System.

The test facility was required to run continuously 24 hours a day for periods up to 6 weeks and would require a life of 5 years. With this in mind the supplier recommended the following control system:

- Optical Digital Encoder (for fitment to the motor to give accurate speed control).
- Brushless DC servo drive.
- Single phase AC to DC power supply unit.

All parts were supplied separately with full connection and operating instructions. The complete manufacturer's drawings, instructions and final wiring schematics are included in Appendix A3.

The system was to be run unattended 24 hours a day, thus there was a requirement to protect the force transducers against overload when the lubricant film began to break down and the friction force exceeded 30N, would require some method to be devised to stop the test. Initially a software solution was sought utilising the commercial data acquisition software package, but due to lack of information of the programming techniques and uncertainties of successful application, an electronic switching solution was designed that used the force measurement to activate a self latching relay to switch off the motor. This type of solution is not uncommon with the type of transducers involved and full details of switching devices are provided with them. Appendix A3 contains the schematic layout for the switching device used.

4.2.7. Load transducers.

The original design incorporated two Kistler piezo electric force links type 9311B (see appendix A4) mounted between the goalpost structure and the moving top carriage. These force links can measure compressive and tensile forces and are particularly suitable for dynamic loads. They have rigid construction and need very little displacement to sense the load. However when measuring static or uni-directional loads, such as those applied in the pin on disk configuration, these type of sensors are not suitable due to the signal decay that is experienced through charge dissipation. Although there are methods of compensating for this signal decay (such as reversing the rotation direction at even intervals) the provision of the load cells described below was deemed by far the simplest and most cost effective solution for uni-directional loads.

The load cells used are produced by Honeywell (type FSG 15N1A see Appendix A4) and consist of a piezoresistive micro-machined silicon sensing element which forms a non compensated Wheatstone bridge circuit that is totally enclosed in a plastic package. A plunger mounted in the centre transmits the load to the silicon disk, deformation of this disk produces a change in the balance of resistance of the strain bridge and hence a change in voltage can be measured which is directly proportional

to the applied load. It should be noted that this plunger is electrically live and required to be insulated from the main test apparatus. This was established by use of adhesive insulation tape between the plunger and the body of the test rig, although this tape is plastic and exhibits some elastic properties the effect of this was taken into consideration during the calibration procedure. Two of these devices were wired in parallel and mounted on the load beam, one each side of centre, this set up would cancel out any off centre loading experienced and allowed greater tolerance of any offset of the specimen holder.

The output from the load cells was fed via an interface described in section 4.2.10. and recorded on a computer using a commercial data acquisition package from Pico Technology of St. Neots. This data acquisition package gives a real time display of readings taken and automatically plots the results graphically so that the test programme can be monitored throughout. Data is automatically saved to hard disk as a “.plw” file and at the end of the test the data file can be saved as a text file allowing input into analysis packages. In this case Microsoft Excel was used for the presentation of all the results.

4.2.8. Temperature and Humidity transducers.

Temperature and humidity was measured by use of a combined transducer described in Appendix A4. This unit (designated RHU-217-AT) is used in commercial applications such as air conditioning units, room humidifiers/dehumidifiers and ventilating systems and is able to measure humidity and temperature without the need for external electronics. The unit requires a supply voltage of 5VDC $\pm 5\%$. Humidity is measured via a linear output of 0 – 3.3 volts corresponding to 0 - 100% humidity full scale. Temperature is monitored by a thermistor and therefore requires a conversion factor to be used to generate a reading in degrees Celsius. Measurement accuracies of ± 0.7 degrees @ 25° C over a range of 0 to 60° C for temperature, and Humidity $\pm 5\%$ RH with a range of 30 - 90% RH. This unit was considered robust and accurate enough to be mounted in the test enclosure on an insulated block. Variation in temperature and humidity was not expected to vary by any significant amount due to the test equipment being housed in a university laboratory and therefore it was decided to monitor these parameters and not control them. Several authors have demonstrated the effect of humidity and temperature on solid lubricants, but due to

this investigation being linked to a commercial application in normal atmospheric conditions it was considered sufficient and more appropriate to record these values, this would, in an unlikely event of a significant change in these parameters (greater than 30%) during testing, allow any effects on the BSL to be observed.

4.2.9. Power supply.

It was necessary to use four variable 0-30 volt laboratory power supplies to power all the data acquisition transducers and also to facilitate the dual rail power requirements of the force overload protection switch for the high load tests. The following schematic Figure 4.39 shows this in detail. The power supply output was calibrated at regular intervals by use of a digital multi meter to ensure the accuracy of measurements taken was consistent between tests.

4.2.10. Data Recording Interface.

All the transducers were wired to an ADC11 interface produced by Pico Technology. This interface has 11 channels of analogue input and 1 digital output, suitable for inputs up to 2.5V with a sampling rate of 10KHz and 10 bit resolution. Full details are included in appendix A3. The interface connects directly to the PC parallel port and a terminal block with screw connections shown in appendix A4. The block obtained from the same supplier, allows for ease of connection to all the external devices. Due to the configuration of the force transducers used, i.e. the measurement of the difference between two voltage outputs, neither of the terminals could be connected to ground. This was achieved by the use of the separate power supplies already described, giving a floating ground for the force transducers and a fixed ground for the other instrumentation. The complete assembly of the apparatus and power supplies is shown in Figure 4.40 and the output from the data acquisition package in Figure 4.42.

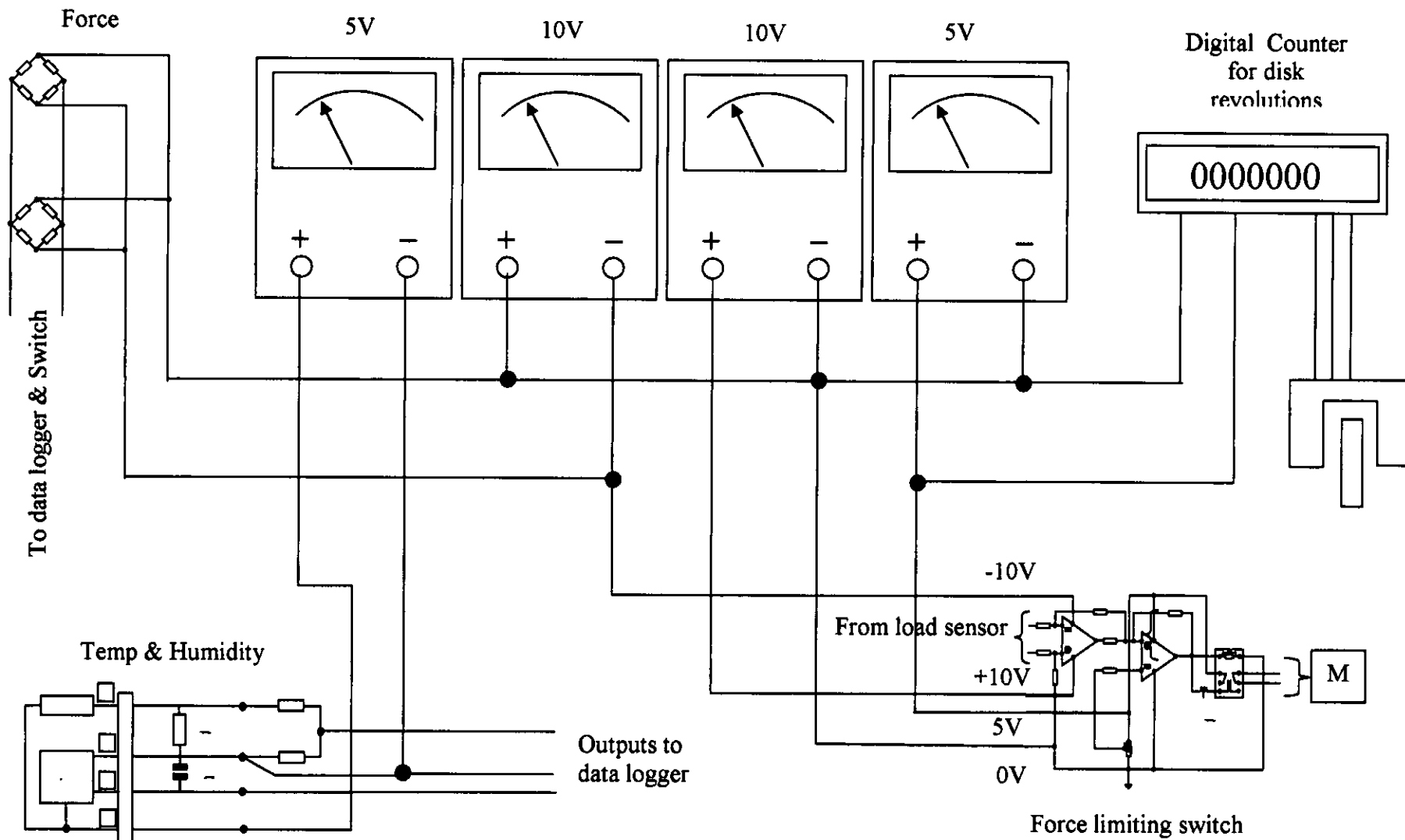


Figure 4.39. Instrumentation Power Supply Schematic

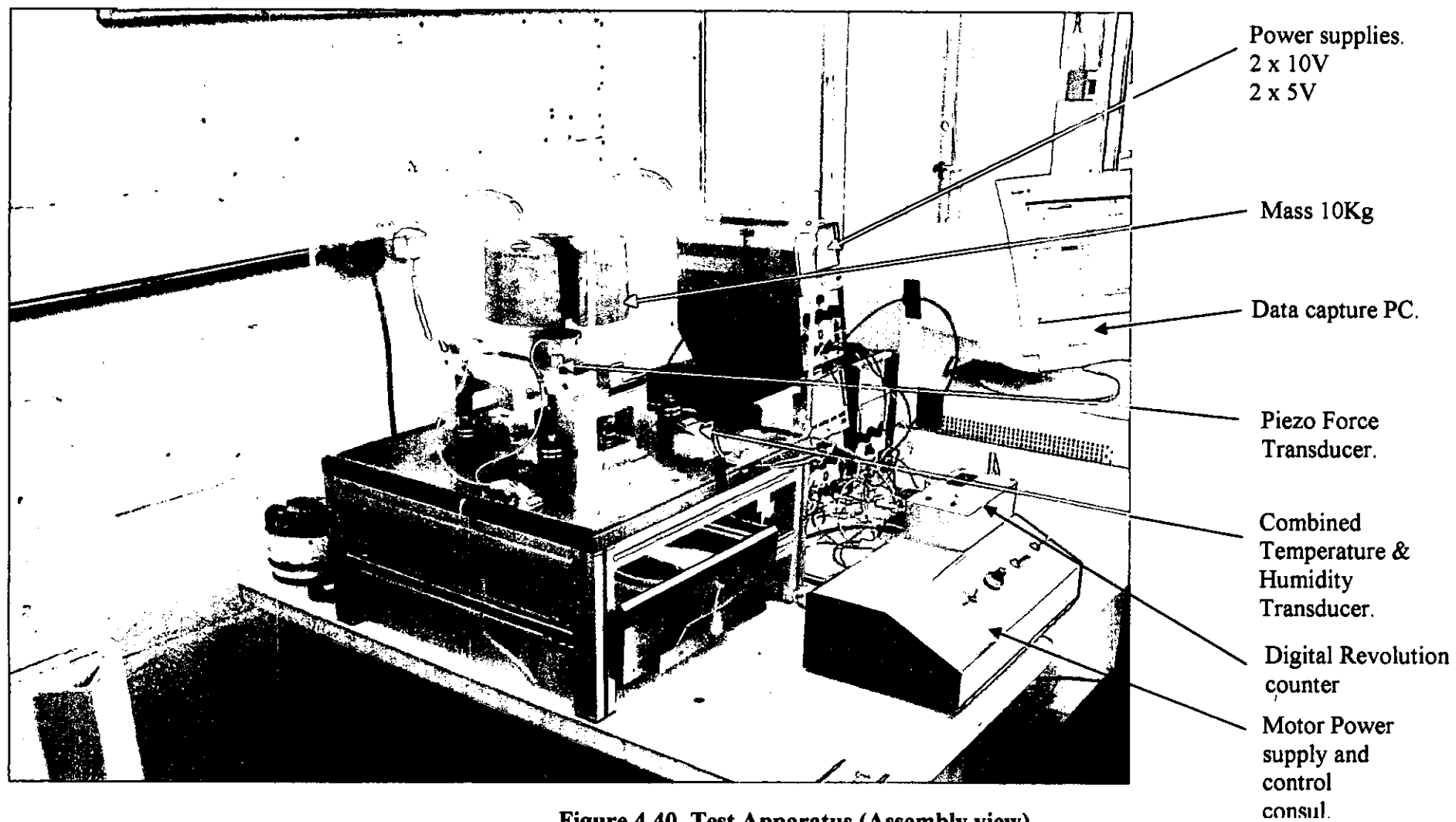


Figure 4.40. Test Apparatus (Assembly view).

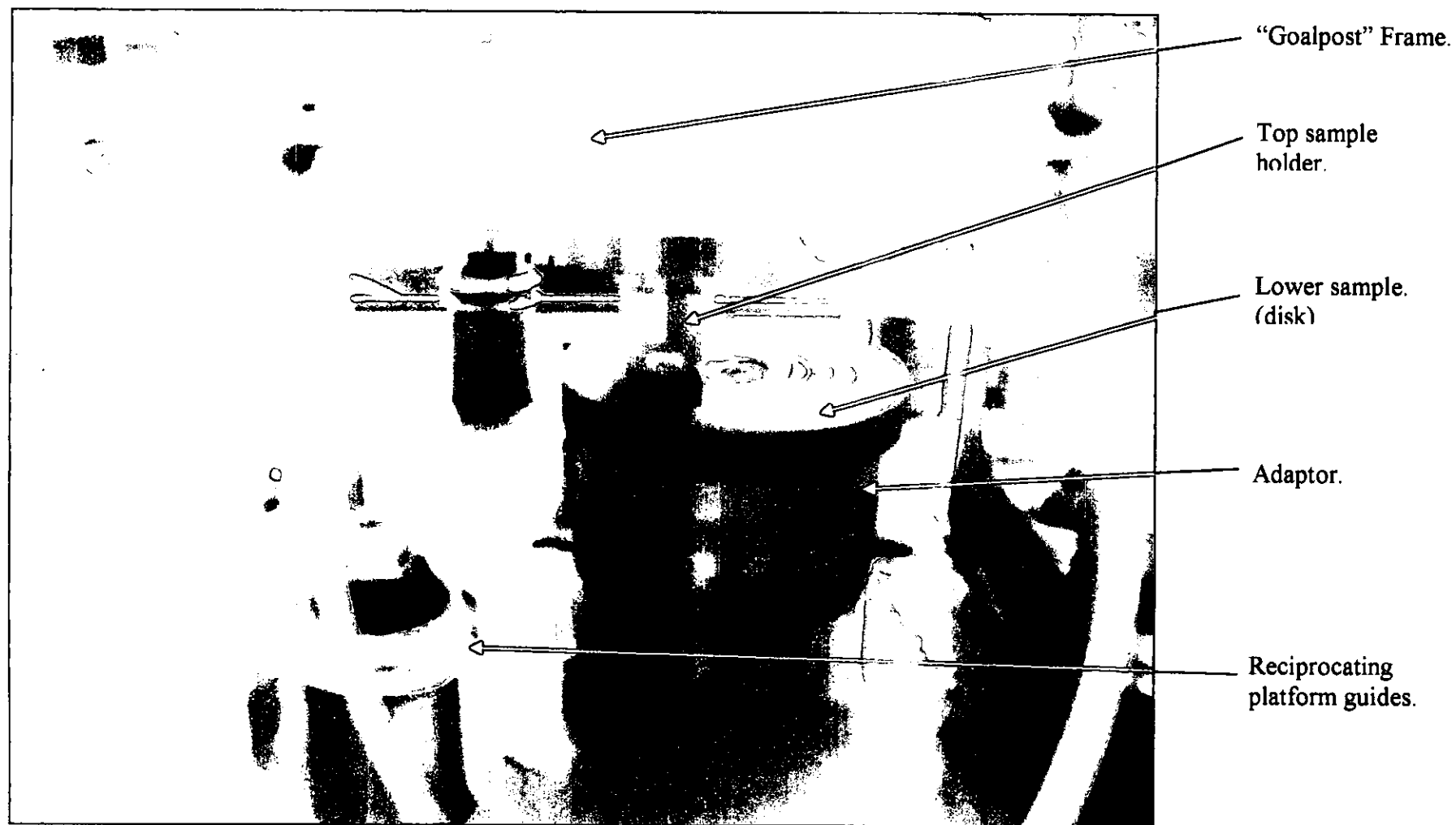


Figure 4.41. Pin on Disk Interface

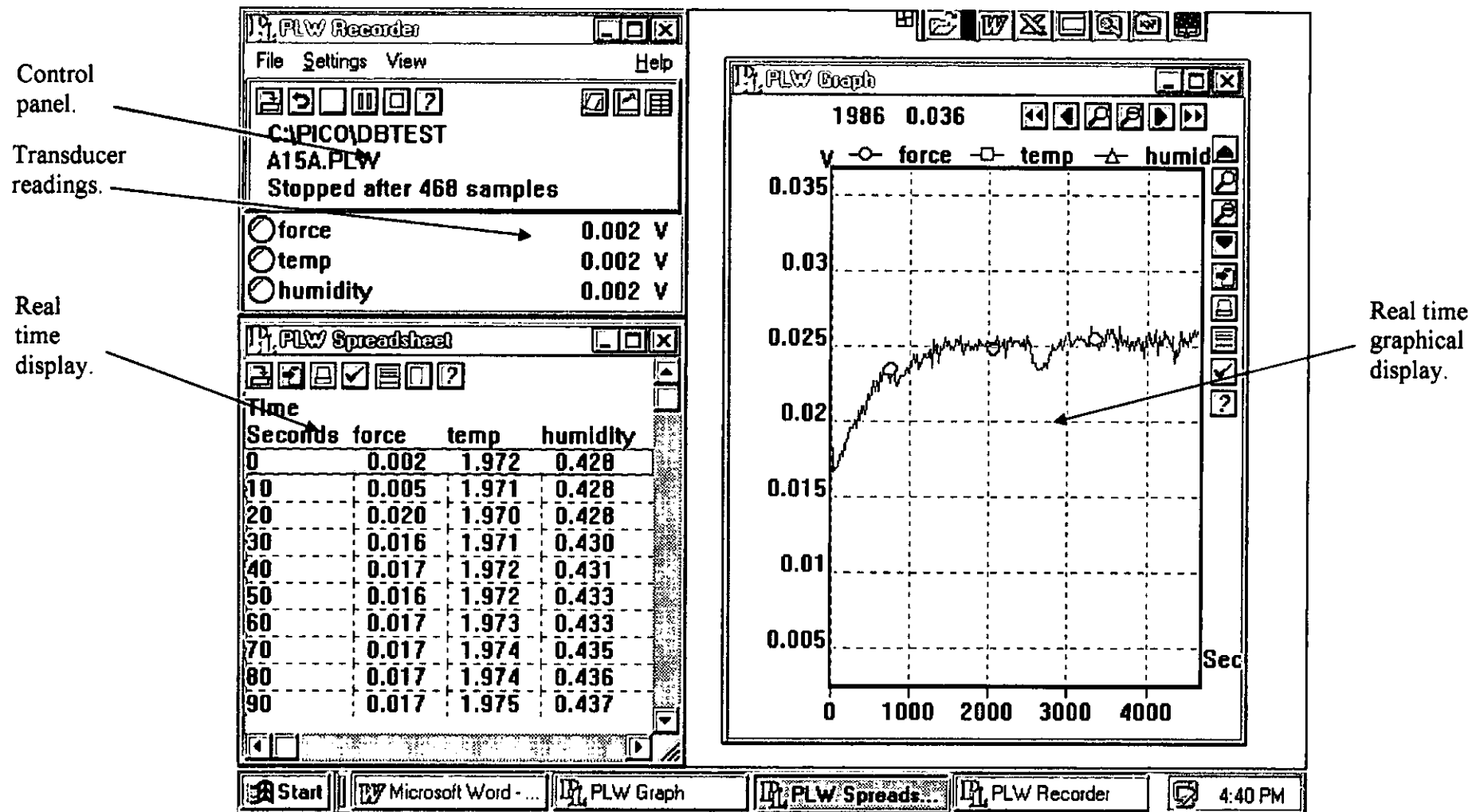


Figure 4.42. Screenshot of Picolog display.

4.2.11. Commissioning and Calibration.

Prior to any test work being performed the base of the apparatus was checked with a precision level and the bench legs on which it was mounted adjusted by means of the screw in feet until the system was level in all directions. The apparatus was checked to ensure there were no loose wires, nuts etc. The electronic motor control was turned on and the motor allowed to run at full speed for an hour, after which the drive belt tension was checked and adjusted, the belt required adjusting only once more during the early experiments. Using a stop watch and the digital counter the electronic motor control was set to give the desired revolutions per minute to comply with the velocities required by adjusting the motor speed control potentiometer setting dial shown in Figure 4.43, these settings are noted in table 7.

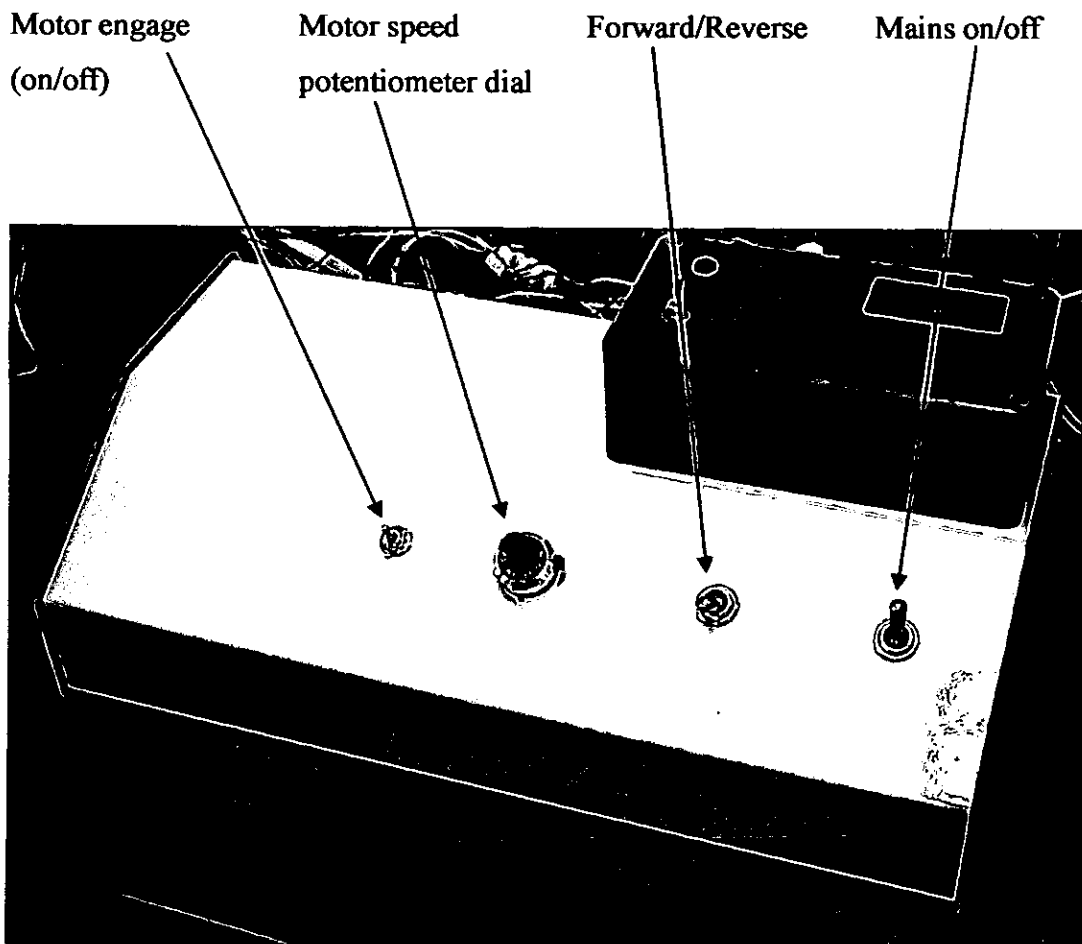


Figure 4.43. Motor speed control unit.

Diameter m	Circumference m	Speed RPM	Speed rev/s	Velocity m/s	Potentiometer setting
0.03	0.09426	65	1.083	0.102	1.0
0.04	0.12568	240	4.000	0.503	4.0
0.05	0.1571	382	6.367	1.000	6.4
0.06	0.18852	638	10.633	2.005	Not used

Table 4.7. Motor control settings.

All masses to be used for the normal load application and calibration of the apparatus were checked using a calibrated digital scale and the actual mass recorded on each individual weight. A free running pulley was clamped securely to the main bed of the test rig in line with the centre of the load application shaft as shown in figure 4.44. A monofilament nylon line (Breaking strain 15Kg) was attached to the upper work holder and the opposite end attached to a small mass holder which had a mass of 50 grams, care was taken to ensure that this line was kept horizontal and in line with the pulley at all times and the specimen holder was held clear of the lower platen.

The recording rate was set on the 'Picollog' data acquisition package to record readings every 10 seconds (sampling rate was set to maximum), a 1kg mass was attached to the mass holder and a reading obtained. Satisfied that everything was in order the mass was removed and the data acquisition package zeroed. Masses were added in 0.5 kg steps and several readings recorded at each level to a maximum of 7kg the masses were then removed again in steps of 0.5 kg to produce the trace shown in figure 4.45.

Temperature and humidity transducers were set up following the instructions supplied Appendix A4 and comparisons made to a calibrated hand held environmental monitoring meter measuring temperature and relative humidity.

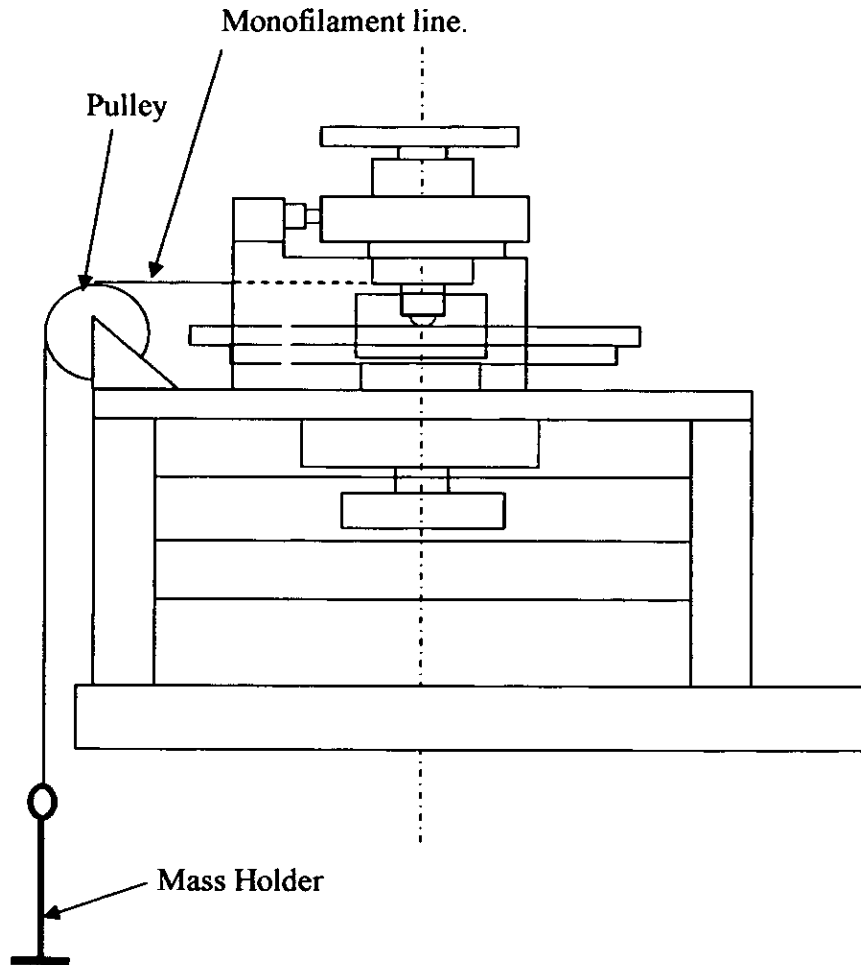


Figure 4.44. Calibration method for force transducers.

Using the readings that generated this trace the calibration curves are plotted in figure 4.46, this procedure was repeated for the high load tests (because a different range setting was needed for the conversion factor as the electronic load protection device changing the load to voltage relationship) and the calibration curve generated. (See figure 4.47.) Both of the curves in Figure 4.46 and 4.47 show a small amount of hysteresis between the measurements taken during loading and unloading, which was deemed to be small enough to ignore, less than 2.25% maximum. Table 4.8 shows the relationship of the nominal mass to the actual mass. Table 4.9 and 4.10 the actual forces applied and the nominal loads (taking account of the mass of shaft and securing bolt.)

The application of the normal loads were checked by use of a digital force gauge on assembly to determine any frictional losses in the sliding supports by lifting the mass

assembly with the force gauge until the counterface was just clear of the disk. Readings were taken of 103N and 10.7N corresponding closely to the calculated values in Tables 4.9 and 4.10.

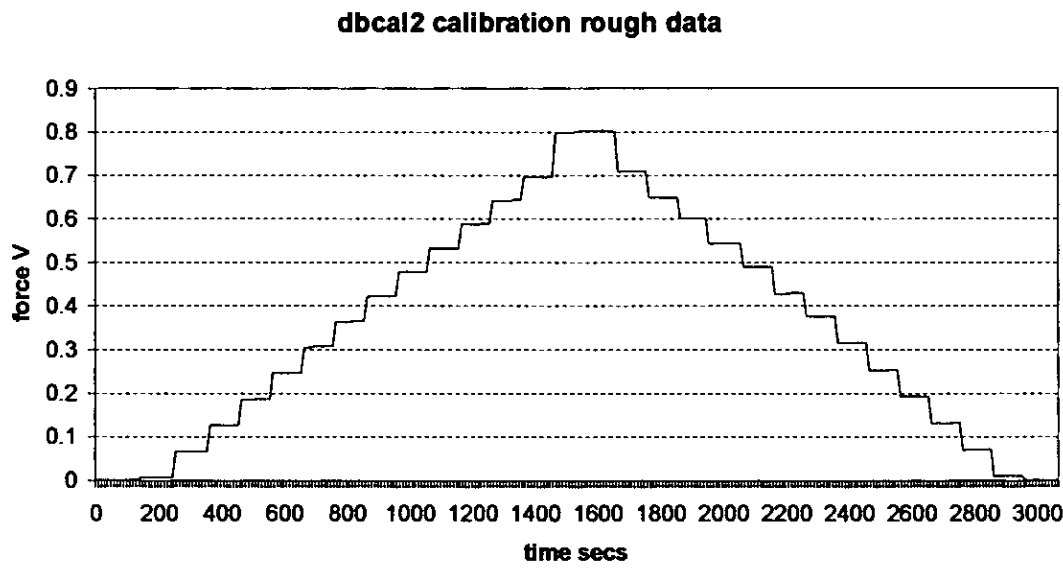


Figure 4.45 Low load calibration data.

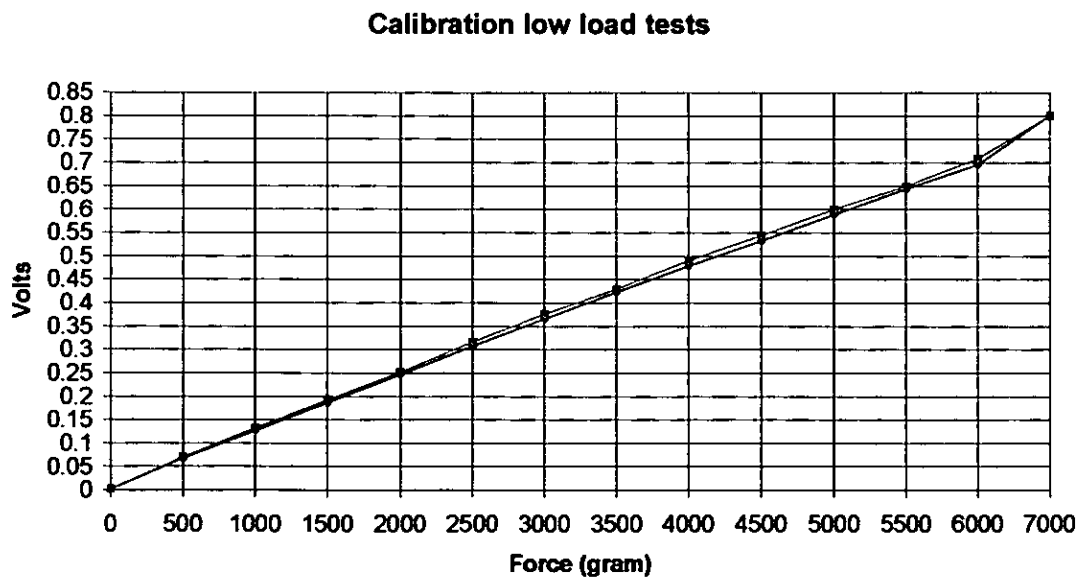


Figure 4.46. Low load Calibration curves.

The data from these curves provided the necessary relationship between the voltage output from the load transducers and the applied load for calculating the friction force and hence the friction coefficient in the graphical data in the experiments described in Chapter 4.

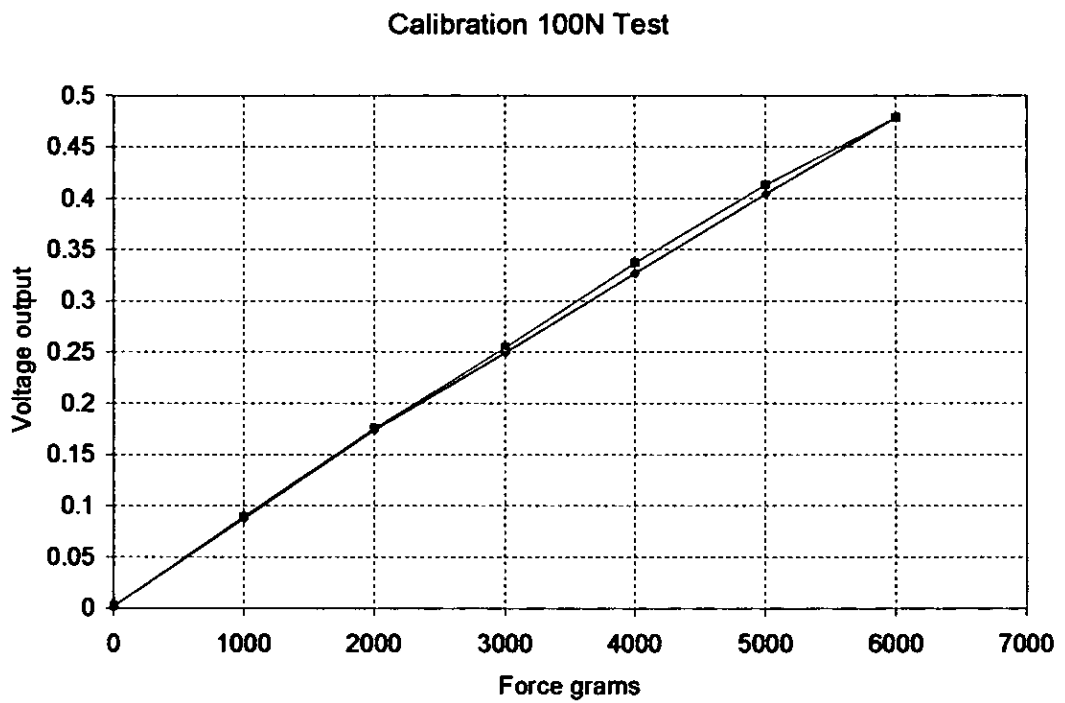


Figure 4.47. Calibration curve 100N tests.

List of masses used.	
Nominal kg	Actual g
0.5	499.5
1	994.4
1	986.1
1	998.8
1	1003.1
2	1995.1
2	1994.0

Table 4.8. Masses used for calibration tests.

Nominal load 10 kg	
Actual Mass g	Nominal kg
9945.9	10
449.1	Shaft assembly
105.8	Bolt & Washer
10500.8	Total
$10.5008\text{Kg} \times 9.81 = 103.013\text{N}$ applied force.	

Table 4.9. Applied force for nominal 100N tests.

Nominal load 1kg	
Actual Mass g	Nominal kg
499.5	0.5
449.1	Shaft assembly
46.4	Screw
100	0.1
1095	Total
$1.095\text{Kg} \times 9.81 = 10.741\text{N}$ applied force	

Table 4.10. Applied force for nominal 10N tests.

It should be noted that all the results given in the following sections are based on the actual values measured as described above i.e. 103 and 10.7

4.2.12. Summary.

The experience gained from the performance of the initial investigation of 12 bonded solid lubricant materials tested on an existing simple reciprocating test facility, indicated that a much more rigid test facility would be required to produce more reliable and consistent results which could be used to investigate the sliding performance of these materials. However the equipment was useful to allow the screening and ranking of the BSLs but not reliable enough for a detailed technical investigation which attempted to quantify effects.

The initial test programme demonstrated the limitations of measuring the deflection of a beam to indicate the friction force in a reciprocating sliding system or in fact any type of sliding contact where a stick slip regime may be present, if the beam is insufficiently damped. Other factors were also observed that could influence the final results such as: motor vibration, inadvertent movement of the specimen holder and application of the normal load.

With these limitations in mind a completely new test facility was designed to allow for pin on disk testing as well as reciprocating type testing, this is described in detail with particular emphasis being given to the rigidity of the apparatus, the vibration free drive and the data acquisition transducers and recording package. Finally, the commissioning and calibration of the new apparatus is described and calibration curves for the load transducers given.

REFERENCES

- [4.1]. Saloman, G., De Gee, A. W. J., Zaat, J. H., "Mechano-chemical factors in MoS₂ lubrication." *Wear* 7, (1964) pp. 87-101.
- [4.2]. "Molykote". Dow Corning. 1991.
- [4.3]. Standard test method for wear life of solid film lubricants in oscillating motion. ASTM 2981-94.
- [4.4]. Standard test method for endurance (wear) life and load-carrying capacity of solid film lubricants. ASTM 2625-94.
- [4.5]. Gee, M. G. "Effect of test machine dynamics on the sliding wear of alumina. Wear testing of advanced materials." Divaker, R., and Blau, P. J., Eds. ASTM STP 1167 Philadelphia (1992) pp. 24-44.
- [4.6]. Alliston-Greiner, A., "Using the energy pulse concept for designing better wear tests." Proceedings of the 21st IRG-OECD meeting "Wear of engineering materials". Amsterdam, Netherlands. (March 1999).
- [4.7]. Plint, M. A., "The energy pulse: A new criterion and its relevance to wear in gear teeth and automotive engine valve trains." Proceedings of the XI NCIT. (January 1995) pp. 185-192.

CHAPTER 5.

DETAILS OF FRICTION MEASUREMENTS ON A BONDED SOLID LUBRICANT FILM AT PRESSURES ABOVE THE YIELD PRESSURE.

A test programme to evaluate the friction performance of a bonded solid lubricant that was selected from the previous screening tests is described. This programme investigates the effects of: counterface surface finish, sliding velocity and applied load. Friction coefficient vs sliding distance data is obtained and the repeatability of the test apparatus demonstrated. These performance curves are discussed and the three distinct regions of performance are identified and discussed.

5.1 Test Programme.

5.1.1 Introduction

Over a period of years, during the routine testing of seat belt buckles at the authors workplace, it had been observed that the surface finish on the mating surface of the connector had a significant effect on their long term performance. Some work has been published on the effect of surface topography of the counterface on the wear of polymers by Jain and Bahadur in 1980 [5.1]. However little work has apparently been published on the effects of the counterface surface finish on the performance of BSLs. This project presents an in depth test programme to study the effects of the counterface surface finish on the lubricant selected from the initial screening test to collect more detailed information for modelling of the performance of this BSL.

operating temperature, operating environment, counterface material, substrate material, substrate hardness, contact pressure, contact geometry, relative motion type,	relative speeds, surface finish, component size and shape, coating thickness, coating uniformity, quantity of parts, economics, including versatility.
--	--

Table 5.1. Factors affecting BSL performance.

If the 15 factors influencing BSL performance listed above in Table 5.1 were to be taken into consideration, the testing time required would be so long that it would not be practical for a PhD project. Therefore most of the variables that can be controlled, were held constant. For example the substrate material hardness and surface finish, was a commercially produced 080M40 Carbon Manganese steel, machined to fine

tolerances and because BSLs are normally applied to hard surfaces, heat treated using the same procedure for each sample. Environmental considerations (humidity and temperature), although not controlled should not vary by more than $\pm 5\%$ in a university laboratory and therefore, can be considered constant. To confirm this humidity and temperature was measured to monitor any variation. This narrowed the parameters of interest to:

- velocity,
- counterface surface finish,
- applied load.

It is acknowledged that tribological effects tend to be more apparent when the variables are in orders of magnitude; this therefore presents a guide to the selection of the velocities and load. The following values were selected taking into consideration the limitations of the apparatus:

- Load 10N and 100N
- Speed 0.1m/s and 1.0m/s

An additional value was selected for the speed (at the mid point of the range selected) at 0.5m/s to be used to give an indication of whether the effects of velocity are linear or otherwise.

5.1.2 Test Specimens

The test specimens consisted of 12mm diameter hardened AISI 51/100 chrome steel balls and ground Disks. The balls were prepared by grit blasting with 3 different grades of carborundum abrasive to achieve the 4 surface finishes as shown in table 5.2

Description	Grit Grade	Roughness $\mu\text{m } R_a$
As Received	None	0.297
Fine (F)	60/80EB	3.01
Medium (M)	24/30EB	4.07
Coarse (C)	16E	4.87

Table 5.2. Surface finish preparation of steel balls.

Figures 5.1, 5.2, 5.3 and 5.4 show the topographic measurements of the ball surface finish (These scans were produced by AEA Technology¹). The topographic data covers a one millimetre square of the ball surface and as well as showing the natural curvature of the ball, illustrate the variation in surface finish generated by the grit blasting process.

Disks of 75mm diameter, 080M40 steel hardened to 55HRC were prepared by radial grinding with the dominant lay direction as illustrated in figure 5.5. They were then grit blasted and manganese iron phosphated prior to coating with the BSL. The disk was coated with a commercial BSL containing PTFE and Graphite in a Polyamide-imide resin binder, the thickness of this coating being $20\mu\text{m} \pm 5\mu\text{m}$. The coating company Armourcote Surface Treatments Limited² used their standard procedure for this particular coating material and no further restraints were exercised.

¹ AEA Technology, Darwin House, 414 The Quadrant, Birchwood Park, Warrington, Cheshire. WA3 6AT

² Armourcote Surface treatments Ltd, Long Causeway, Cross Green, Leeds. LS9 0NY

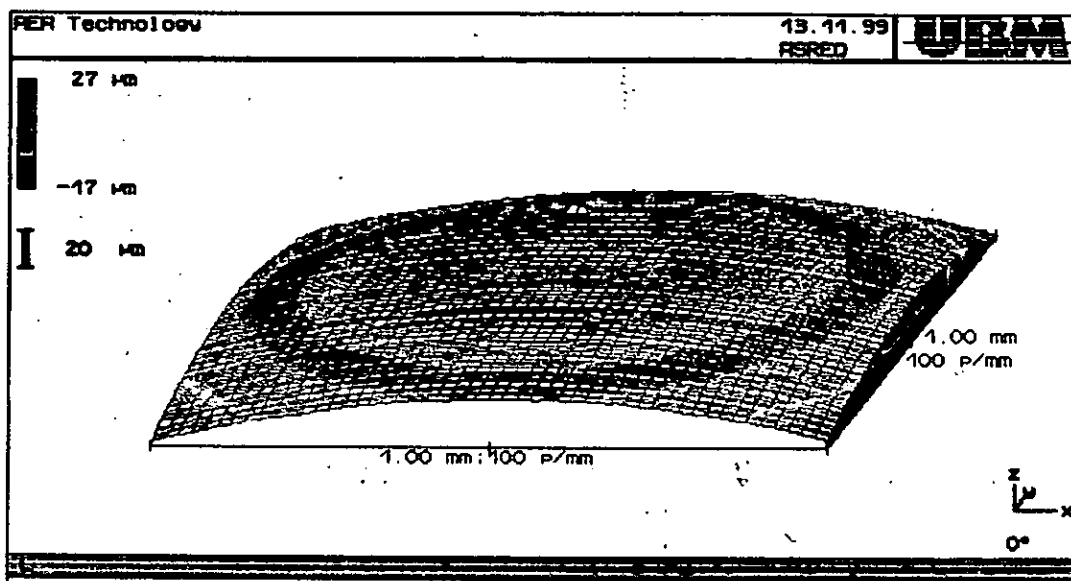


Figure 5.1. Surface scan of as received sample.

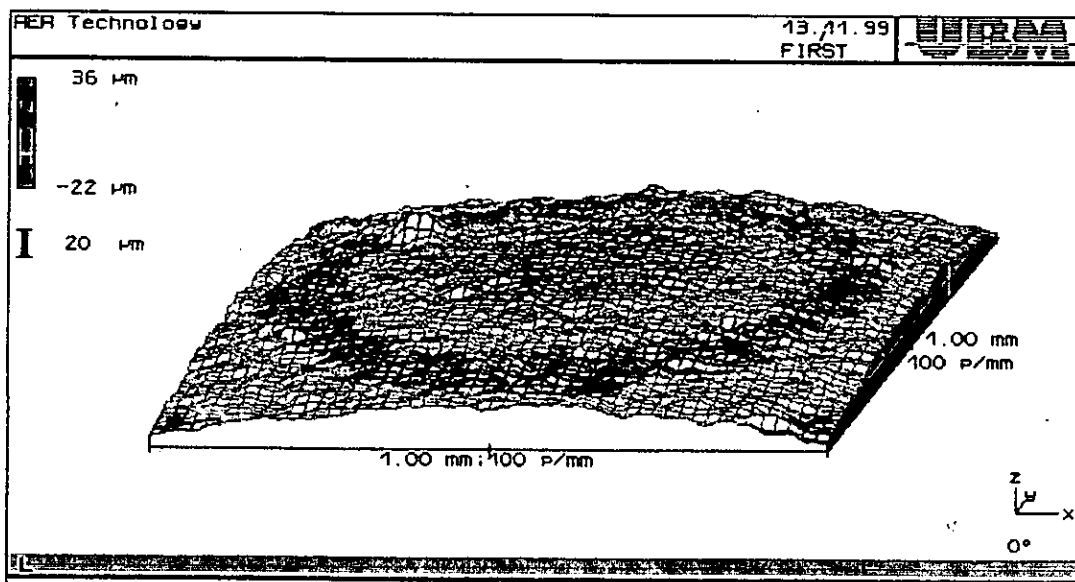


Figure 5.2. Surface scan of fine grit blasted sample.

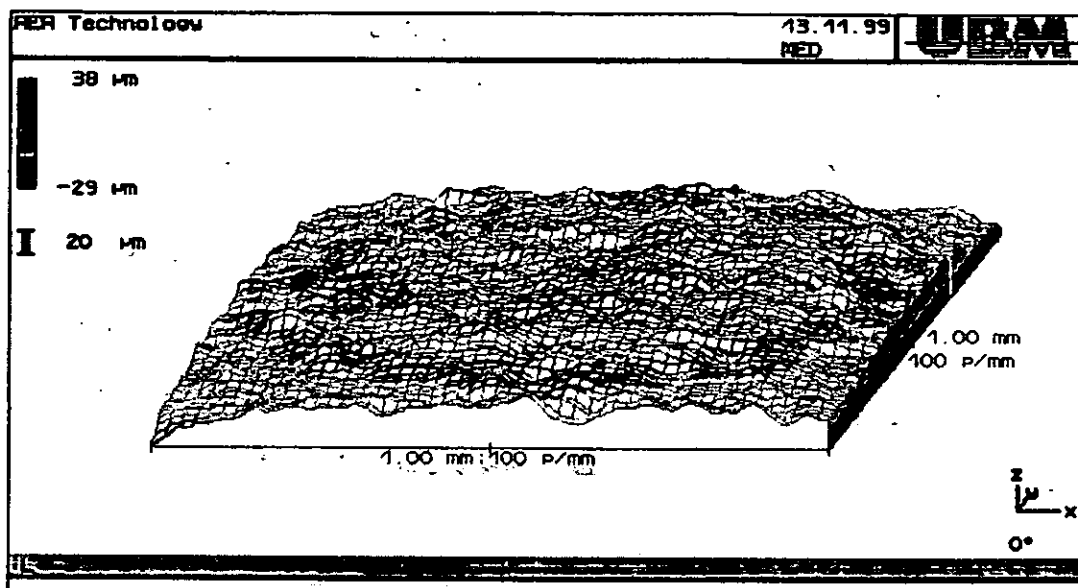


Figure 5.3. Surface scan of medium grit blasted sample.

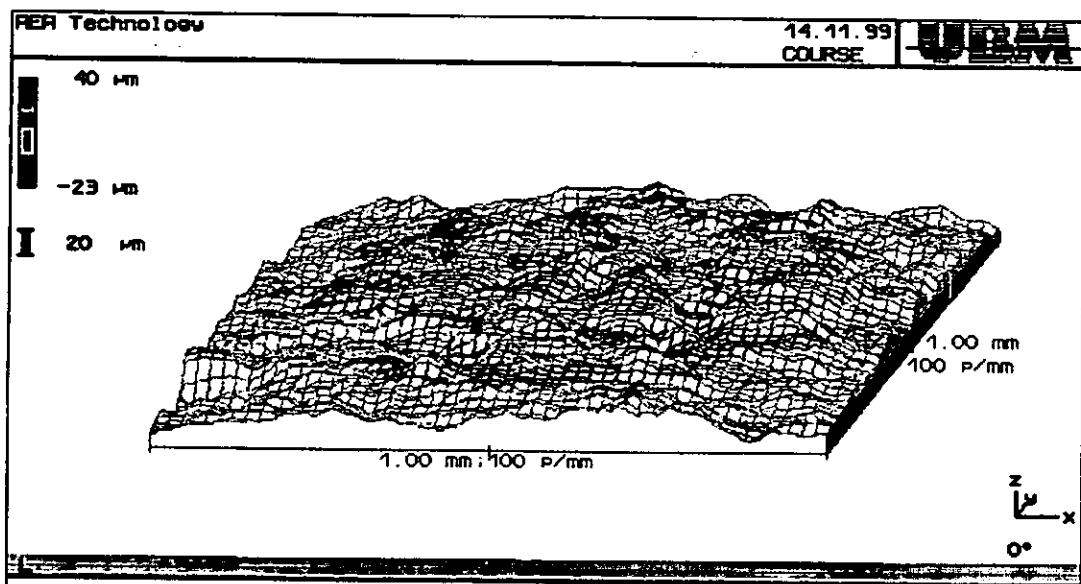


Figure 5.4. Surface scan of coarse grit blasted sample.

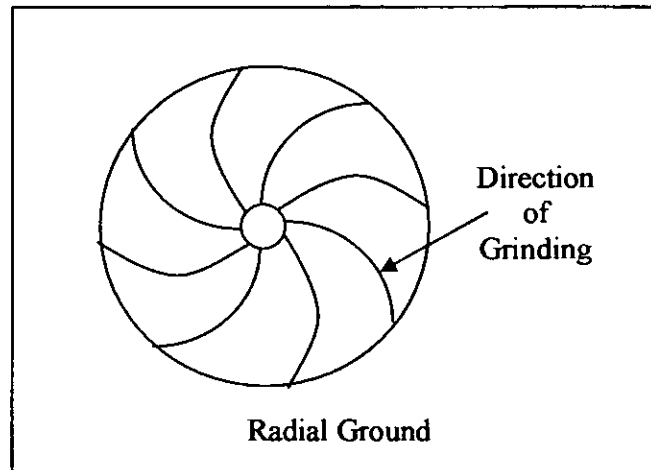


Figure 5.5. Disk grinding pattern.

5.1.3 Test conditions.

The test apparatus described in Chapter 4 was used in the pin on disk configuration for all the tests. The three sets of variables to be tested are presented in table 5.3. An 'X' denotes one test run, giving 24 tests in total. For a check of repeatability of experiments one repeat would give 48 test runs, the actual tests repeated are indicated with an 'x', the basic test programme is illustrated more clearly in tree format in figure 5.6.

Speed ms^{-1}	0.1		0.5		1.0	
	10N	100N	10N	100N	10N	100N
Finish						
As rec'd	X	Xx	X	Xx	Xx	Xx
Fine	X	Xx	X	Xx	Xx	Xx
Med	X	Xx	X	Xx	X	Xx
Coarse	X	Xx	X	Xx	Xx	Xx

Table 5.3. Test matrix.

Table 5.4 presents a matrix listing the combinations of motor RPM / sliding velocity / sliding distance employed and is used to estimate the test duration. Table 5.5 gives

details of the operating conditions for each test. The test programme of 48 test runs could be accomplished by conducting 3 tests per side (6 per Disk) and therefore required eight disks.

Diameter m	Circumference m	Speed RPM	Speed Rev s ⁻¹	Velocity ms ⁻¹	Distance mhr ⁻¹	Distance covered in 24hr m
0.03	0.094	65	1.083	0.102	367.2	8,812
0.04	0.125	240	4	0.502	1807.2	43,372
0.05	0.157	382	6.366	1.002	3607.2	86,572
0.06	0.188	319	5.316	1.002	3607.2	86,572

Table 5.4. RPM – Velocity – Sliding distance matrix.

Test No	Velocity ms ⁻¹	Track diameter m	Finish	Load	
				H	L
1 & 13	0.1	0.03	As rec'd	1	13
2 & 14	0.1	0.03	F	2	14
3 & 15	0.1	0.03	M	3	15
4 & 16	0.1	0.03	C	4	16
5 & 17	0.5	0.04	As rec'd	5	17
6 & 18	0.5	0.04	F	6	18
7 & 19	0.5	0.04	M	7	19
8 & 20	0.5	0.04	C	8	20
9 & 21	1.0	0.05	As rec'd	9	21
10 & 22	1.0	0.05	F	10	22
11 & 23	1.0	0.05	M	11	23
12 & 24	1.0	0.05	C	12	24

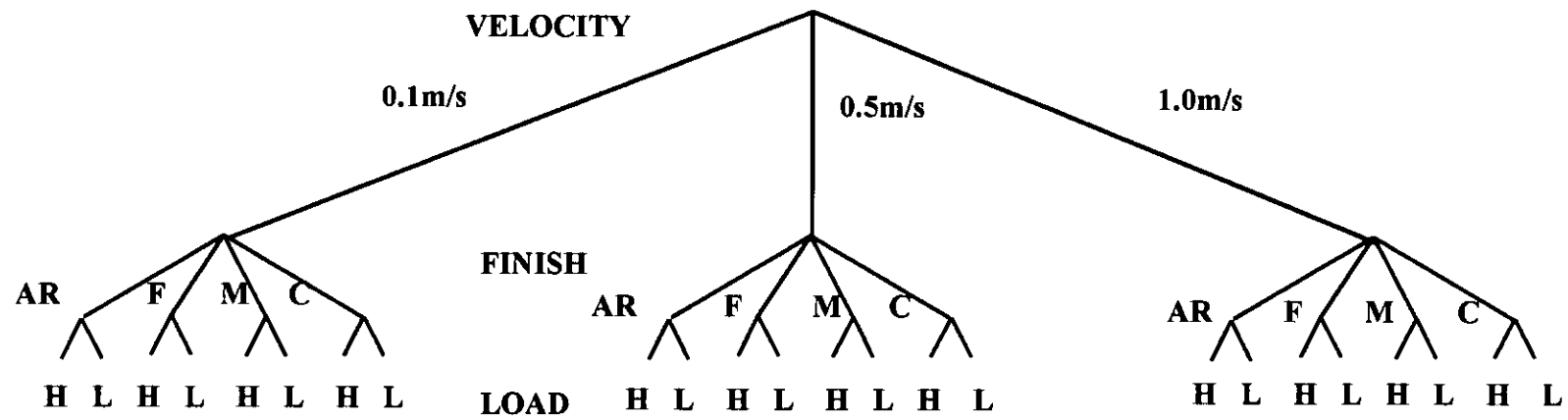
L = 10N H = 100N

Table 5.5. Matrix of test conditions.

5.1.4 Test procedure.

The tests were conducted by mounting the samples in the pin on disk apparatus which had previously been set to the relevant parameters, i.e. speed, test diameter and load. The Pico soft data acquisition package was set to record readings of friction force, temperature, relative humidity and time every 10 seconds. The main drive motor was switched on and the ball lowered slowly into contact with the disk. This setup was allowed to run for two hours until the friction signal began to level off. Readings were then taken every 5 minutes until the completion of the test (when the friction coefficient reached 0.3). In the case of test 21 (and its repeat 45), the test was stopped on reaching a sliding distance of 500km, due to the length of time required and there being no indication of failure. Data was transferred approximately every 12 hours to an Excel spreadsheet and the friction coefficient / distance traces generated.

The same procedure was used for the 100N load tests except that the load protection switch was wired in circuit, this automatically stopped the main drive motor when a friction force of 30N (friction coefficient of 0.3) was reached. All of the 100N load tests were repeated to assess the repeatability of the test apparatus with three of the 10N load tests being repeated, it was decided at this point that the repeatability had been demonstrated and the last nine tests would not be conducted due to the length of time required.



H = 100N

L = 10N

AR as received.

F Fine

M Medium

C Coarse

Figure 5.6. Test programme diagram.

5.2. Results and Discussion.

5.2.1. Results.

The following figures 5.7 - 5.10 contain the friction coefficient data plotted against distance travelled for the 10N load tests. In each case the colours of the traces are consistent throughout the series of graphs, blue representing the as received (smoothest) counterface, pink the fine grit blasted sample, green the medium grit blasted sample and orange the coarse sample. Likewise figures 5.11 – 5.16 contain the data for the 100N load tests, again the colours of the traces follow the same regime as the 10N tests.

It should be noted that although the friction coefficient axis is common throughout, the distance axis is not, figures 5.17 and 5.18 are included to show the overall comparison of each series of tests.

If the point of failure is specified to be where the friction coefficient begins its sharp rise towards the end of the graphs then the distances at this point can be recorded. These are shown in figures 5.20 and 5.21 distance against velocity and figures 5.22 to 5.24 for distance against load.

In general the figures 5.7 – 5.16 highlight the effect of surface finish on the sliding performance whereas figures 5.17 and 5.18 highlight the more dramatic effect of velocity on the sliding performance of the BSL.

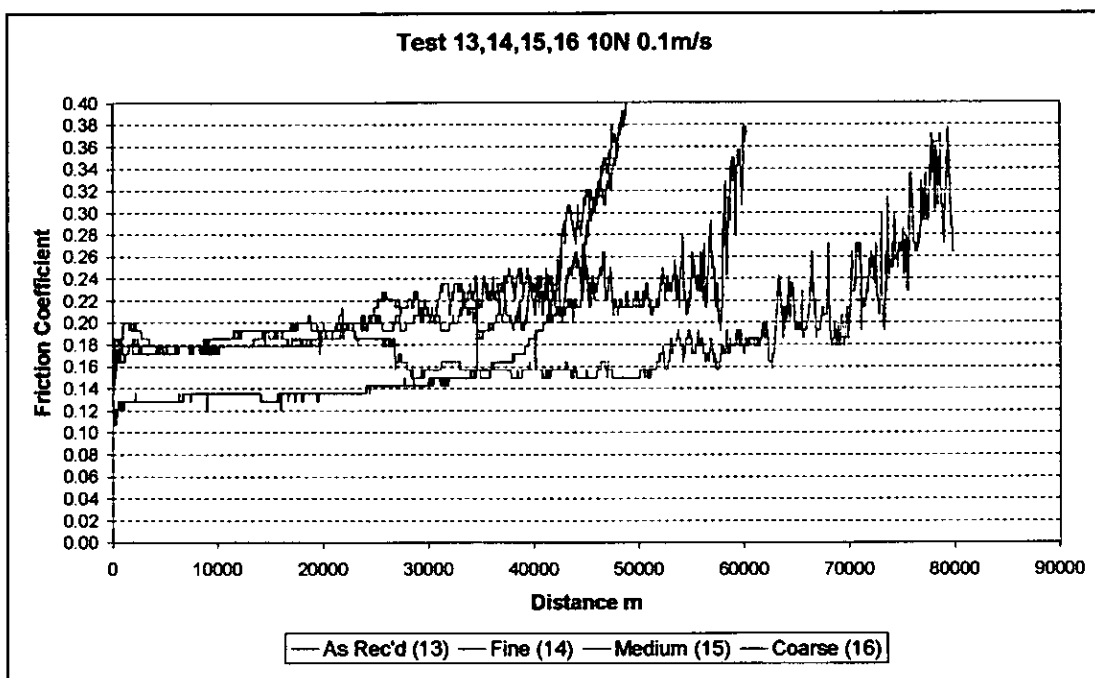


Figure 5.7. Friction coefficient vs distance for 10N load @ 0.1ms^{-1}

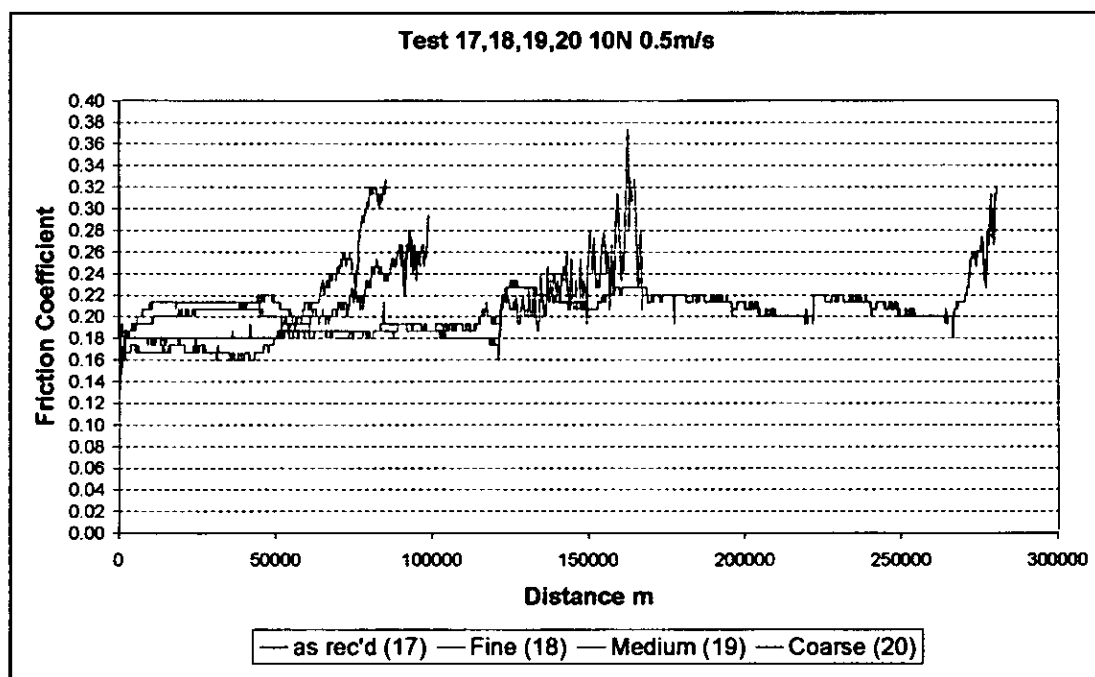


Figure 5.8. Friction coefficient vs distance for 10N load @ 0.5ms^{-1}

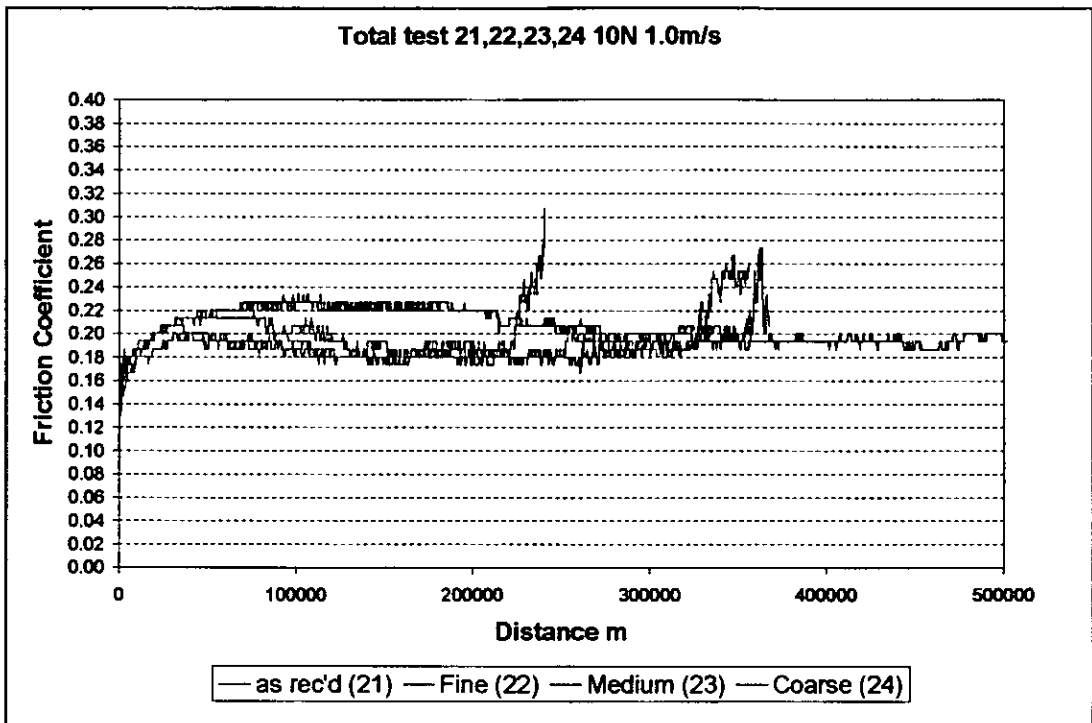


Figure 5.9. Friction coefficient vs distance for 10N load @ 1.0ms^{-1}

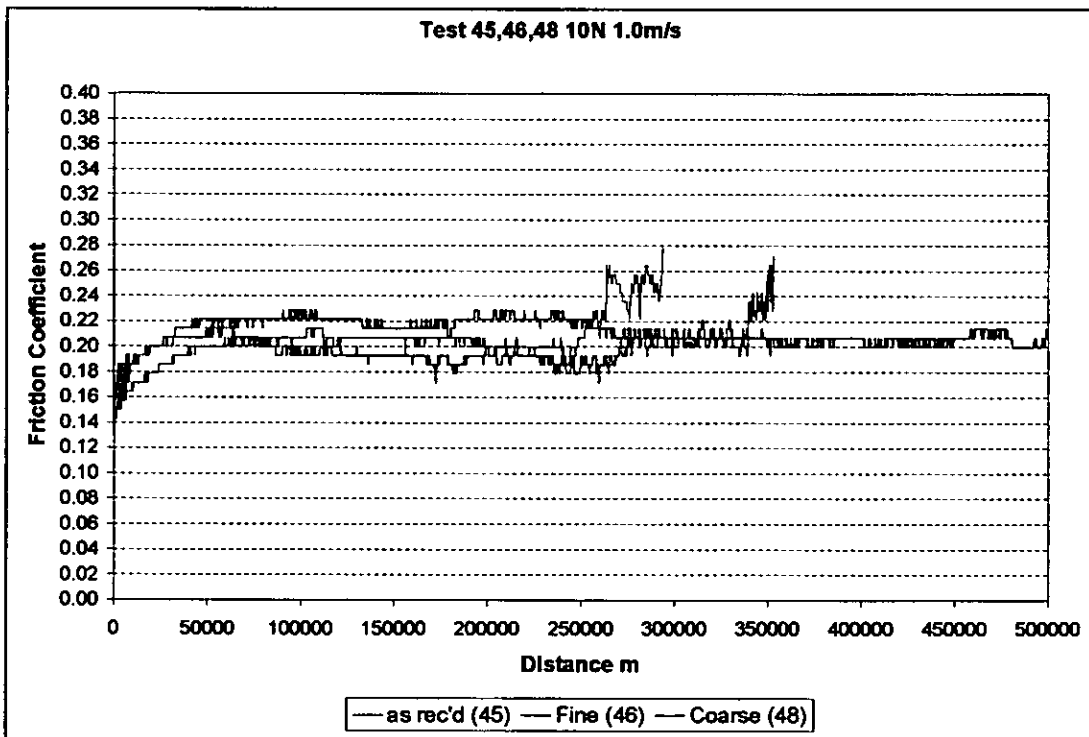


Figure 5.10. Repeat of 10N @ 1.0ms^{-1} test.

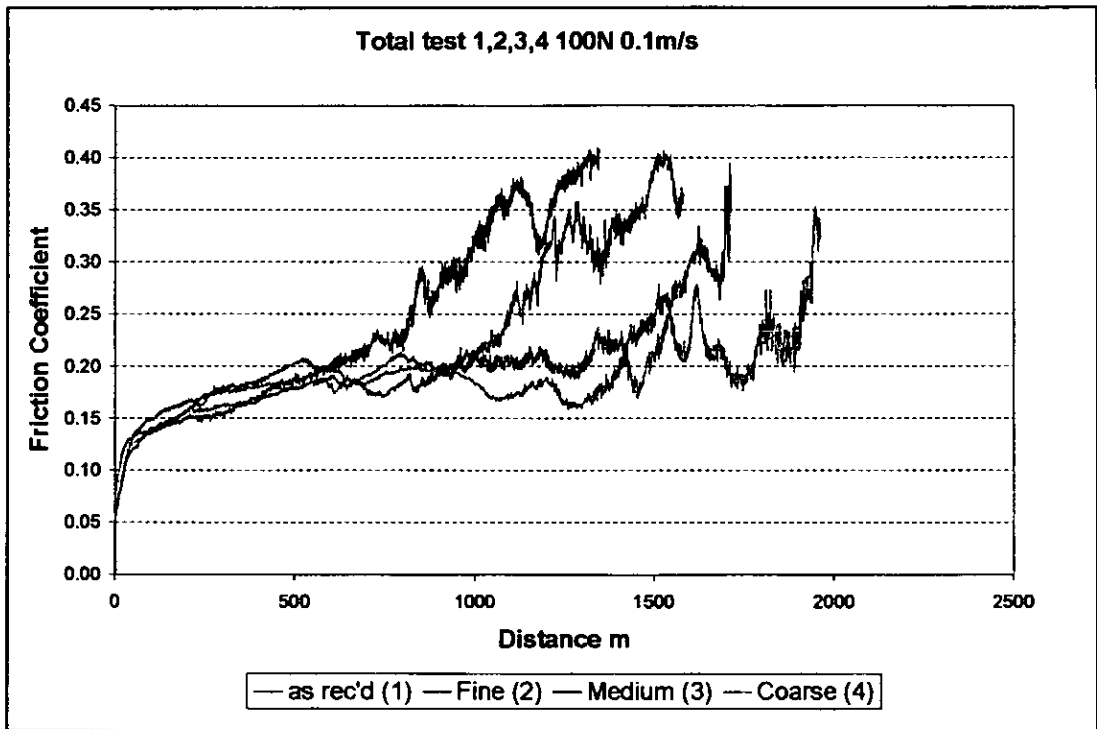


Figure 5.11. Friction coefficient vs distance for 100N load @ 0.1ms^{-1}

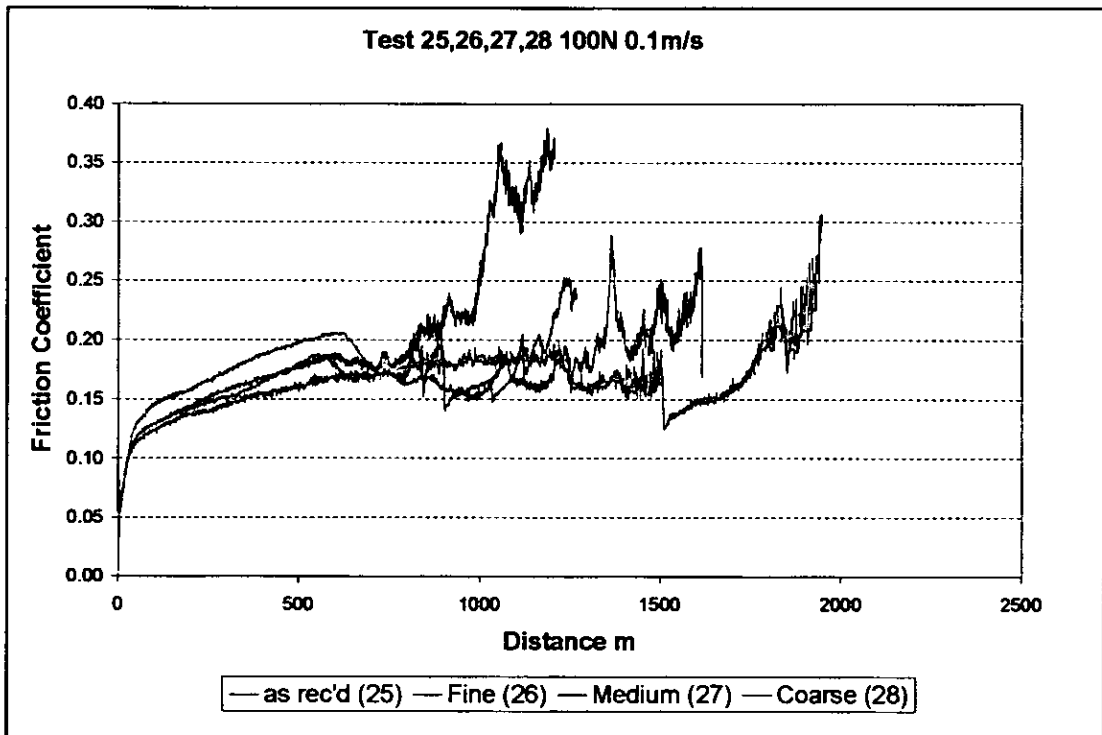


Figure 5.12. Repeat of 100N @ 0.1ms^{-1} test.

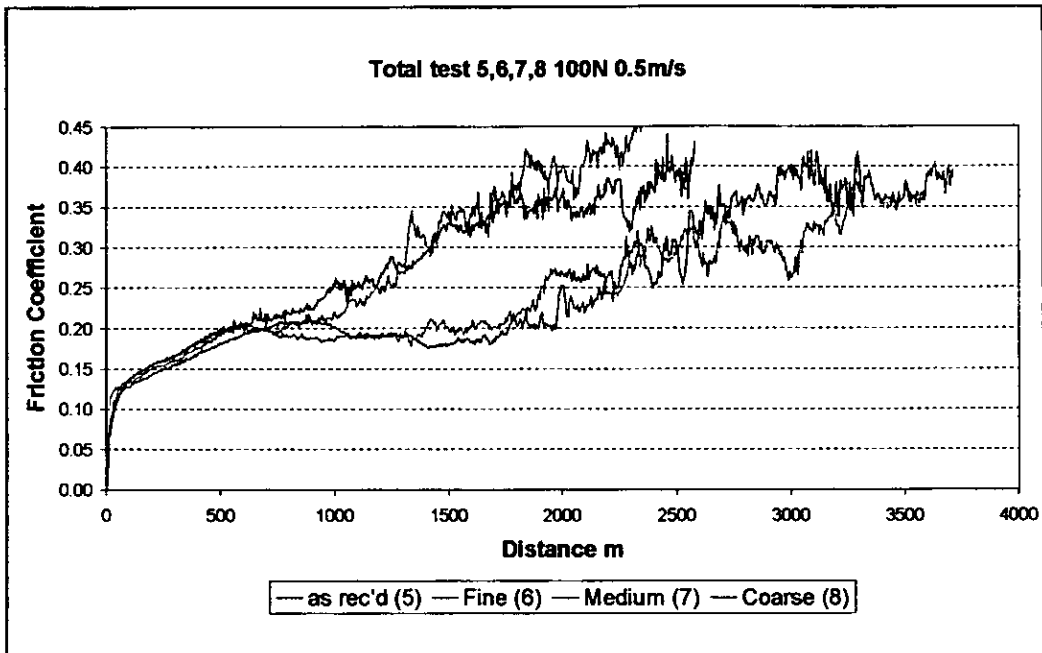


Figure 5.13. Friction coefficient vs distance for 100N load @ 0.5ms^{-1}

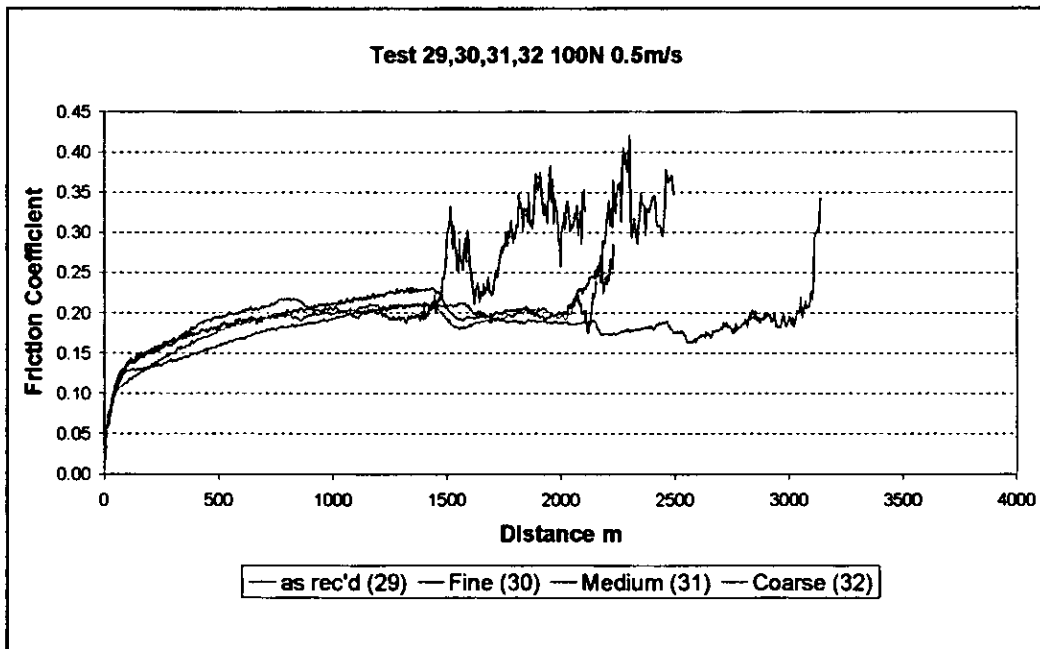


Figure 5.14. Repeat of 100N @ 0.5ms^{-1} test.

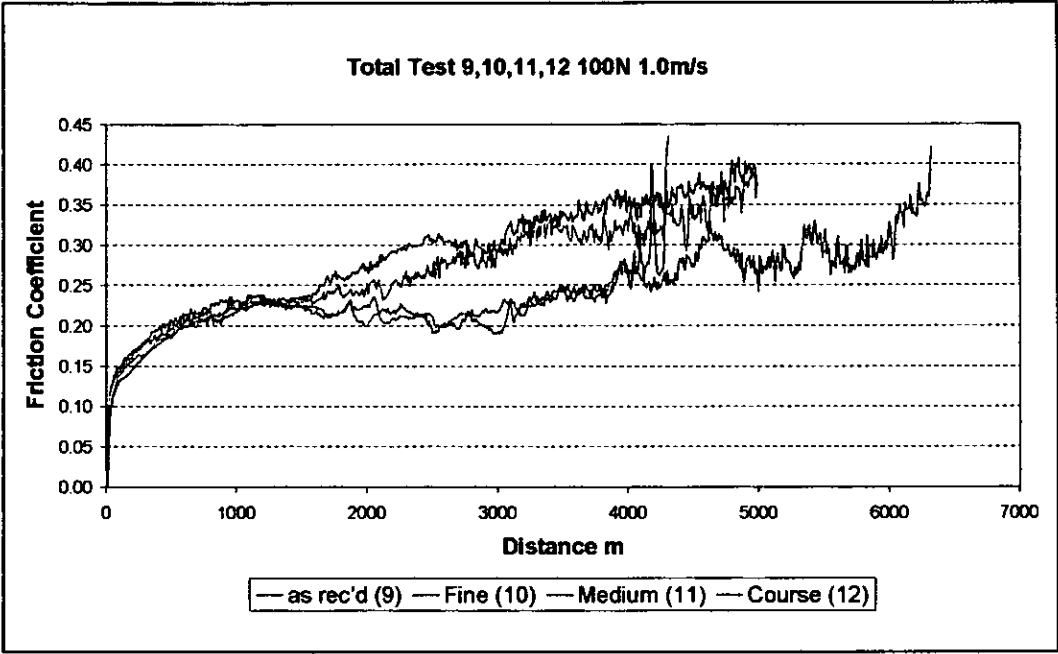


Figure 5.15. Friction coefficient vs distance for 100N load @ 1.0ms^{-1}

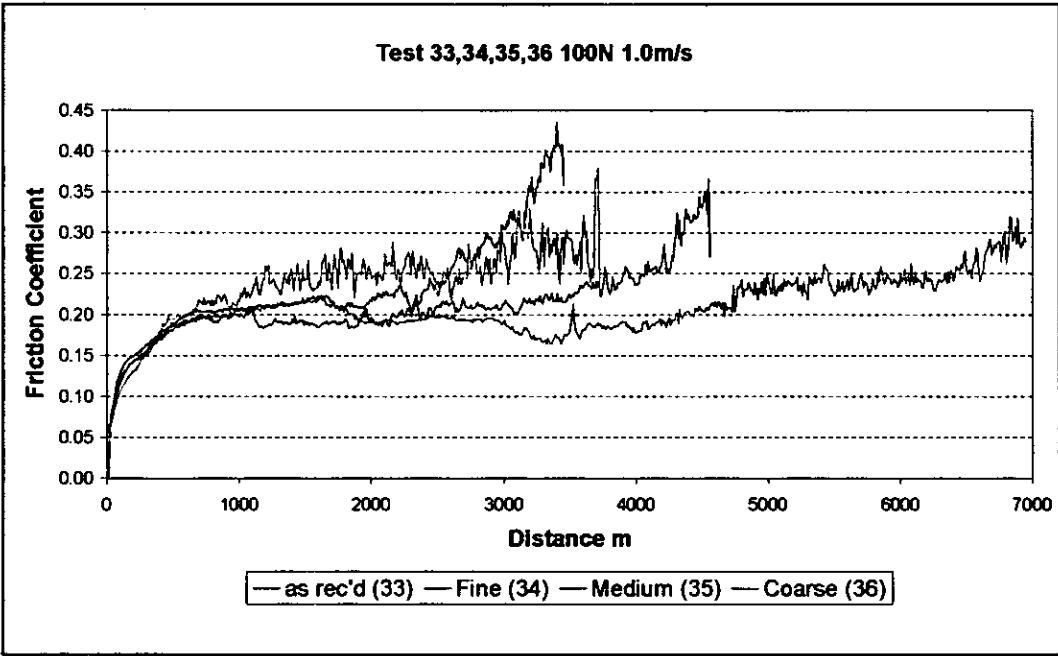


Figure 5.16. Repeat of 100N @ 1.0ms^{-1} test.

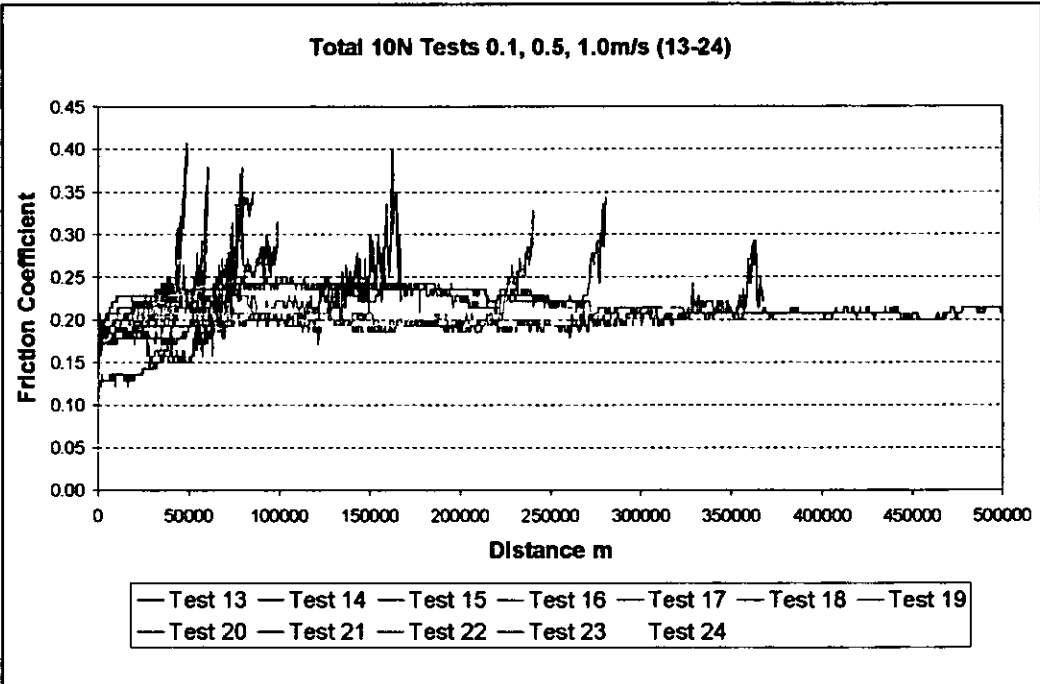


Figure 5.17. All results 10N load tests.

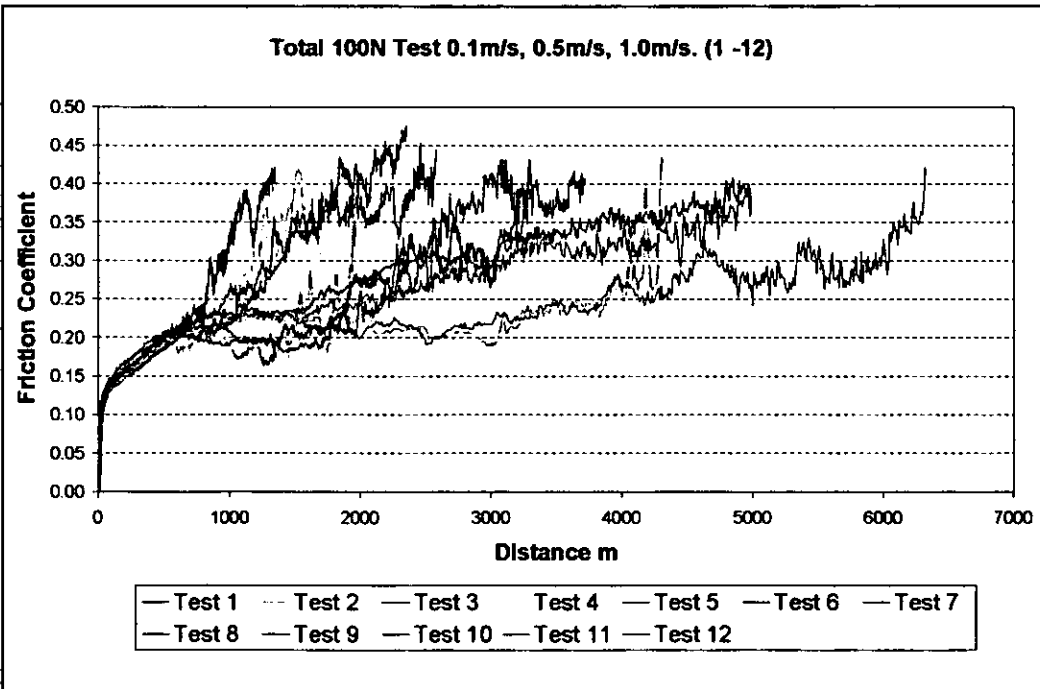


Figure 5.18. All Results 100N load tests.

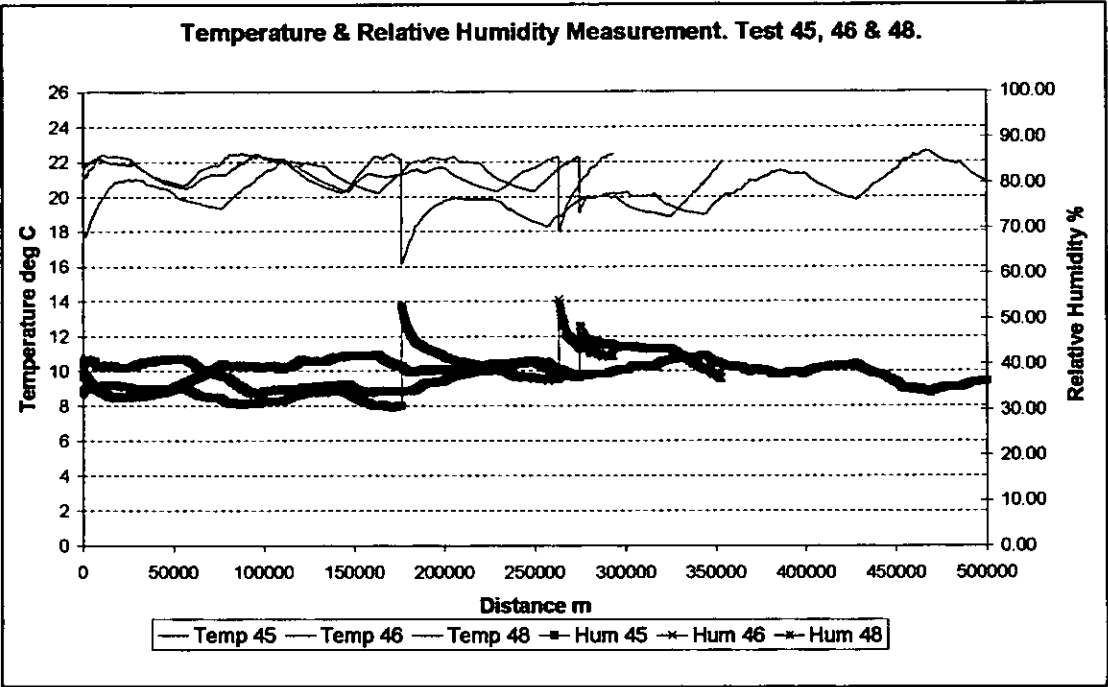


Figure 5.19. Temperature and Relative Humidity Measurement.

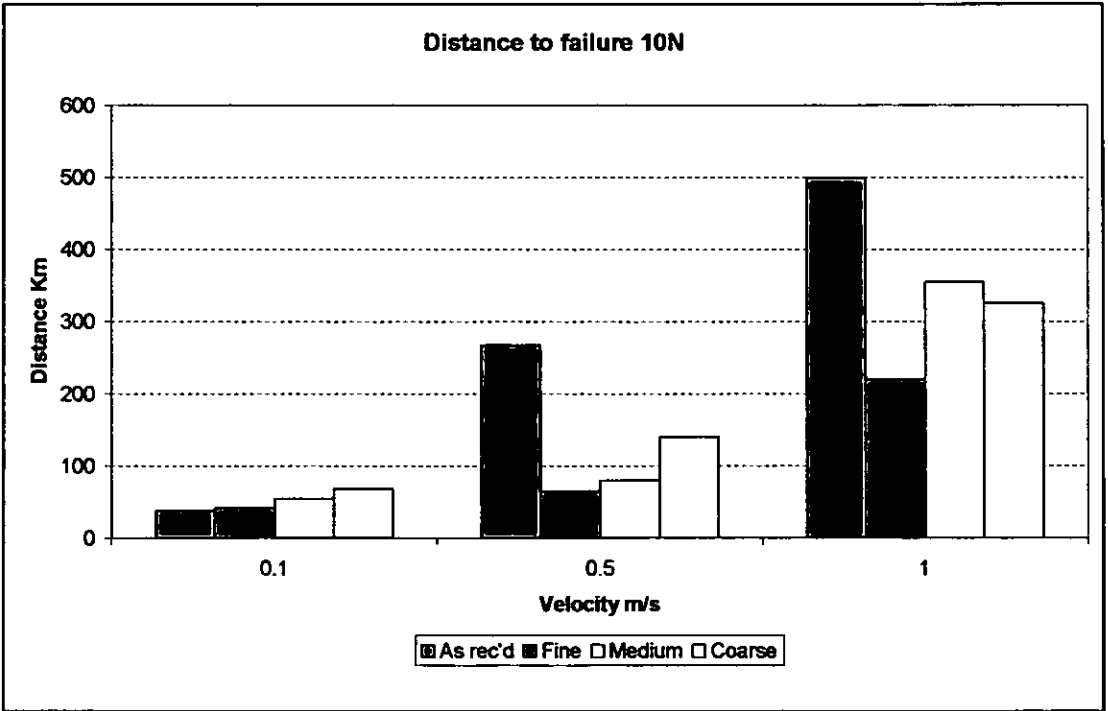


Figure 5.20 Distance to failure 10N load.

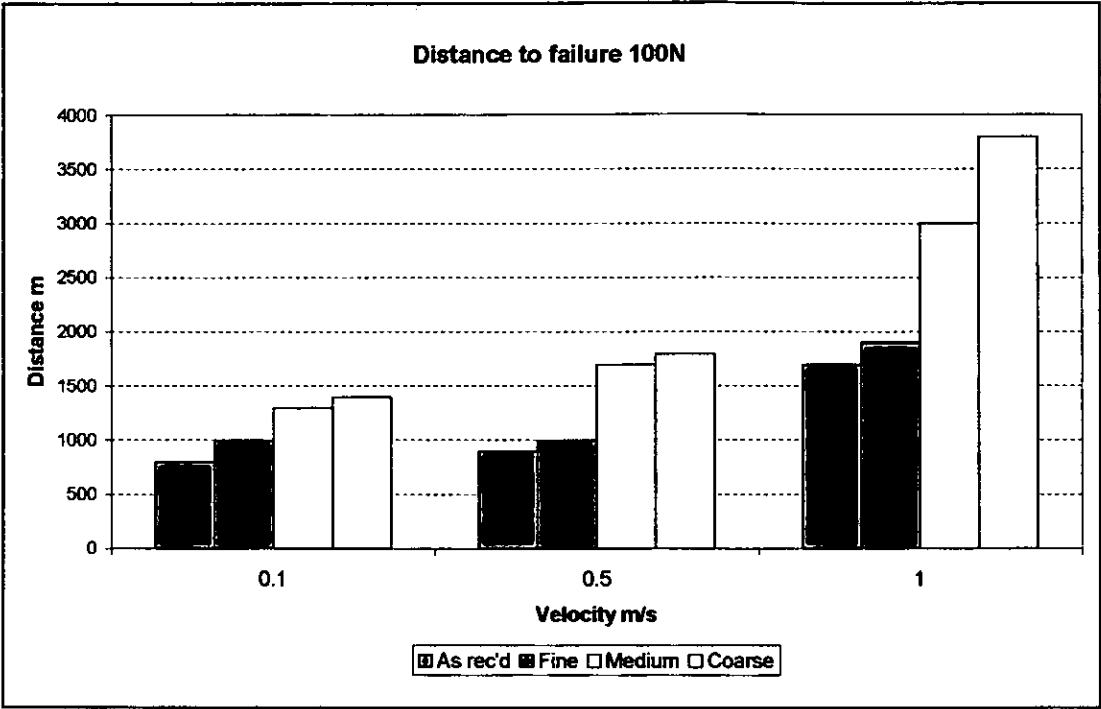


Figure 5.21 Distance to failure 100N load.

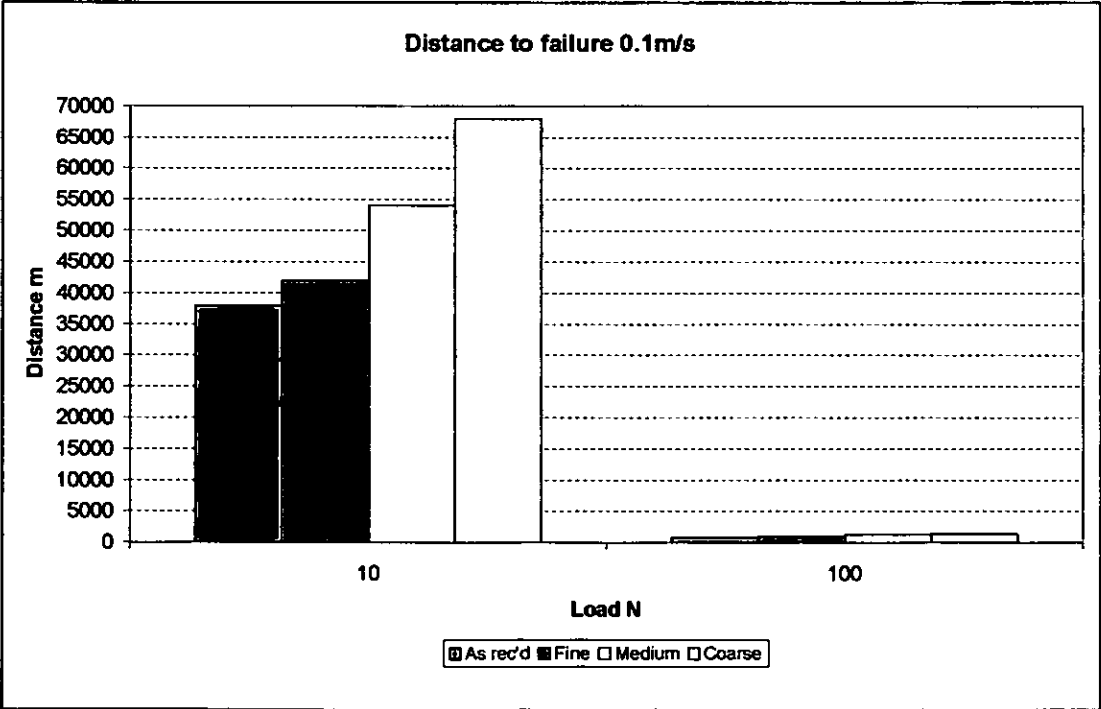


Figure 5.22 Distance to failure 0.1ms⁻¹

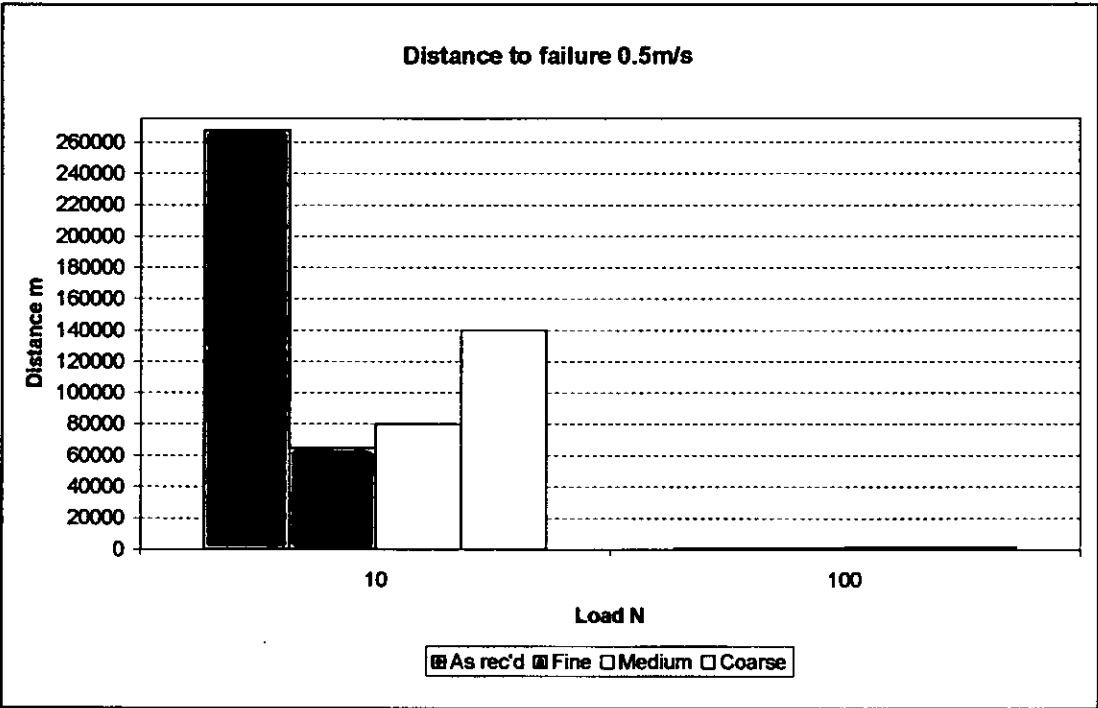


Figure 5.23 Distance to failure 0.5ms⁻¹

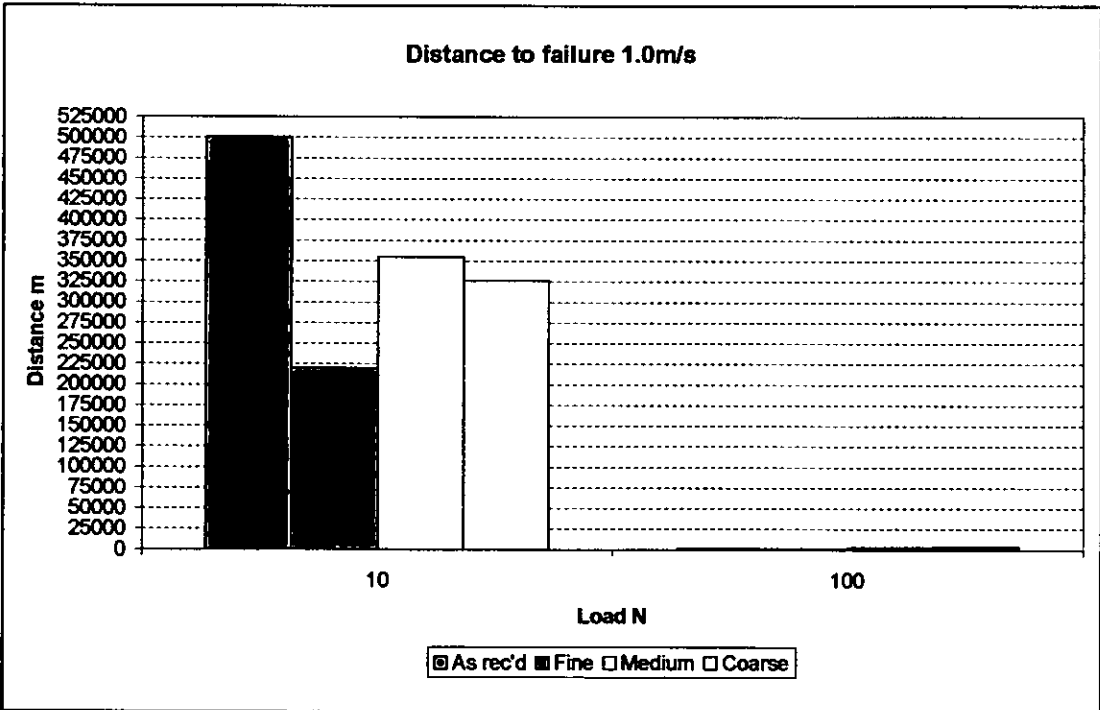


Figure 5.24 Distance to failure 1.0ms⁻¹

5.2.2. Discussion of results.

The results obtained demonstrate three distinct regions of performance as a function of sliding distance and friction coefficient:

- A region where the friction coefficient increases slowly over similar periods of time for each particular finish (This is not as apparent as velocity reduces in the 10N load tests).
- A region where the friction coefficient remains relatively stable (This is also barely noticeable for some of the high load tests).
- A region where the friction coefficient is erratic and increases rapidly.

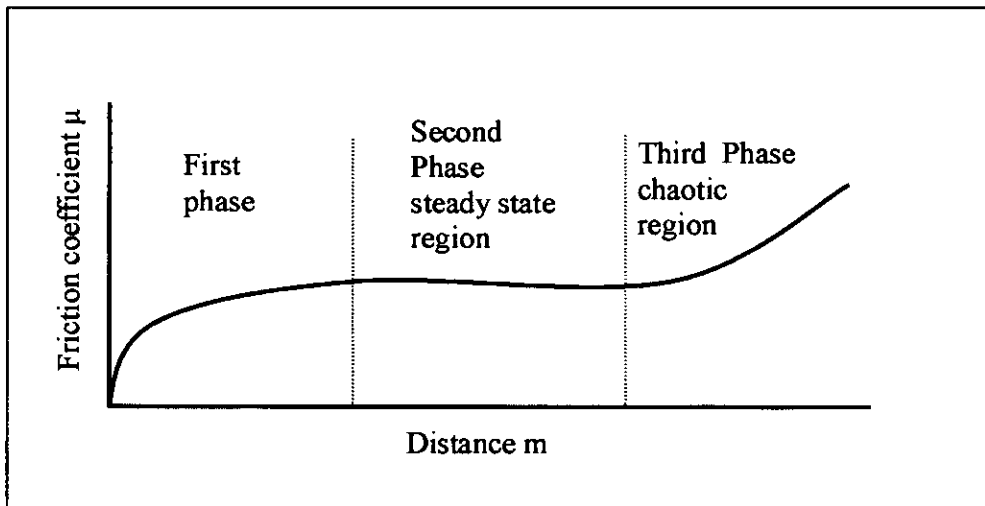


Figure 5.25. Generalised performance phases.

In general the friction coefficient is comparable at the steady state region for all test samples lying between $\mu = 0.18$ and $\mu = 0.24$.

If the useful life is taken as the length of time or distance to where the friction coefficient begins to ramp up rapidly, then in general the following observations can be made with respect to velocity, counterface roughness, wear behavior, friction coefficient and load, for the 10N Load tests:

- Life / sliding distance reduces as velocity reduces.
- Counterface roughness has little effect on the friction coefficient in the initial stage.
- Increased counterface roughness markedly affects the life in the second and third stages but not as may be intuitively expected i.e. the fine grit blasted finish produced the shortest overall sliding life and the as received finish (the smoothest) the longest, however for tests performed at 0.1ms^{-1} the sliding life increases marginally as roughness increases figures 5.20 and 5.22.

For the 100N load tests:

- Behaviour is similar to the low load tests, life / sliding distance reduces as velocity reduces.
- Counterface roughness has little effect on the friction coefficient in the initial stage but does affect the sliding life in the second and third stages, in general an increase in roughness provides an increase in sliding distance when compared with the as received finish.
- Test results are repeatable for the first region with reasonable repeatability for the later stages.

Figures 5.20 and 5.21 show the effect of counterface surface finish and velocity at each loading condition. The figures 5.22 to 5.24 demonstrate the effect of the applied load for each velocity.

Typical example of Temperature and Humidity measurements are shown in figure 5.19 the upper traces show the temperature data recorded over the life of the tests and the lower traces the recorded relative humidity data. The discontinuities in the traces are due to the tests being stopped over the weekend.

5.3. Summary.

The friction data for a particular BSL and four counterface surface finishes has been generated for both high and low load conditions at three velocities and the friction coefficient / Distance graphs plotted. The effect of velocity on sliding life of the lubricant has been demonstrated i.e. sliding distance reduces as velocity is reduced. Also the surface finish has been demonstrated to have an effect on sliding life but not as significant as sliding velocity.

One of the problems with the testing of BSL materials highlighted in this test programme is the amount of time required for each individual test, initially the first tests at a velocity of 1.0 metre per second were only allowed to be performed during normal working hours (08:00 to 20:00 hours) taking 5 weeks in total to complete, even running 24 hours a day these tests took 15 days (running continuously). Therefore in a commercial environment the scant amount of data generated may be seen as not to be economically viable.

REFERENCES.

- [1] Jain. V. K. Bahadur. S. Surface topography changes in polymer-metal sliding – 1. Transactions of the ASME Vol 102 (1980) 520-525.

CHAPTER 6.

OPTICAL EXAMINATION OF TEST SAMPLES AND WEAR SCAR GENERATION UNDER DIFFERENT REGIMES OF DRY SLIDING CONTACT.

In the first part of this chapter the ball wear scars and disc wear tracks produced by the test programme described in chapter 5 are examined by optical microscopy and their digital photographs reproduced. The characteristics of these scars and tracks are discussed.

The second part of the chapter describes the test programme to evaluate the evolution of the wear scar and track during the early stages of sliding and the corresponding friction coefficient at each stage. The development of the wear scars are discussed from 25m to 50km sliding distance.

In the third part the friction performance of a bonded solid lubricant below the yield pressure of the film is described. This programme evaluates the effects of: counterface surface finish, sliding velocity and at various loads that generate a pressure at the counterface that is below or close to the yield pressure of the applied film. The friction coefficients are obtained for each condition and analysed statistically. The wear scar on the ball and corresponding wear track on the disc are illustrated and discussed.

Finally the individual contact spots generated by the static loading a 12mm diameter ball from 10 to 100N in increments of 10N are examined and recorded graphically. A methodology for predicting the contact spot diameter for hard materials that are coated with BSLs is discussed and values calculated.

6.1. Optical examination of test samples.

6.1.1 Introduction.

After completion of the test programme described in chapter 5 the samples were examined under an optical microscope and digital photographs taken of the ball wear scar and the disc wear track. The wear scar and disc track were also measured for the first 24 tests and are recorded in table 6.1 and 6.2.

Test No	Ball wear scar diameter	Disc track width	Ball finish	Disc velocity ms^{-1}
1	3.04	3.13	As rec'd	0.1
2	3.03	3.30	Fine	0.1
3	2.48	2.73	Med	0.1
4	2.48	2.97	Coarse	0.1
5	3.70	3.80	As rec'd	0.5
6	3.62	3.90	Fine	0.5
7	3.32	3.51	Med	0.5
8	3.48	3.68	Coarse	0.5
9	4.20	4.31	As rec'd	1.0
10	4.22	4.45	Fine	1.0
11	3.55	3.68	Med	1.0
12	3.49	2.95	Coarse	1.0

Table 6.1 Wear scar and disc track 100N test loads tests 1to12.

For the 100N tests the wear scars and wear tracks were all very similar in appearance and only varied as recorded above. The wear scar on the ball on the as received finish and fine finish being almost the same size in each velocity group, as are the wear scars on the medium and coarse finished balls. This wear scar being composed of scratches and grooves in the direction of sliding with small protrusions to either side that correspond to the track width, these are shown in the following figures 6.1 – 6.4.

Test No	Ball wear scar diameter	Disc track width	Ball finish	Disc velocity ms⁻¹
13	3.21	3.40	As rec'd	0.1
14	2.6	2.84	Fine	0.1
15	3.09	3.26	Med	0.1
16	2.87	3.15	Coarse	0.1
17	3.34	3.52	As rec'd	0.5
18	3.15	3.45	Fine	0.5
19	3.53	3.63	Med	0.5
20	2.94	3.33	Coarse	0.5
21	3.60	3.80	As rec'd	1.0
22	3.34	3.56	Fine	1.0
23	3.91	4.26	Med	1.0
24	3.53	3.75	Coarse	1.0

Table 6.2 Wear scar and disc track 10N test loads tests 13 to 24.

For the 10N load the wear scars and wear tracks again were very similar in appearance to those of the 100N tests and varied in size as above.

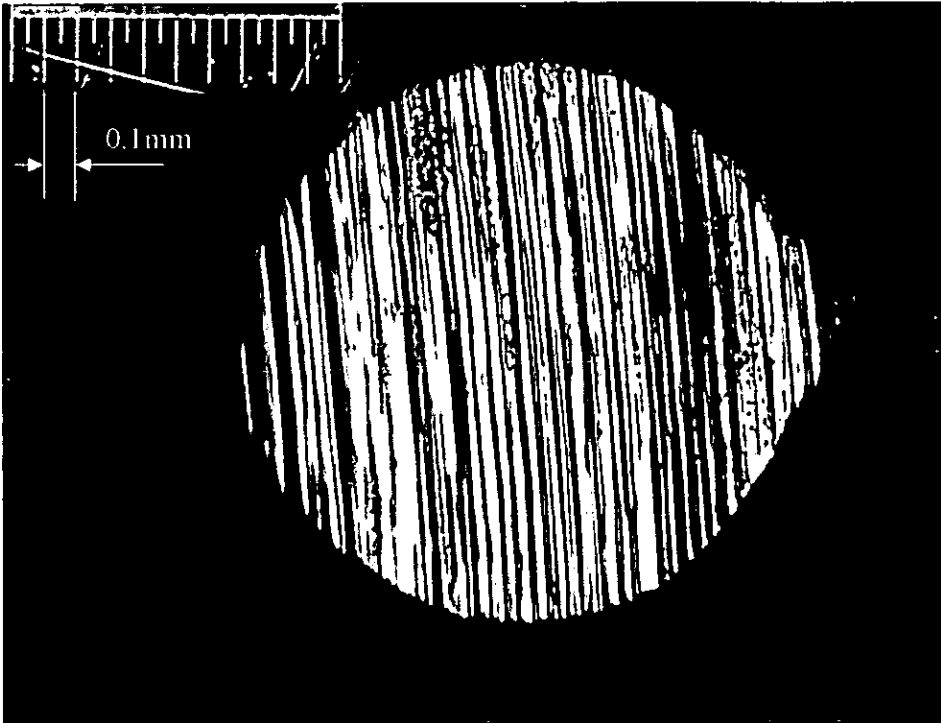


Figure 6.1 Ball wear scar.

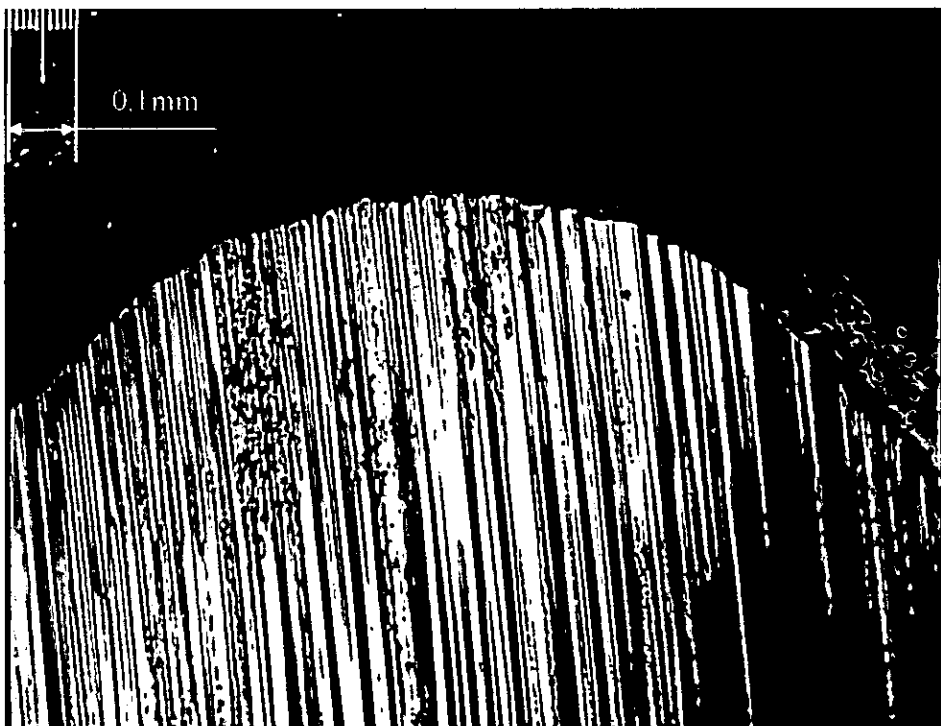


Figure 6.2 Trailing edge of ball wear scar.

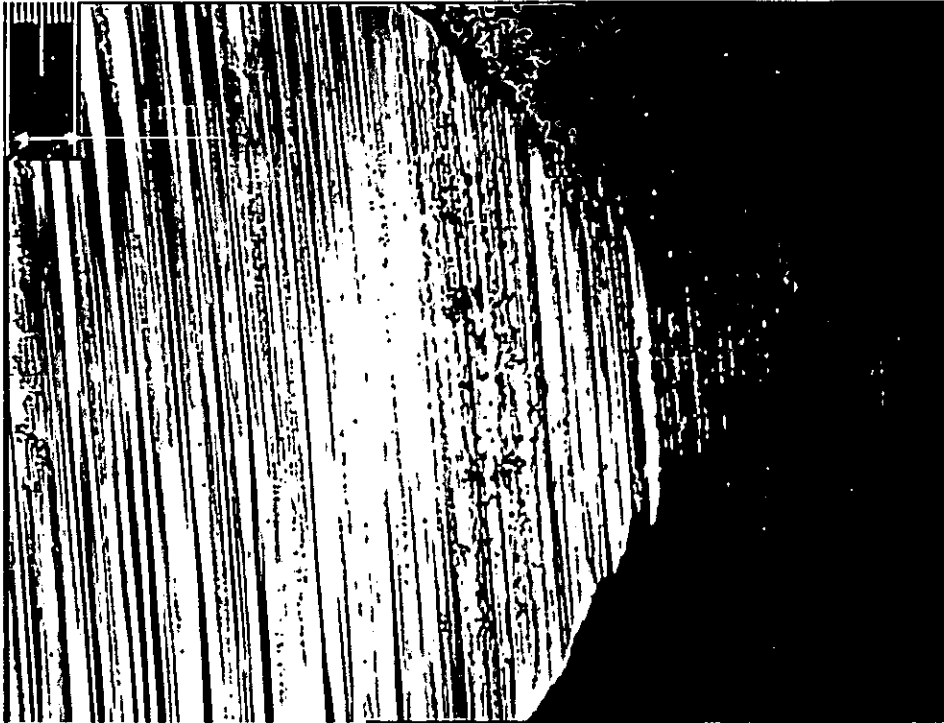


Figure 6.3 RHS of ball wear scar showing side protrusion.

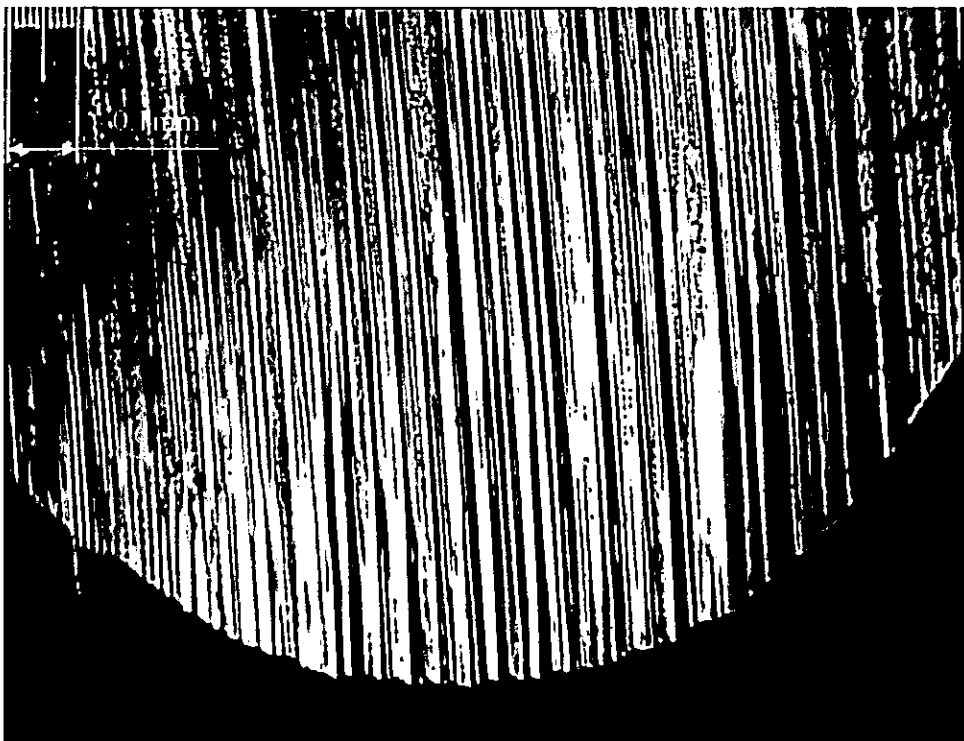


Figure 6.4 Leading edge of ball wear scar.

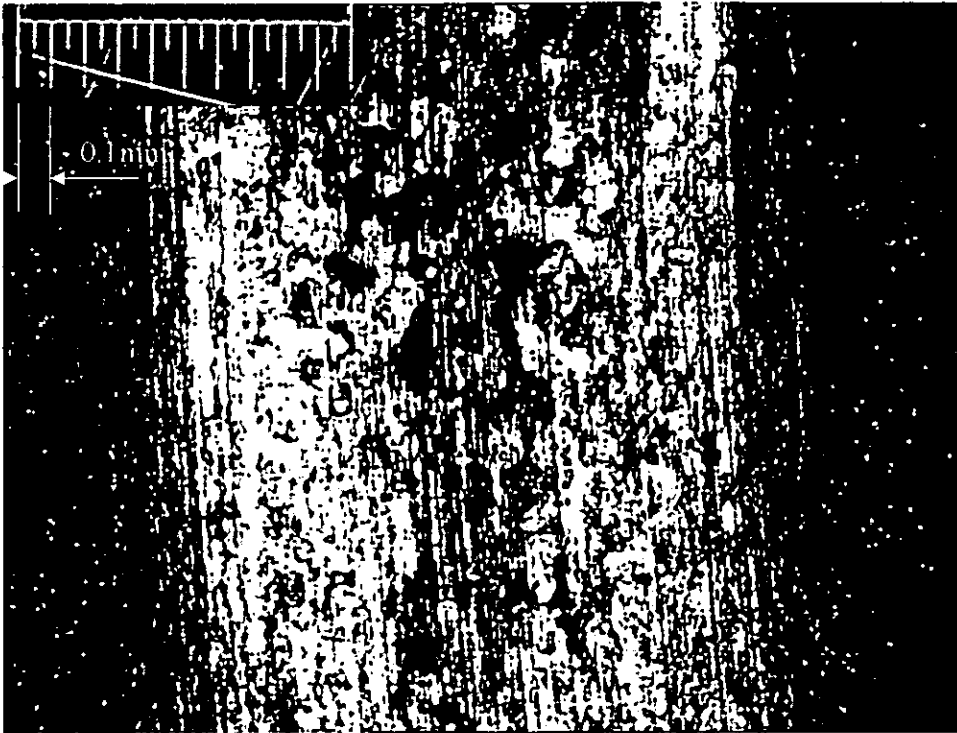


Figure 6.5 Disc wear track full width.



Figure 6.6 Centre of wear scar at higher magnification.

Figure 6.1 shows the total ball wear scar comprising scratches and grooves formed in the direction of sliding, the scale in the top left hand side being 1mm total. Figure 6.2 shows the the trailing edge of the ball wear scar, with wear debris visible to the right hand side, and mottled areas to the centre. The edge of the scar is not quite as well defined as the leading edge. The scale in the top left hand side in increments of 0.01mm with a total range of 0.1mm. Figure 6.3 shows the right hand side of the wear scar illustrating the side protrusions where contact/sliding has mainly occurred between the ball and lubricant film. Figure 6.4 shows the sharp well defined leading edge of the scar. All the photographs show bright colours and mottled areas of wear debris, possibly due to the thin transfer films being formed and wear particles being re-incorporated into the sliding interface. Figure 6.5 shows the corresponding disc wear track with the centre portion enlarged in figure 6.6.

6.2 A study of the contact evolution during the early stages of sliding.

The generation of the contact wear scar at different stages of the friction test was observed during the following test programme to determine the friction coefficient and contact development at various stages of sliding from 25m to 50km.

6.2.1 *Materials and Methods.*

Using 7 separate 12mm diameter balls and existing discs previously described the apparatus was set to utilise the unused 60mm dia track at a speed of 1ms^{-1} allowed samples to be generated at various intervals in the sliding life as shown in table 6.3.

The wear scars generated in these tests and there respective relationship with friction coefficient and sliding distance are shown in figures 6.7 and 6.8. Figure 6.9 – 6.22 show the wear scars and their corresponding disc tracks in greater detail.

Test No	Disc No/side	Distance m	Speed ms ⁻¹	Load N
1	1a	25	1	10
2	1b	50	1	10
3	2a	100	1	10
4	2b	500	1	10
5	3a	1000	1	10
6	3b	10000	1	10
7	4a	50000	1	10

Table 6.3. Sequence of Wear Scar generation tests.

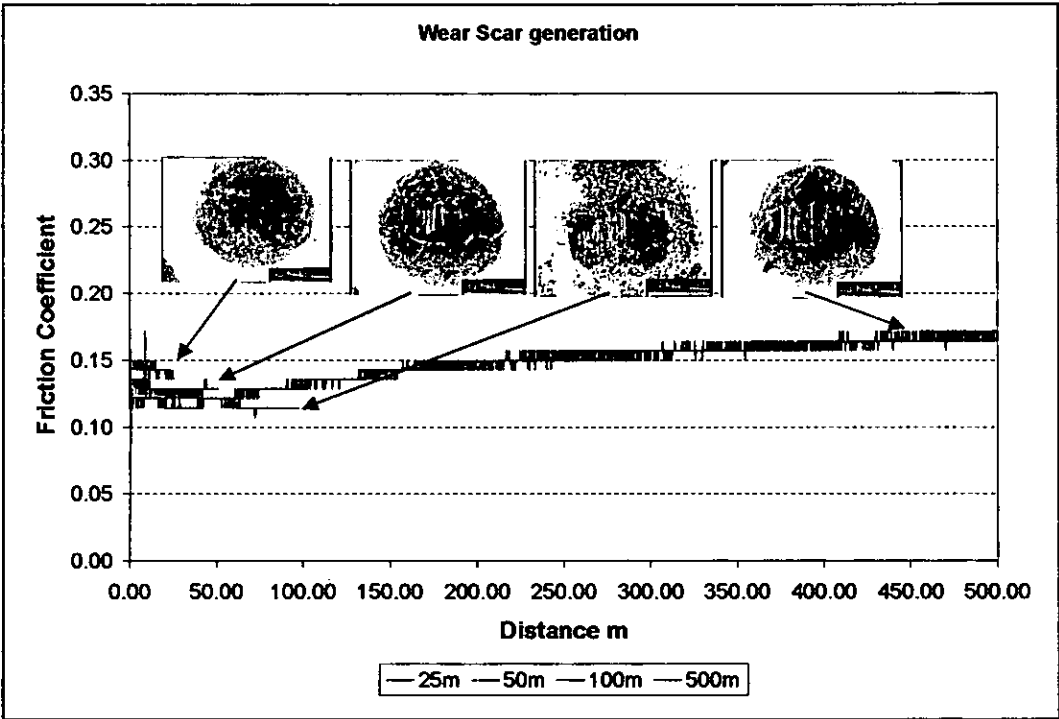


Figure 6.7. Wear Scar generation 25 to 500m

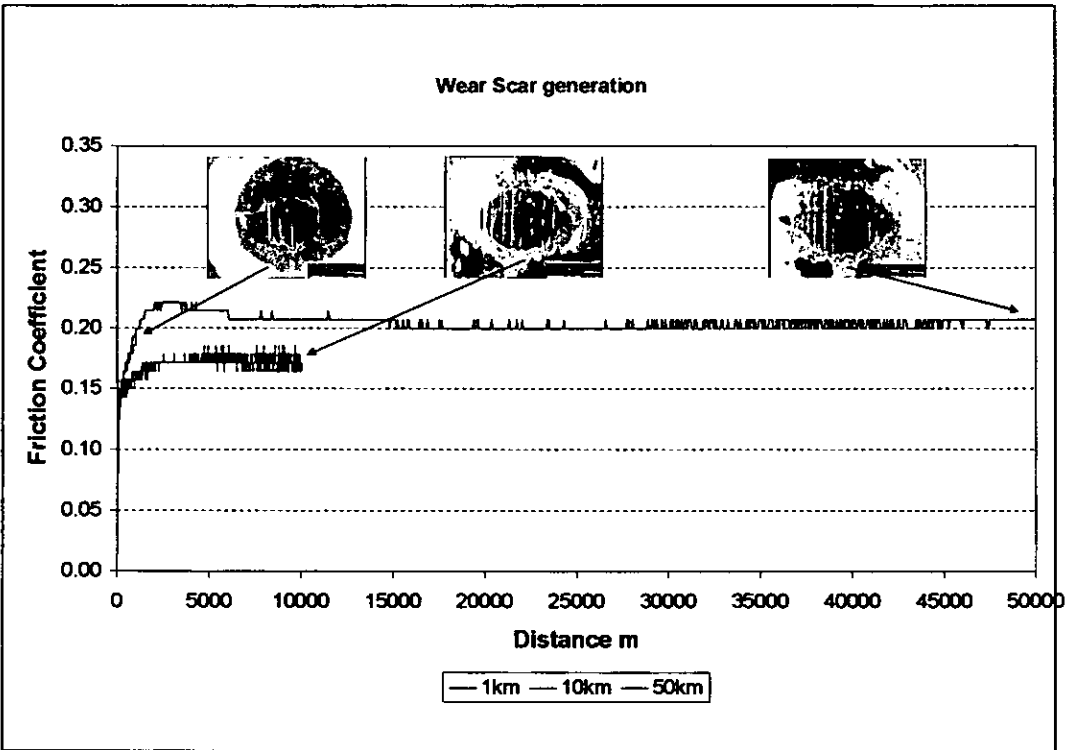


Figure 6.8. Wear Scar generation 1 to 50Km.

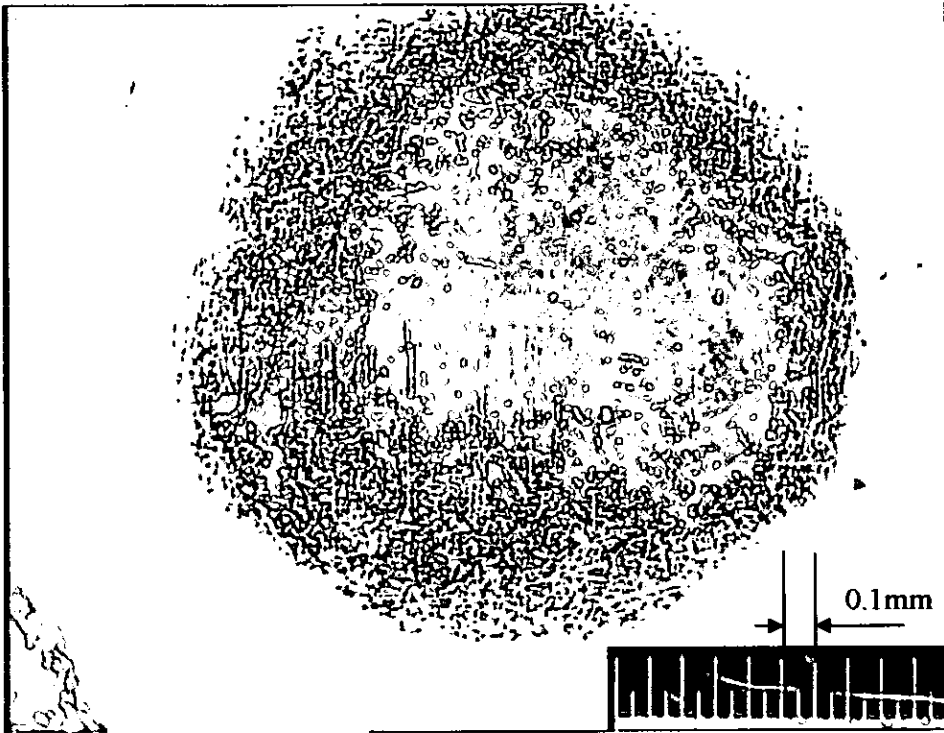


Figure 6.9. Ball Wear Scar 25m

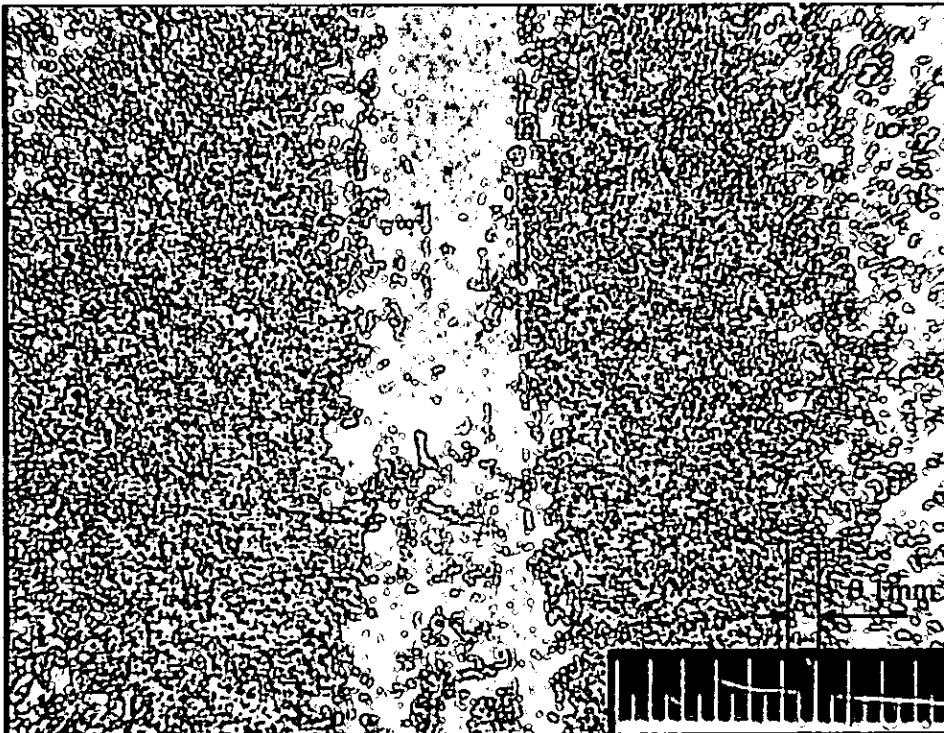


Figure 6.10. Disc Wear Track 25m

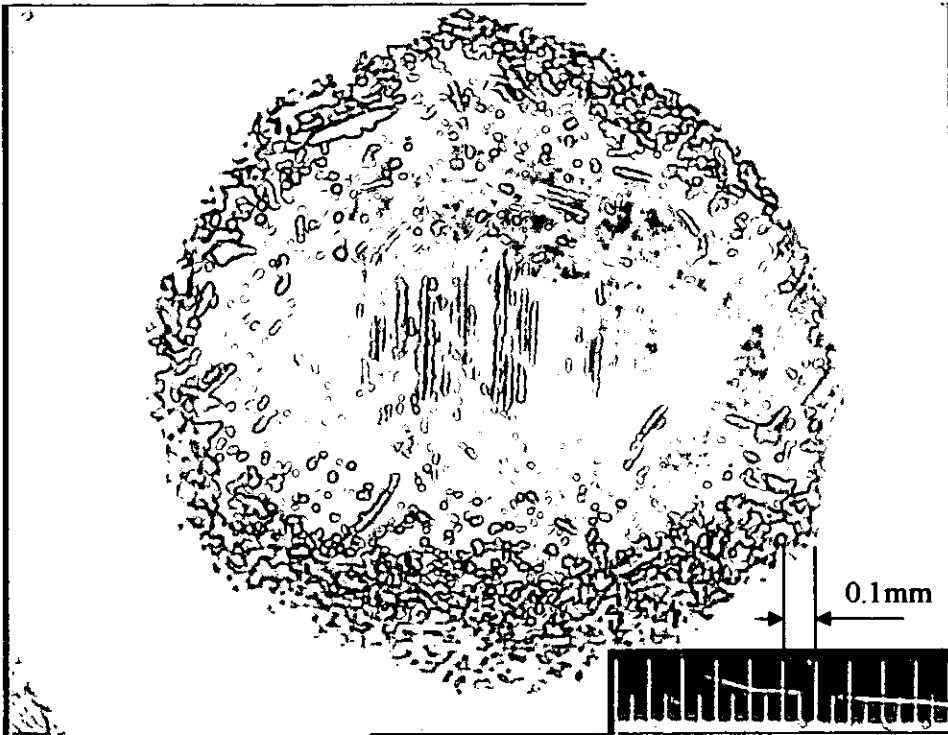


Figure 6.11. Ball Wear Scar 50m

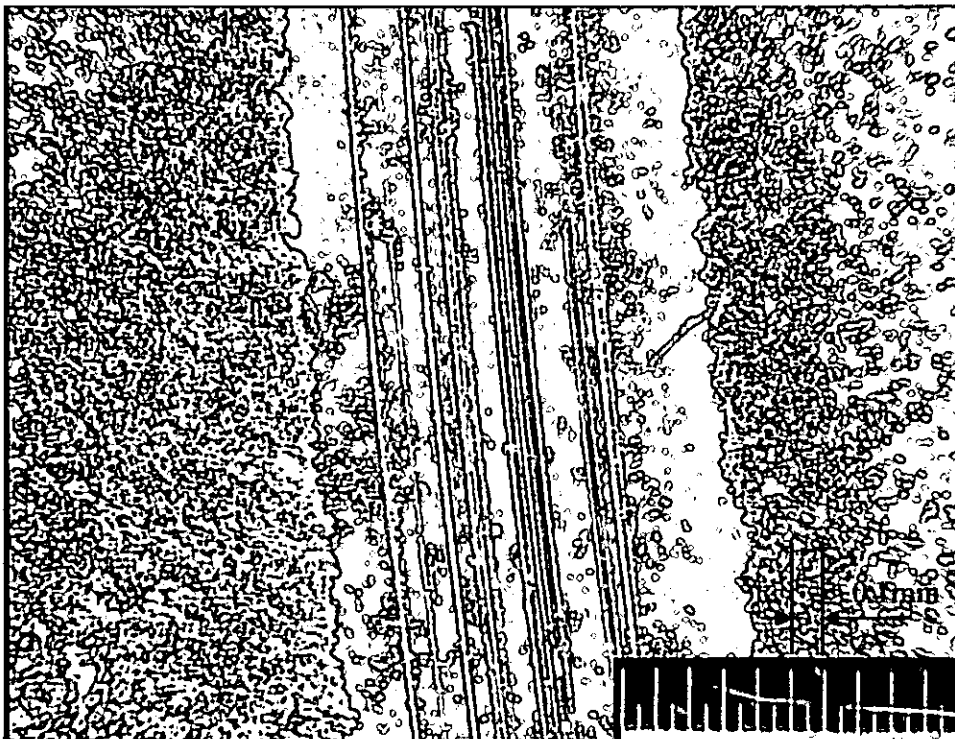


Figure 6.12. Disc Wear Track 50m



Figure 6.13. Ball Wear Scar 100m

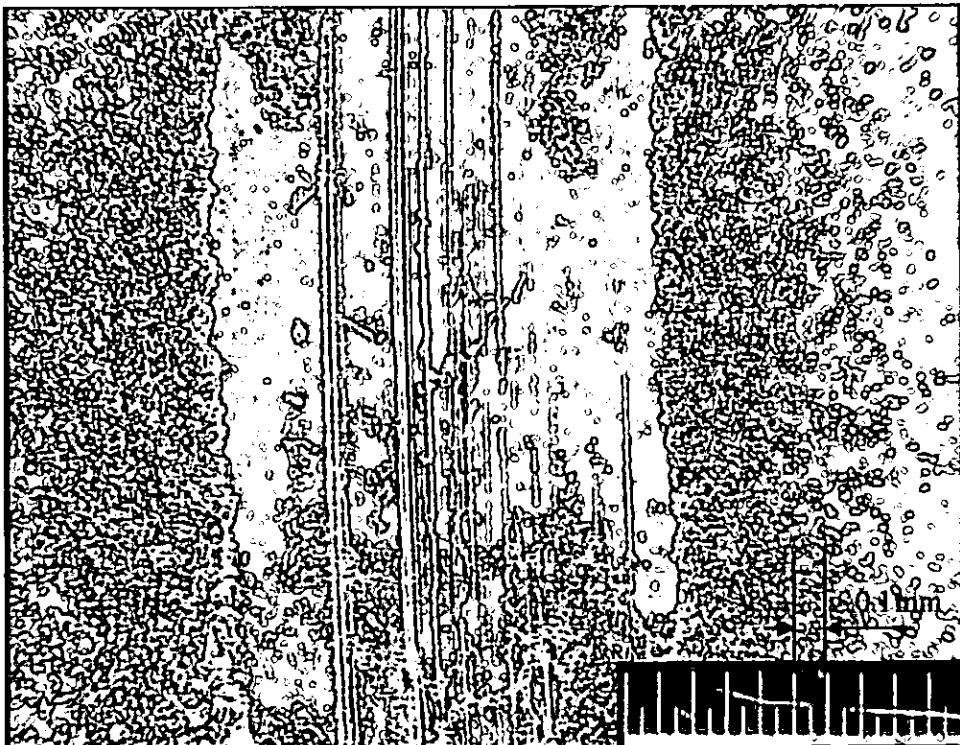


Figure 6.14. Disc Wear Track 100m

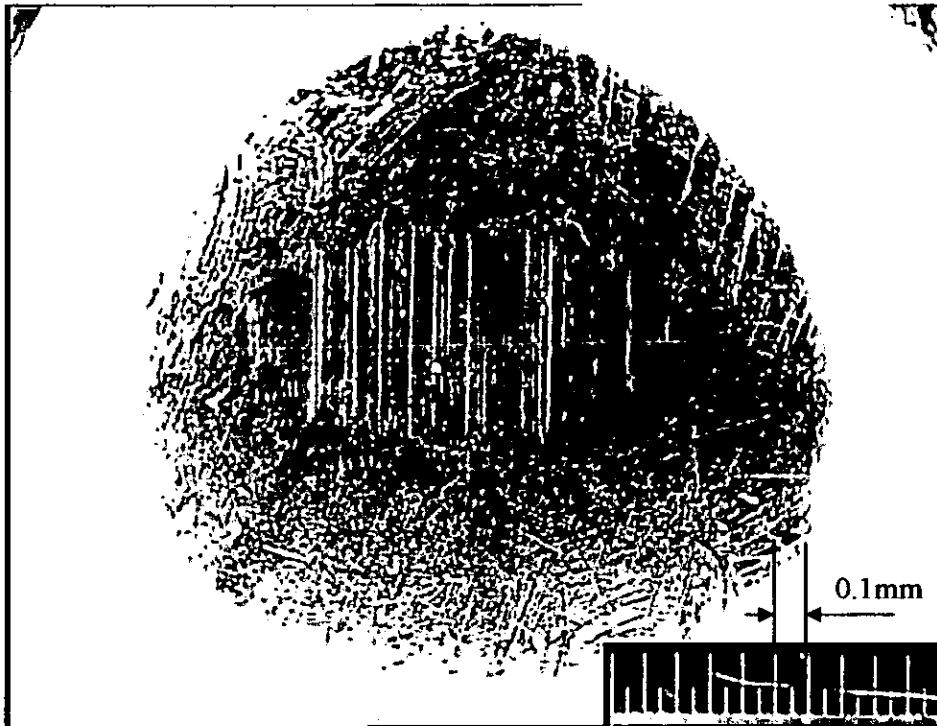


Figure 6.15. Ball Wear Scar 500m

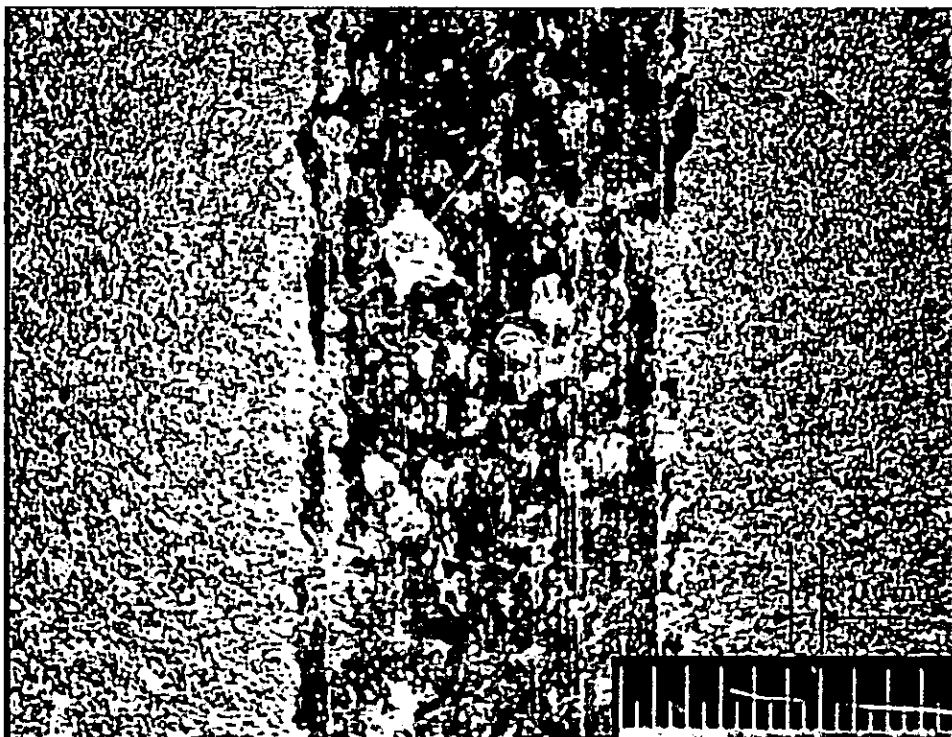


Figure 6.16. Disc Wear Track 500m

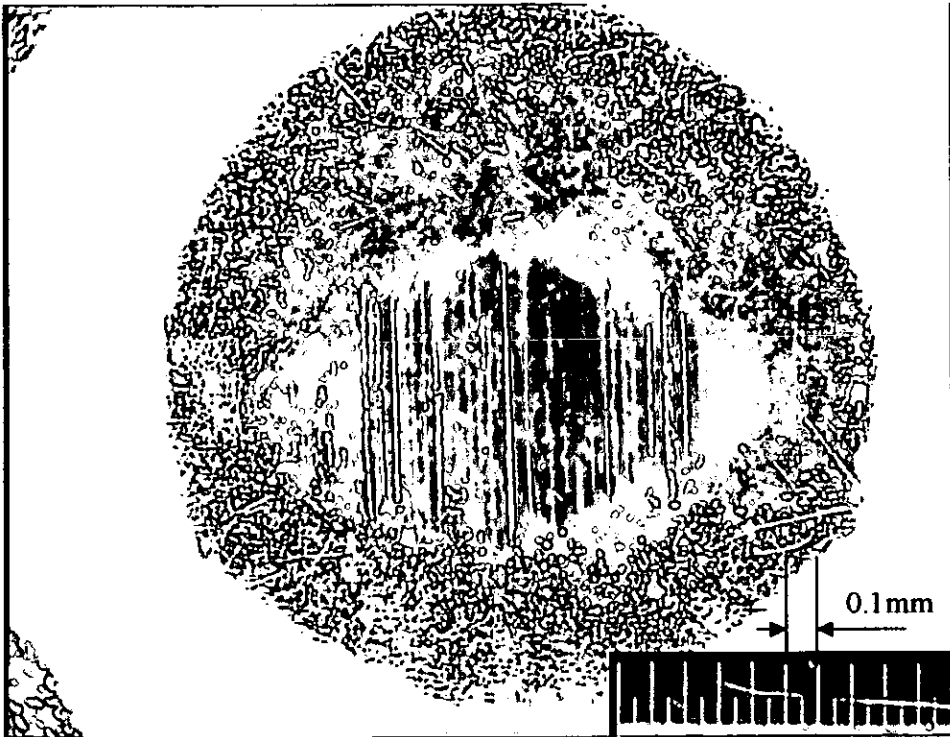


Figure 6.17. Ball Wear Scar 1000m

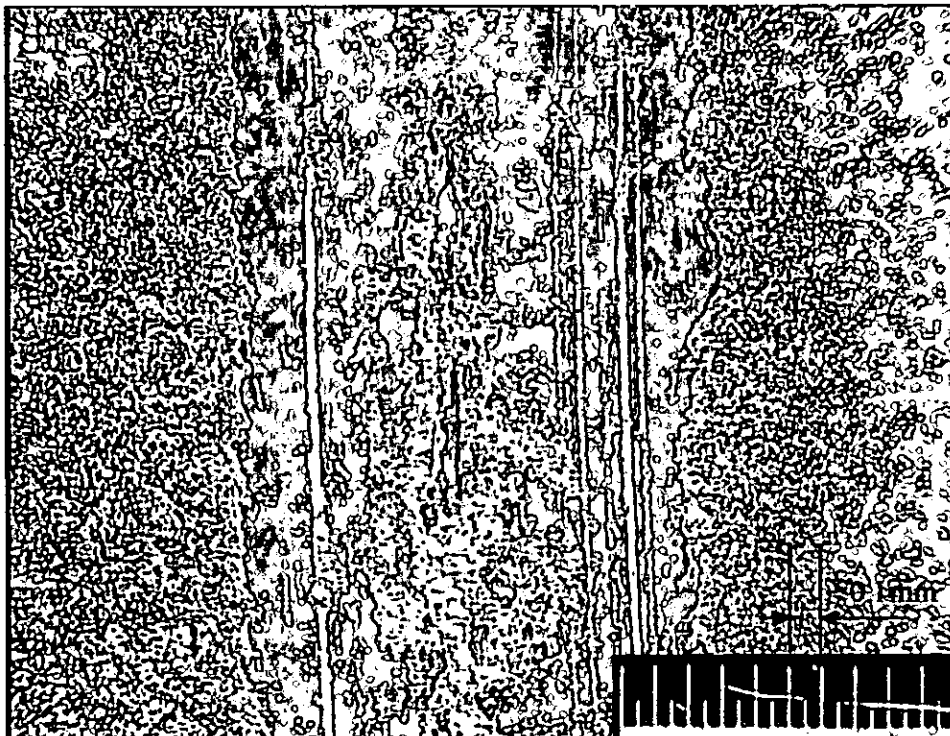


Figure 6.18. Disc Wear Track 1000m

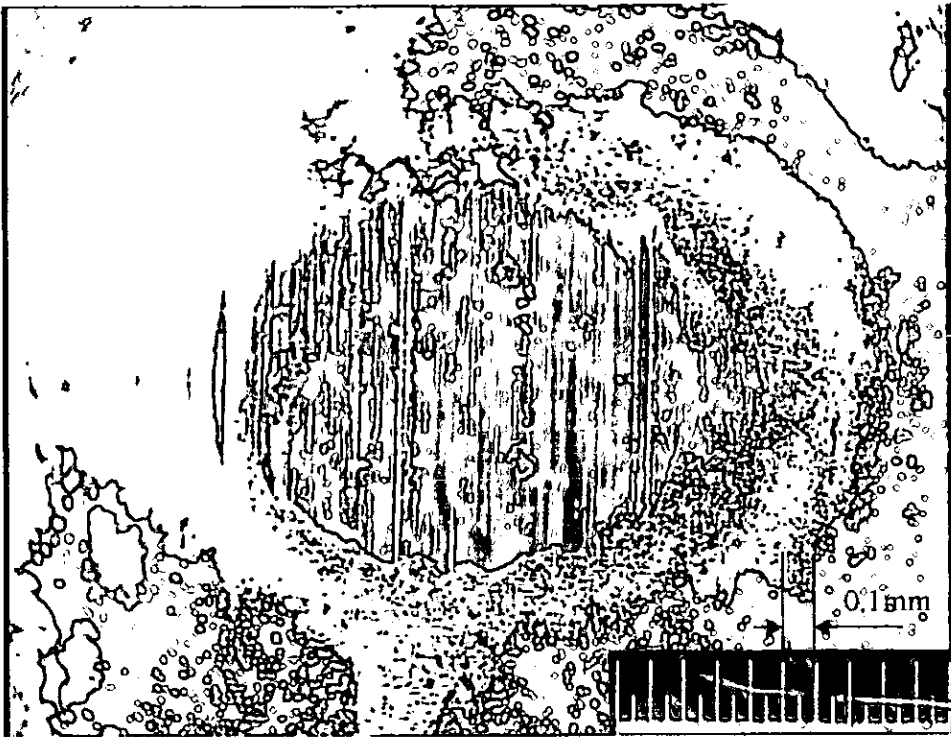


Figure 6.19. Ball Wear Scar 10,000m

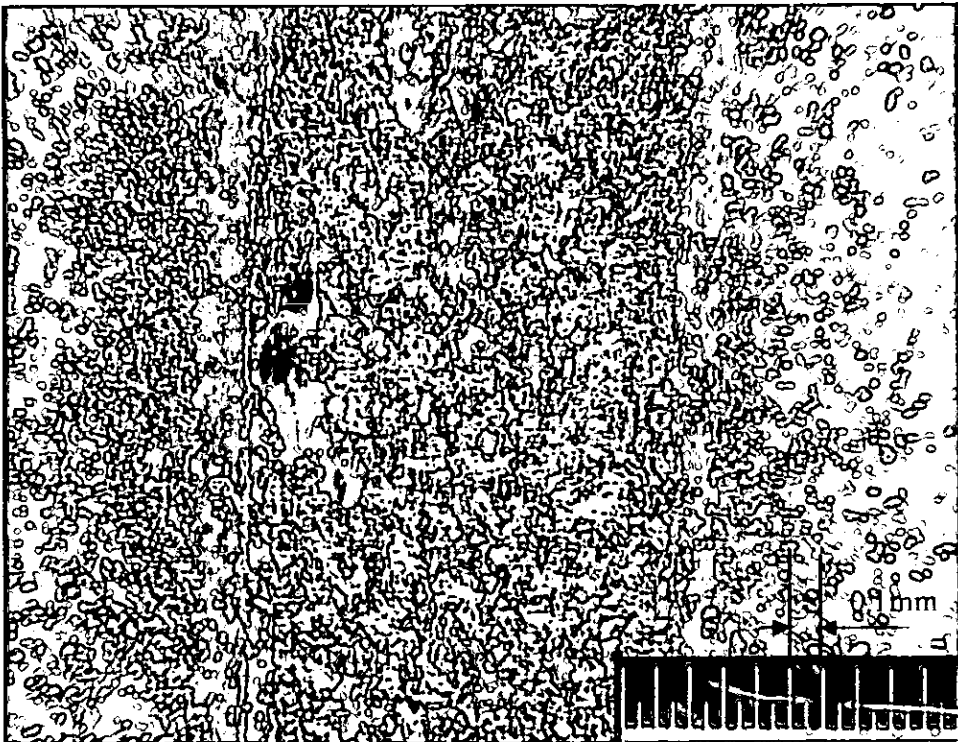


Figure 6.20. Disc Wear Track 10,000m

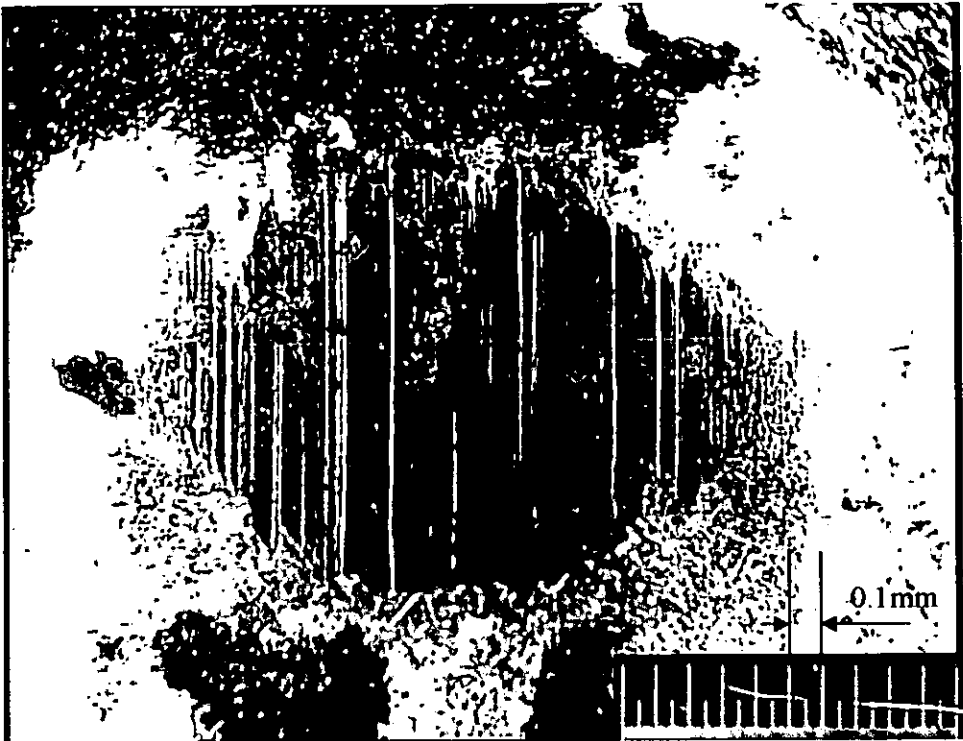


Figure 6.21. Ball Wear Scar 50,000m

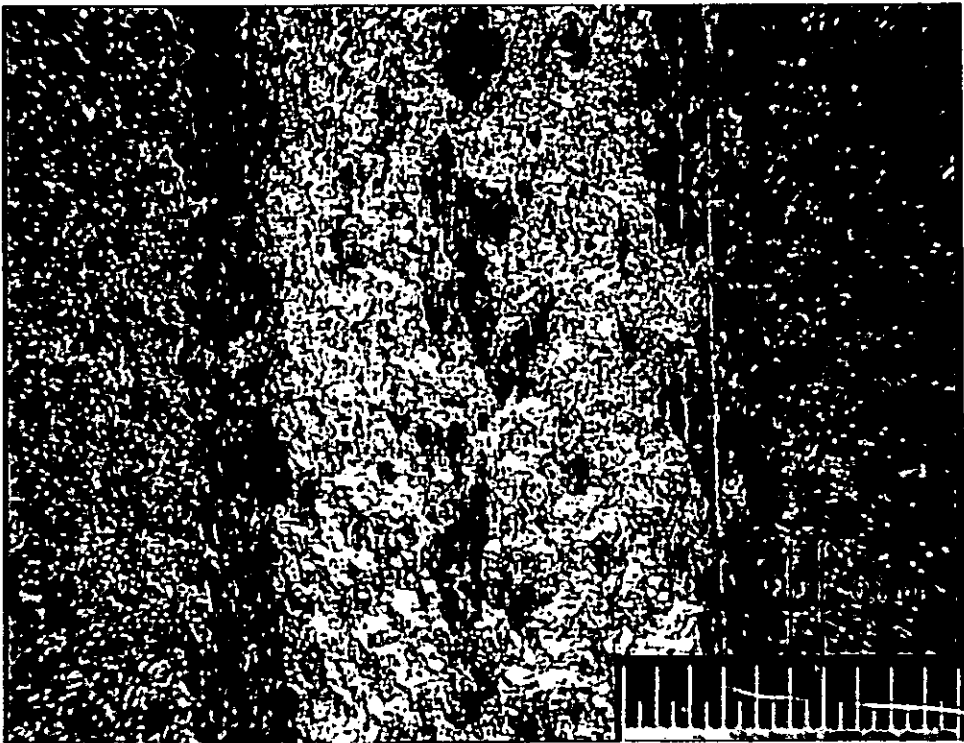


Figure 6.22. Disc Wear Track 50,000m

6.2.2 Observation of results

After a sliding distance of 25m the wear scar can be seen as a half moon shaped blemish on the ball surface figure 6.9, at this stage it is thought the this blemish is made up from a thin film transferred from the disc. The scar itself appears to be twice as wide as the corresponding track on the disc figure 6.10, this can be attributed to the slight undulations in the film thickness causing the lighter coloured areas on the sides of the blemish. The lightly stained area above the scar is a thin film of debris formed at the rear of the interface. At this stage the friction coefficient is 0.13-0.14.

The blemish becomes more apparent after 50m sliding, figure 6.11, as the ball continues to plough through the film, again it is thought that at this stage the blemish consists of a thicker film being built up as the sliding process continues. The corresponding wear track on the disc is almost the same width as the more defined area of the blemish. Very pronounced striations can now be seen towards the centre of the blemish with matching features in the wear track. The friction coefficient is still in the area of 0.13-0.14. Figure 6.23 illustrates the formation of the half moon shape of the blemish.

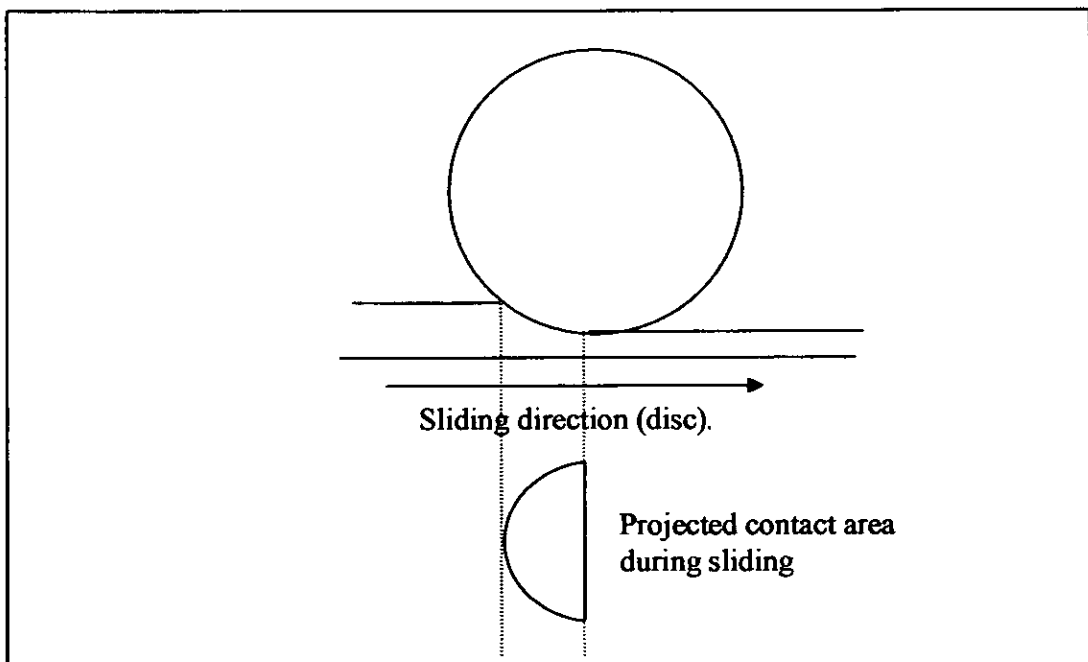


Figure 6.23 Blemish formation due to ball ploughing through film.

After 100m the blemish is now starting to become elliptical due to the transfer film being “drawn” to the rear of the feature by the action of sliding, figure 6.13 and the grooves have become more pronounced. Wear debris is visible around the blemish and a tail of debris is apparent to the rear.

At 500m figure 6.15 the blemish has a distinctive centre with closely spaced grooves, small particles of wear debris are apparent on these grooves and around the feature. The wear track, figure 6.16 still has features that can be seen to match the ball but large particles of wear debris are visibly distributed across the width.

The development of the distinctive centre of the blemish continues until after 1000m of sliding a circular spot can be seen, figure 6.17, it is still thought at this stage that this is comprised mainly from the material transferred from the disc, although it is probable that the ball is now sliding on this transfer film and a mixture of the phosphate pretreatment and the lubricant on the disc. The disc wear now appears more “turbulent” in the centre of the track but still contains matching grooves to the side. The friction coefficient at this stage has progressively risen from about 0.13 to 0.19.

Between 1000m and 3000m sliding, a distinct change can be seen to take place in the friction coefficient, figure 6.8. Up to this point the friction has risen steadily and then levelled off to a steady value. It is thought that this is due to the change over from a contact consisting of a thick, greater than $5\mu\text{m}$, transfer film on the ball and the matrix of the disc film to one of very thin, less than $2\mu\text{m}$, transfer films on the ball with a mixture of the film constituents, PTFE, graphite, polyamide-imide plus manganese phosphate on the disc with some metal to metal contact occurring, at this point the circular metallic scar is formed as shown in figure 6.19. The wear track on the disc has almost lost the grooved appearance and now exhibits an area that contains regions that appear to have been melted and flowed, figure 6.20. This phase continues up to and beyond 50000m, figure 6.21, with the scar and track increasing in diameter and width until they reach a size where the film breaks down with a rapid increase in the coefficient of friction.

6.3 Friction measurement close to the yield pressure.

6.3.1 Introduction.

With very thin films 1-2µm thick deposited by Physical Vapour Deposition and similar techniques it has been demonstrated by Singer that the mechanical properties of the film do not greatly influence the contact geometry and their frictional properties can be related directly to Hertzian contact theory [6.1]. However BSL films are relatively thick 10 - 25µm for the film thickness and approx 5µm for the substrate pretreatment film, this 'thick' film may be a factor in determining the initial frictional properties of the tribo couple. At very low loads it may be the main contributor to friction. To assess the frictional effects of the BSL under low loading conditions the yeild strength or pressure of the film is required.

It has been shown by Rabinowicz [6.2] that the Yield strength is proportional to the hardness stress of the material, H, as follows:

$$H = 3.2\sigma_y$$

Where σ_y is the yield stress at which the plastic strain in the material is 0.002. Since the Vickers micro hardness number is actually in units of pressure/stress, this now becomes a simple calculation of the hardness number divided by 3.2 to give the yield pressure in MPa.

Microhardness readings where taken at 5 possitions on one of the disc faces with results as shown in table 6.4.

Test	1	2	3	4	5	Average
Hardness Hv/0.1	264	239	239	234	265	248

Table 6.4 BSL film hardness.

Using the average of these five readings, then:

$$\sigma_y = \frac{H}{3.2} \quad \text{where } H = 248$$

$$\sigma_y = 77.5\text{MPa}$$

Data given in the literature for σ_y for polyamide- imide and PTFE bulk materials are given as 93 – 160MPa average 120MPa and 9 – 30 MPa average 11.6MPa. using the average values then a ratio of mixtures of 60% Polyamide-imide to 40% PTFE would give a yield pressure of :

$$0.6 \times 120 + 0.4 \times 11.6 = 76.64\text{MPa}$$

Therefore in order to evaluate the friction performance below or close to the yield pressure the applied loads will require to exert a maximum pressure less than the above, table 6.5 has been generated using Hertzian contact theory to give the average and maximum pressures, using the average modulus of elasticity for the film as 4.6 GPa.

Normal Load N	Contact spot radius a mm	Contact area mm ²	Pressure max MPa	Pressure average MPa
5	0.1657	0.0862	86.92	57.95
4	0.1538	0.0743	80.69	53.79
3.5	0.1471	0.0680	77.18	51.45
2.5	0.1315	0.0543	68.99	45.99
1.5	0.1109	0.0387	58.19	38.79
1.0	0.0969	0.0295	50.84	33.89
0.8	0.0900	0.0254	47.19	31.46
0.6	0.0817	0.0209	42.88	28.58
0.4	0.0714	0.0160	37.46	24.97
0.2	0.0567	0.0100	29.73	19.82

Table 6.5 Maximum and average contact pressures.

6.3.2 Test Specimens.

The test specimens were prepared as described in chapter 5, the discs were coated with material from the same batch used for the test programme also described in chapter 5 and the 12mm diameter balls taken from the samples originally produced for the test programme described in this chapter, these were cleaned and degreased prior to use.

6.4 Test Conditions.

6.4.1 Apparatus.

The pin on disc apparatus used for the original test programme was designed to allow test programmes to be conducted at loads of 10 – 100N and required modifications to accommodate applied loads as small as 0.2N. This was achieved by providing a simple pulley system and counterbalance as shown in figure 6.24 to negate the mass of the load application shaft which had a mass of 390 grams. The load applied was checked by

inserting a digital pocket scale between the counterface and the disc platform, then loading the load application shaft with weights in increments of 20g and the calibration graph, figure 6.25 was produced.

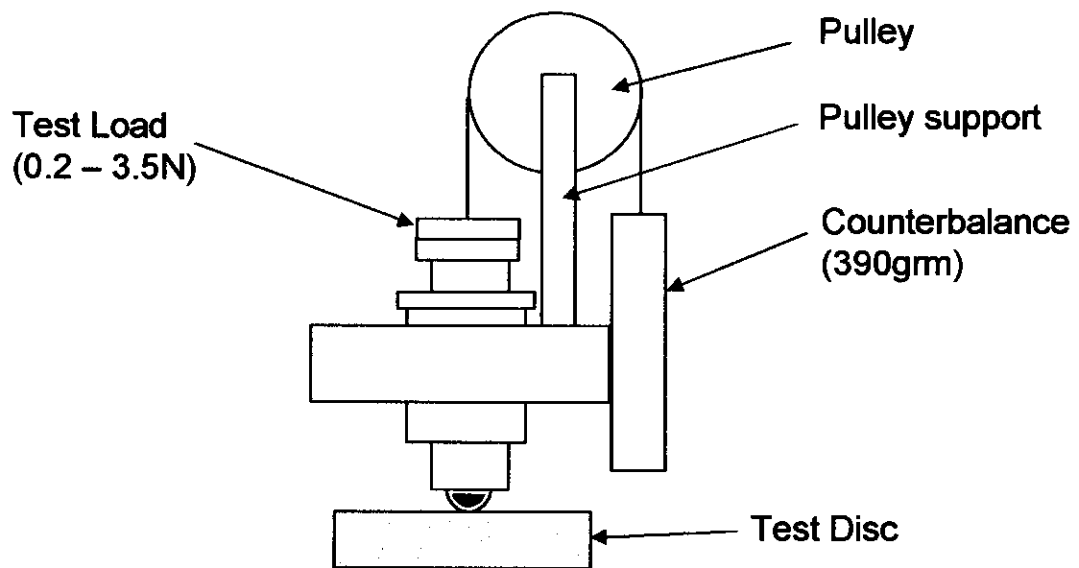


Figure 6.24 Test apparatus modifications.

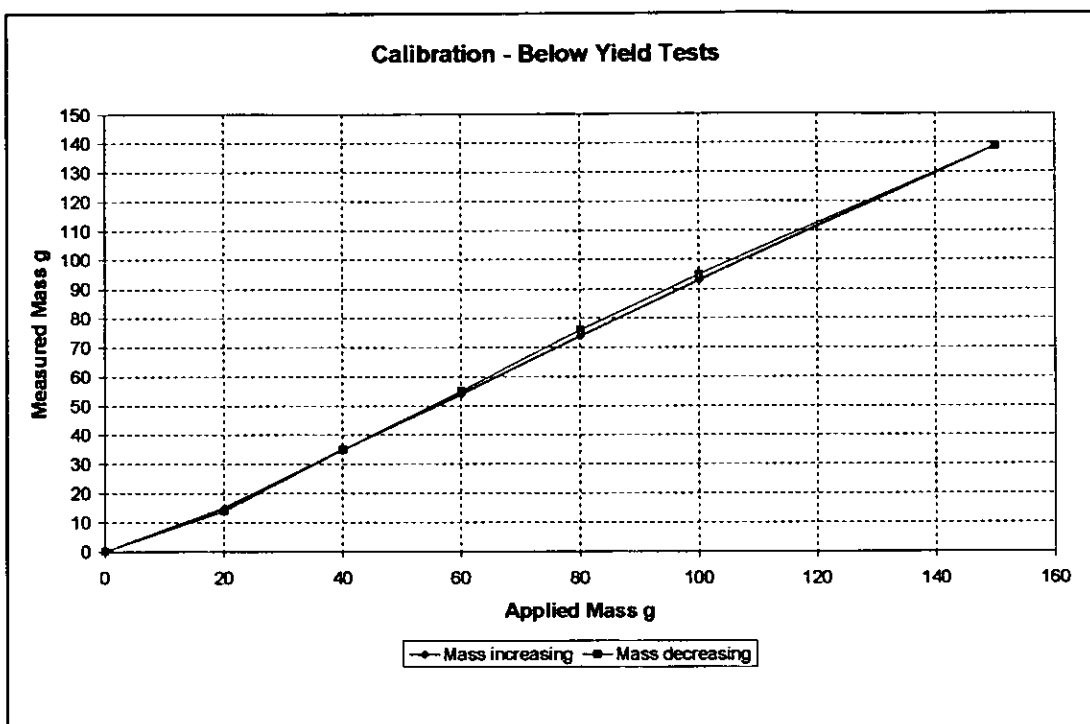


Figure 6.25 Calibration graph applied load.

6.4.2 Test Procedures.

Testing was conducted with applied loads from 0.2N to 3.5N at velocities of 0.1, 0.5 and 1.0ms^{-1} and is shown in table 6.6. The tests were conducted by mounting the samples in the modified pin on disc apparatus which had previously been set to the relevant parameters, i.e. speed and test diameter. The Pico soft data acquisition package was set to record readings of friction force every 100ms. A 0.2N load was added to the load application shaft and the ball lowered slowly into contact with the disc, the main drive motor was switched on and the data acquisition package started. This setup was allowed to run for 350 revolutions then another 0.2N added, repeated loads were added every 350 revolutions until the test was complete. Each test configuration was performed in the same manner until all combinations had been tested.

Test Number	Velocity ms⁻¹	Counterface Surface Finish
3001	0.1	AR
3002	0.1	F
3003	0.1	M
3004	0.1	C
4001	0.5	AR
4002	0.5	F
4003	0.5	M
4004	0.5	C
5201	1.0	AR
5202	1.0	F
5203	1.0	M
5204	1.0	C
AR – as rec'd, F – fine, M – medium, C – coarse		

Table 6.6 Test programme matrix.

6.5 Results.

A typical output trace is shown in figure 6.26 showing voltage against time in milliseconds. This data was then transferred to an excel spreadsheet and the central 100 readings plotted for each individual load as shown in figure 6.27. Further analysis was performed by loading the data into a statistical analysis package (Minitab) and box plots generated. These box plots show the mean, median, lower quartile, upper quartile and total spread of the data with any outliers highlighted by an asterisk, four typical box plots are shown here figures 6.28 – 6.31, the bulk of the data being included in Appendix 4. The means of all the data are plotted for comparison in figure 6.32.

6.6 Discussion of results.

The results obtained show a distinct negative correlation of friction coefficient against applied load, that is, as the load increases the friction coefficient reduces. This correlation applies across all the tests irrespective of finish or velocity. In general the spread of the data for each individual applied load reduces as load increases and this is shown in figures 6.28 – 6.39. The data generated with the 0.2N load applied generally has the largest spread and may not be a true reflection of the friction at this level, this can be attributed to the limitations of the apparatus and the phenomenon of stick slip occurring in the linear bearing that housed the load application shaft, and pulley system employed. The outliers illustrated by an asterisk in the figures are data points that lie outside the normal plus or minus three standard deviations of the normal data, these are probably due to noise from the apparatus, test specimens and surrounding area, it should be noted that very low levels of load are being measured, 0.015 – 0.05N and hence very low output voltages recorded 0.5 to 10 mV. The final chart, figure 6.40 shows a summary of all the data means plots for the entire test series,

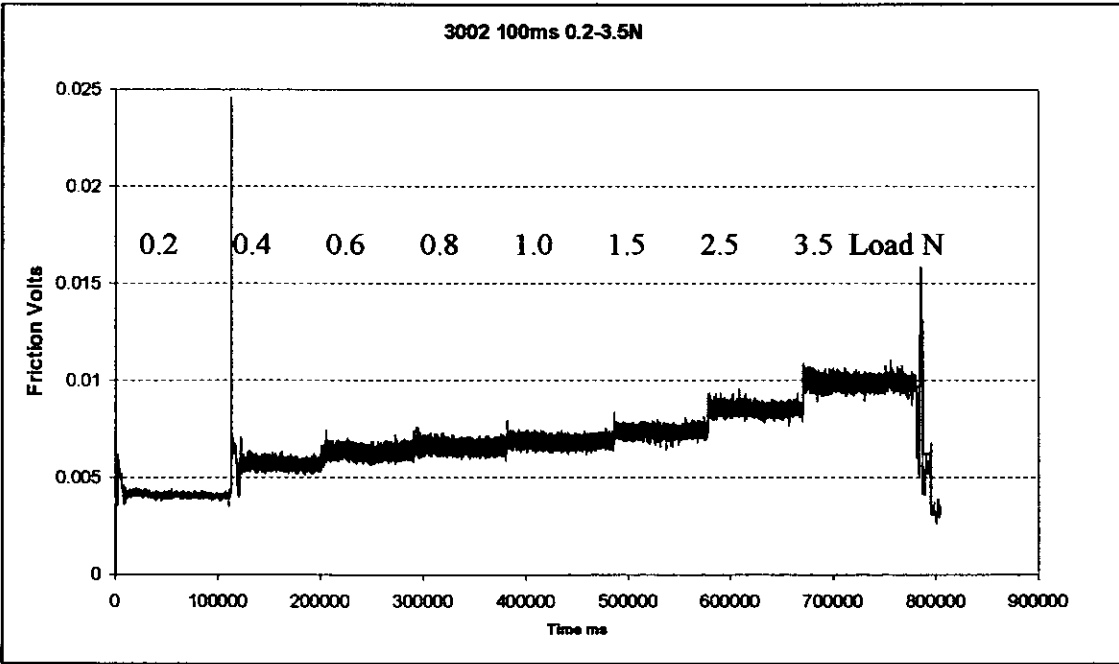


Figure 6.26 Typical output trace raw data.

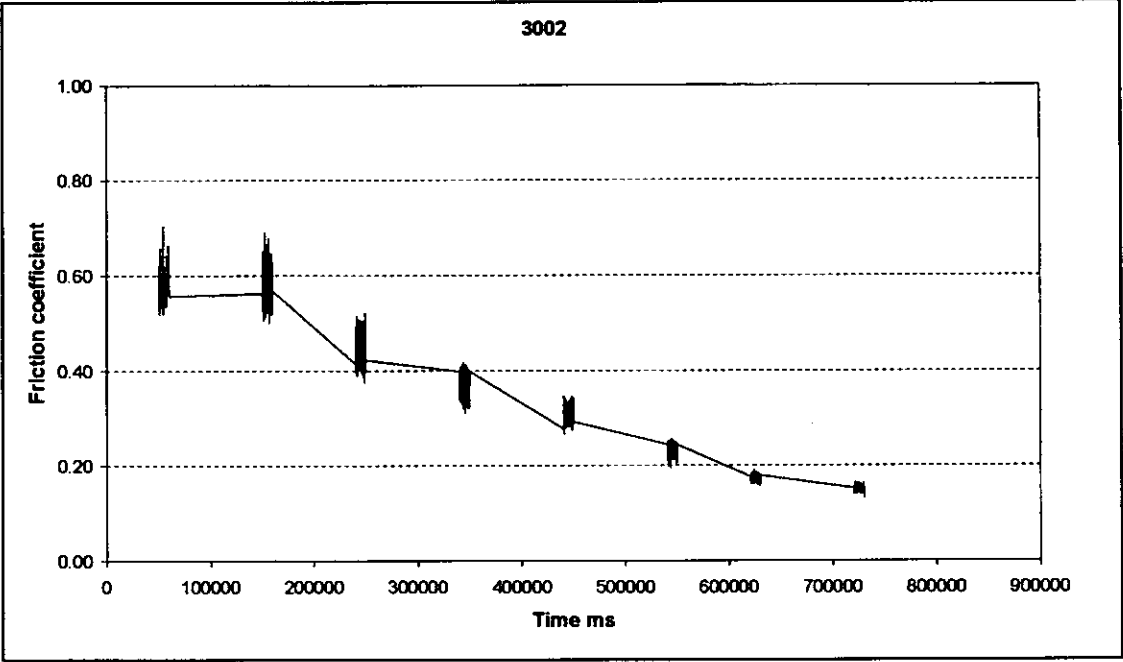


Figure 6.27 Typical friction coefficient data vs. time.

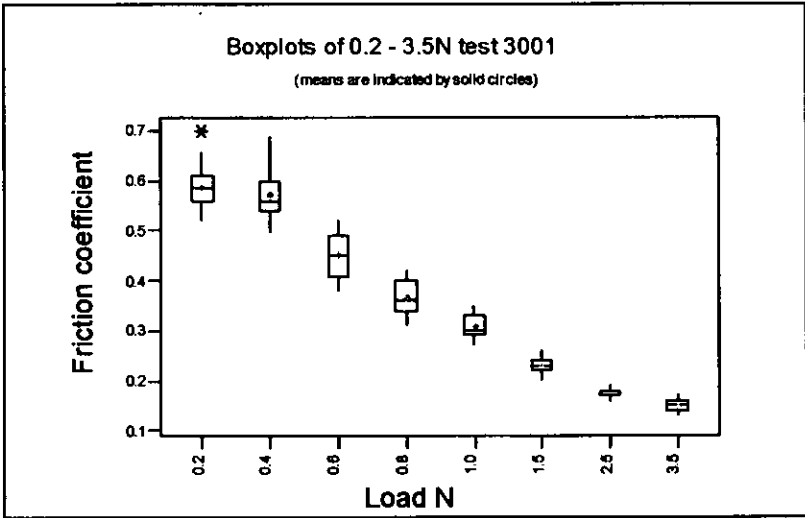


Figure 6.28 Box plots of friction data for 0.1ms⁻¹ as rec'd finish.

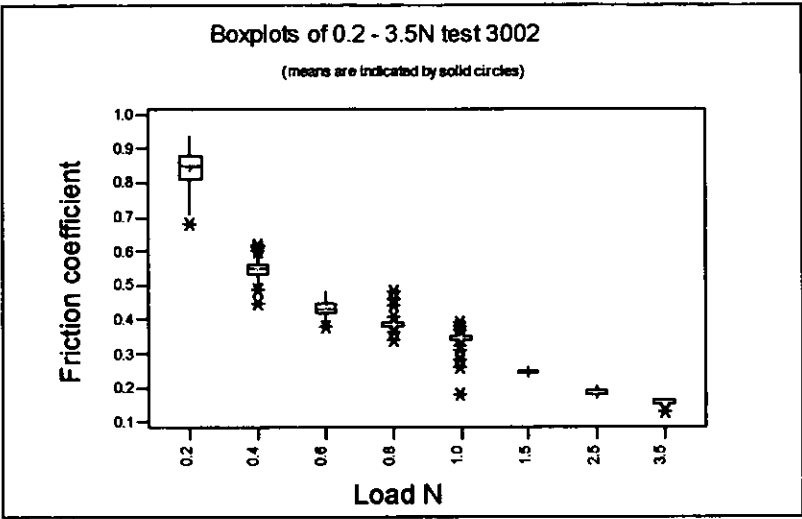


Figure 6.29 Box plots of friction data for 0.1ms⁻¹ fine finish.

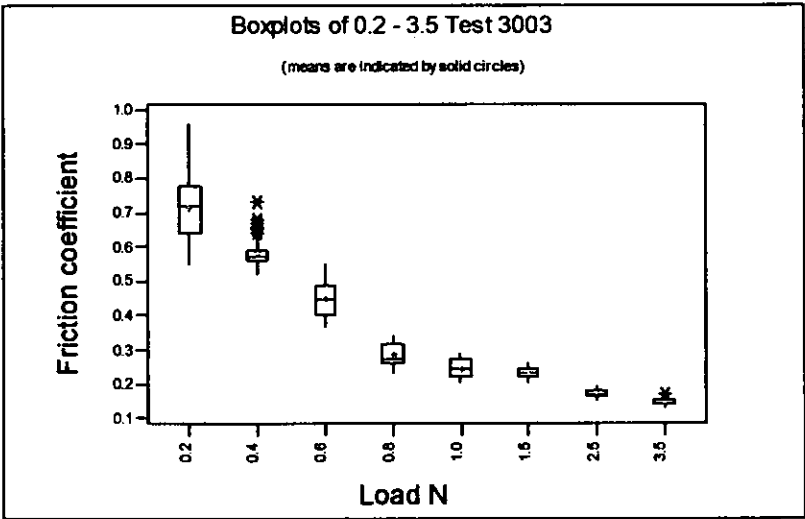


Figure 6.30 Box plots of friction data for 0.1ms⁻¹ medium finish.

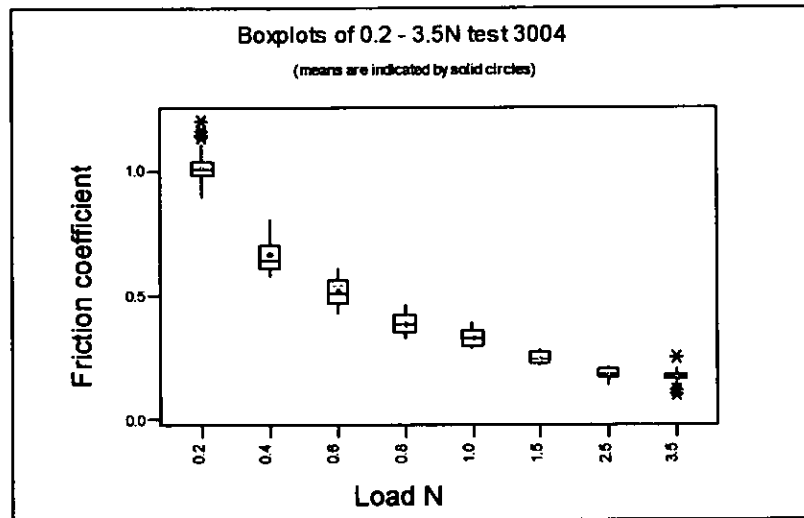


Figure 6.31 Box plots of friction data for 0.1ms^{-1} coarse finish.

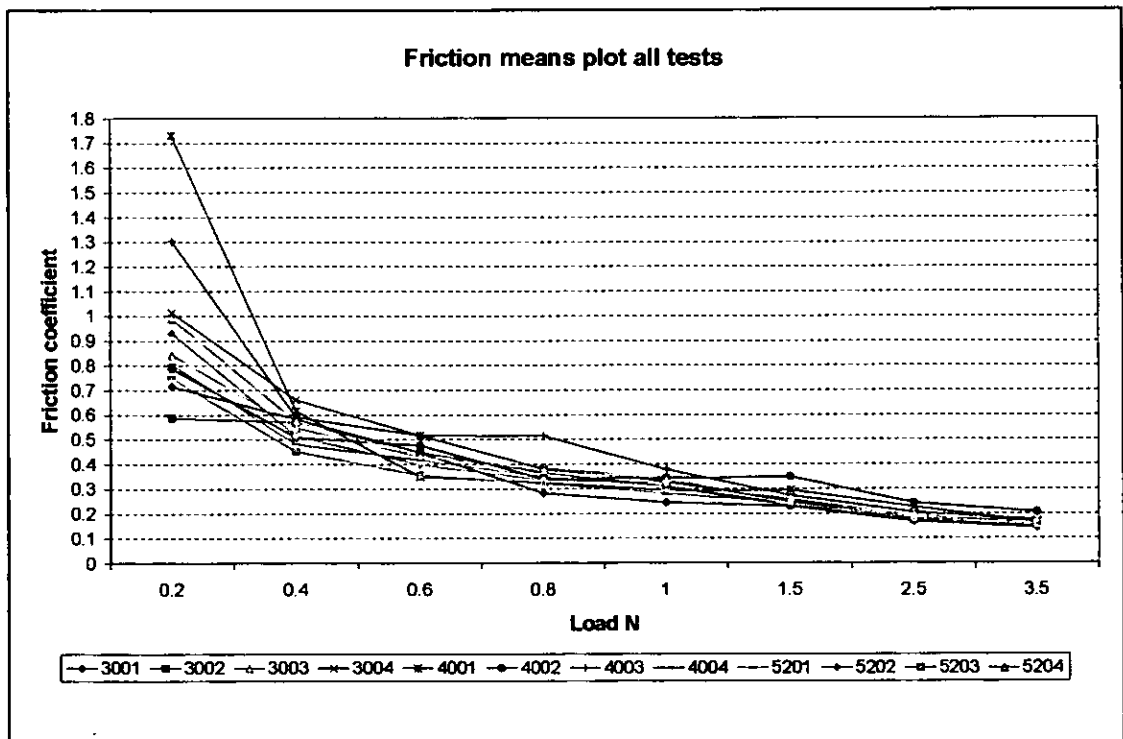


Figure 6.32 Means plot of friction coefficient all tests.

6.7 Optical examination of the counterface and wear track.

6.7.1 *Introduction.*

Digital photographs were taken of the individual counterfaces and their corresponding wear track after the tests were completed using an optical microscope and imaging system. These photographs are reproduced in Figures 6.33 to 6.44 the top photograph is the ball, counterface, the lower photograph the corresponding wear track on the disc. The scale in the top left hand corner of each photograph representing 0.1 mm.

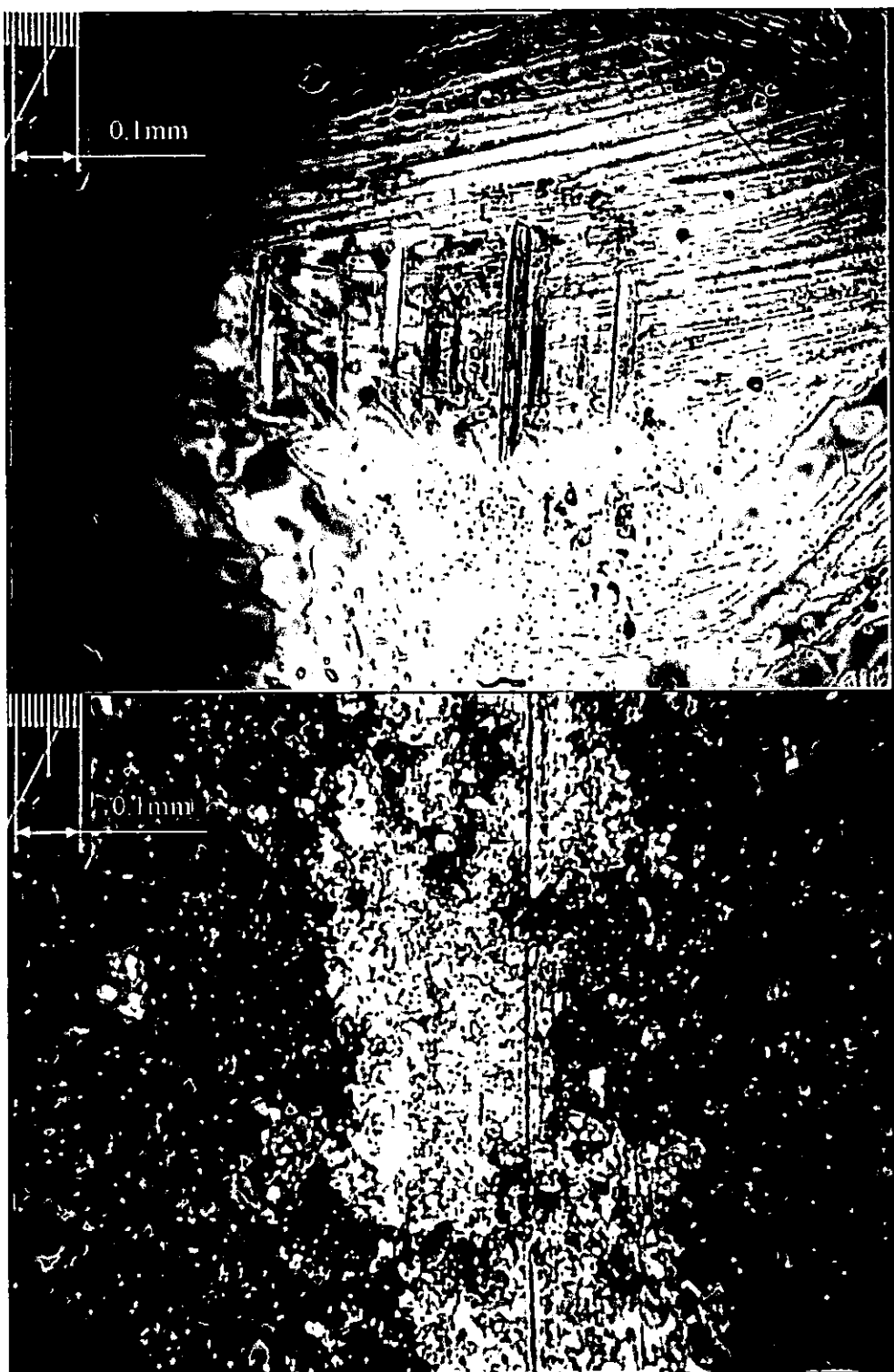


Figure 6.33 Test 3001 as rec'd finish 0.1ms^{-1}

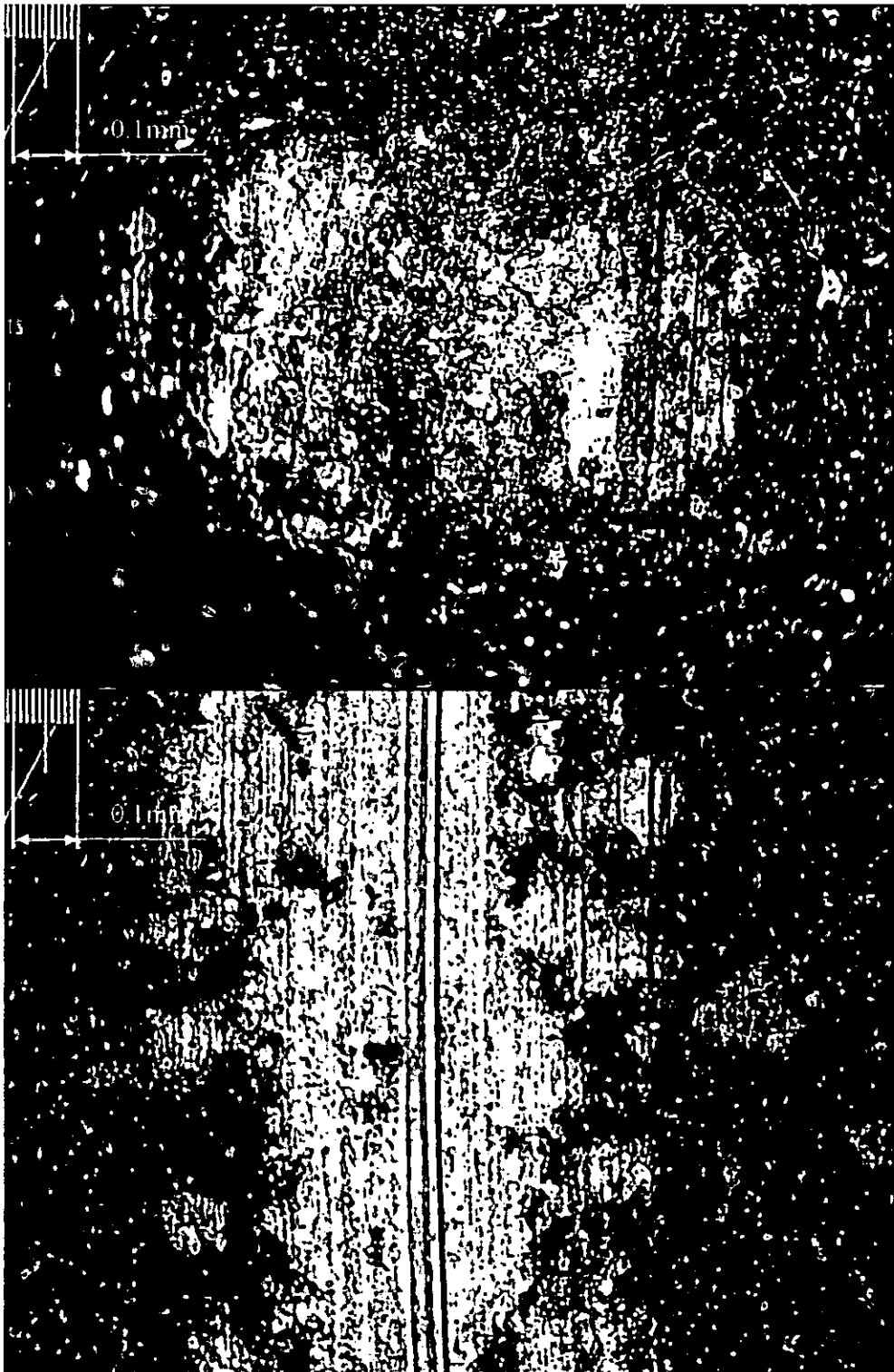


Figure 6.34 Test 3002 fine finish 0.1ms^{-1}

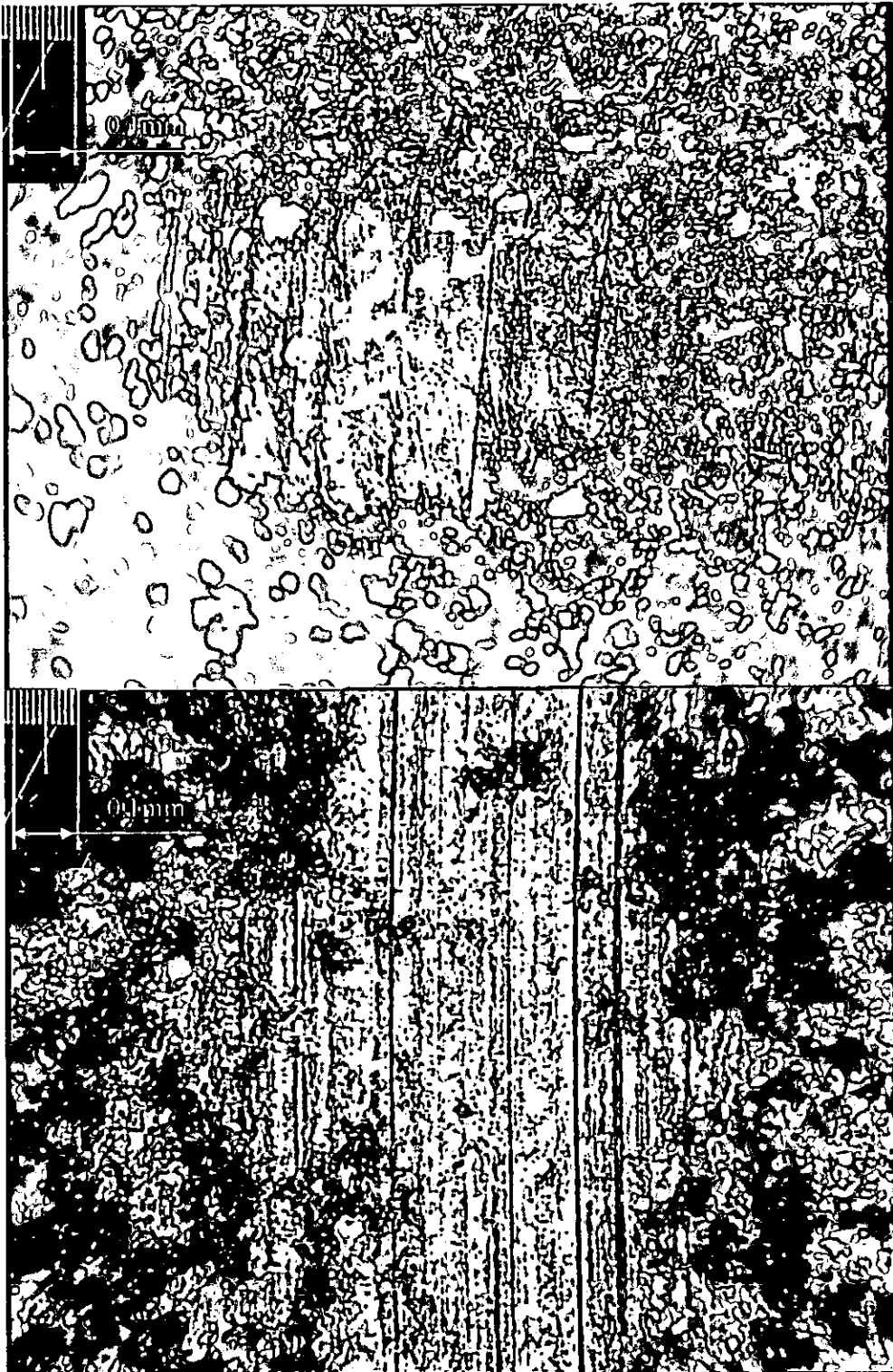


Figure 6.35 Test 3003 medium finish 0.1ms^{-1}

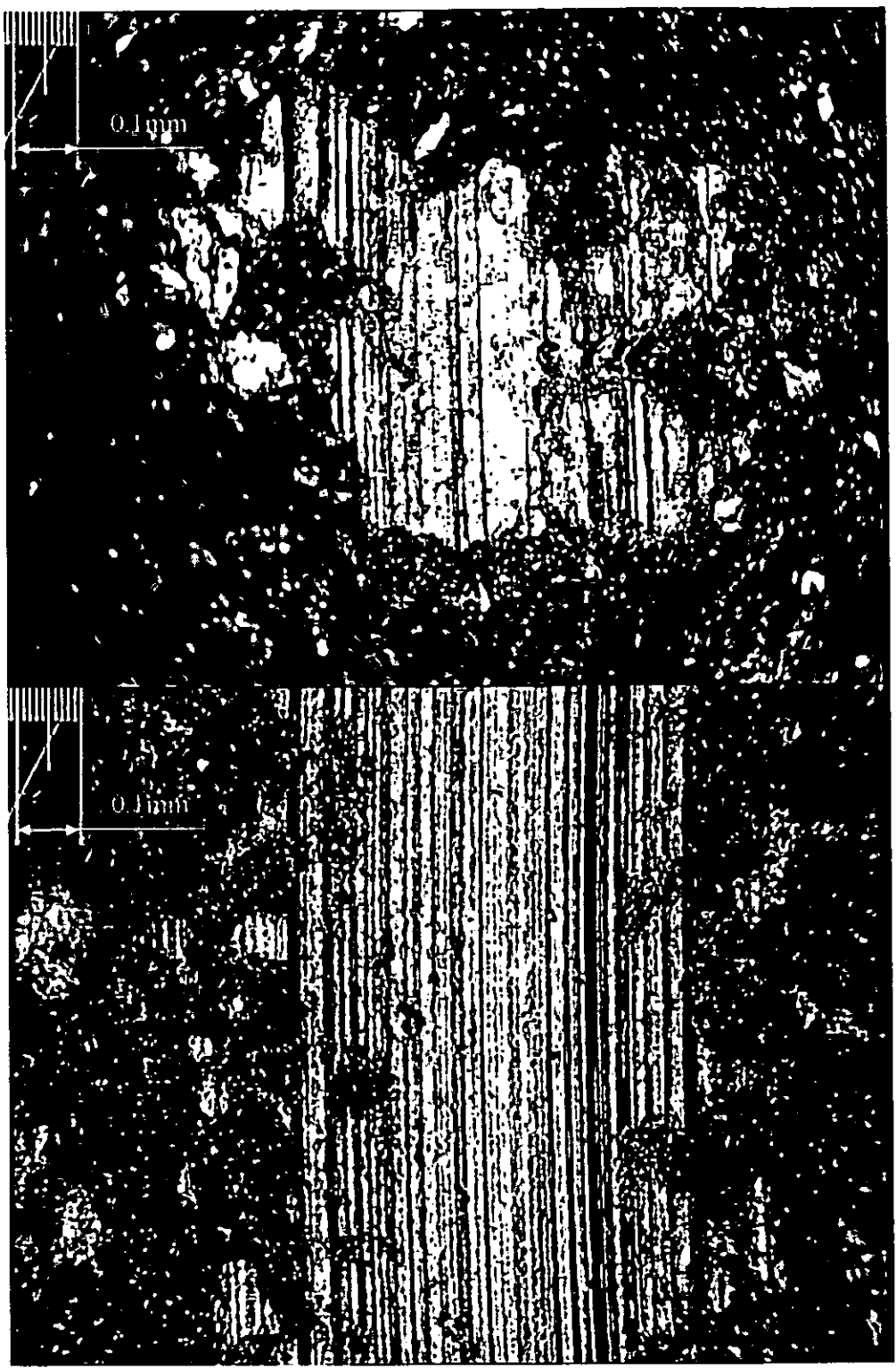


Figure 6.36 Test 3004 course finish 0.1ms^{-1}



Figure 6.37 Test 4001 as rec'd finish 0.5ms^{-1}



Figure 6.38 Test 4002 fine finish 0.5ms^{-1}

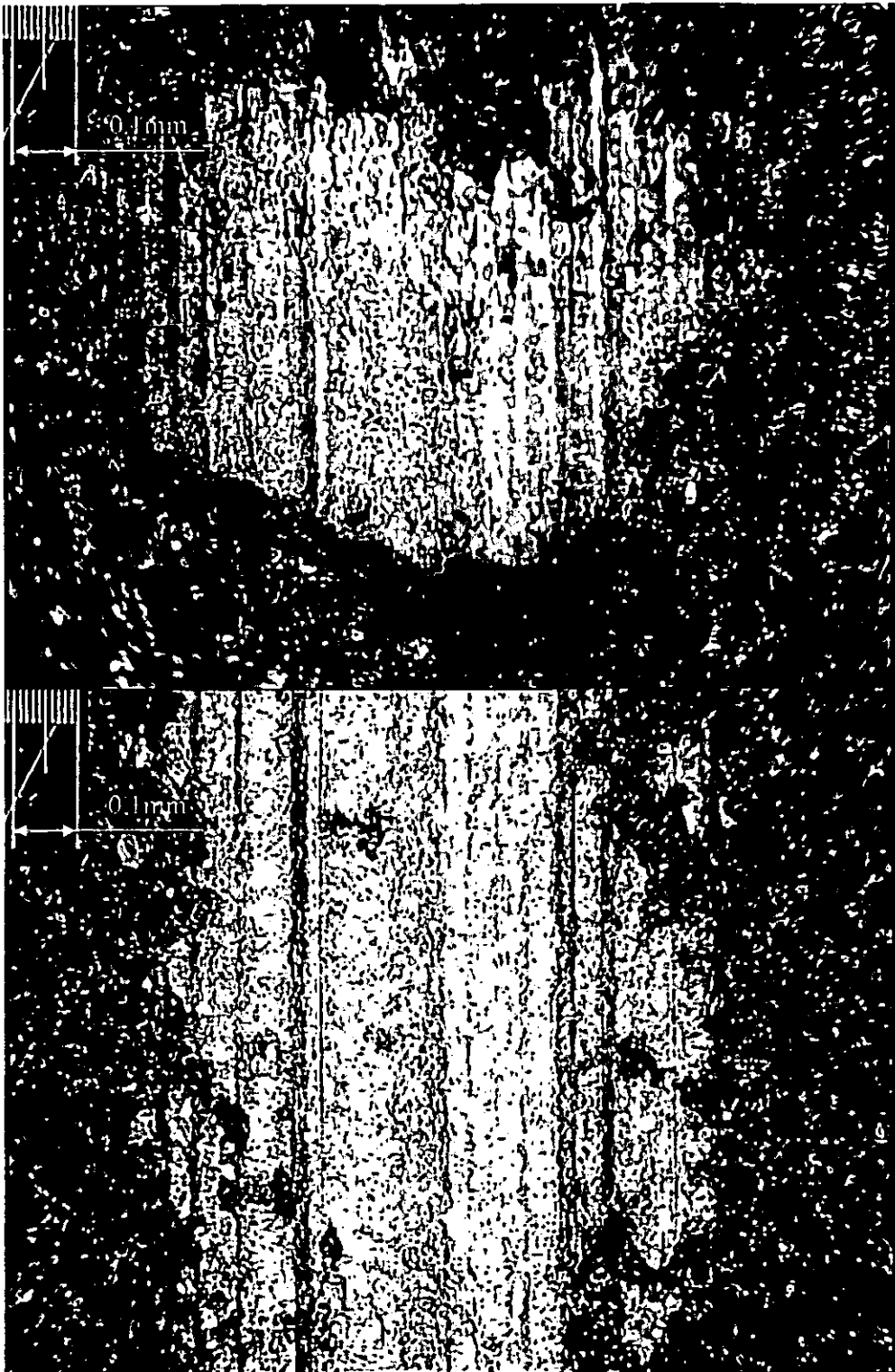


Figure 6.39 Test 4003 medium finish 0.5ms^{-1}

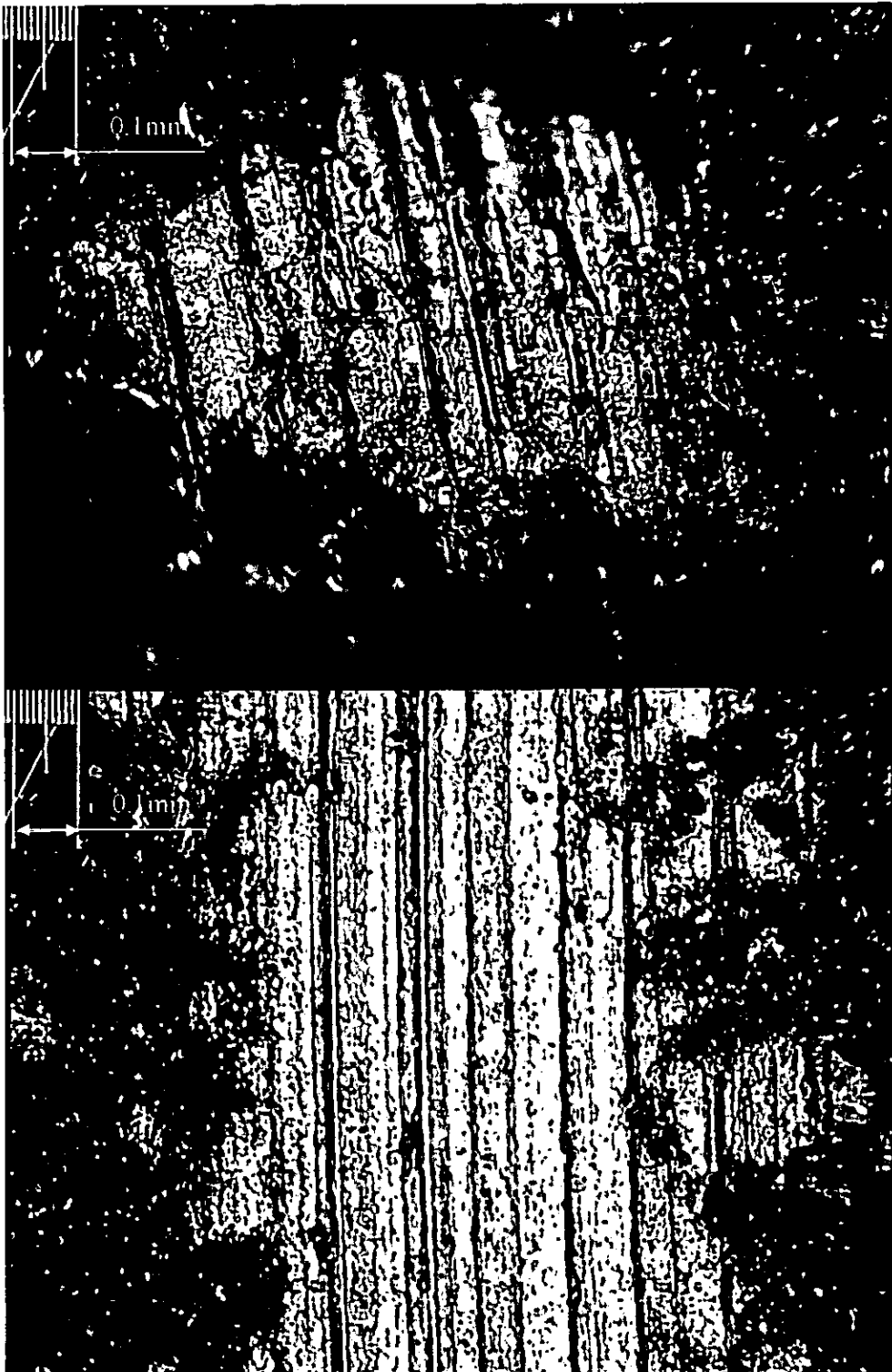


Figure 6.40 Test 4004 course finish 0.5ms^{-1}

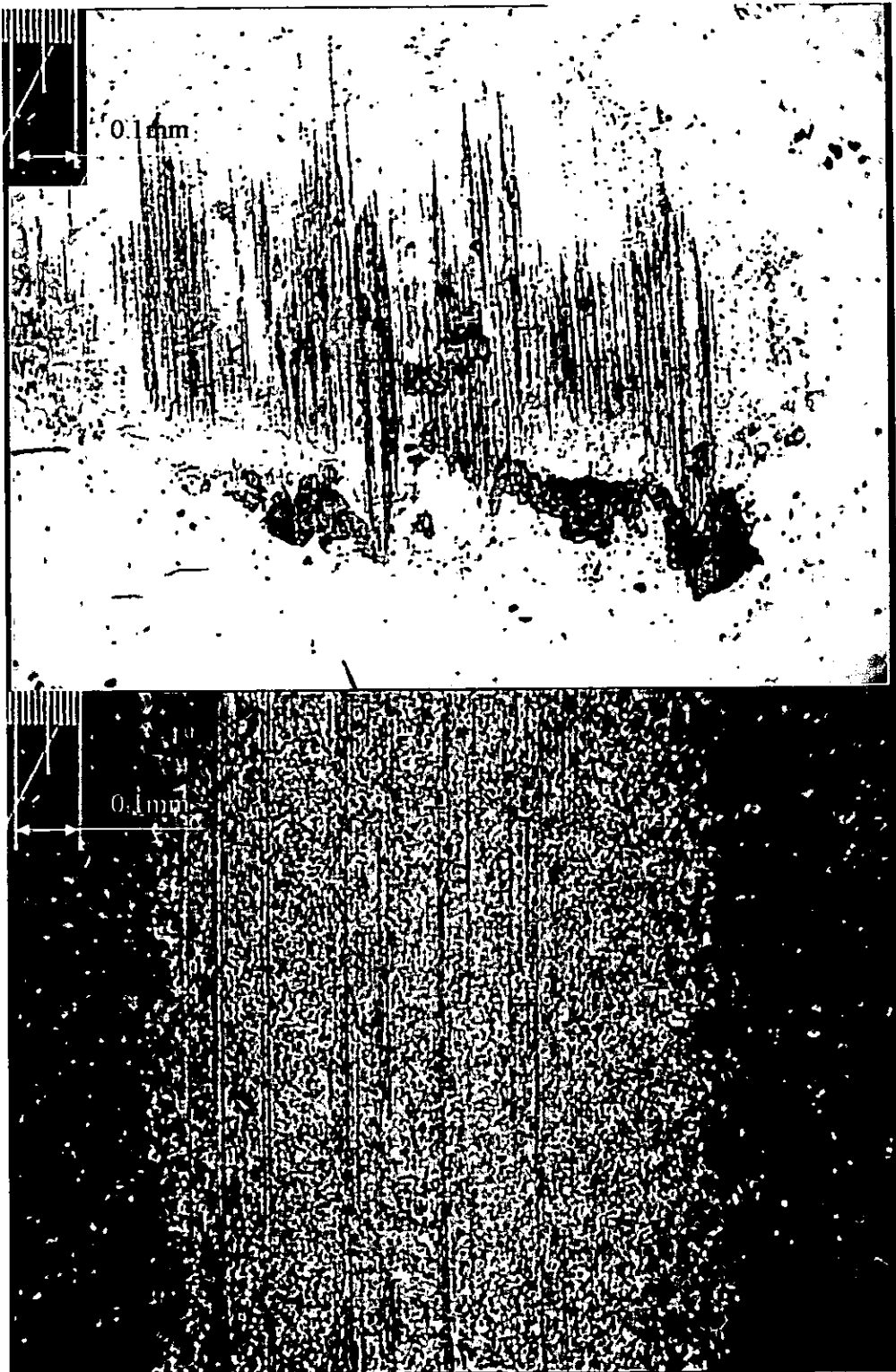


Figure 6.41 Test 5201 as rec'd 1.0ms^{-1}

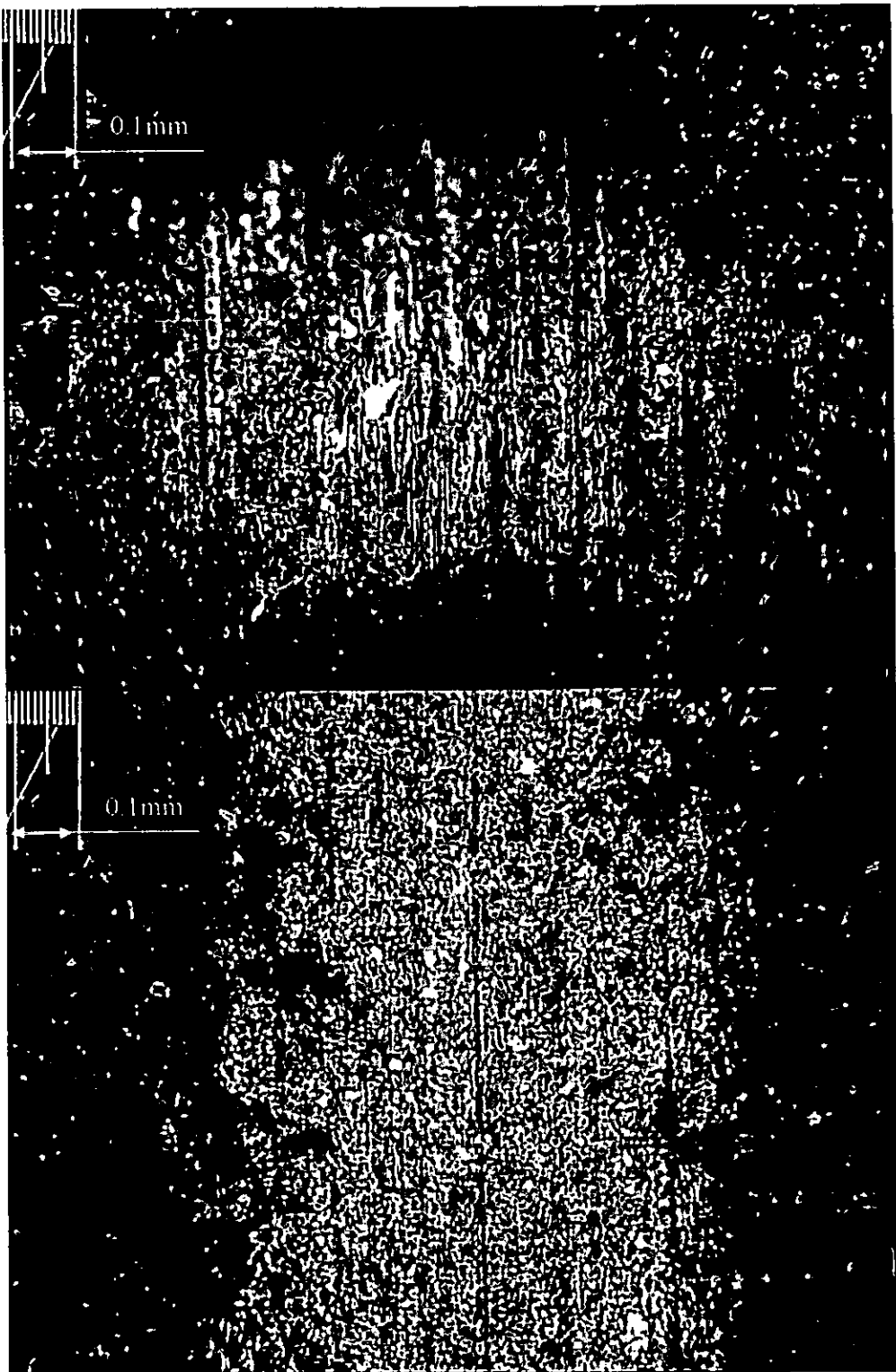


Figure 6.42 Test 5202 fine finish 1.0ms^{-1}

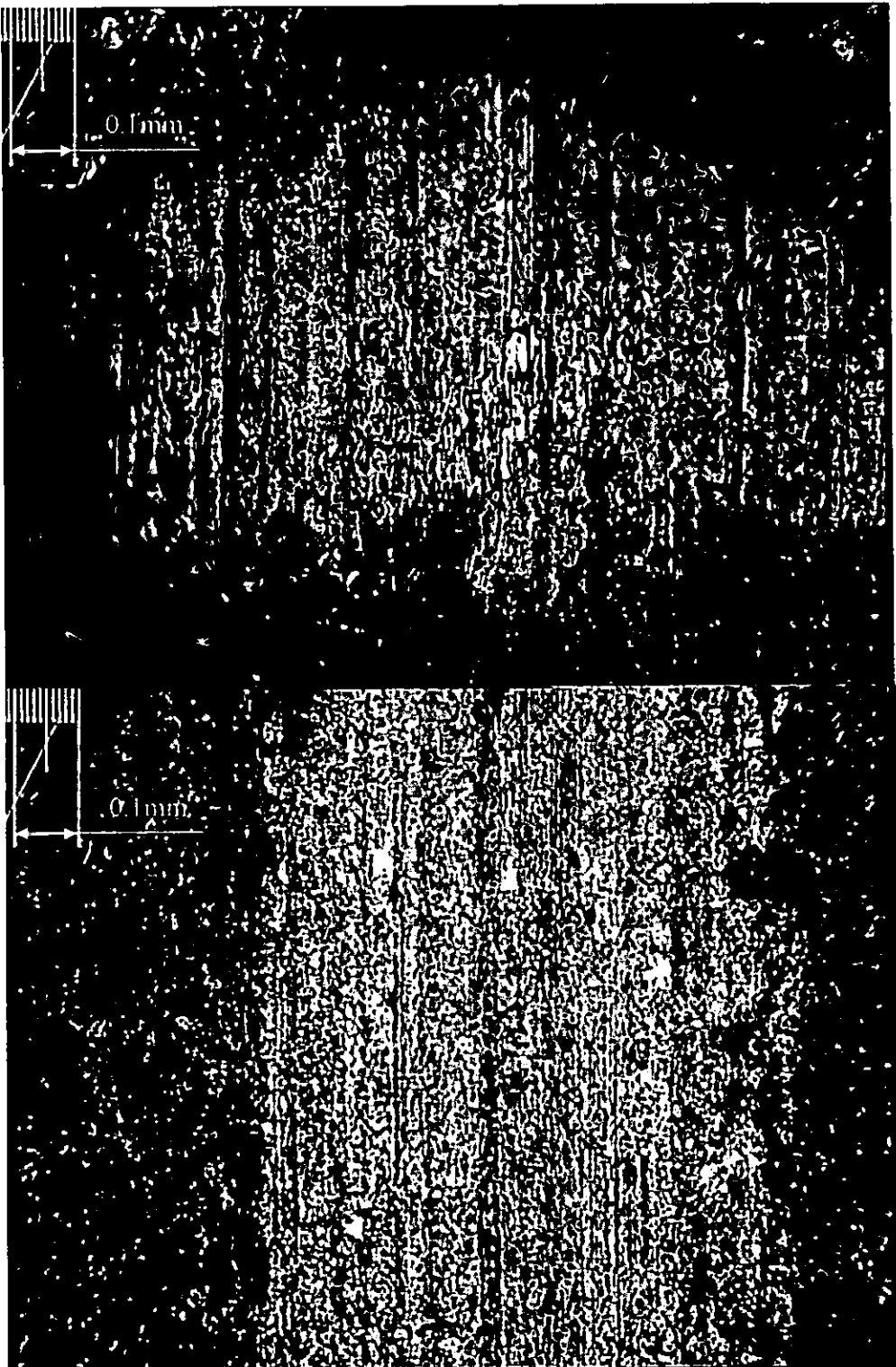


Figure 6.43 Test 5203 medium finish 1.0ms^{-1}

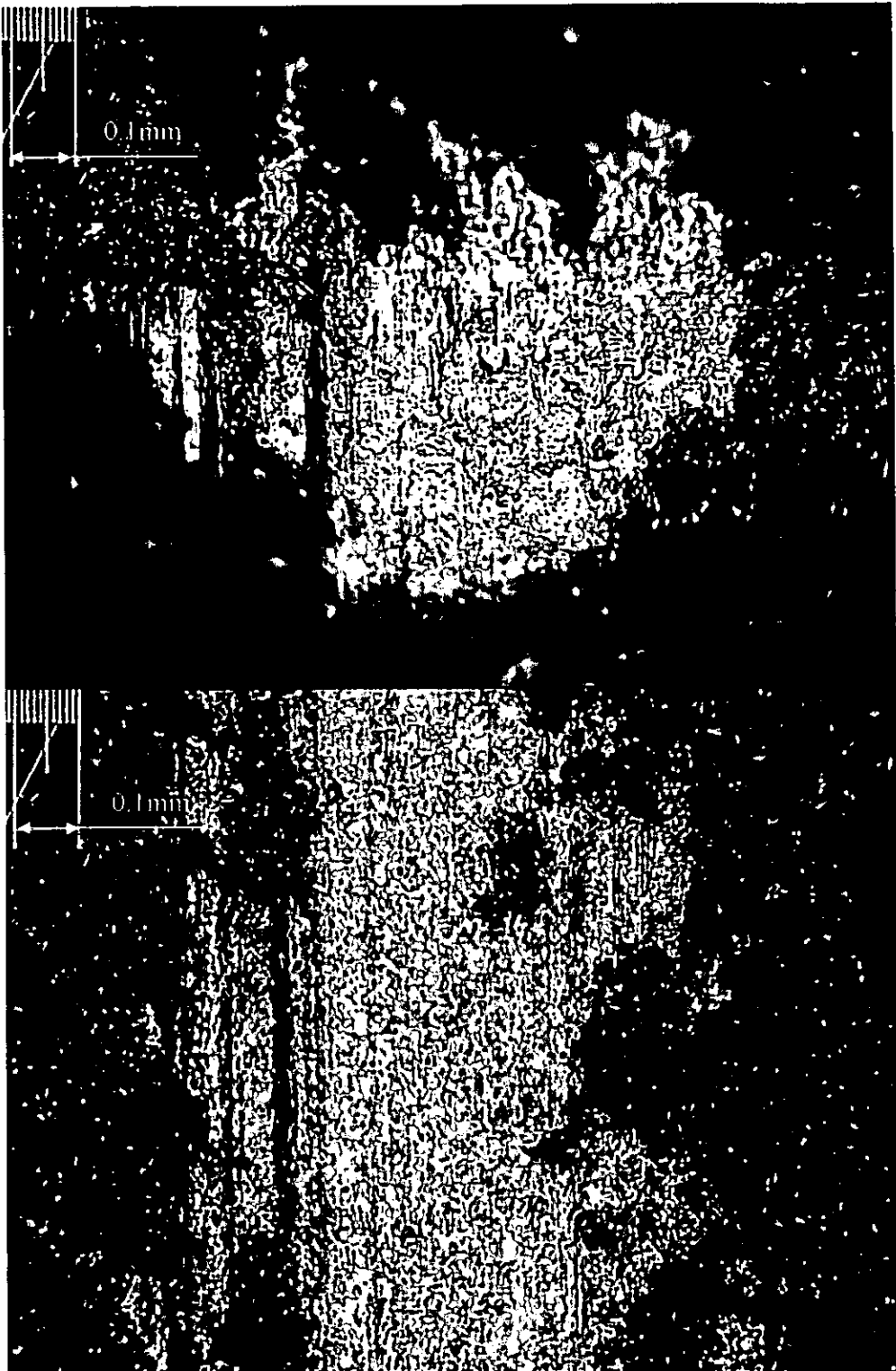


Figure 6.44 Test 5204 course finish 1.0ms^{-1}

6.7.2 Observations of results.

All the photographs have distinct similarities in that all the counterfaces have a “wear spot” which varies both in size and composition dependent on the surface finish of the ball. These “spots” comprising an area of apparently linear striations surrounded by dark areas and spots of wear debris. The coloured fringe patterns visible in figure 6.41 are due to the inadequate cleaning/degreasing of the ball prior to test.

The as received finish samples in figures 6.41, 6.42 and 6.49 increase in width, length and intensity as the test velocity increases, with figure 6.49 exhibiting distinct colour fringe patterns and large areas of wear debris at the trailing edge of the spot. The fringe patterns have been demonstrated by Fusaro [6.] to be the result of very thin transfer films deposited on the counterface, the thickness of which is proportional to the wavelength of the particular colour of light. It is thought that these wear spots are composed wholly of material that has been transferred from the disc with very little or no wear occurring on the ball.

The counterface samples that have been grit blasted all exhibit relatively thick transfer films that again vary in size with the test velocity. The samples tested at 0.1ms^{-1} look rather flaky, as if small areas have been dislodged during testing. In general as roughness increases the spot and corresponding striations become more defined. The samples that were tested at 1.0ms^{-1} exhibit some highly polished areas in a greyish matrix more like the wear track on the disc. This could possibly be caused by the localised melting of the film at the ball/disc interface.

The disc wear tracks again exhibit distinct striations but are visibly radial in nature, these striations correspond to the counterface profiles in the majority of the samples. The width of the wear track tends to increase with the increase in roughness of the surface finish of the ball and a distinct change occurs in the appearance at the 1ms^{-1} test velocity, again this may be caused by localised heating and melting of the film. In some of the photographs the wear spot appears wider than the width of the corresponding wear track, the most probable cause for this is small variation in the film thickness due

to the application process and the slight run out in the flatness of the discs, approx 0.01mm, which were produced to commercial tolerances.

6.8 Contact Spot Generation above the yield pressure of the coating.

By utilising the unused outer track on one disc it was possible to generate imprints in the BSL at various loads from 10 to 100N. Ignoring any elastic deformation (spring back) an approximation of the contact spot diameter can be made. Figure 6.53 shows the digital photographs of these imprints with a reference scale in the lower right hand corner of each record, full scale is equal to 1mm. Table 6.6 shows the measured and calculated diameters and these are plotted in figure 6.54

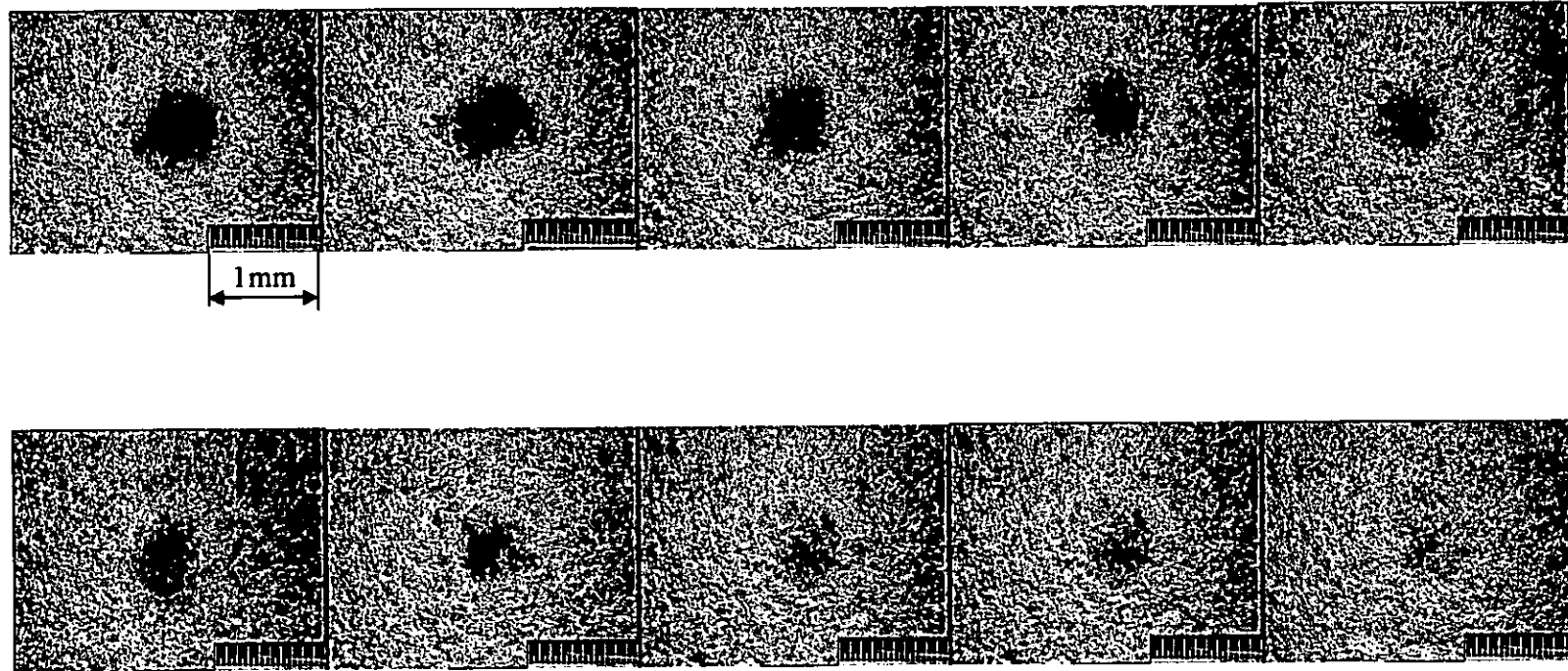
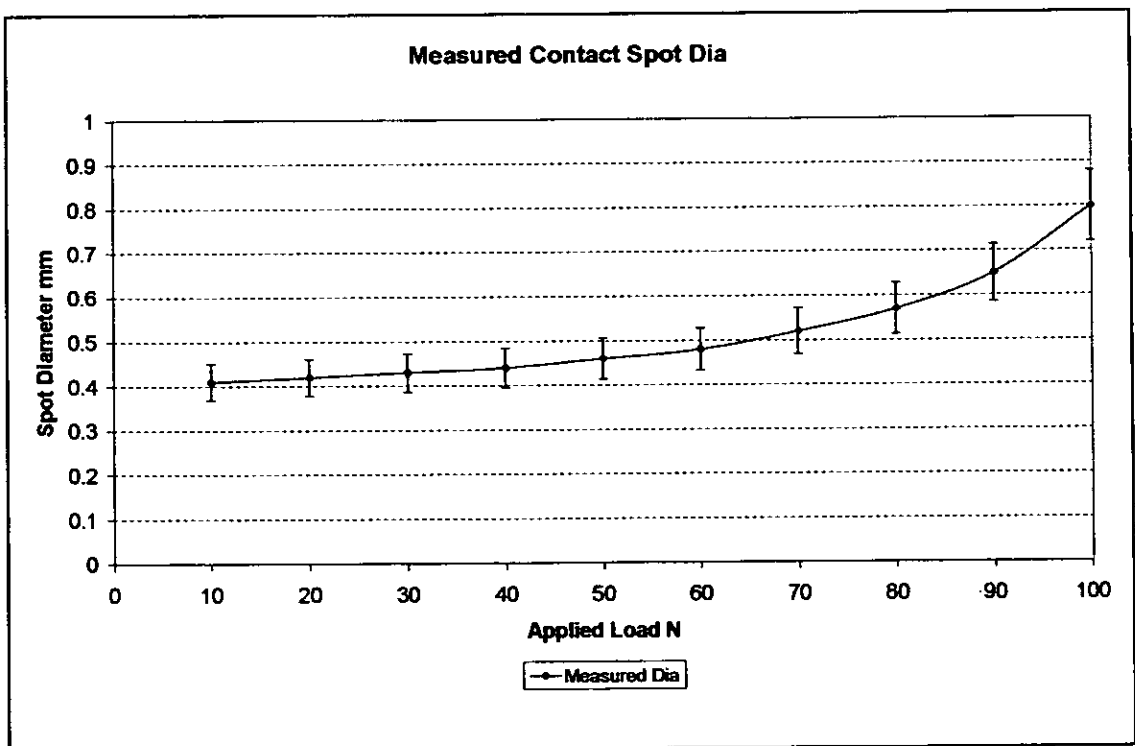


Figure 6.45 Ball Indentation Imprints. Top line left to right 100N -60N. Bottom line left to right 50N – 10N.

Applied Load N	Measured Spot Diameter mm
100	0.8
90	0.65
80	0.57
70	0.52
60	0.48
50	0.46
40	0.44
30	0.43
20	0.42
10	0.41

Table 6.7 Spot Diameter Measured.



**Figure 6.46. Measured Contact Spot diameters
With 10% error bars.**

6.9 Calculation of the predicted contact spot from Hertzian contact mechanics.

The contact diameter for a sphere in contact with a flat plain is given by the Hertzian elastic contact theory given in Chapter 3.

$$\text{Contact radius } a = \left(\frac{3WR}{4E^*} \right)^{\frac{1}{3}}$$

Therefore for an applied load W , where R is 0.006m and E^* is the combined modulus again given in Chapter 3:

$$\frac{1}{E^*} = \frac{1 - \nu_1^2}{E_1} + \frac{1 - \nu_2^2}{E_2}$$

The elastic modulus for the steel ball does not present any problems and can be found in any number of textbooks on the subject with 210 GPa being an accepted value. However when it comes to thin films of BSLs there is little or no information in the public domain, therefore approximations must be made from the information that is available for the bulk material. Unfortunately, with BSLs we are dealing with a mixture of several materials e.g. Polyamide-imide, graphite, PTFE and several other additives. If the ratios of the main constituents were known then an approximation could be made by proportioning the moduli in the ratios of the mixture. Due to the commercial sensitivity of this, the material manufacturers will not divulge this information. Therefore several informed guesses have been made in order to give some sort of comparison with the theoretical values. Table 6.8 contains the mechanical properties of the two main constituents which are to be used in calculating the contact spot diameter. Table 6.9 shows the effects of the ratio of mixture on these values for three mixture ratios, graphite is not included due to lack of information, also it is thought that only small amounts of this material have been added to the particular BSL.

Material	Modulus E GPa	Shear strength MPa	
Polyamide-imide	4.6	85	
PTFE	0.65	5	
Graphite	No information available for material in powder form.		

Table 6.7 Mechanical properties of bulk materials.

Identification	Mixture ratio %	Modulus E GPa
75-25	75% polyamide-imide 25% PTFE	$4.6 \times 0.75 + 0.65 \times 0.25 = 3.612$
50-50	50% - 50%	$4.6 \times 0.5 + 0.65 \times 0.5 = 2.625$
25-75	25%-75%	$4.6 \times 0.25 + 0.65 \times 0.75 = 1.637$

Table 6.8 Mixture moduli.

Using the above moduli in the excel spreadsheet calculator described in the next chapter gives the following contact spot diameters for an applied load of 10N.

75-25	Diameter 0.451
50-50	Diameter 0.501
25-75	Diameter 0.586

For an applied load of 100N

75-25	Diameter 0.973
50-50	Diameter 1.081
25-75	Diameter 1.263

6.10 Discussion.

The test programmes described for the contact evolution at constant load and velocity and the friction measurement below the yield pressure of the film, demonstrate two distinct phases in the contact conditions. In the early stages of sliding a thick deposit is formed on the counterface and sliding occurs between this deposit and the film, the amount, shape and size of the deposit being dependant on the initial surface finish of the counterface, the applied load and the velocity of sliding. At loads below or approaching the yield point of the film, the deposit appears to be relatively thick on the surfaces that had been grit blasted, whereas the as received finish samples exhibit an apparently thinner transparent deposit.

Above the yield point of the film the shape and size of the contact is more defined and can be explained by the initial geometry of the interface, again it is thought that in the early stages of sliding a thick deposit is generated, however under this condition the contact changes with distance travelled, as the wear track in the film deepens. At some point, determined by the applied load the contact conditions change to the more familiar circular scar illustrated in figure 6.1, at this point it is thought that sliding occurs between very thin transfer films on the wear scar, a very thin film on the disc, with the wear debris formed in the early stages acting as a reservoir of lubricant to replenish the bearing surfaces, this phase represents 90% of the sliding life of the BSL.

The values for the calculated contact spot diameter for a mixture are all higher than the measured values for 10N and 100N this could be due to the elasticity of the film not being taken into account and difficulty in assessing the actual diameter due to the “fuzzy” boundary produced, also the uncertainty of the film mechanical properties.

6.11 Summary.

The friction coefficient at various loads below and approaching the yield pressure of the material have been measured at three velocities and four counterface surface finishes

and the data plotted. The reduction in friction coefficient as load increases is shown with a summary chart demonstrating the minimal effect of surface finish and velocity.

The formation of the different contact conditions that exist at various times during the sliding life of a sphere in contact with a bonded solid lubricant and the differences and similarities at loads above and below the yield pressure of the lubricant film discussed

The generation and measurement of the contact spot under static loading conditions from 10 to 100N with a 12mm ball have been undertaken and a comparison made with the predicted values.

Reference.

- [6.1] Singer, I. L., Bolster, R. N., Wegand, J. C., Feyeulle, S., Stupp, B. C., "Hertzian stress contribution to low friction behaviour of thin MoS₂ coatings." Appl. Phys. Lett. 57. 1990, pp. 995.
- [6.2] Rabinowicz, E., "Wear coefficients." Wear Control Handbook, Peterson, M. B., Winer, W. O., (eds) ASME New York, 1980, pp. 475 - 506
- [6.3]. Fusaro, R. L., "Effect of load, area of contact and contact stress on the tribological properties of polyimide bonded graphite fluoride films." ASME Proceedings of the International conference on wear of materials. 1981, pp.625-636.

CHAPTER 7.

COMPARISON OF EXPERIMENTAL AND THEORETICAL RESULTS.

In this chapter an empirical model is developed for the first phase of sliding under loading conditions above the yield point of the BSL film. The experimental results are reviewed against the accepted simple and modified theories of friction.

Finally three spread sheets are included for calculation the Hertzian contact area and friction coefficients at various loads and with differing models.

The following table is a summary of the subject detail discussed in this chapter.

Section	Contact condition	Model
7.1.1	Mixed	Empirical
7.2.1	Elastic	Hertzian $\mu = kW^{-1/3}$
7.2.3	Elastic/plastic	Ploughing $F = A.s + p_e$
7.3	Elastic/plastic	Simple $F = A.s$
7.4.1	Elastic/plastic	Modified theory with tangential load $\mu = \frac{1}{W} \left(\frac{A^2 p_0^2 - W^2}{\alpha} \right)^{\frac{1}{2}}$
7.4.2	Contaminated surface	s_f / p_0
7.5	Elastic, above yield strength but below the hardness plastic limit.	Hertzian
7.6	Flat / mixed	Simple $F = A.s$

7.1 Empirical model of time dependant friction.

In this section an empirical model is developed from the experimental data obtained from the test programme in chapter 5.

7.1.1 Generalised performance phases.

From the results obtained in chapter 5 where friction coefficient was plotted against sliding distance it can be seen that there are three distinct phases during the sliding life of a BSL in contact with a sphere:

- A region where the friction coefficient increases slowly over similar periods of time for each particular finish (This is not as apparent as velocity reduces in the 10N load tests).

- A region where the friction coefficient remains relatively stable (This is also barely noticeable for some of the high load tests).
- A region where the friction coefficient is erratic and increases rapidly.

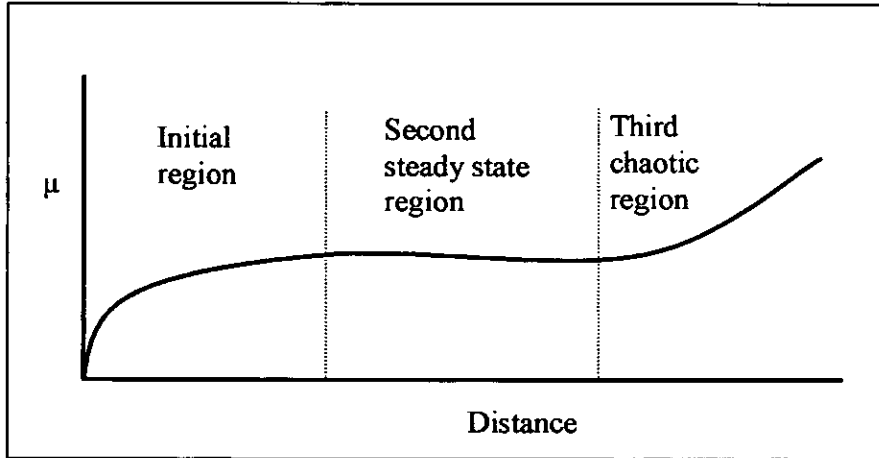


Figure 7.1 Generalised performance phases.

7.1.2 Modelling of the first phase.

During the first phase of sliding the friction coefficient initially rises sharply with respect to sliding distance then more slowly as illustrated in figure 7.2

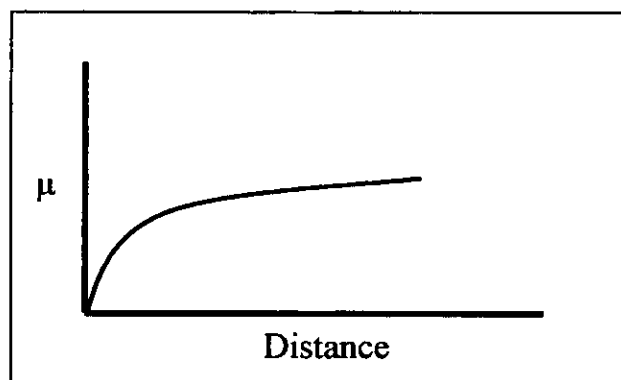


Figure 7.2 Shape of first phase of friction curve.

This type of curve can normally be described by the function:

$$y = a \cdot \ln x + b$$

By using the trend line function in 'Excel' trend lines have been generated for all of the results, an example of which is shown in figure 7.3 with the function describing it and the confidence indicator R^2 , this is an assessment of how closely the trend line fits the data and is most reliable as it approaches 1.

Figure 7.4 is a collection of all the data up to a sliding distance of 700 metres from test 1 – 12 and illustrates the similarity of all the tests in this sequence. Figure 7.5 is the repeat of the tests shown in figure 7.3 (25 –36).

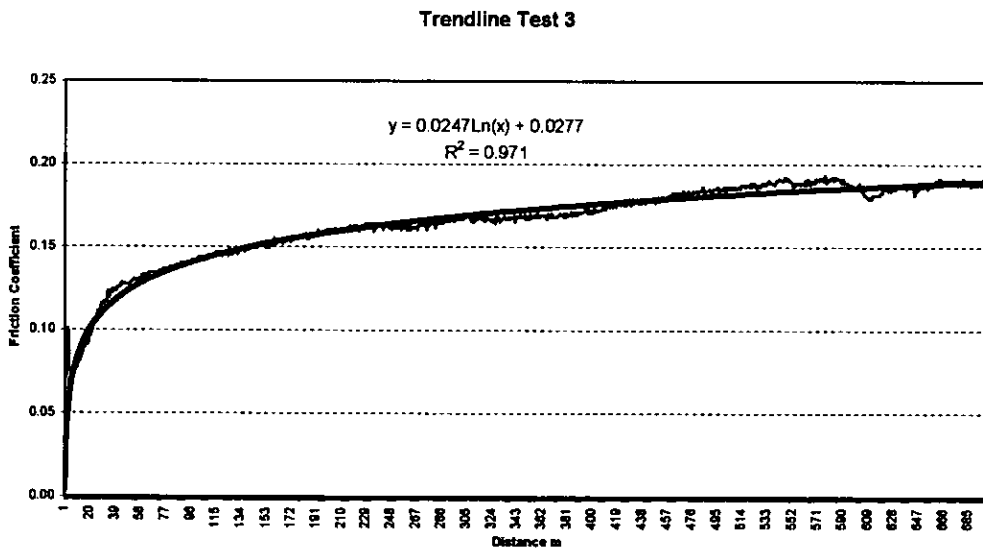


Figure7.3 Test Number 3 with trendline.

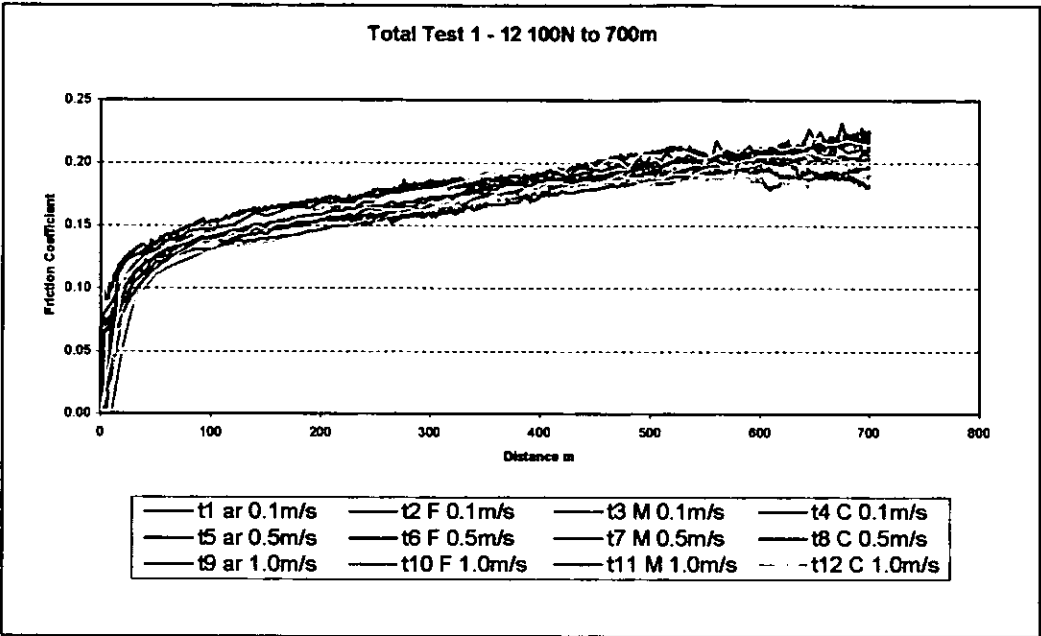


Figure 7.4 100N Tests 1 – 12 to 700 metres.

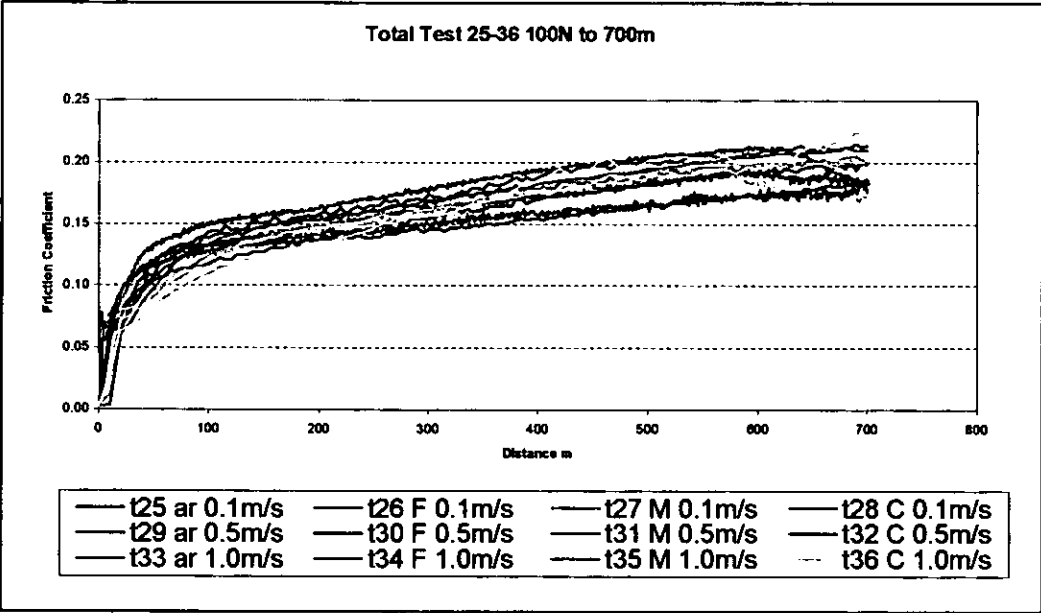


Figure 7.5 Repeat of Tests 1 – 12 (25 – 36)

By taking the average of all the individual curve constants an empirical model for the friction coefficient can be derived for this series of tests that is independent of sliding velocity and counterface finish.

For the 100N tests:

$$\mu = 0.035.Ln (D) + 0.035$$

Where D is the distance travelled, and an average confidence indicator of 0.95 is obtained.

Similarly for the 10N Load tests the average of all the individual curves the empirical model for the friction coefficient would be:

$$\mu = 0.02.Ln (D) + 0.065$$

With an average confidence indicator of 0.85

7.1.3 Discussion.

The empirical model developed here has not been assessed for other BSL mixtures but it is thought that in general they will follow the same behaviour with changes to the constants, giving the friction coefficient independent of load, velocity and counterface surface finish. The model could also be used to predict the friction coefficient in the second phase of performance. However from the results in chapter 5 it can be seen that the useful sliding life is affected by both surface finish and the velocity of sliding, the velocity of sliding having the greatest impact and therefore the model is limited to where sliding speeds are sufficient to produce the long steady states seen in the 1ms^{-1} tests.

7.2 Models dependant on contact geometry.

Here the experimental results are compared with accepted theoretical models for sliding under elastic conditions and combined elastic / plastic deformation.

7.2.1 Elastic contact model.

It has been shown, see references in chapter 3 that the frictional force is the result of ploughing the surface by asperities and particles, the adhesion between the surfaces in contact and by asperity deformation. In elastic contact the friction coefficient decreases as load increases. The relationship between the friction coefficient μ and load W is given by [7.1]:

$$F = As$$

Hertzian contact area is proportional to load $^{2/3}$ and the friction force F is proportional to A

$$A_H \propto W^{2/3} \text{ and } F \propto A_H$$

therefore the friction coefficient, F/W is proportional to the load $W^{-1/3}$

$$\mu = kW^{-1/3}$$

where k is derived from the material constants, shear stress s , combined tensile modulus E^* and the radius of the asperity R these are given in the Hertzian friction model in chapter 3.

$$k = \frac{s\pi 3R^{\frac{2}{3}}}{4E^*{}^{\frac{2}{3}}}$$

The Minus 1/3 power can be interpreted as arising from an adhesion mechanism, with the contact area being determined by elastic deformation. In elastic contact frictional energy is dissipated during sliding by shearing at the interface. In contrast, where plastic contact occurs the friction coefficient increases as the load increases and frictional energy is dissipated by shearing at the interface and by plastic deformation of the softer material, in the case of a sphere on a flat surface, ploughing through the coating.

The data generated in chapter 6 figure 6.32 clearly follows the above relationship in that the friction coefficient reduces as the load increases. It follows then that at very

low loading conditions that generate pressures close to or below the yield pressure of the film the mechanism of sliding follows Hertzian elastic behaviour. Figure 7.8 shows the experimental data points with a trend line for one of the test series. The test numbers referring to the velocity i.e. 3000 – 0.1ms^{-1} , 4000 – 0.5ms^{-1} and 5000 – 1.0ms^{-1} .

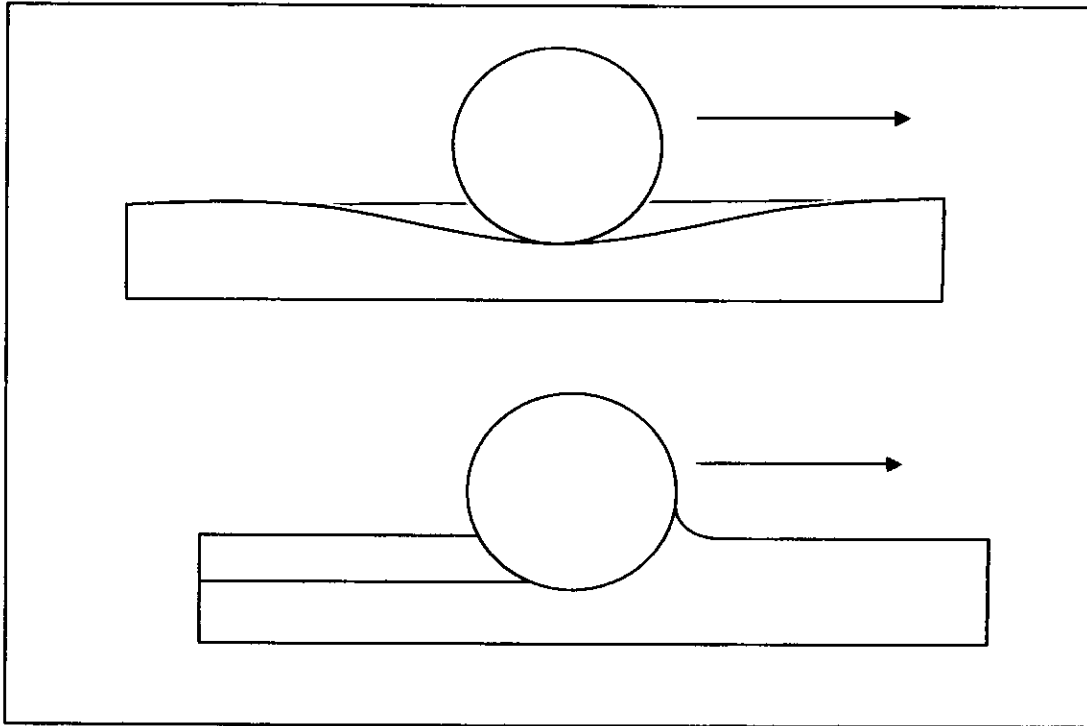


Figure 7.6 Top, sliding with elastic deformation, bottom, sliding with plastic deformation, ploughing.

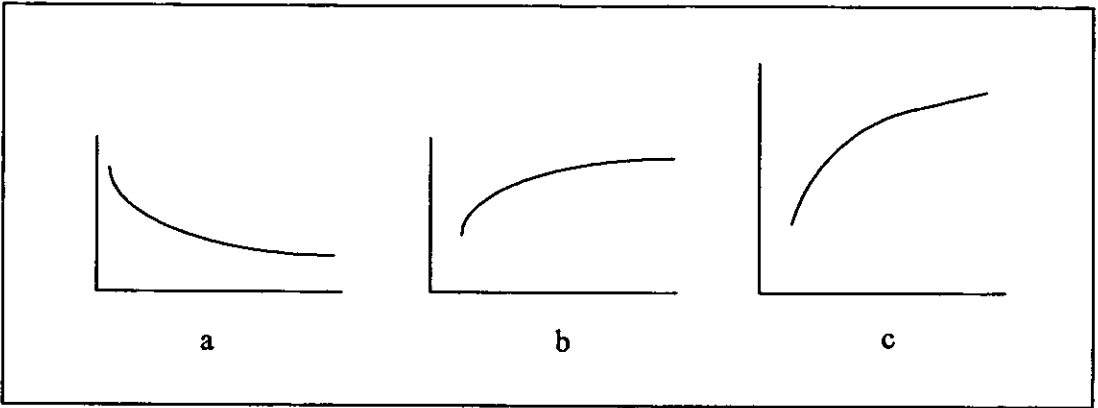


Figure 7.7 Schematic representation of load effect on friction coefficient for spherical, hard pin sliding on a flat soft solid. (a) Elastic contact. (b) Plastic contact. (c) Brittle contact.

Adapted from Solid Lubrication Fundamentals and applications [7.2]

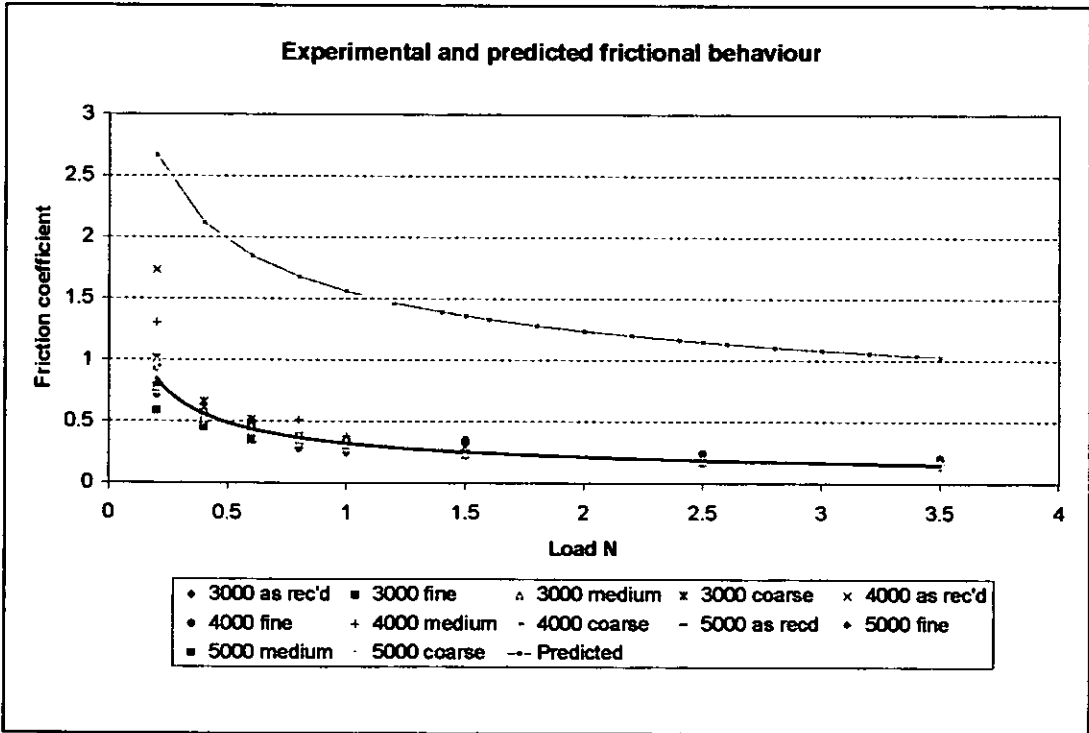


Figure 7.8 Experimental and predicted frictional behaviour.

The surface finish of the counterface appears to have little effect on the frictional performance, this can probably be explained by the build up of the thick deposits seen in the photographs in chapter 6 on the grit blasted samples, with sliding taking place between this deposit and the bulk of the film. It should be noted that even with loads as low as 0.2N a mark is produced on the film, indicating that some abrasion of the surface occurs, this could be due to the films being applied by spraying which produces a fine granular surface. It is well known that these surfaces can be “polished” by gently rubbing against a sheet of paper, this action removing the tops of the grains Figure 7.9 and 7.10.

Continuous sliding under elastic conditions eventually leads to breakdown of the film due to fatigue and in some cases thermal effects causing film delamination, some evidence of this is shown in the photographs in chapter 6 by the difference in appearance between the tests performed at 0.1ms^{-1} and those performed at 1.0ms^{-1} .

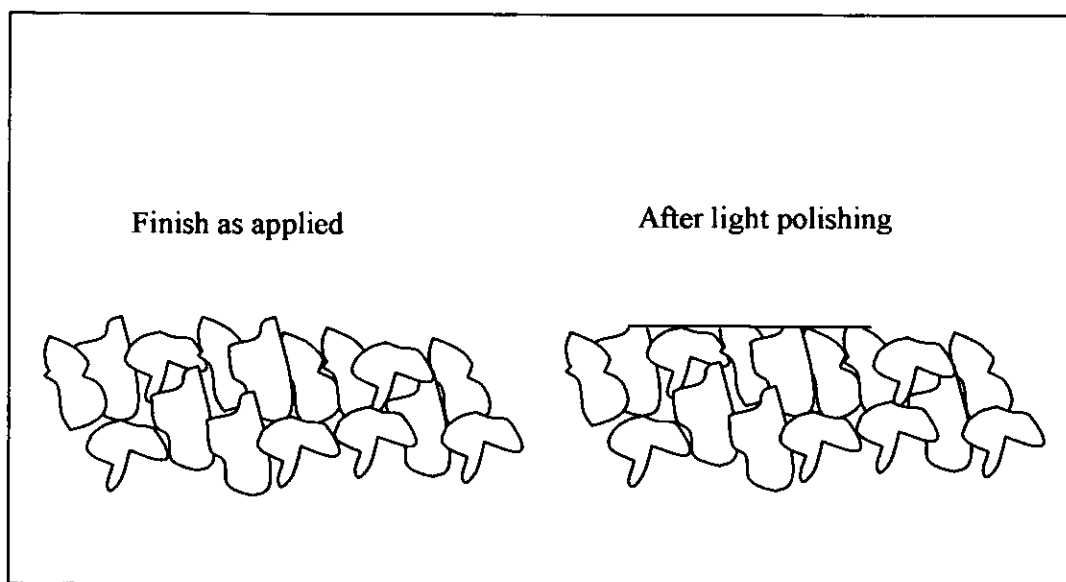


Figure 7.9 Effect of light polishing.



Figure 7.10 Film before and after light polishing.

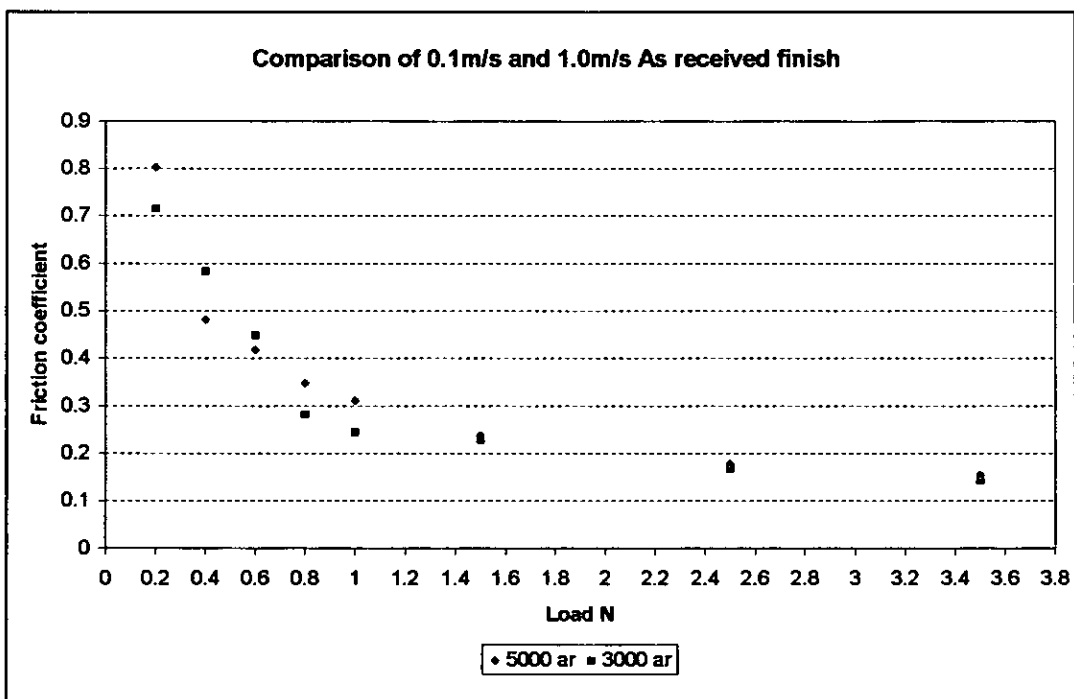


Figure 7.11 As received finish 0.1 and 1.0ms⁻¹ velocity.

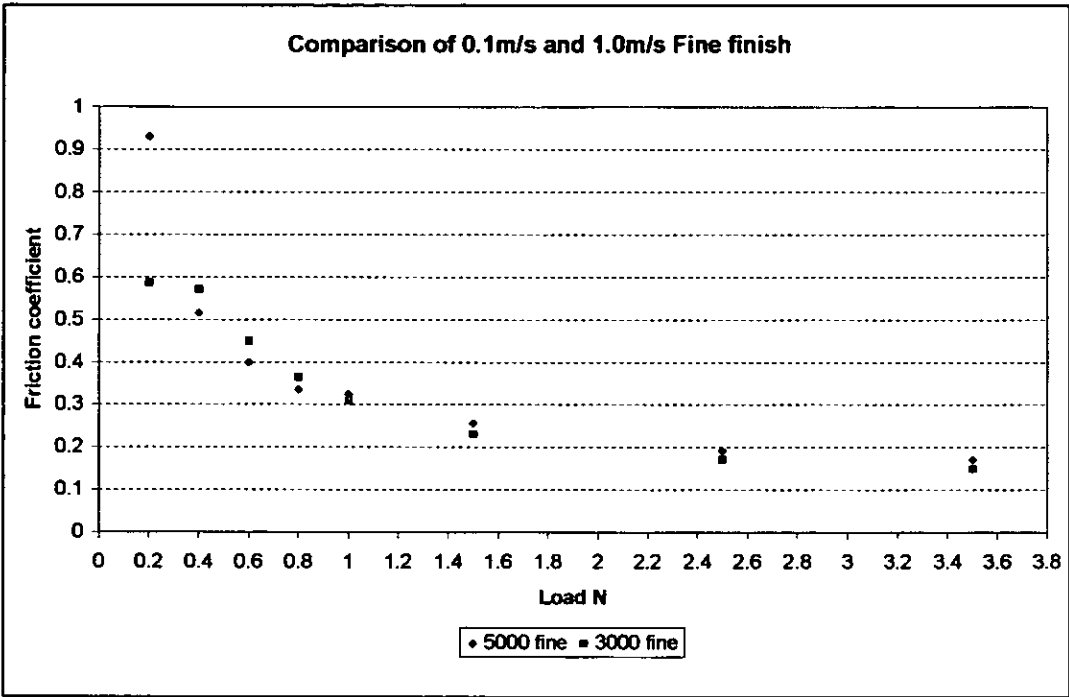


Figure 7.12 Fine finish 0.1 and 1.0ms⁻¹ velocity.

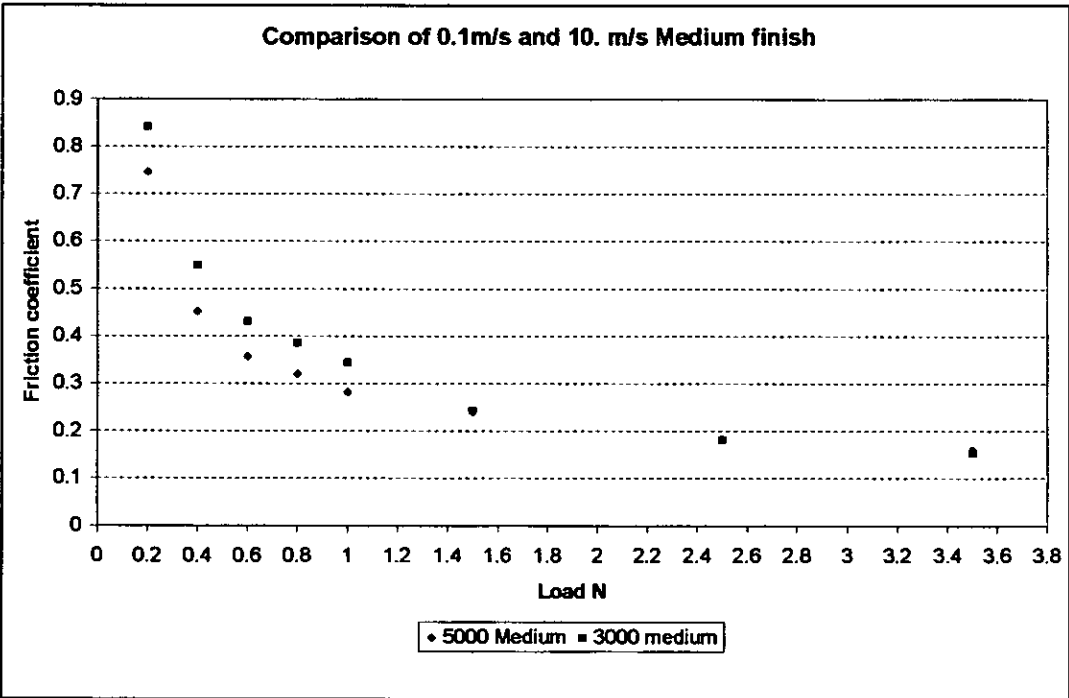


Figure 7.13 Medium finish 0.1 and 1.0ms⁻¹ velocity.

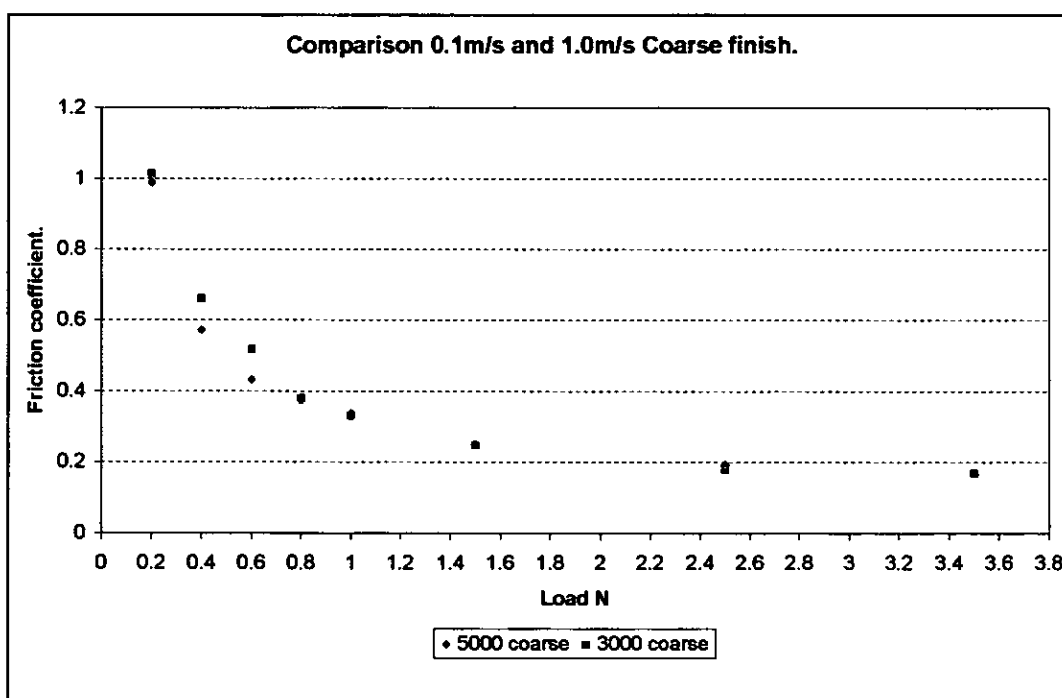


Figure 7.14 Coarse finish 0.1 and 1.0ms⁻¹ velocity

Velocity does not appear to have any great effect on the friction performance under these low loading conditions and this can be seen in the comparison between the 0.1ms⁻¹ and 1.0ms⁻¹ tests in figures 7.11 to 7.14.

7.2.2 Contact spot dimensions.

The areas of the contact spots generated on the samples used in the test programme were estimated by generating a grid pattern with reference to the scale contained in the photographs in figures 6.33 – 6.44. Two of these photographs complete with grid pattern are reproduced here for reference figure 7.15 and 7.16 and the corresponding areas for all the samples plotted in figure 7.17, this figure also contains the plot for the calculated Hertzian contact area for a 12mm diameter sphere at the final load of 3.5N.

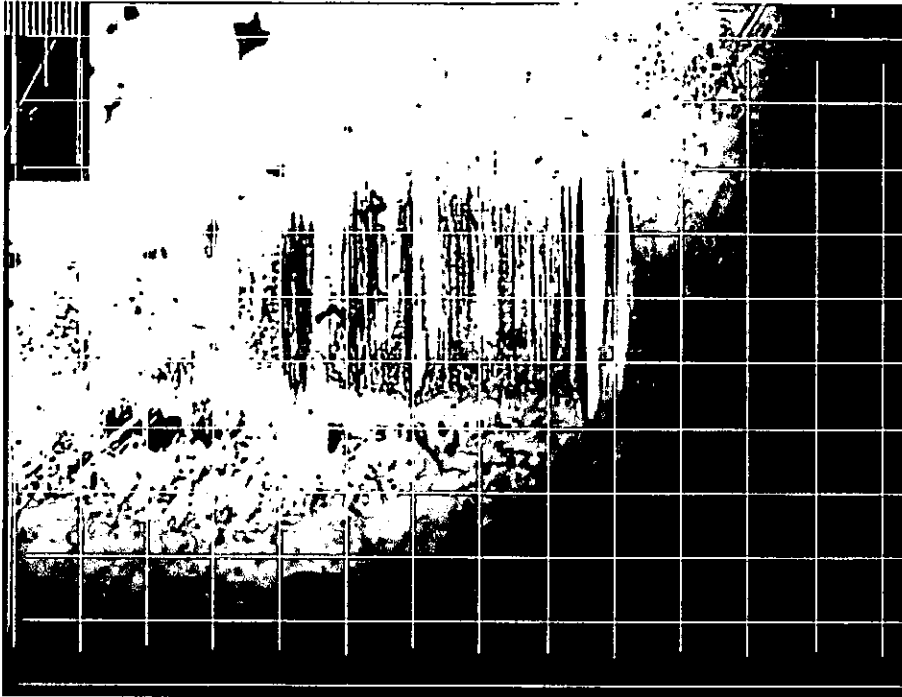


Figure 7.15 Sample 4001 with 0.1mm grid pattern.

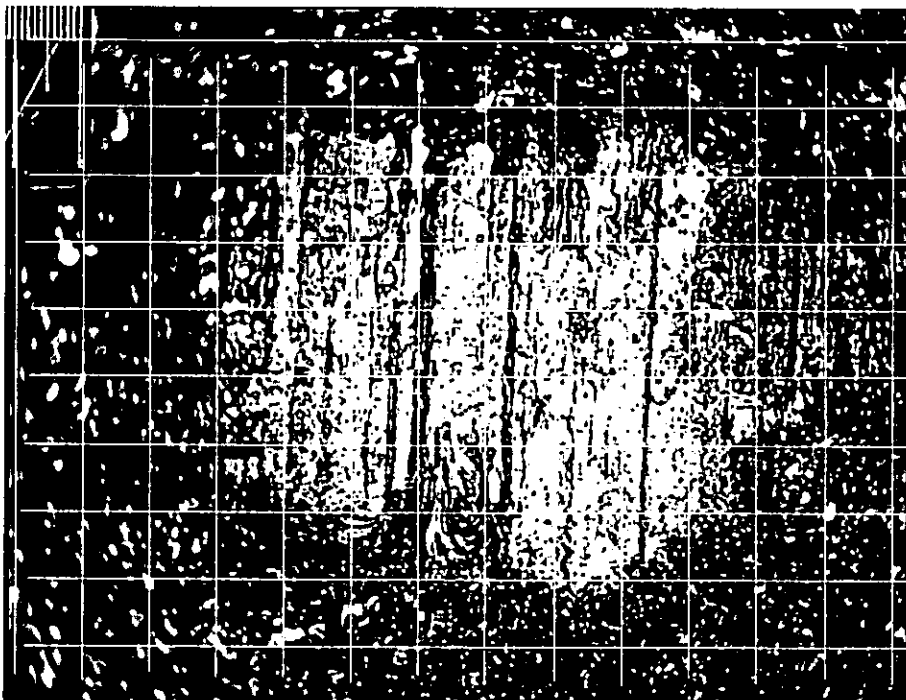


Figure 7.16 Sample 4002 with 0.1mm grid pattern.

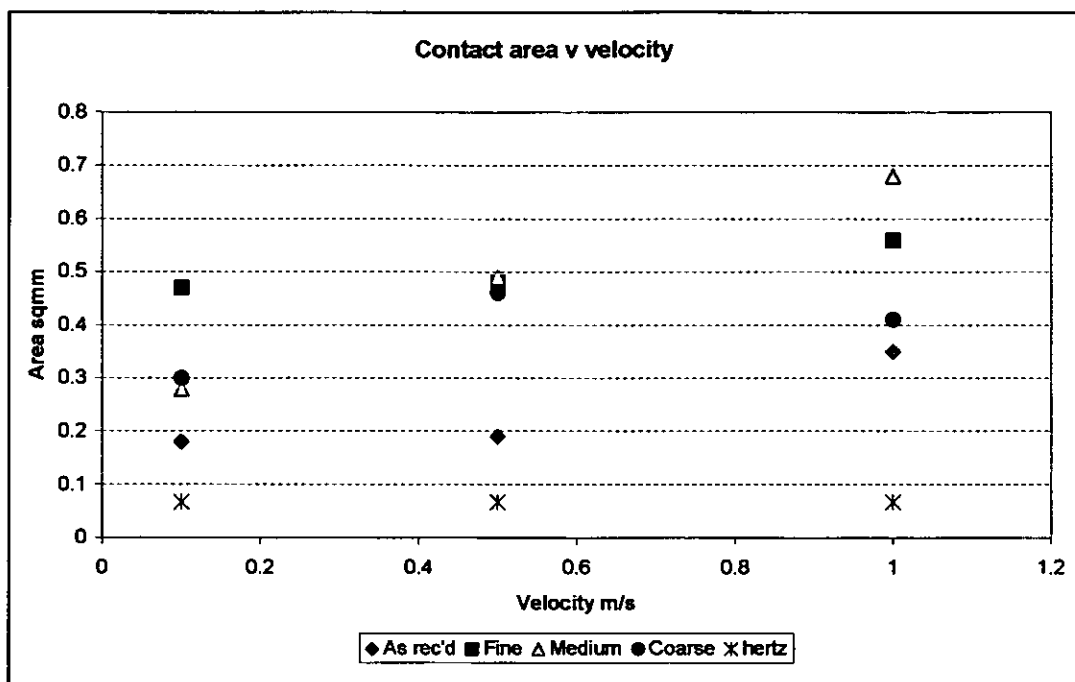


Figure 7.17 Apparent contact area vs. velocity.

The plot of contact area at each velocity shows a gradual increase in area as velocity increases and similarly as counterface roughness increases area increases. The areas measured for each velocity are approximately 2.5 – 10 times greater than those calculated using the accepted Hertzian contact theory for a sphere in contact with a flat plane. This can be explained by the build up of the thick deposit which may not all be in contact with the main body of the film at any one time i.e. the real area of contact may move about in this general area due to small movements in the apparatus or the unevenness in the track generated, or even by sections of the deposit breaking off and being replaced as sliding continues. Some evidence of this can be seen in figure 6.34 which is repeated here in figure 7.18.

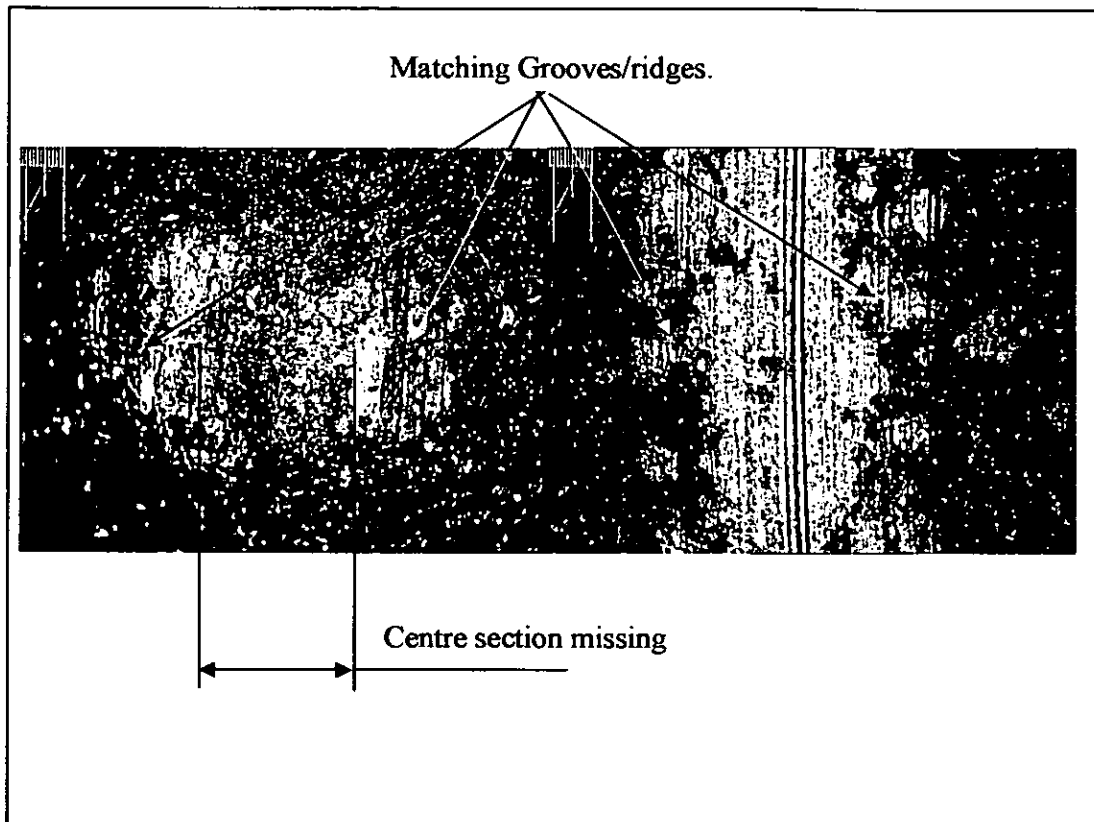


Figure 7.18 Missing section in contact deposit.

7.2.3 Models with simple elastic / plastic contact (no tangential load).

At loading conditions that produce contact pressures above the yield pressure of the film plastic deformation may occur as well as elastic deformation, this is illustrated in figure 6.45 in the previous chapter where permanent indentations were produced by pressing a 12mm diameter ball for 30seconds into the film under various loads, it is assumed that the marks left by the ball are due to the plastic deformation of the film, this is discussed later in section 7.5.

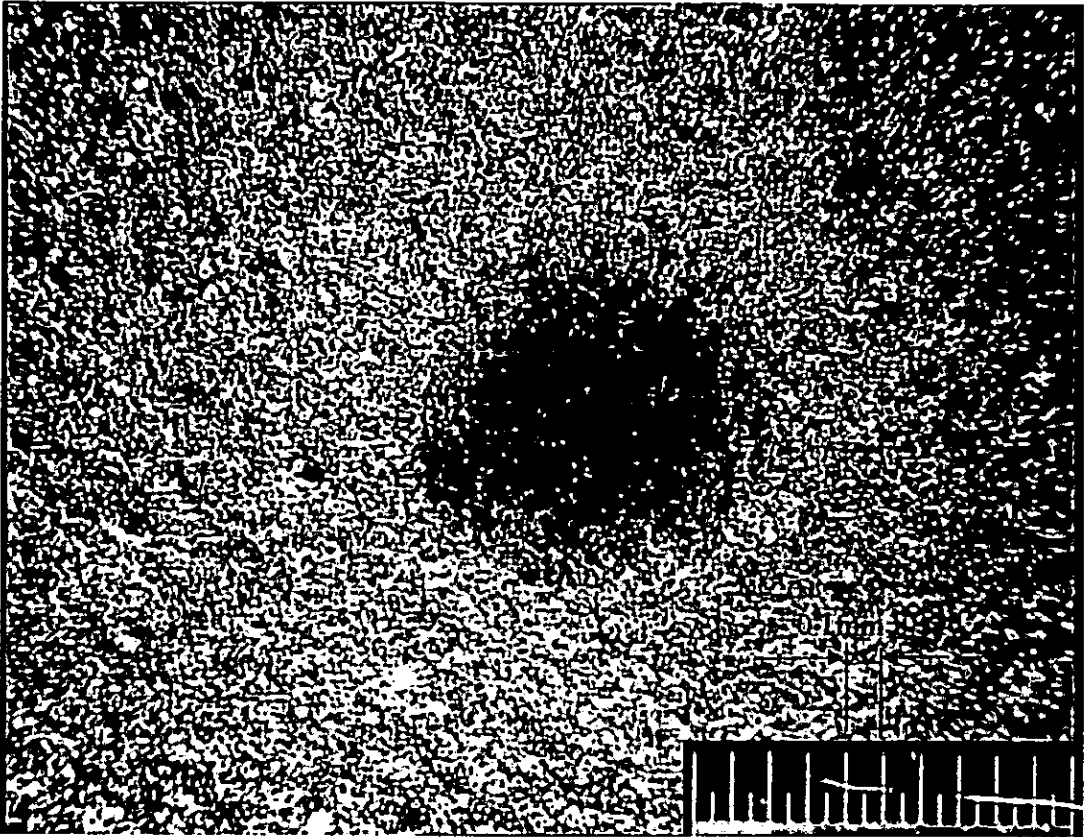


Figure 7.19 Plastic deformation of film 12mm ball 100N load.

In sliding contacts under these conditions there will be a combination of elastic behaviour and plastic behaviour. This was recognised by Bowden and Tabor in their simple theory of friction by the addition of the ploughing force p_e to take account of the force required to “plough” hard asperities through a softer surface, where:

$$F = A_s + p_e$$

The ploughing term for a spherical asperity in contact with a soft flat surface is related to the load due to half the vertically projected area divided by the resistive force due to the horizontal projected area. In the same way a sphere in contact with a soft film can be treated as a single large asperity then:

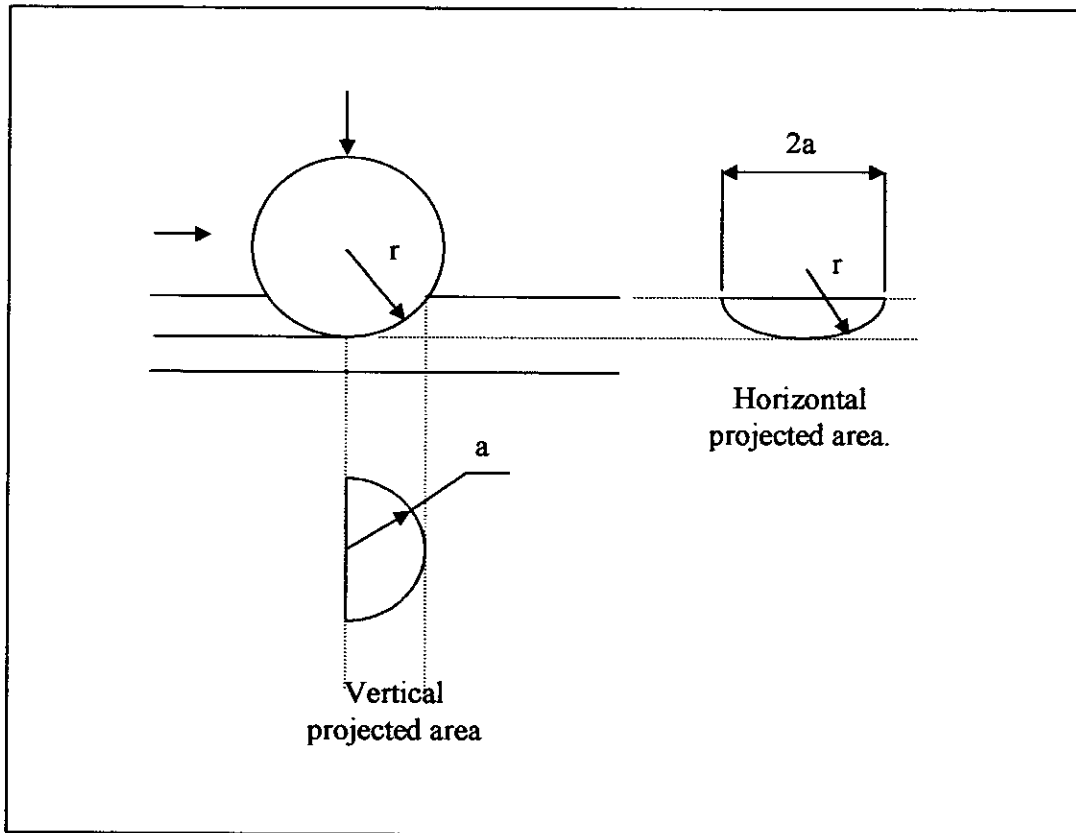


Figure 7.20 Single large spherical asperity projected areas.

For the vertically projected area:

$$\text{Area of a semi circle} = \frac{\pi a^2}{2} \text{ where } a = r \sin \frac{\theta}{2}$$

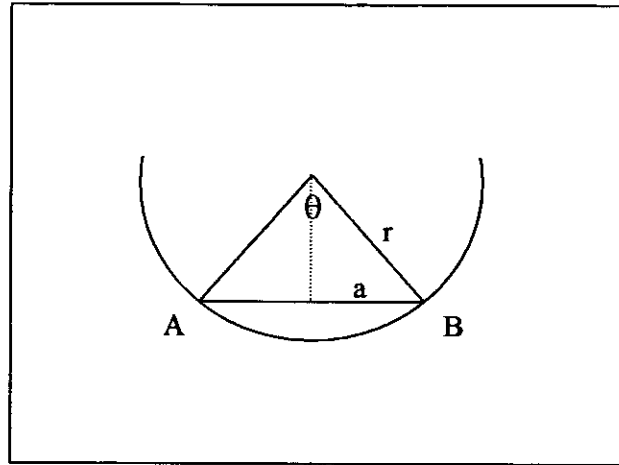


Figure 7.21 Horizontal projected area.

For the horizontal projected area:

$$\text{Arc AB} = r\theta$$

$$\text{Area of sector} = \frac{1}{2}r^2\theta$$

$$\text{Area of triangle} = \frac{1}{2}r^2\sin\theta$$

$$\text{Area of segment} = \frac{1}{2}r^2\theta - \frac{1}{2}r^2\sin\theta$$

$$A = \frac{1}{2}r^2(\theta - \sin\theta)$$

$$W = Ap_H = \frac{\pi \left(r \sin \frac{\theta}{2} \right)^2}{2} p_H$$

where p_H is the average or maximum Hertzian pressure.

and friction force

$$F = \frac{1}{2}r^2(\theta - \sin\theta)p_0$$

where p_0 is the yield pressure of the film.

$$\mu = F/W = \frac{\frac{1}{2} r^2 (\theta - \sin \theta) p_0}{\frac{\pi \left(r \sin \frac{\theta}{2} \right)^2}{2}}$$

$$\mu = \frac{(\theta - \sin \theta) p_H}{\left(\sin \frac{\theta}{2} \right)^2 p_0}$$

Using the diameter of the impression in figure 7.19 ignoring elastic deformation AB = 0.8mm and ball radius = 6mm.

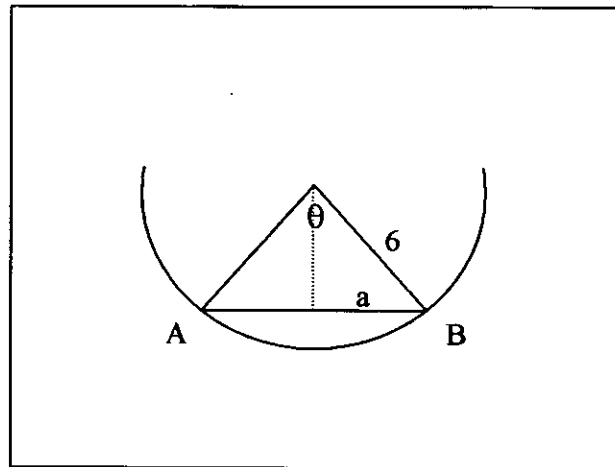


Figure 7.22 Impression generated by 100N load.

For very small indentations arc AB is almost equal to chord AB hence $\theta \approx AB/r$

$$\theta = 0.8 \times 10^{-3} / 6 \times 10^{-3} = 0.1333 \quad \text{and } \theta/2 = 0.0666$$

For maximum Hertz pressure

$$\frac{(\theta - \sin \theta) p_H}{\left(\sin \frac{\theta}{2} \right)^2 p_0} = \frac{(0.1333 - 0.1328) 235 \times 10^6}{(0.0666)^2 \times 77 \times 10^6}$$

$$\mu = 0.344$$

and from

$$F = As$$

Where the resulting deformation just reaches plastic behaviour then the real area of contact A_r becomes dependant on the hardness of the material H and the applied force:

$$A_r = W/H$$

At the onset and during sliding only half the above area will be in contact, from chapter 6 the hardness of the coating $H_v = 248$, then for 100N applied load:

$$A_r = 100 / (248 \times 10^6) \times 0.5$$

If the shear strength is taken as the bulk polymer value, polyamide-imide has a value of 85.3MPa and the value for PTFE is 5Mpa, using the 60/40 mixture assumed in chapter 6, the combined shear strength would be 53.18MPa and the friction force F would be:

$$F = A.s$$

$$\begin{aligned} F &= 0.201 \times 10^{-6} \times 53.18 \times 10^6 \\ &= 10.69\text{N} \end{aligned}$$

For 100N load

$$\begin{aligned} \mu &= F/W \\ &= 10.69/100 \\ &= 0.1069 \end{aligned}$$

Total friction coefficient

$$\begin{aligned} \mu &= \mu_e + \mu_p \\ \mu &= 0.1069 + 0.344 \\ \mu &= 0.4509 \end{aligned}$$

It is expected that this value will only occur for one revolution of the disc with a pin on disc test regime due to the contact area changing from revolution to revolution as a wear track is formed on the disk.

7.3 Real area of contact.

In this section the area of contact generated during the study of the wear scar generation is estimated and the interfacial shear stress is calculated using this area and the measured coefficient of friction. However the question arises, what is the real area of contact? The area required to support a load of 10N for a sphere on a flat surface is given by Hertzian contact theory, for this particular example it would be 0.15mm^2 , then why are the areas that follow due to wear much larger? The possibility is that they are not the real contact area, but the footprint generated by the real area moving around and becoming more dispersed, this will depend on the topography of the contacts themselves.

7.3.1 Area generated at various stages of sliding 10N load.

By overlaying a grid corresponding to the attached scale, using figures 6.9 – 6.22 the areas of contact can be estimated at the various stages of sliding. Two examples are shown in figure 7.23 and 7.24 with the measurements for all the samples given in table 7.1. this data is plotted in figure 7.25, for each of the sliding distances along with their corresponding measured friction coefficient.

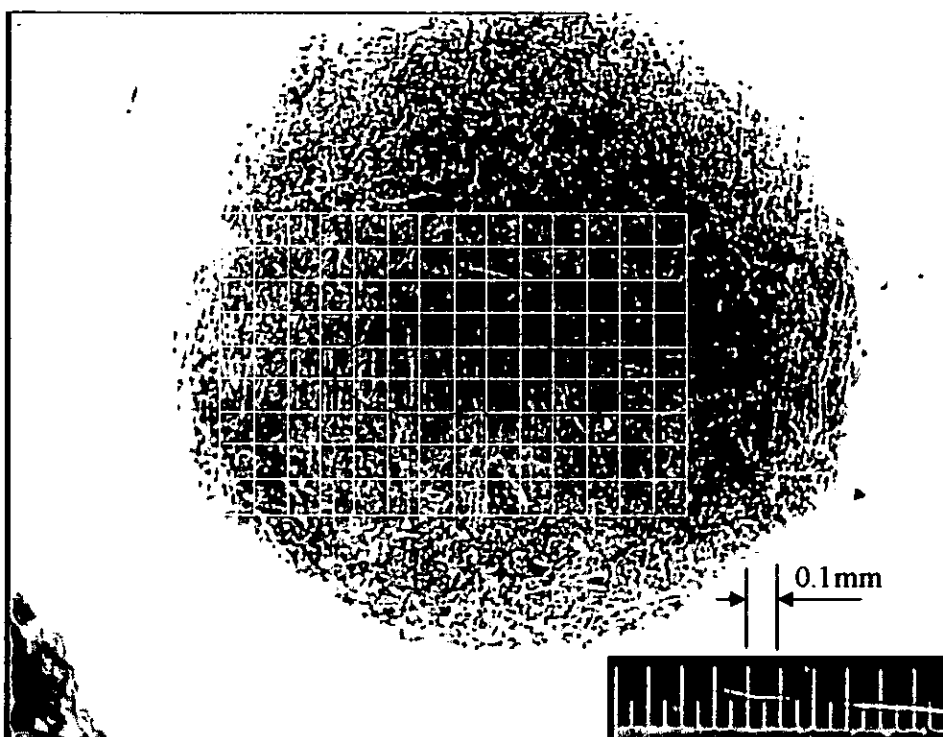


Figure 7.23 Wear scar and grid pattern 25m 10N load.

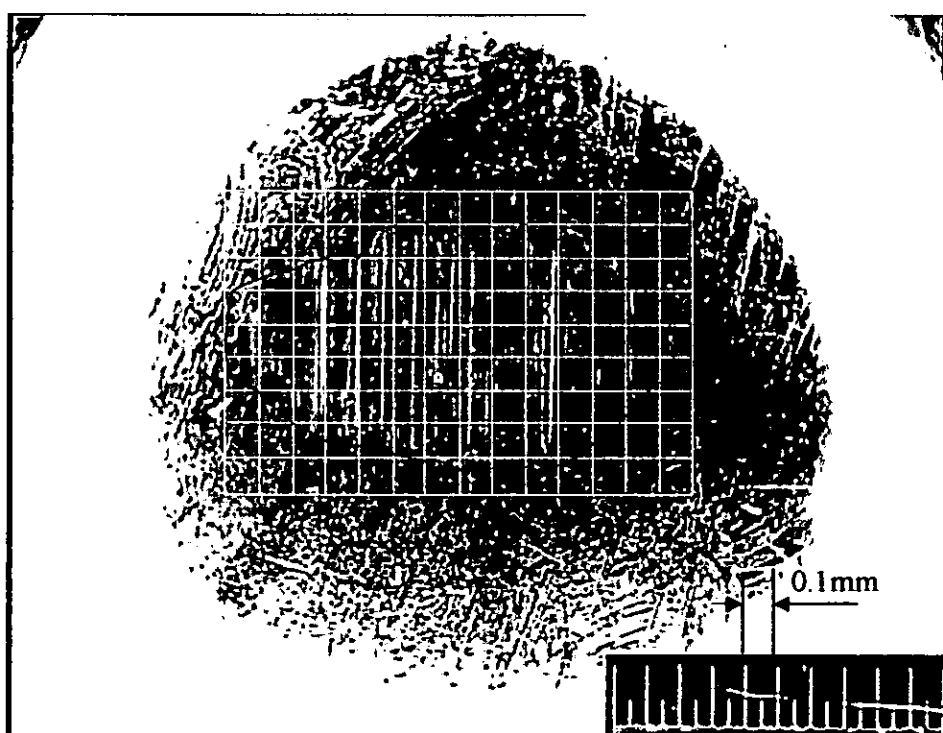


Figure 7.24 Wear scar and grid pattern 500m 10N load.

Distance m	Area mm ² Measured	μ Measured	Hertzian area to support 10N mm ²
25	0.29	0.14	0.15
50	0.55	0.13	0.15
100	0.6	0.11	0.15
500	0.75	0.17	0.15
1000	0.88	0.19	0.15
10000	1.22	0.17	0.15
50000	1.88	0.21	0.15

Table 7.1 Apparent and real area of contact vs. sliding distance.

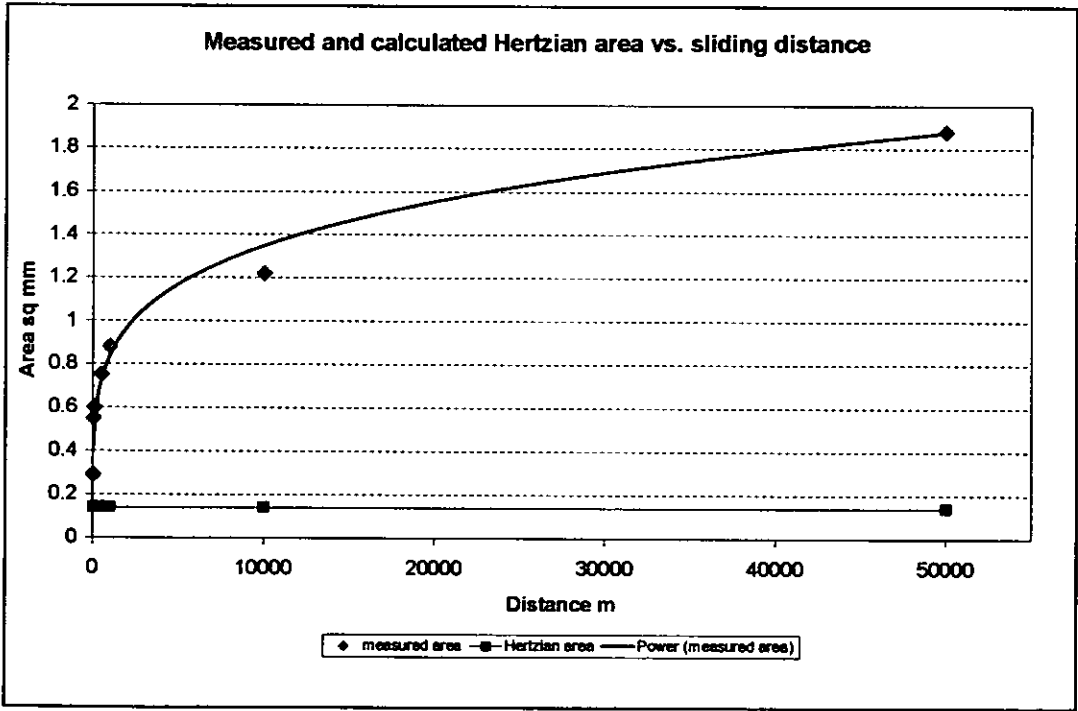


Figure 7.25 Area plotted against sliding distance to 50km.

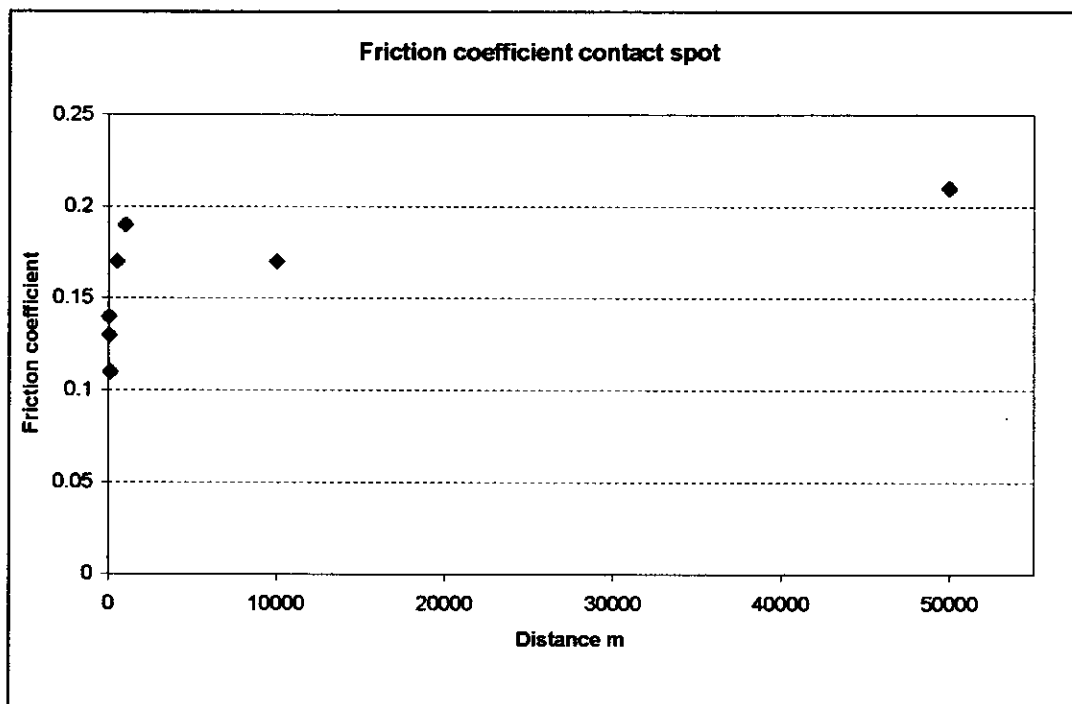


Figure 7.26 Friction coefficient at each stage of sliding measured.

With the measured area and friction coefficient for each sliding interval, the shear strength, s , of the interface can be determined at each stage:

$$F = As \quad \mu = F/W$$

Then, $s = \mu W/A$

if the average and recorded friction coefficients are used then the following table 7.2 is produced, when $W = 10\text{N}$.

Distance m	Area mm ²	μ Measured	Shear strength average coefficient $\mu = 0.16$ MNm ⁻²	Shear strength measured coefficient μ MNm ⁻²	Shear strength using Hertzian contact area MNm ⁻²
25	0.29	0.14	5.52	4.82	9.33
50	0.55	0.13	2.91	2.36	8.66
100	0.6	0.11	2.67	1.83	7.33
500	0.75	0.17	2.13	2.26	11.33
1000	0.88	0.19	1.82	2.15	12.66
10000	1.22	0.17	1.31	1.39	11.33
50000	1.88	0.21	0.85	1.11	14
Average		0.16	2.45	2.27	10.66

Table 7.2 Shear strength of interface using an average friction coefficient of 0.16 and actual recorded value and the Hertzian contact area.

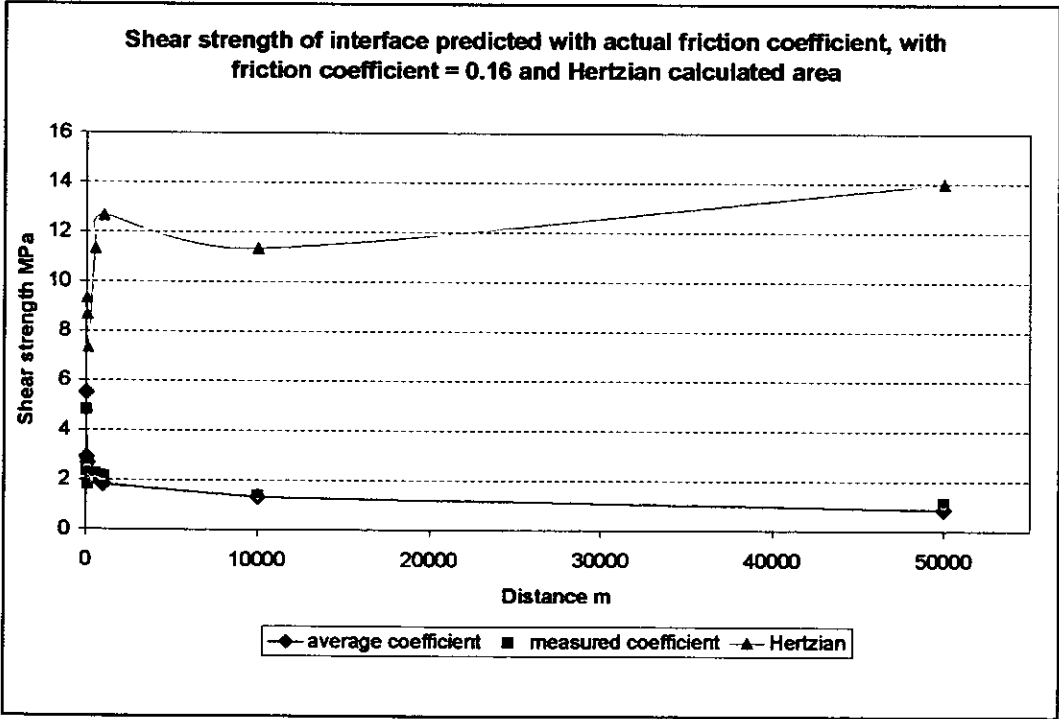


Figure 7.27 Shear strength of sliding interface from the measure friction coefficient and real area of contact.

7.4 Tangential force effects and coated surfaces above the film yield pressure.

“Simple theory” of sliding friction ignores the stress generated due to the side load generated in sliding. Additionally, no account is taken of the effect of varying coverage of the BSL. In this section the experimental results are reviewed with respect to Bowden and Tabor’s modified theory of friction.

7.4.1 Tangential force (side load).

In the previous section where the elastic-plastic interface was explored no account was taken of the effect of the friction force produced by tangential forces due to movement. Bowden and Tabor address this by the addition of the term $\alpha(F/p_0)^2$ representing the increase caused by the shear or friction force and W/p_0 is the area of contact derived from the simple theory, α is a constant derived from the ratio of the squares of the critical shear stress s_0 , as it approaches the value of the maximum shear stress s , and the yield pressure of the softer material, p_0 , [7.3].

In a dynamic system where a tangential force is applied, yielding will take place due to the normal and shear stresses and it can be shown that [7.3]:

$$A^2 = \left(\frac{W}{p_0} \right)^2 + \alpha \left(\frac{F}{p_0} \right)^2$$

$$A^2 = \frac{W^2}{p_0^2} + \alpha \frac{F^2}{p_0^2}$$

$$A^2 p_0^2 = W^2 + \alpha F^2$$

$$A^2 p_0^2 - W^2 = \alpha F^2$$

$$F^2 = \frac{A^2 p_0^2 - W^2}{\alpha} \quad F = \mu W$$

$$\mu = \frac{1}{W} \left(\frac{A^2 p_0^2 - W^2}{\alpha} \right)^{\frac{1}{2}}$$

If the apparent area of contact recorded in table 7.2 is used then the following is generated:

Distance m	Area m ² x 10 ⁻⁶	μ
25	0.29	0.22
50	0.55	0.46
100	0.6	0.50
500	0.75	0.63
1000	0.88	0.74
10000	1.22	1.04
50000	1.88	1.60

Table 7.3 Friction coefficient calculated from the modified friction theory and measured area of contact $\alpha = 9$.

For metals $p_0 = 5s_0$ giving $\alpha = 25$. However experiments with metals indicates that α should be less than this and Bowden and Tabor assumed $\alpha = 9$ implying that $p_0 \approx 3s_0$. For metals this approximation is reasonable and it can be shown that α does not greatly affect the junction growth. However for metals with thick films on their surface this may not be the case and α may have a significant effect. Table 7.3 shows the first approximation using $\alpha = 9$ gives a friction coefficient which is approx ten times too large, when compared with the measured data. A closer approximation can be made by increasing α , figure 7.28 shows the plots for $\alpha = 9, 14, 17, 25$ and 35 , also the measured coefficient is shown. This implies that at $\alpha = 35$, p_0 would be approx $6s_0$

compared with $5s_0$ assumed for metals. The above equation only recognises changes in contact area and assumes a single large asperity contact that has “just reached” plastic deformation. However, as wear takes place and the contact area grows contact is really becoming increasingly elastic.

Another way this issue could be approached is to consider the actual contact pressures, p , approximated from the measured apparent areas of contact and the applied load then:

$$A^2 = \left(\frac{W}{p}\right)^2 + \left(\frac{F}{p_0}\right)^2$$

$$A^2 - \left(\frac{W}{p}\right)^2 = \left(\frac{F}{p_0}\right)^2$$

$$F^2 = p_0^2 \left(A^2 - \left(\frac{W}{p}\right)^2 \right)$$

$$\mu = \frac{1}{W} \left[p_0^2 \left(A^2 - \left(\frac{W}{p}\right)^2 \right) \right]^{\frac{1}{2}}$$

alternatively including the constant α

$$A^2 = \left(\frac{W}{p}\right)^2 + \alpha \left(\frac{F}{p_0}\right)^2$$

$$A^2 - \left(\frac{W}{p}\right)^2 = \alpha \left(\frac{F}{p_0}\right)^2$$

$$F^2 = \frac{p_0^2}{\alpha} \left(A^2 - \left(\frac{W}{p} \right)^2 \right)$$

$$\mu = \frac{1}{W} \left[\frac{p_0^2}{\alpha} \left(A^2 - \left(\frac{W}{p} \right)^2 \right) \right]^{\frac{1}{2}}$$

where $p = W/A_m$ and A_m is the measured area at 10N load, from table 6.7 the diameter of the contact spot is $0.41 \times 10^{-6} \text{m}^2$. Therefore $A_m = \pi \times 0.205^2 = 0.132 \times 10^{-6} \text{m}^2$. This value is fairly close to the value of $0.15 \times 10^{-6} \text{m}^2$ obtained from the Hertzian calculation.

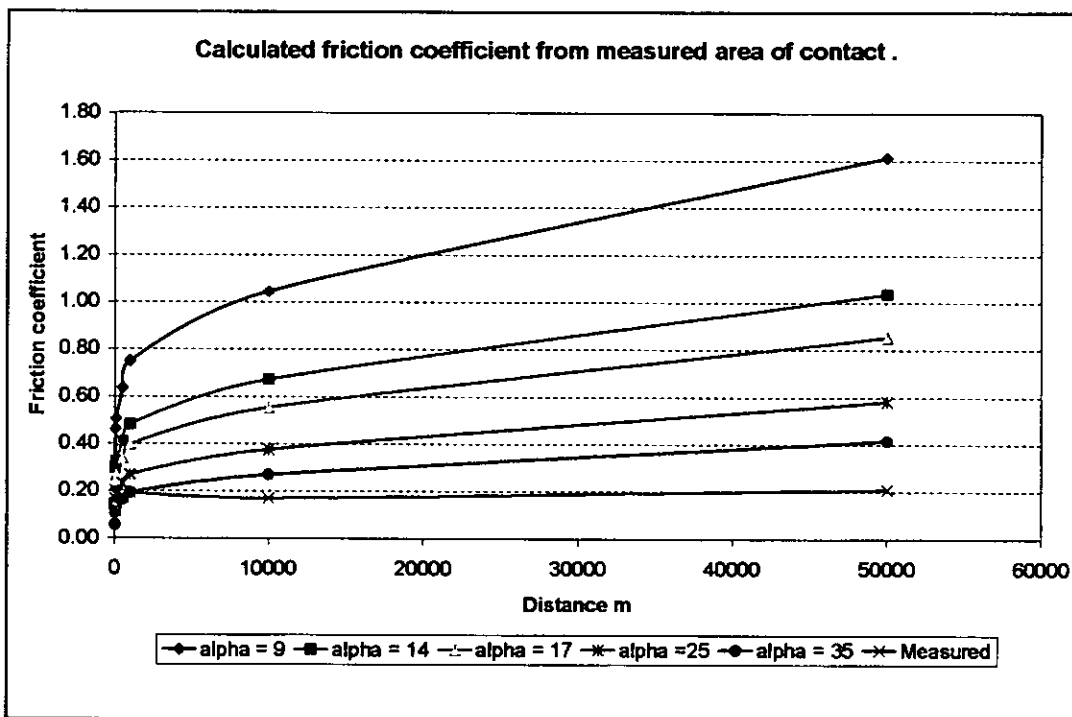


Figure 7.28 Friction coefficient calculated from the modified friction theory and measured area of contact $\alpha = 9$ to 35.

This second approximation using the measured values gives a friction coefficient which is approximately 100 times too large, inserting the constant α improves the

approximation of μ by moving it closer to the measured value and $\alpha = 9$ is plotted in figure 7.29. Possible reasons for this error are:

- The assumption that the contact spot measurement is accurate, no account is taken of elastic behaviour.
- The assumption that the estimated area of contact from the photographs in figure 6.45 is actually the real area of contact.
- p is assumed to be the same over all the area of contact, this is obviously not true for a sphere where the pressure will increase towards the centre of the contact.

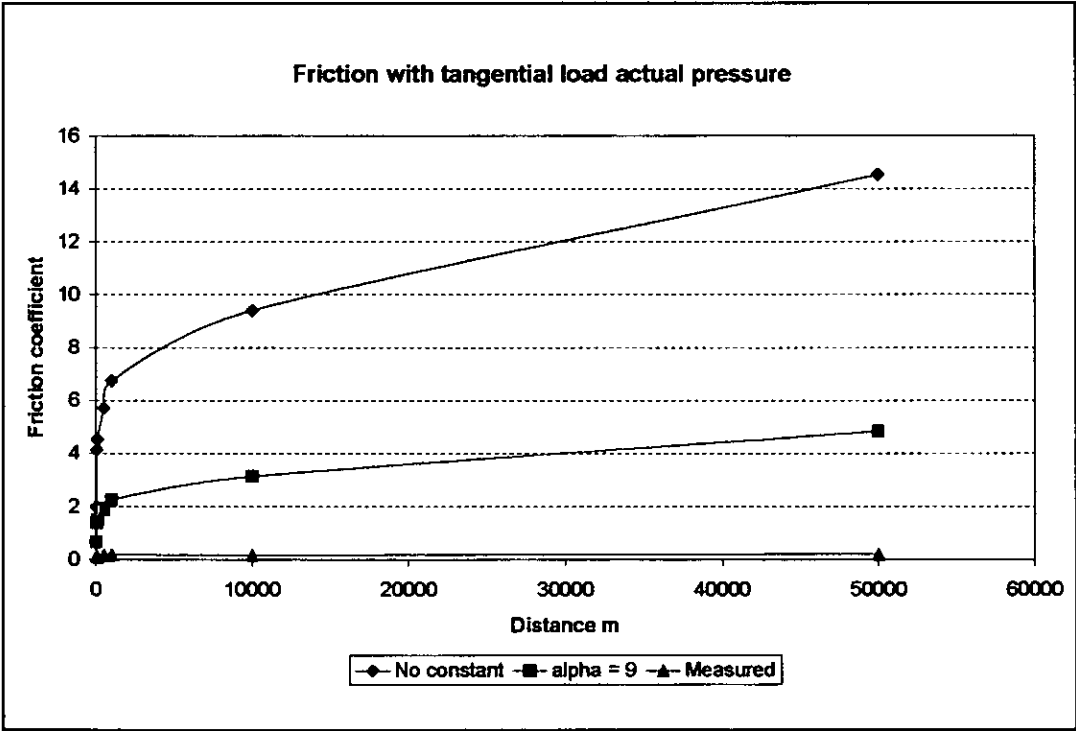


Figure 7.29 Friction coefficient calculated from the modified friction theory and measured area of contact and contact pressure.

7.4.2 Contaminated surfaces.

Most of the theoretical work on the friction of materials by Bowden and Tabor deals with clean metal surfaces. With materials that incorporate a surface film such as a BSL the surface film will reduce the asperity contact, junction growth and asperity welding. Therefore the theory discussed in chapter 3.2.2 should apply, where for the initial contact:

$$\mu = s_f/p_0$$

If the critical shear stress s_f is taken as the shear stress developed from the measured data in table 7.2, in this example the shear strength generated using the average friction coefficient is used, and $p_0 = 77.5$, is taken from the hardness testing on a 25 μ m film, then at the onset of sliding:

$$\begin{aligned}\mu &= 5.52 \times 10^6 / 77.5 \times 10^6 \\ &= 0.0712 \text{ at 25m sliding}\end{aligned}$$

In figure 7.29 the friction values are plotted up to 50000 metres of sliding from the above, again using the shear strength from table 7.2

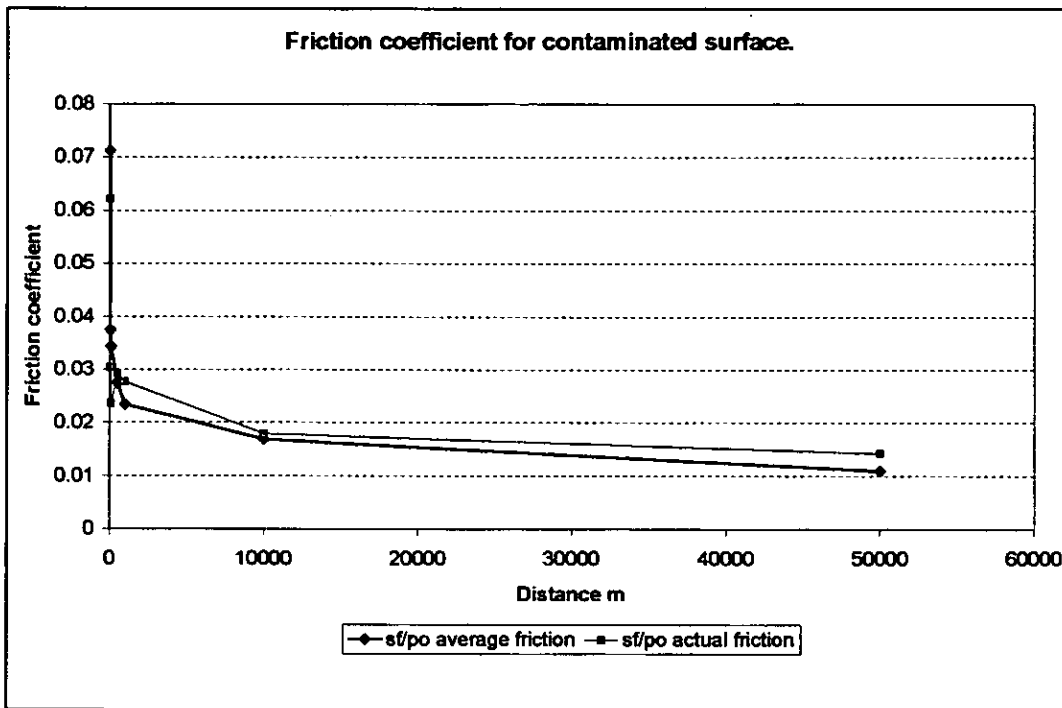


Figure 7.30 Friction coefficient for contaminated surface using data for critical shear stress from table 7.2.

Unlike all the previous estimates for the friction coefficient which overestimate the actual value, this method underestimates the value by a factor of 2 at the beginning of sliding to a factor of 20 at 50000 metres. This is one of the problems that people encounter when trying to estimate the friction coefficient from measured data, the assumption is made that the measured area is the real area of contact which in this example generates the shear strength for the film that is not constant. A better approximation can be made by using the shear strength generated from the Hertzian contact area, this would be more representative of the asperity contact area, this would give:

$$\mu = s_{H}/p_0 = 8.8 \times 10^6 / 77.5 \times 10^6 \text{ using the average value.}$$

$$= 0.114$$

Alternatively if the pressures used are calculated from the apparent A_a and the applied load then for 10N load, table 7.4 and figure 7.31 can be generated:

Distance m	Area m ² x 10 ⁻⁶	Pressure W/A MNm ²
25	0.29	34.48
50	0.55	18.18
100	0.6	16.66
500	0.75	13.33
1000	0.88	11.36
10000	1.22	8.19
50000	1.88	5.32

Table 7.4 Apparent contact pressure.

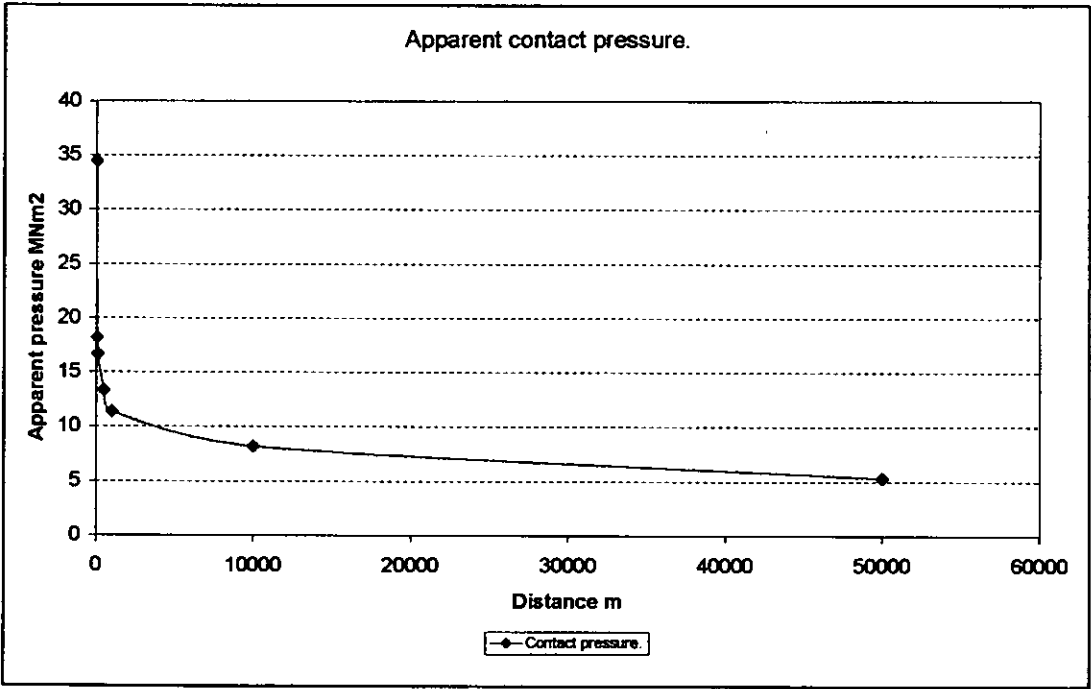


Figure 7.31 Graph of contact pressure from applied load and measured area.

In this case the friction coefficient would be:

$$s_f/p_a$$

therefore:

$$\mu = 5.52 \times 10^6 / 34.48 \times 10^6$$

= 0.16 at 25m sliding.

Figure 7.32 contains the friction values up to 50000 metres of sliding from the above using the shear strength from table 7.2 and apparent pressures from table 7.4

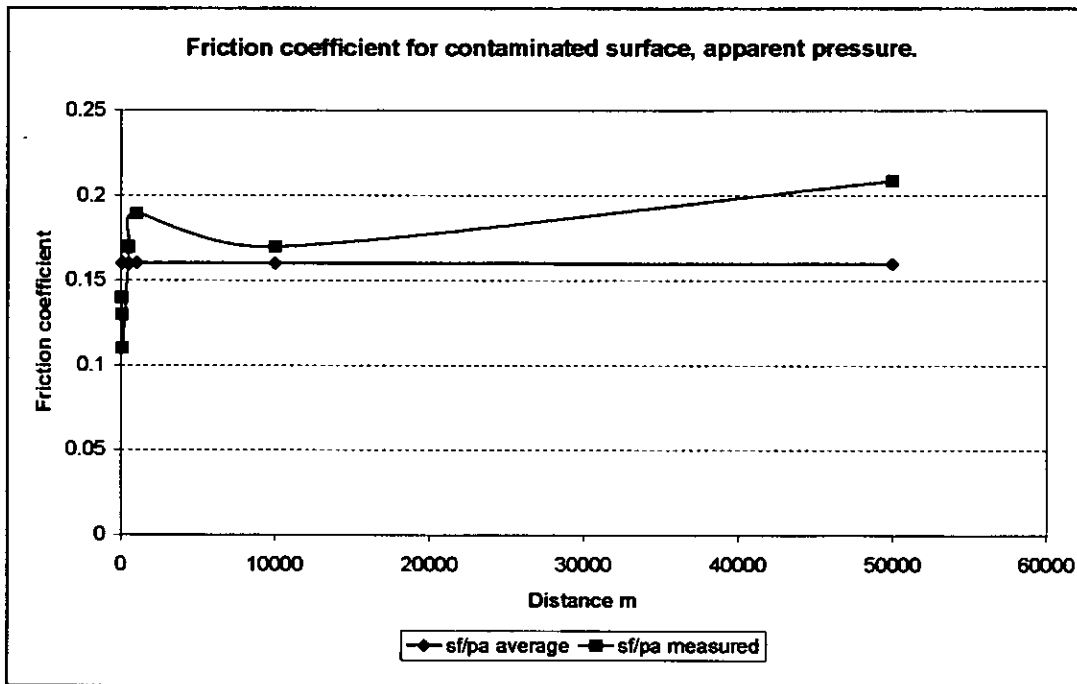


Figure 7.32 Friction coefficient for contaminated surface using data for critical shear stress from table 7.2. and apparent contact pressure table 7.4

The above graph using values of shear stress and contact pressure calculated from the measured friction values and contact areas compares fairly well with the experimental results obtained in chapter 4.

7.5 Hertzian contact with pressures above the yield point.

When a sphere in contact with a flat surface is loaded, deformation will occur at the contact interface, it has been shown by Hertz that the deformation of the bodies in contact is proportional to the elastic modulus, poisons ratio and radius of each of the bodies. If the bodies have the same elastic modulus then the deformation will be equal for each of them, if the modulus is smaller for one of the bodies then the deformation will be proportionally greater on that body depending on the geometry of the two surfaces. In either case the projected area of the contact will remain the same. It has also been demonstrated by Singer [7.4] that for very thin films that the low friction properties are dependant on the Hertzian stress distribution.

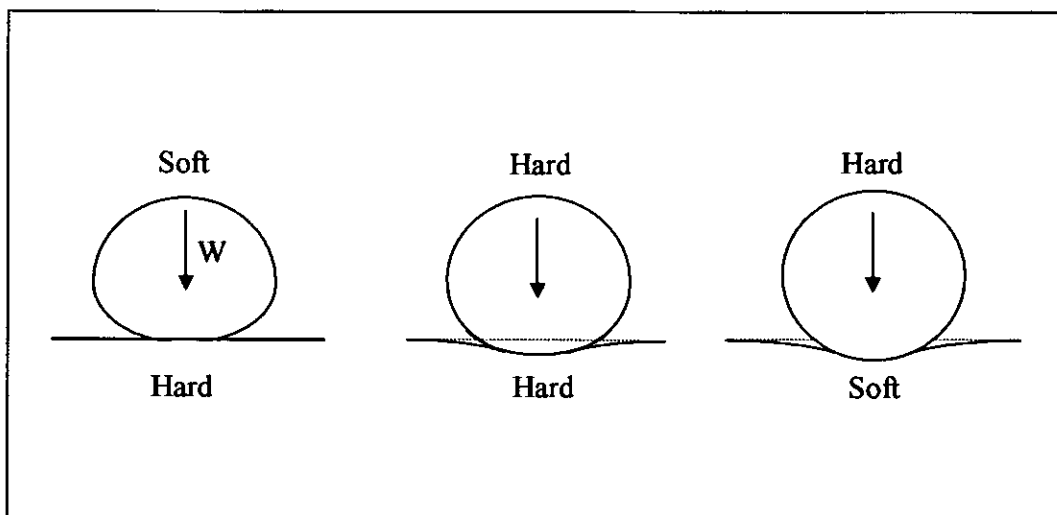


Figure 7.33 Deformation of contact zone for hard/soft bodies.

The elastic modulus of the materials used in BSLs is small compared to that of steel. E.g. 4.6GPa for Polyamide-imide and 0.61GPa for PTFE compared to steel at 209GPa, this would mean for thick films, the majority of the deformation will occur in the BSL.

For loads that generate contact pressures above the yield pressure of the film, the friction force generated by a sphere sliding on a flat surface will depend on the elastic deformation and some plastic deformation, with a pin on disk apparratus this will

occur for a very short period at the start of sliding due to the groove or track being progressively deeper after each revolution of the disc until the film becomes so thin that the load is supported by a thin coating of transfer film on the substrate. This is illustrated in figures 6.9 – 6.22. In these tests the friction coefficient gradually increased over a sliding distance of 2500 metres where a change took place and the friction coefficient became constant. During this latter phase it is assumed that sliding took place between the transfer film on the sphere and the bulk of the film with some plastic deformation and some ploughing occurring at the centre, where the pressure is at a maximum figures 7.34 and 7.35.

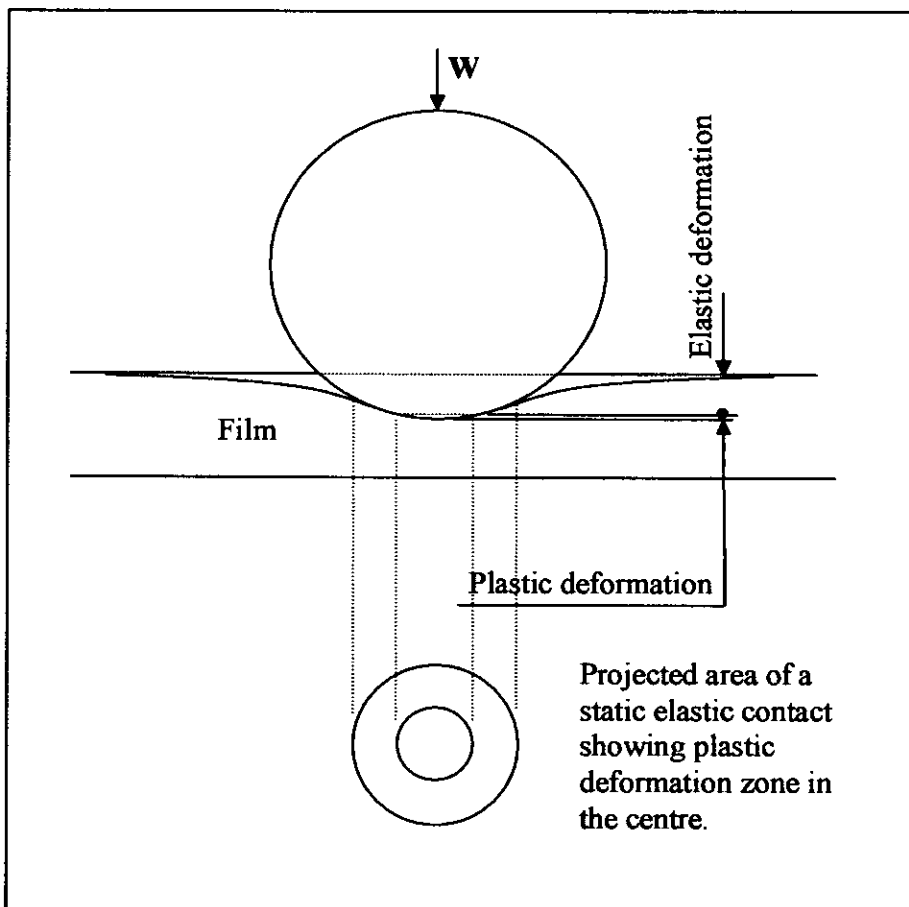


Figure 7.34 Elastic plastic deformation for a hard spherical asperity in a soft flat film.

The friction due to the elastic deformation may be given by the model discussed in section 7.2:

$$\mu_e = kW^{-1/3}$$

and the friction due to ploughing will occur at the centre where the Hertzian pressure is maximum and exceeds the yield pressure of the film material.

At low pressures the majority of the sliding will be under elastic conditions and the ploughing term will be small, whereas under high contact pressure conditions the ploughing term will dominate.

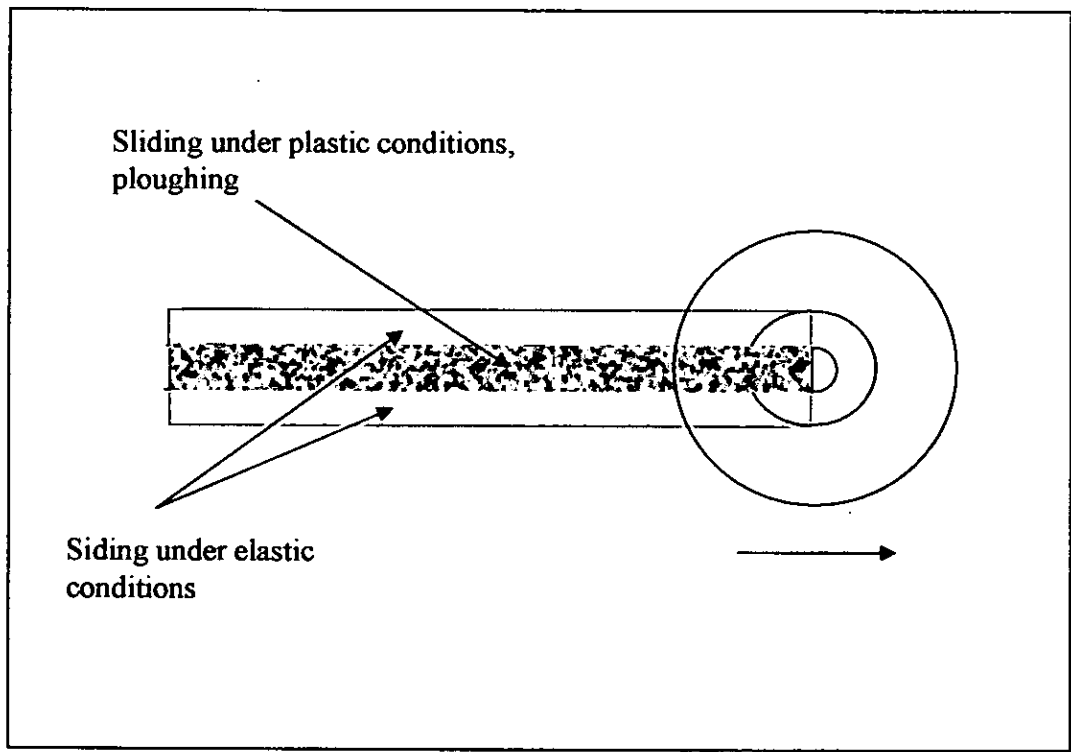


Figure 7.35 Idealised wear track form by elastic/plastic sliding by a sphere on a flat plate.

It has been shown for metals that the maximum shear stress τ_{max} under Hertzian contact occurs below the surface at a distance of $0.67a$ where a is the radius of the contact spot due to loading. It has also been demonstrated [7.5] that contact pressures

in excess of the yield value for the material do not result in plastic deformation at the surface, so that higher loads than might be expected can be carried, apparently elastically, figure 7.36. When yielding has taken place below the surface very little plastic deformation occurs because the plastic zone is surrounded by elastic material on all sides. As load is increased, the plastic zone will increase in size and eventually reach the surface of the material. Plastic flow will then occur and the pressure at this point will be 3 times the critical shear stress at which the yield initially occurred. The mean pressure under these conditions is the indentation hardness value of the material and hence

$$H = 3Y$$

Where Y is the tensile yield strength of the material.

In the experimental programme in chapter 5, the maximum load used was 100N. This produces a maximum Hertzian contact pressure of 200MPa. The indentation hardness of the 25µm film from chapter 6 is given as 248MPa, therefore, under these conditions it is possible that plastic deformation at the surface of the film will not occur and the frictional behaviour would be as for elastic contact.

If the above is the case, then the question arises “why is there an apparent indentation left when a sphere is pressed into the film”, as in figure 7.19? It has already been mentioned that these films are applied by spraying and have a granular texture, if a sphere is pressed into this, the tips of the grains will deform plastically under fairly low load conditions, but it is possible that the main deformation will still be elastic. On removal of the load the film would return to its original shape, but the tips of the grains will be remain deformed and may have even flowed into each other as illustrated in figure 7.37.

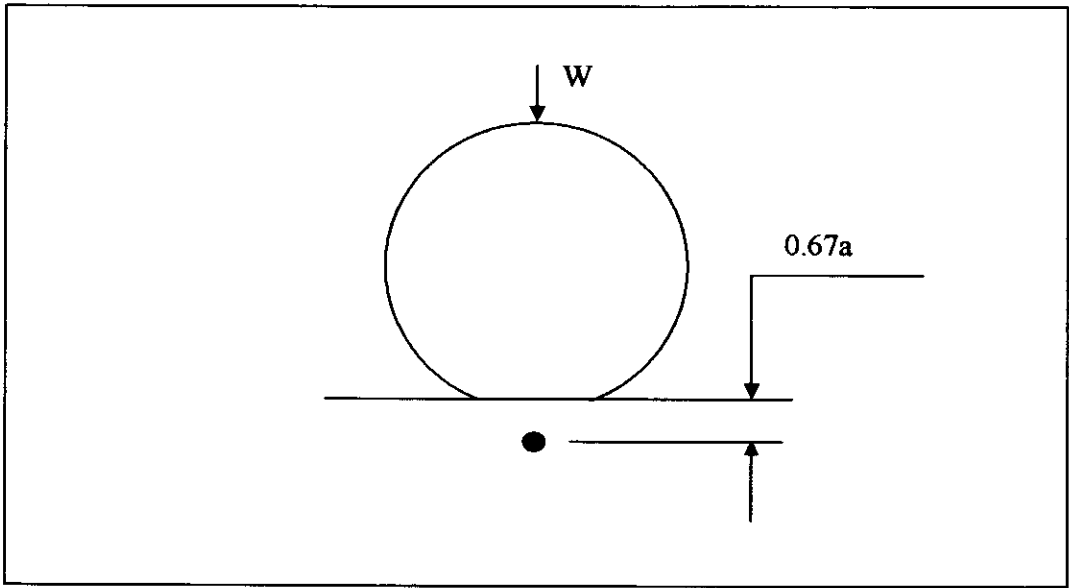


Figure 7.36 Position of τ_{\max} for a sphere in static contact with a flat plane.

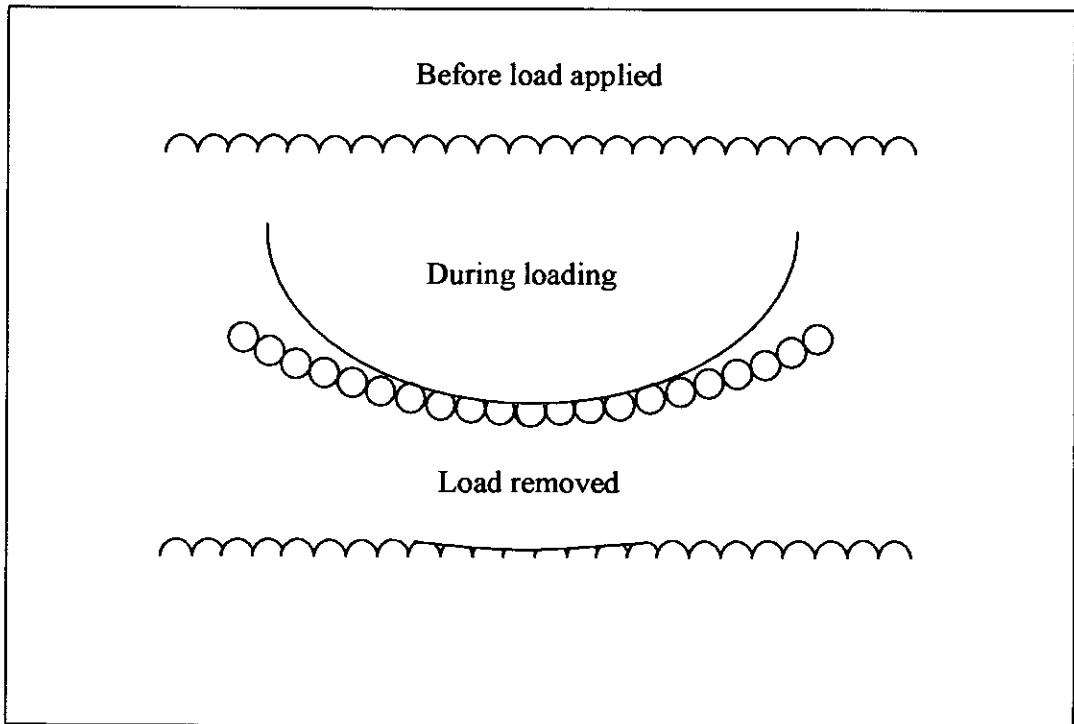


Figure 7.37 Schematic of film deformation showing elastic and plastic deformation area to tips of “grains”.

7.6 Friction due to sliding taking place between a thin film and a wear scar.

It has already been mentioned that at some point during sliding a change in mechanism occurs, in the tests in section 7.3 this occurs at about 2500 metres, after this point sliding occurs between the wear scar on the ball as shown in chapter 6 and a thin film on the disc, as this scar grows lubricant is continually replaced by wear from the sides of the track, it has been shown for thin PVD films that it is this mechanism of lubricant replacement that gives these films their longevity [7.4]. Eventually the scar reaches a size where the amount of lubricant is insufficient to provide a stable system and the frictional performance becomes erratic and deteriorates rapidly.

From chapter 6 figures 6.17 and 6.19 the diameter of the wear scar can be estimated to somewhere between 0.7mm and 1.0mm at a distance of 2500 metres. Also the final scar diameter has been recorded as 4.2mm for the as received finish then these measurements should allow the friction force and hence the friction coefficient to be estimated at these two points.

From $F = A_r s$ $A_r = \text{real area of contact}$

However the real contact area is much more complex and consists of asperity contacts within the circular scar illustrated in the photographs which run on a thin film with some metal to metal contact, some transfer film contact and the areas to the sides that are running on the thick film. Figure 7.37 shows this. When the circular scar is small, at the beginning of sliding after 2000 to 3000m the majority of the contact area will be in area 2, towards the end of sliding when the friction force begins to increase and becomes erratic the contact area will be mainly in the circular scar area 1. Considering only apparent contact areas the friction force can be estimated as follows:

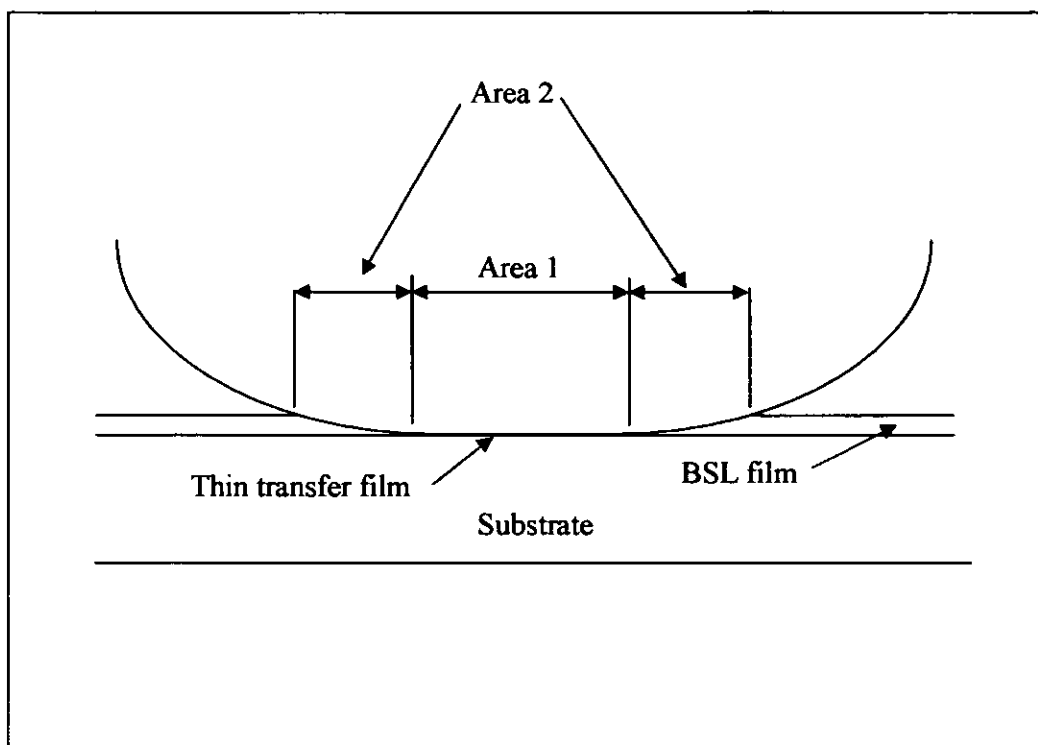


Figure 7.37 Apparent area of contact for a sphere sliding on a BSL film.

At the beginning of this phase the apparent area of contact can be assumed to be $A_1 + A_2$ if A_1 is taken to be just larger than the area predicted due to Hertzian contact mechanics say from a spot diameter of 0.42 mm $A_1 = \pi r^2 = 0.14 \times 10^{-6} \text{m}^2$ and A_2 estimated from the film thickness of 25 μm assuming elastic contact. The following assumes that the projected area is a close approximation to the surface area of the partial spherical contact to give a reasonable approximation of the friction coefficient.

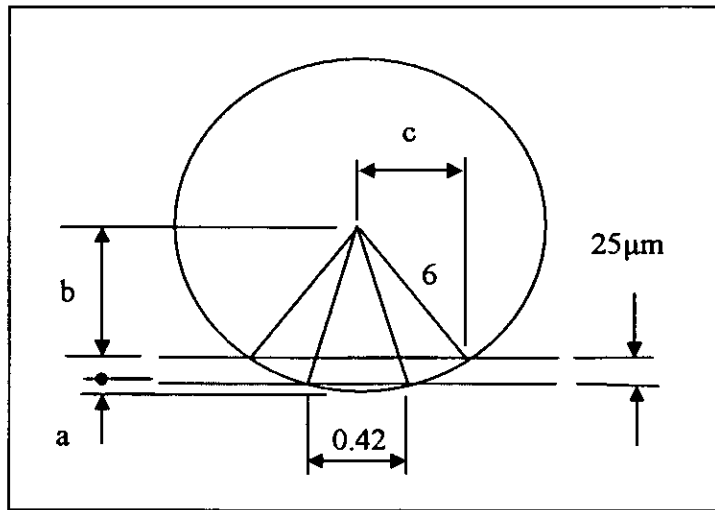


Figure 7.38 Area of contact for a 25μm film.

$$a = 6 - \sqrt{6^2 - 0.21^2} = 0.004 \text{ mm} \quad b = 6 - 0.025 - 0.004 = 5.971$$

$$c = \sqrt{6^2 - 5.971^2} = 0.5899$$

$= 0.5899^2 \pi - 0.21^2 \pi = 0.9548 \text{ mm}^2$ this would be the area if there was no track on the disk TW.

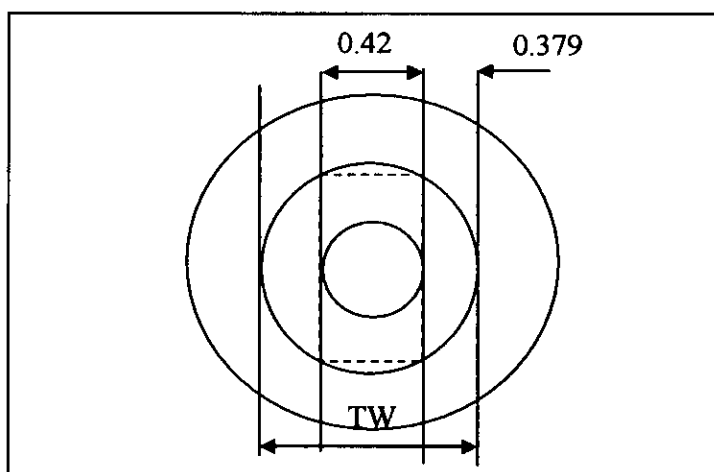
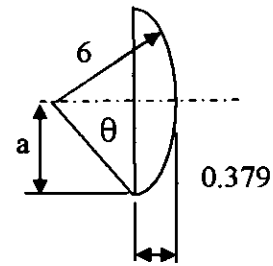


Figure 7.39 Area contacting thick film during sliding.

Area of segment contained by 0.379 dimension:

$$\begin{aligned}\text{Length } a &= 6 - \sqrt{6^2 - 5.621^2} \\ &= 2.09\end{aligned}$$



$$\begin{aligned}\sin \theta &= 2.09/6 \\ &= 0.3483\end{aligned}$$

$$\text{Area of segment} = \frac{1}{2}r^2\theta - \frac{1}{2}r^2\sin\theta$$

Where $\theta = .3557$ rads

Therefore area of segment = 0.1332mm^2 this is the apparent area that would be in contact with the thick film during sliding, due to there being two segments but only the front half of each segment would be in contact.

$$\begin{aligned}\text{Total area } A_a &= A_1 + A_2 = 0.14 \times 10^{-6} + 0.132 \times 10^{-6} \\ &= 0.272 \times 10^{-6}\text{m}^2\end{aligned}$$

$$\text{Friction force} \quad F = A_a \cdot s$$

$$\begin{aligned}F &= 0.272 \times 10^{-6} \times 53.18 \times 10^6 \\ &= 14.46\text{N}\end{aligned}$$

$$\begin{aligned}\mu &= 14.46/10 \\ &= 1.44\end{aligned}$$

This is approximately a factor of ten times too high considering that ploughing, metal to metal contact, and tangential forces have been ignored. It also assumes that the value for the shear pressure is that of the bulk film, it is possible that as sliding takes place that the PTFE and Graphite molecules are dragged to the surface and sliding takes place between the transfer film on the ball and this layer of PTFE and graphite in which case the shear strength of the PTFE and graphite will dominate. The shear strength of PTFE is given as 5MPa, this would give a friction coefficient of 0.14 which does compare with the experimental results, data is not available for the shear strength of graphite.

At the other end of the scale where the scar is 4.2mm diameter, just before failure of the film at 500km sliding distance, the contact area of the thick film will be much smaller and the majority of the friction will be due to the scar. Substituting in the above:

$$a = 6 - \sqrt{6^2 - 2.1^2} = 0.38\text{mm} \quad b = 6 - 0.025 - 0.038 = 5.935$$

$$c = \sqrt{6^2 - 5.935^2} = 2.16$$

Diameter of the apparent area in contact with thick film would be $2.16 \times 2 = 4.32$ but circular scar is 4.2 diameter, therefore segment in contact would be 0.06mm wide as this will produce an extremely small area compared to the wear scar, it is reasonable to ignore this and the component of friction will be from the wear scar.

$$F = (2.1 \times 10^{-3})^2 \times 3.142 \times 53.18 \times 10^6$$

$$= 736.8$$

$$\mu = 736.8/10$$

$$= 73.68$$

This is a factor of 300 times larger than the experimental values and it is obvious that the simple theory can not be used to approximate the friction coefficient from the apparent area of contact. The areas used here are not the true area of contact during sliding due to the reasons given previously in section 7.4. If the real area of contact is taken as the area that is required to support 10N from the Hertzian calculation the total number of asperities in contact would need to have an area of $0.15 \times 10^{-6} \text{ m}^2$ these areas of asperity contact would be distributed around the wear scar and could change position as sliding progresses, figure 7.40. This would give a friction coefficient of 0.74 using the shear strength of the bulk film.

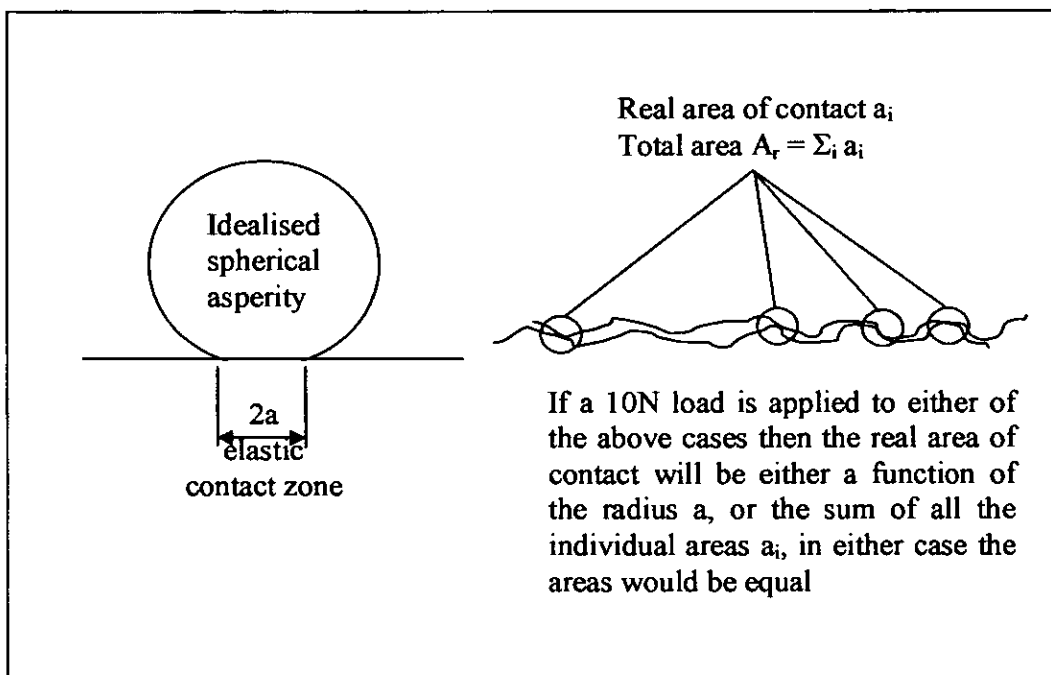


Figure 7.40 Illustration of area required to support a load of 10N.

It has already been noted that as the circular wear scar increases in size, the area in contact with the thick film reduces. It is thought that when this area reaches some critical limit the friction begins to increase and the sliding couple begins to fail. It is assumed that up to this critical limit there is sufficient lubricant being worn from the film and re integrated into the contact to replenish the sliding interface. However at the critical limit the supply of lubricant becomes insufficient, hence the erratic rise in

friction. It is possible that this critical limit may be determined by experiment, this would require stopping the test immediately a distinct rise in friction force is encountered, unfortunately all the tests in chapter 5 were allowed to run until they reached a friction coefficient of 0.3+ taking them past this critical point.

7.7 Friction calculators.

The following spreadsheets and graphs can be used to estimate the friction coefficient at various loads for this particular BSL for the conditions discussed in this chapter.

Figure 7.41 shows the friction coefficient due to adhesion calculated from the film shear strength and the calculated maximum pressure with applied loads from 0.1 to 1.0N. Similarly figure 7.44 shows the friction coefficient due to adhesion with loads 1 to 10N, and figure 7.47 at loads of 10 to 100N.

The friction due to tangential force using the contact areas generated from Hertzian contact theory are shown in figures 7.42, 7.45 and 7.48 for 0.1 to 1N, 1 to 10N and 10 to 100N respectively. The friction due to elastic contact theory are given in figures 7.43, 7.46 and 7.50 again for the same load ranges. Figure 7.49 shows the friction due to abrasion for loads of 10 to 100N

TITLE: HERTZIAN CONTACT & FRICTION DATA, BALL ON PLATE 0.1 to 1N.

AUTHOR: DAVID BURKE DATE: 04/10/2004

$$\delta = \left(\frac{9}{16} \frac{W^2}{E^* R} \right)^{\frac{1}{3}}$$

$$P_{max} = \left(\frac{6WE^*}{\pi^3 R^2} \right)^{\frac{1}{3}} \quad P_{ave} = (2/3)P_{max}$$

$$\tau = 0.31P_{max}$$

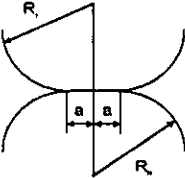
$$z_0 = 0.48r$$

$$a = \left(\frac{3WR}{4E^*} \right)^{\frac{1}{3}}$$

$$\mu = \frac{aR^{\frac{1}{3}}}{W^{\frac{1}{3}}4E^*^{\frac{1}{3}}}$$

$$\frac{1}{E^*} = \frac{(1-\nu_1^2)}{E_1} + \frac{(1-\nu_2^2)}{E_2}$$

$$\frac{1}{R} = \frac{1}{R_1} + \frac{1}{R_2}$$



Parameter		Units
Ball Radius R	0.006	Metre
Shear Strength	53.18	MPa
Modulus E1	210	GPa
Modulus E2	4	GPa
Poissons ratio ν_1	0.3	
Poissons ratio ν_2	0.3	
Combined Mod E*	4.313	GPa
	0.231833333	

Note! Shear strength taken from 60/40 ratio PTFE - Polyamide-Imide

Assumed - no data

Normal Load W, N	a	Spot dia mm	Spot Area A mm2	Pmax (MPa)	Pave (MPa)	δ (10-6)	ADHESIVE		ABRASIVE	Hertz	θ
							μ (s/Pmax)	μ a side load	μ_{ab}	μ	
1	0.1014	0.2028	0.032317	46.40	30.93	9.43	1.1461	0.7654		1.5600	
0.9	0.0979	0.1958	0.030125	44.80	29.87	8.79	1.1871	0.7979		1.6157	
0.8	0.0942	0.1883	0.027850	43.07	28.72	8.13	1.2346	0.8353		1.6803	
0.7	0.0901	0.1801	0.025478	41.20	27.47	7.44	1.2908	0.8792		1.7567	
0.6	0.0855	0.1711	0.022990	39.14	26.09	6.71	1.3589	0.9320		1.8493	
0.5	0.0805	0.1610	0.020358	36.83	24.55	5.94	1.4440	0.9976		1.9650	
0.4	0.0747	0.1495	0.017544	34.19	22.79	5.12	1.5555	1.0829		2.1166	
0.3	0.0679	0.1358	0.014483	31.06	20.71	4.23	1.7120	1.2017		2.3294	
0.2	0.0593	0.1186	0.011052	27.14	18.09	3.23	1.9597	1.3881		2.6661	
0.1	0.0471	0.0942	0.006963	21.54	14.36	2.03	2.4691	1.7675		3.3583	

$$\mu_a = \frac{1}{W} \left(\frac{A^2 \rho_0^2 - W^2}{\alpha} \right)^{\frac{1}{2}}$$

$$\mu_{ab} = \frac{(\theta - \sin \theta) p_H}{\left(\sin \frac{\theta}{2} \right)^2 p_0}$$

TITLE: HERTZIAN CONTACT & FRICTION DATA, BALL ON PLATE 1 to 10N.

AUTHOR: DAVID BURKE DATE: 04/10/2004

$$\delta = \left(\frac{9}{16} \frac{W^2}{E^* R} \right)^{\frac{1}{3}}$$

$$P_{max} = \left(\frac{6WZ}{\pi^3 R^2} \right)^{\frac{1}{3}} \quad P_{ave} = (2/3)P_{max}$$

$$\tau = 0.31P_{max}$$

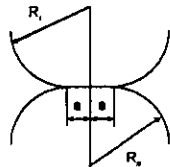
$$z_0 = 0.48r$$

$$a = \left(\frac{3WR}{4E^*} \right)^{\frac{1}{3}}$$

$$\mu = \frac{\tau_p 3R^{\frac{1}{3}}}{W^{\frac{1}{3}} 4E^*}$$

$$\frac{1}{E^*} = \frac{(1-\nu_1^2)}{E_1} + \frac{(1-\nu_2^2)}{E_2}$$

$$\frac{1}{R} = \frac{1}{R_1} + \frac{1}{R_2}$$



Parameter		Units
Ball Radius R	0.006	Metre
Shear Strength	53.18	MPa
Modulus E1	210	GPa
Modulus E2	4	GPa
Poissons ratio ν_1	0.3	
Poissons ratio ν_2	0.3	
Yield strength p_0	77.5	MPa
Combined Mod E^*	4.313	GPa
	0.231833333	

Note! Shear strength taken from 60/40 ratio PTFE - Polyamide-imide

Assumed - no data

Normal Load W, N	a	Spot dia mm	Spot Area A mm ²	Pmax (MPa)	Pave (MPa)	δ (10 ⁻⁶)	ADHESIVE		ABRASIVE	Hertz μ	Imp dia	θ
							μ (a/Pmax)	μ side load				
10	0.2185	0.4370	0.1500	99.96	66.64	43.78	0.5320	0.1976	0.039	0.7274	0.41	0.068333
9	0.2110	0.4219	0.1398	96.51	64.34	40.81	0.5510	0.2235		0.7534		
8	0.2028	0.4057	0.1293	92.79	61.86	37.72	0.5731	0.2513		0.7836		
7	0.1940	0.3880	0.1183	88.75	59.17	34.51	0.5992	0.2817		0.8193		
6	0.1843	0.3686	0.1067	84.31	56.21	31.14	0.6308	0.3162		0.8624		
5	0.1734	0.3469	0.0945	79.34	52.89	27.58	0.6703	0.3587		0.9185		
4	0.1610	0.3220	0.0814	73.65	49.10	23.77	0.7220	0.4068		0.9872		
3	0.1483	0.2926	0.0672	66.92	44.61	19.62	0.7847	0.4732		1.0866		
2	0.1278	0.2556	0.0513	58.46	38.97	14.97	0.9097	0.5727		1.2438		
1	0.1014	0.2028	0.0323	46.40	30.93	9.43	1.1461	0.7654		1.5671		

16.60827 22.83146
22.04361
21.19501
20.27239
19.25713
18.12176
16.82288
15.28475
13.35264
10.59824

$$\mu_a = \frac{1}{W} \left(\frac{A^2 \rho_0^2 - W^2}{\alpha} \right)^{\frac{1}{2}}$$

$$\mu_{ab} = \frac{(\theta - \sin \theta) p_H}{\left(\sin \frac{\theta}{2} \right)^2 p_0}$$

TITLE: HERTZIAN CONTACT & FRICTION DATA, BALL ON PLATE 10 to 100N.

AUTHOR: DAVID BURKE DATE: 04/10/2004

$$\delta = \left(\frac{9}{16} \frac{W^2}{E^* R} \right)^{\frac{1}{3}}$$

$$P_{max} = \left(\frac{6WE^*}{\pi^3 R^2} \right)^{\frac{1}{3}} \quad P_{ave} = (2/3)P_{max}$$

$$\tau = 0.31P_{max}$$

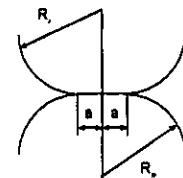
$$z_0 = 0.48r$$

$$a = \left(\frac{3WR}{4E^*} \right)^{\frac{1}{3}}$$

$$\mu = \frac{a}{W} \left(\frac{R}{4E^*} \right)^{\frac{2}{3}}$$

$$\frac{1}{E^*} = \frac{(1-\nu_1^2)}{E_1} + \frac{(1-\nu_2^2)}{E_2}$$

$$\frac{1}{R} = \frac{1}{R_1} + \frac{1}{R_2}$$



Parameter		Units
Ball Radius R	0.006	Metre
Shear Strength	53.18	MPa
Modulus E1	210	GPa
Modulus E2	4	GPa
Poissons ratio ν_1	0.3	
Poissons ratio ν_2	0.3	
Combined Mod E*	4.313	GPa
	0.231833333	

Note! Shear strength taken from 60/40 ratio PTFE - Polyamide-Imide

Assumed - no data

Normal Load W, N	a	Spot dia mm	Spot Area A mm2	Pmax (MPa)	Pave (MPa)	$\delta (10^{-6})$	ADHESIVE		ABRASIVE	Hertz	Imp dia	θ
							$\mu (s/P_{max})$	μ_a slide load	μ_{ab}	μ		
100	0.4708	0.9415	0.6962	215.34	143.56	203.15	0.2470	0.3723	0.165	0.3377	0.8	0.133333
90	0.4545	0.9090	0.6490	207.90	138.60	189.38	0.2558	0.3723	0.129	0.3497	0.63	0.108333
80	0.4370	0.8740	0.6000	199.90	133.27	175.08	0.2660	0.3723	0.109	0.3637	0.57	0.095
70	0.4180	0.8360	0.5489	191.20	127.47	160.17	0.2781	0.3723	0.095	0.3803	0.52	0.086667
60	0.3971	0.7941	0.4953	181.82	121.08	144.52	0.2928	0.3723	0.083	0.4003	0.48	0.08
50	0.3736	0.7473	0.4386	170.92	113.94	127.99	0.3111	0.3723	0.075	0.4254	0.46	0.076667
40	0.3469	0.6937	0.3780	158.67	105.78	110.30	0.3352	0.3724	0.067	0.4583	0.44	0.073333
30	0.3151	0.6303	0.3120	144.16	98.11	91.05	0.3689	0.3724	0.059	0.5044	0.43	0.071667
20	0.2753	0.5506	0.2381	125.94	83.96	69.49	0.4223	0.3724	0.051	0.5774	0.42	0.07
10	0.2185	0.4370	0.1500	99.96	66.64	43.78	0.5320	0.3724	0.039	0.7274	0.41	0.068333

16.60827 49.18512
47.48788
45.65976
43.67219
41.48504
39.03916
36.24101
32.92746
28.78518
22.83146

$$\mu_a = \frac{1}{W} \left(\frac{A^2 \rho_0^2 - W^2}{\alpha} \right)^{\frac{1}{2}}$$

$$\mu_{ab} = \frac{(\theta - \sin \theta) p_H}{\left(\sin \frac{\theta}{2} \right)^2 p_0}$$

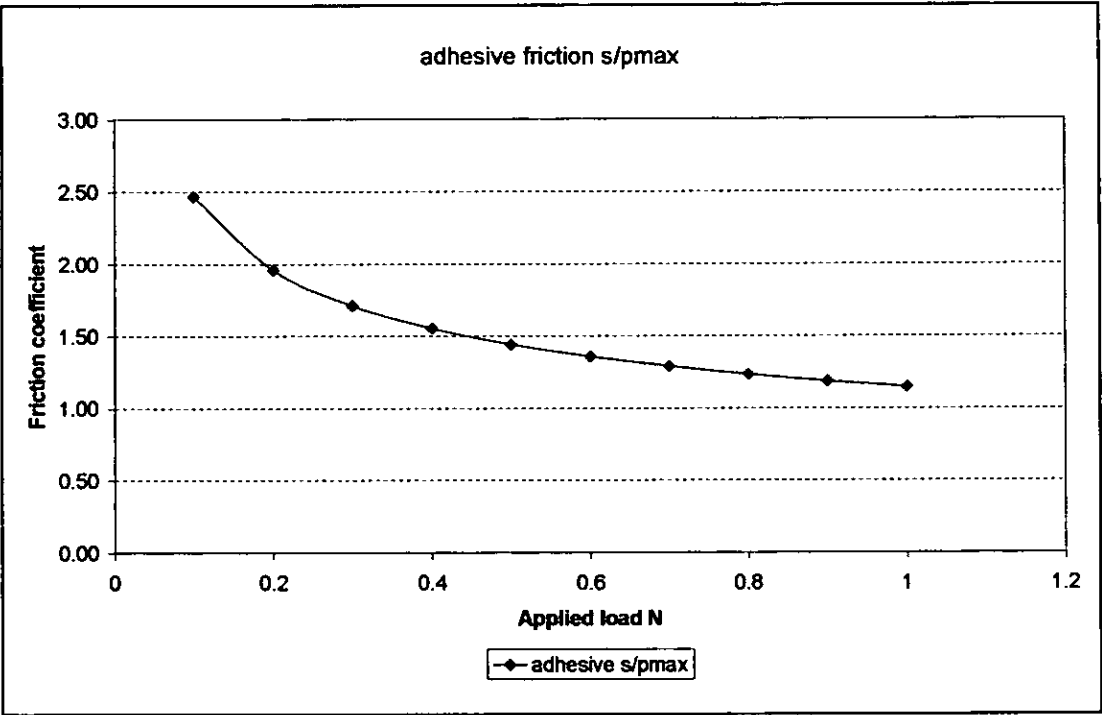


Figure 7.41 Friction due to adhesion s/p_{max} 0.1 to 1N

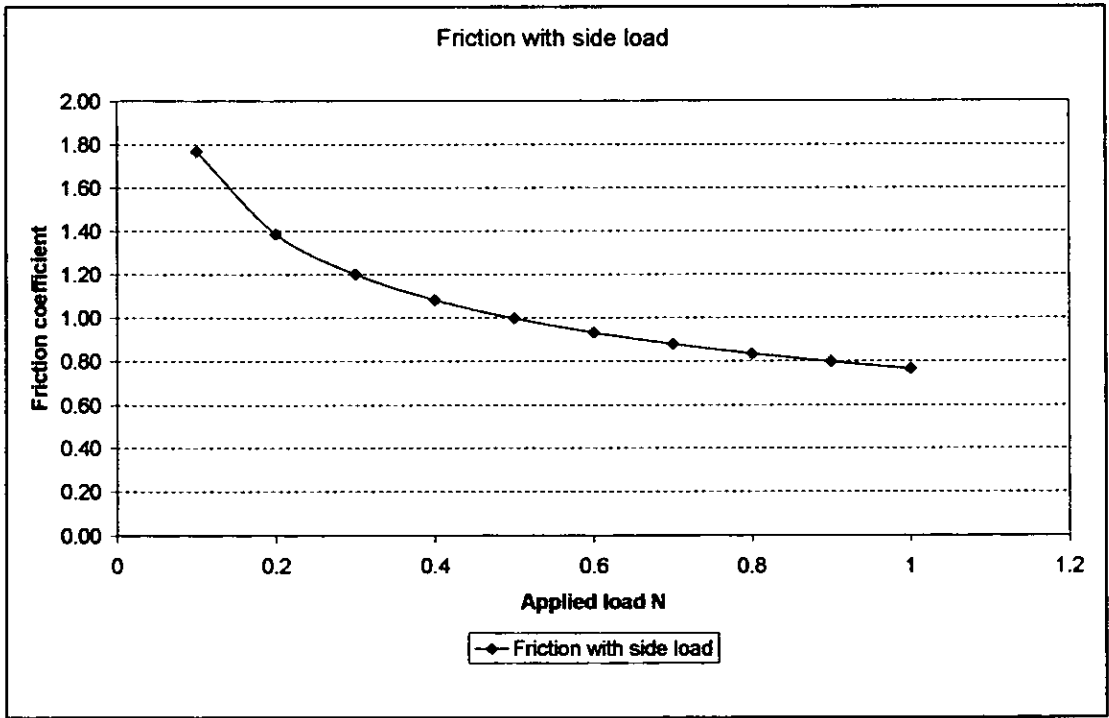


Figure 7.42 Friction with side load (tangential) 0.1 to 1N

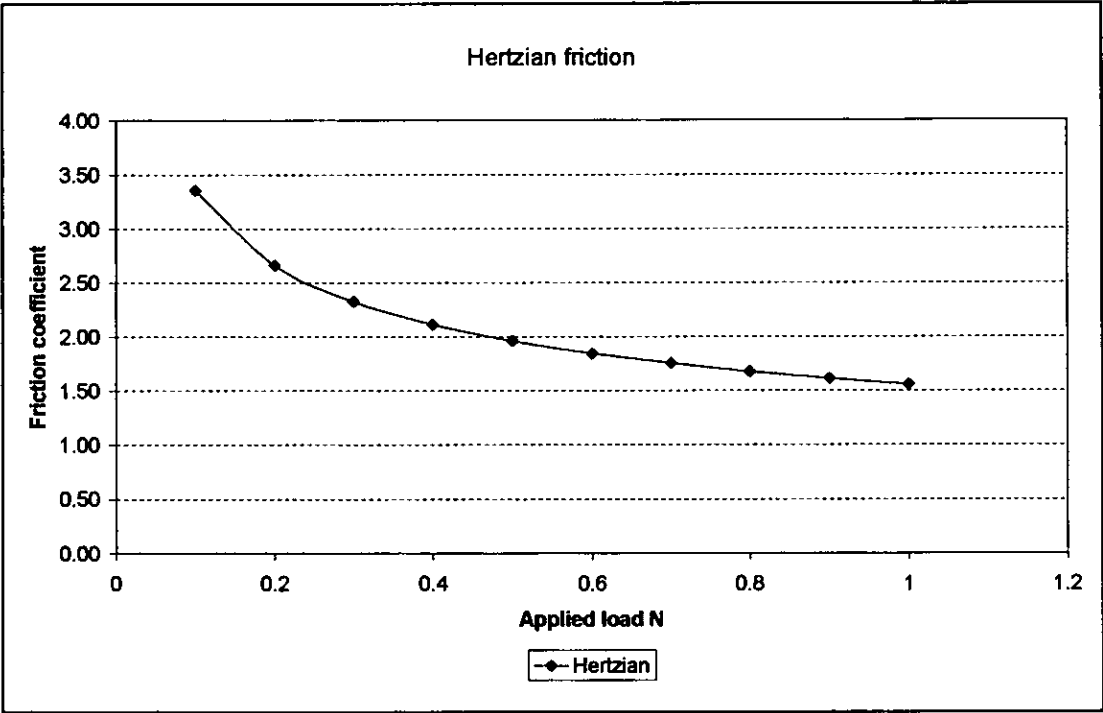


Figure 7.43 Friction due to Hertzian contact. 0.1 to 1N

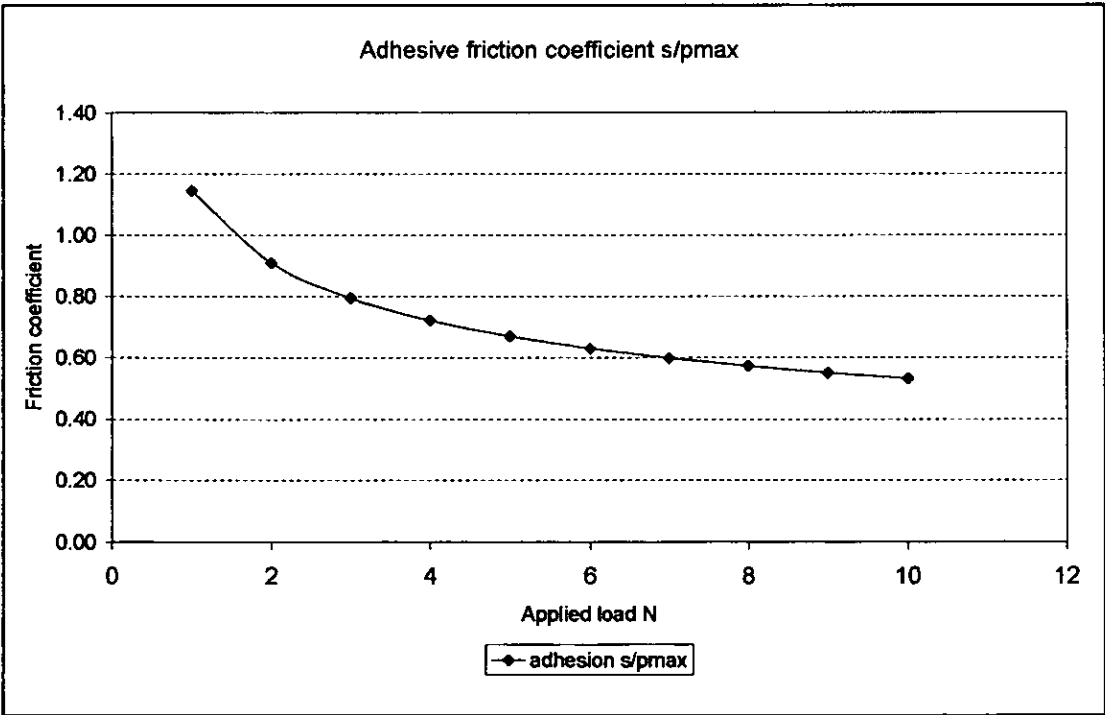


Figure 7.44 Friction due to adhesion s/p_{max} 1 to 10N

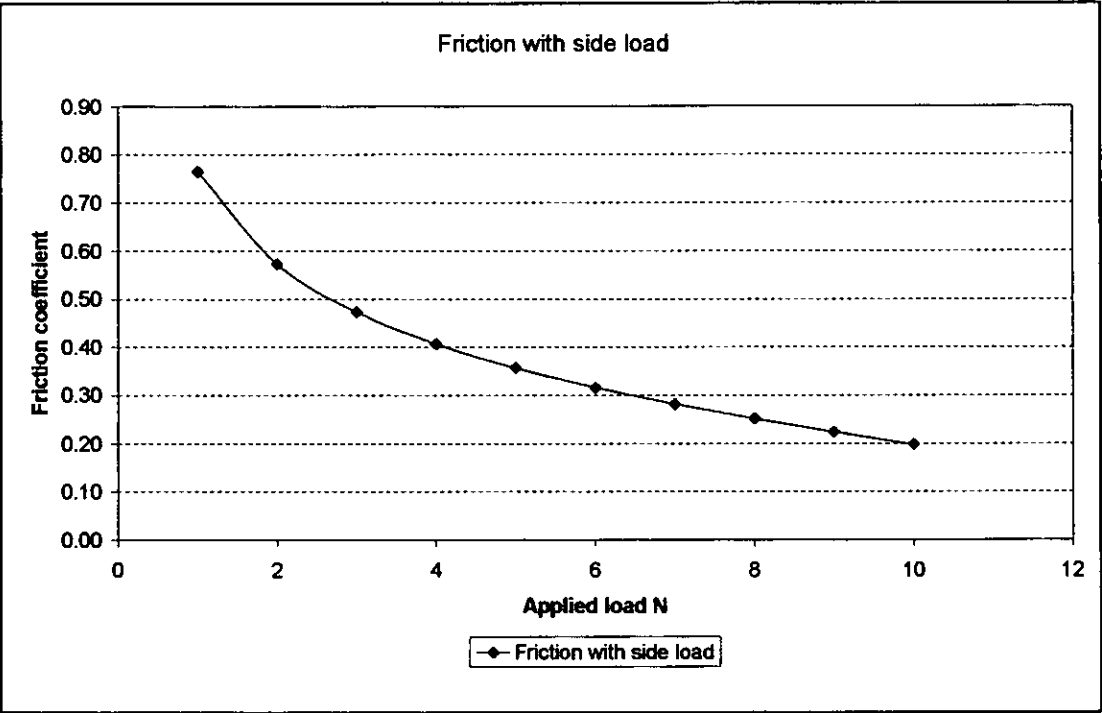


Figure 7.45 Friction with side load (tangential) 1 to 10N

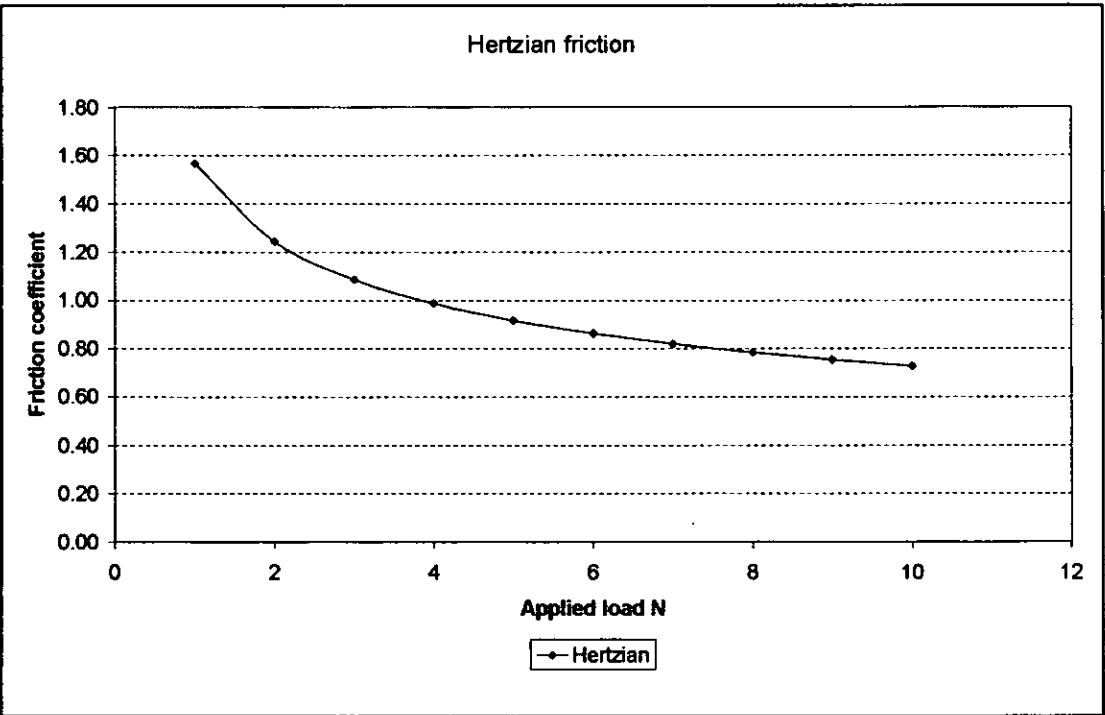


Figure 7.46 Friction due to Hertzian contact. 1 to 10N

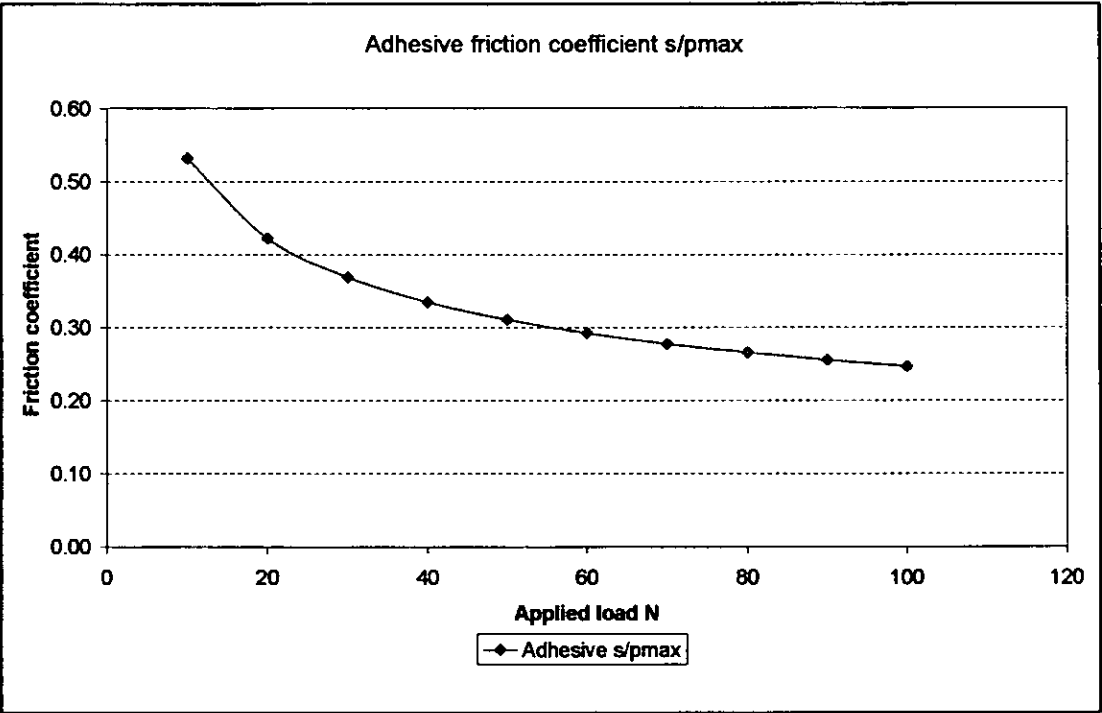


Figure 7.47 Friction due to adhesion s/p_{max} 10 to 100N

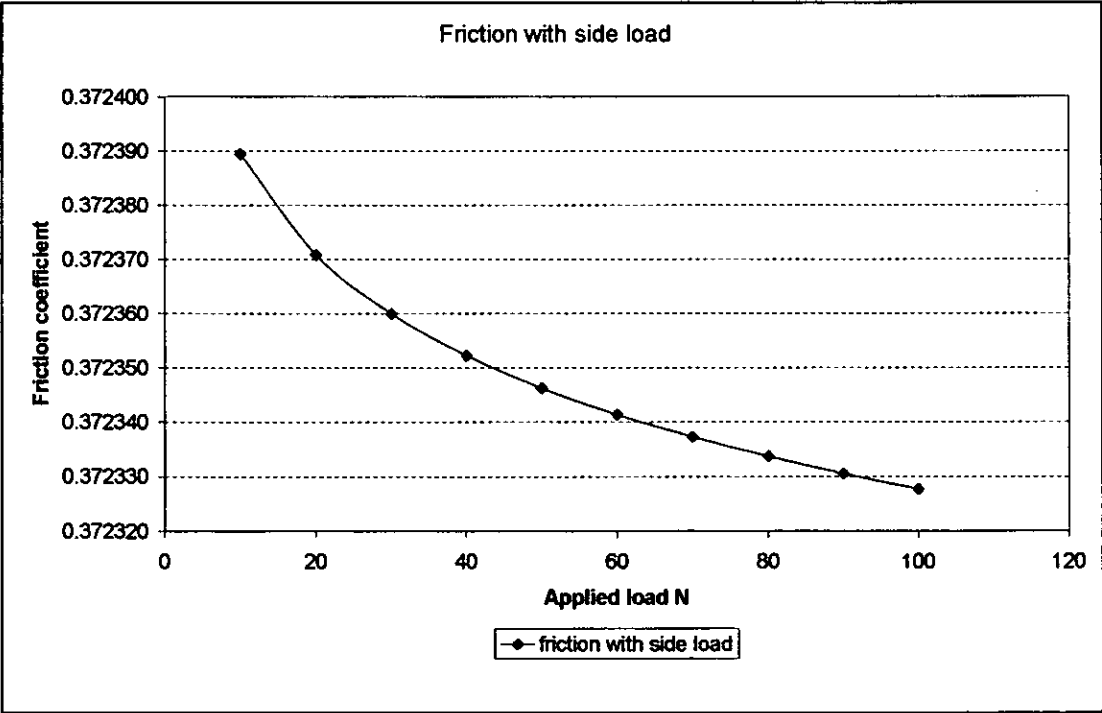


Figure 7.48 Friction with side load (tangential) 10 to 100N

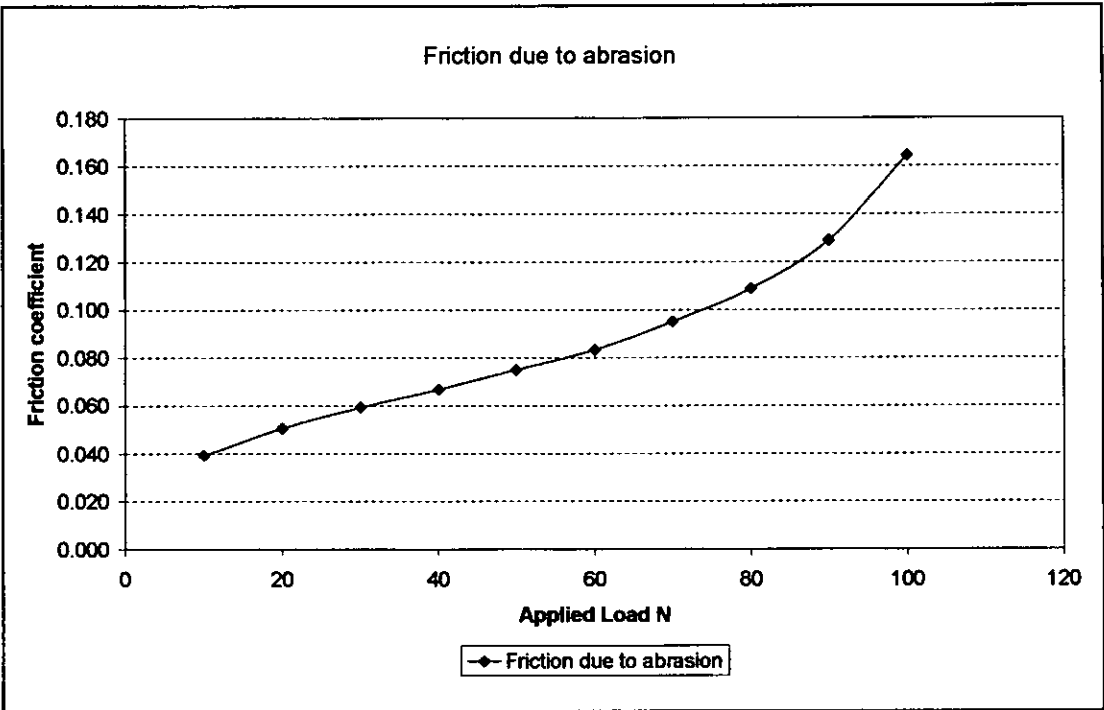


Figure 7.49 Friction due to abrasion 10 to 100N

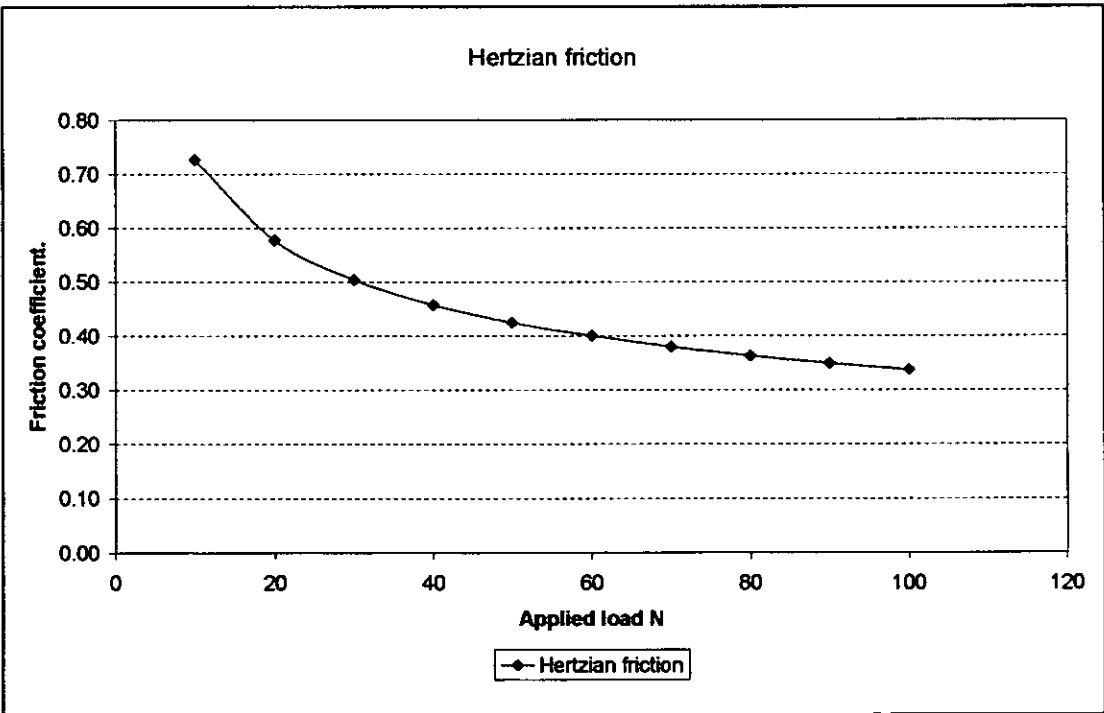


Figure 7.50 Friction due to Hertzian contact. 10 to 100N

7.8 Summary

An empirical model has been developed from the experimental results for the coefficient of friction of a sphere sliding on a flat surface. This model is independent of applied load, surface finish and velocity. It has also been demonstrated that for loading conditions that produce contact pressures below or close to the yield pressure of the film that the mechanism of sliding follows Hertzian elastic behaviour and that the surface finish on the counterface appears to have little effect on the frictional performance.

A study of the wear scar on the ball and the track on the disc, under loading conditions below and close to the yield pressure of the film, during sliding has demonstrated the apparent contact area to be much larger than the calculated Hertzian contact area. This study also demonstrated the thick build up of lubricant due to sliding on the counterface of the grit blasted balls. An equation for the ploughing term for the film was derived for a spherical contact and the friction coefficient calculated.

The wear scar generated on the as received finish ball under a load of 10N and a velocity of 1 ms^{-1} was investigated and the apparent area of contact, friction coefficient and shear strength compared with the calculated values derived from Hertzian contact theory. An expression is derived from Bowden and Tabor's modified theory to include tangential loads and example graphs of friction coefficient plotted against sliding distance using the yield pressure and apparent pressures obtained from the measurements.

Hertzian contact conditions are discussed in combination with ploughing of the film and a possible reason why this may not occur for these 'thick' films up to an applied load of 100N. A possible reason is demonstrated for the impressions made in the film under static loading conditions. The large wear scars generated are discussed and simple theory used to evaluate the friction coefficient in the early and late stages of sliding these are compared with the experimental values and possible reasons given for their non compliance.

Finally three spreadsheets are included that are used to calculate the various theoretical friction conditions and the associated graphs plotted.

Reference.

- [7.1] Bowden, F. P., Tabor, D., "The friction and lubrication of solids, Part II". Clarendon Press, Oxford, UK. 1964, pp. 158-185
- [7.2] Miyoshi, K., "Solid Lubrication Fundamentals and Applications." NASA/TM – 2001-210749/ Chapter 5. 2001. pp. 1 - 10
- [7.3] Halling, J., "Principles of Tribology" The Macmillan Press Ltd. 1975. pp. 51 – 53, 82 – 84.
- [7.4] Singer, I. L., Bolster, R. N., Wegand, J. C., Feyeulle, S., Stupp, B. C., "Hertzian stress contribution to low friction behaviour of thin MoS₂ coatings." Appl. Phys. Lett. 57. 1990, pp. 995.
- [7.5] Johnson, K. L. "Contact Mechanics." Cambridge University Press, 1985.

CHAPTER 8.
CONCLUSION AND FURTHER WORK.

8.1 Conclusion.

The literature survey described in chapter 2 discusses the scientific study of solid lubricants back to the early 1940s. The study of BSLs begin around 1965, to date only 50 or so papers have been published, one of the possible reasons for this is the introduction of PVD films in the late 1970s, these films taking over the more technically demanding aerospace roles and possibly being more attractive for researcher. Apart from these scientific papers there is very little information in the public domain, the material that is in the public domain is normally provided by the material suppliers, who only supply the basic information such as the friction coefficient, wear life, corrosion resistance and guidelines for application. The tribological information is normally from a specific test regime and may be of little use to a designer or engineer for the material selection for a specific application.

In the first experimental phase of this study, a screening programme was conducted using an existing test facility on 12 bonded solid lubricants to identify an optimum coating for a specific application in a seat belt buckle. In general the friction coefficients measured tended to be higher than those quoted by the manufacturer, it was concluded that this was probably as a consequence of the difference in test methods. The screening programme also gave an insight into some of the problems encountered in tribological testing i.e. vibration, uncontrolled oscillation of the friction measuring device and data processing.

In the second test programme on the new test facility a BSL selected from the first screening programme was tested with various counterface finishes, loads and velocities. The results of this programme demonstrated:

- There were three distinct phases of performance for all of the test conditions.
- With high loads the contact life increased with velocity.
- The counterface surface finish had a significant effect on performance, in general the smoother the finish, lower R_a value, the shorter the life.
- With low load conditions the smooth as received counterface finish lasted over 500km sliding without failure.

- In general the friction coefficient for all the tests in the steady state phase is between 0.18 and 0.22.
- From this test programme it was possible to develop an empirical equation to describe the friction coefficient to the point just before failure begins to occur, although it was not possible to predict at what point this would be. It was also shown that the curves generated for all of the tests were remarkably similar, conforming to a band on the friction coefficient scale that was only 0.05 wide.

The third test programme concentrated on the development of the contact wear during sliding of the as received ball on the BSL at a velocity of 1ms^{-1} at a load of 10N. This programme shows that the friction coefficient gradually increases up to a sliding distance of 2500m with the surface scar on the ball consisting of, initially, a thin transfer film, that gradually became thicker as sliding progressed. After 2500m sliding the friction coefficient changed and became almost constant, at this point the thick film surface scar on the ball changed to the circular wear scar possibly indicating that metallic contact was occurring, from the previous tests it is assumed that this scar would continue to increase in size until the area in contact with the coating was insufficient to continue to supply the interface with the amount of lubricant to maintain sliding and the friction coefficient would begin to rise and become erratic.

In the forth test programme the performance of the BSL was evaluated at pressures below the yield pressure of the film. The results from this programme demonstrate that as the load increases, the friction coefficient decreases and is assumed to be associated with the Hertzian stress component of the contact. A comparison of the data with the predicted friction coefficient generated using the bulk shear strength of the film as 53.18MPa calculated by using the mixture ratio of 60/40 and similarly the elastic modulus at 4GPa. Gives a value that is approximately 4 to 5 times the experimental value, this is illustrated in figure 8.1. If this was used by designers and engineers in designing mechanisms, it would give a very conservative estimate of the friction with the results that the loading to operate such mechanisms, and hence the power required, would be much greater and lead to waste. In figure 8.1 the results reduce in range as the load increases, on the left hand side at the very low load, 0.2N, the range is very wide, it is thought that this is due to the limitations of the test facility, which was originally designed for loads in excess of 10N, but adapted to

accommodate loads down to this level. At this level of loading the natural resistance, stick-slip, of the load application shaft and counter balance system could have influenced the applied load.

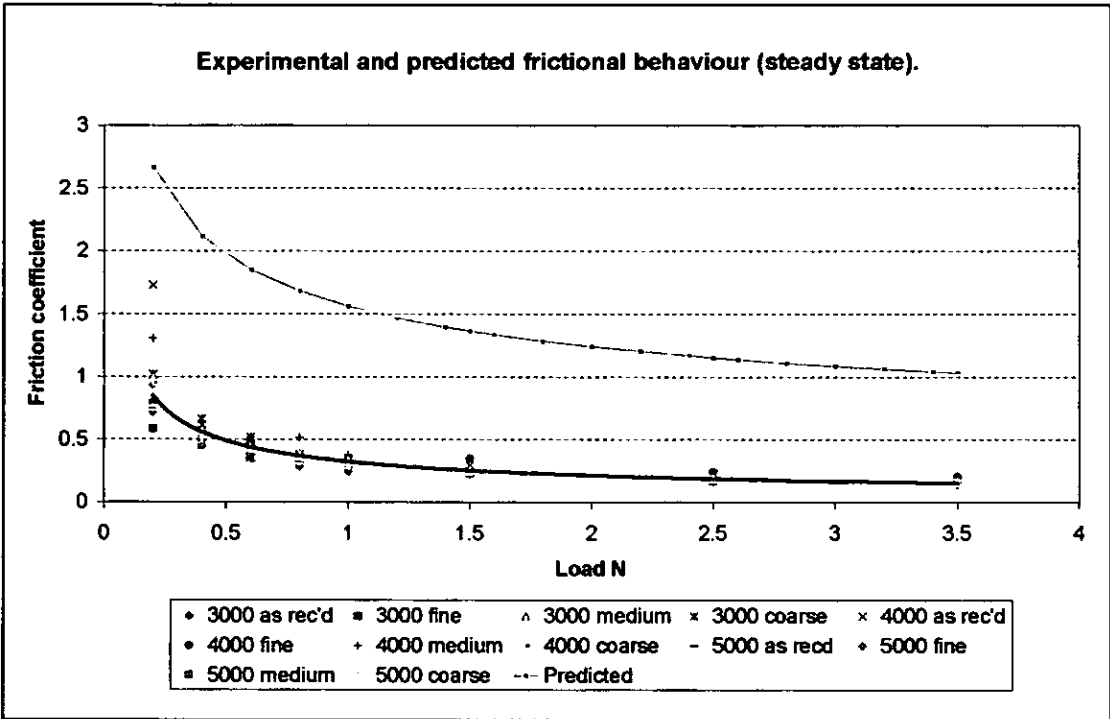


Figure 8.1 Experimental and predicted friction coefficient below the yield pressure of the film.

The calculation of the friction coefficient using the Hertzian approximation is a standard technique and may not be appropriate, as it gives the wrong result, possible reasons for the overestimation are: the bulk modulus may not be representative of the real film modulus, the shear strength may not be representative of the real shear strength of the film interface, both these values have been calculated from data obtained from the moulded polymers, due to there not being any data available for the materials in the dry film form. Additionally the shear strength at the interface may be totally different, due to the build up of transfer films on the ball and coating, comprising the PTFE and graphite components of the film. However it is though that it is the determination of the real area of contact that is the problem. Having said this, the experimental data does follow the general trend of the predicted data.

In predicting the friction coefficient from the “simple theory” of sliding, it is difficult to predict the real area of contact, if the area is calculated from the hardness of the film $A = W/H$, is used, where H is the film hardness, then:

$$F = As$$

Substituting $F = \frac{W}{H}s$ and $F = \mu W$

$$\mu W = \frac{W}{H}s$$

$$\mu = s/H$$

then for any applied load this would give a friction coefficient of $53.18 \times 10^6 / 248 \times 10^6 = 0.21$ this is a close approximation to the experimental results. If the Hertzian prediction of contact area is used, $A = 0.15$ at 10N and 0.696 at 100N giving $\mu = 0.79$ and 0.37, which does not compare favourably with the experimental values.

The modified theory of sliding produces results that require an α value in excess of 35 to obtain a close approximation, when the yield pressure of the film is used. When the apparent pressures and areas are used, a smaller value of α is required to obtain a closer approximation.

If the coated surface is treated as a contaminated surface, then the shear strength of interface calculated from the apparent area, measured friction coefficient and the apparent pressure taken from the applied load and measured apparent area, which is known to be too big:

$$s_a = \mu W/A_a \quad \text{and} \quad p_a = W/A_a$$

then $\mu = s_a/p_a$

this gives a fairly close approximation, see figure 7.32, to the performance curves generated in the experiments. Whereas using the accepted ratio of the shear strength of the contaminating film, in this case the BSL, to the yield pressure, s_0/p_0 gives:

$$\begin{aligned}\mu &= 53.18 \times 10^6 / 77.5 \times 10^6 \\ &= 0.68\end{aligned}$$

This is approximately 3 times the experimental value.

During the steady state phase where the circular wear scar is generated, approximations by estimating the apparent area of contact greatly over estimate the friction coefficient by a factor between 10 and 300. Using the Hertzian contact area expression an approximation that is 3 to 4 times the experimental value is obtained when using the shear strength and elastic modulus of the bulk film material.

In general all the accepted models of friction over estimate the friction coefficient of a sphere sliding on a flat surface. If the real area of contact in the simple theory of sliding friction is calculated from the film hardness then a close approximation to the experimental data is achieved, this is probably one of these easiest to perform in practice and means that the friction coefficient of the sliding couple is equal to the bulk shear modulus divided by the film hardness. i.e. assumes limited junction growth.

8.2 Further work.

The work performed in this study was concerned with one specific type of bonded solid lubricant, for which an empirical equation was developed to predict the friction coefficient for a specified sliding distance. However it is thought that this model would apply to other types and mixtures of BSL, possibly with changes to the constants. The same test facility could be used with a range of BSLs to verify this.

It was noticed when performing the test programme described in chapter 5 that wear debris accumulated at the edges of the track, at the end of one of the tests when the friction began to display erratic behaviour the debris was inadvertently disturbed,

being swept back into the track with the result that the friction trace settled back to slightly below its old level, this was allowed to run for 20 minutes before being stopped, during which time the friction trace remained stable. Perhaps the management of this debris in sealed systems could be a method of prolonging the useful life of these lubricants, or even produce a new type of lubrication by providing just the solid lubricant in powder form.

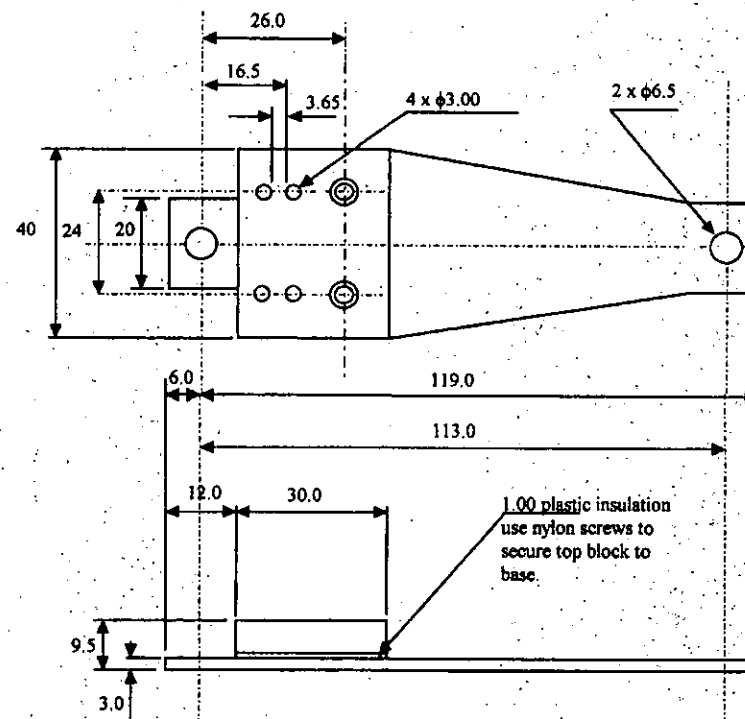
The shear strength of the film used in this study is calculated by assuming a 60/40 mixture ratio of the main constituents, polyamide-imide and PTFE with data from the bulk moulded material. The assumption is made due to the lack of information from the material manufacturers and understandably, their unwillingness to divulge the make up of the BSL. A study of BSLs with known mixture ratios could be used to verify the use of the ratio of mixtures method. A further study on these same samples could examine the effects of the individual components e.g. their effect on the friction coefficient, sliding life, load carrying capacity etc.

The manufacturers of BSLs normally specify the optimum thickness of these films as an arbitrary 10 to 15 μm , the films used in this study were specified at 20 $\mu\text{m} \pm 5\mu\text{m}$, developed from the screening test and in product testwork, in practice the films vary between 20 and 35 μm due to the application process. A study could be conducted to determine the effect of film thickness, taking into consideration the limitations of the application process.

In chapter 7 an illustration is given of three conditions of a sphere pressed against a flat surface, soft sphere hard surface, hard sphere hard surface and hard sphere soft surface it would be interesting to investigate the real contact area for these conditions, this may provide information that is useful for analysing thick films.

APPENDIX A1.

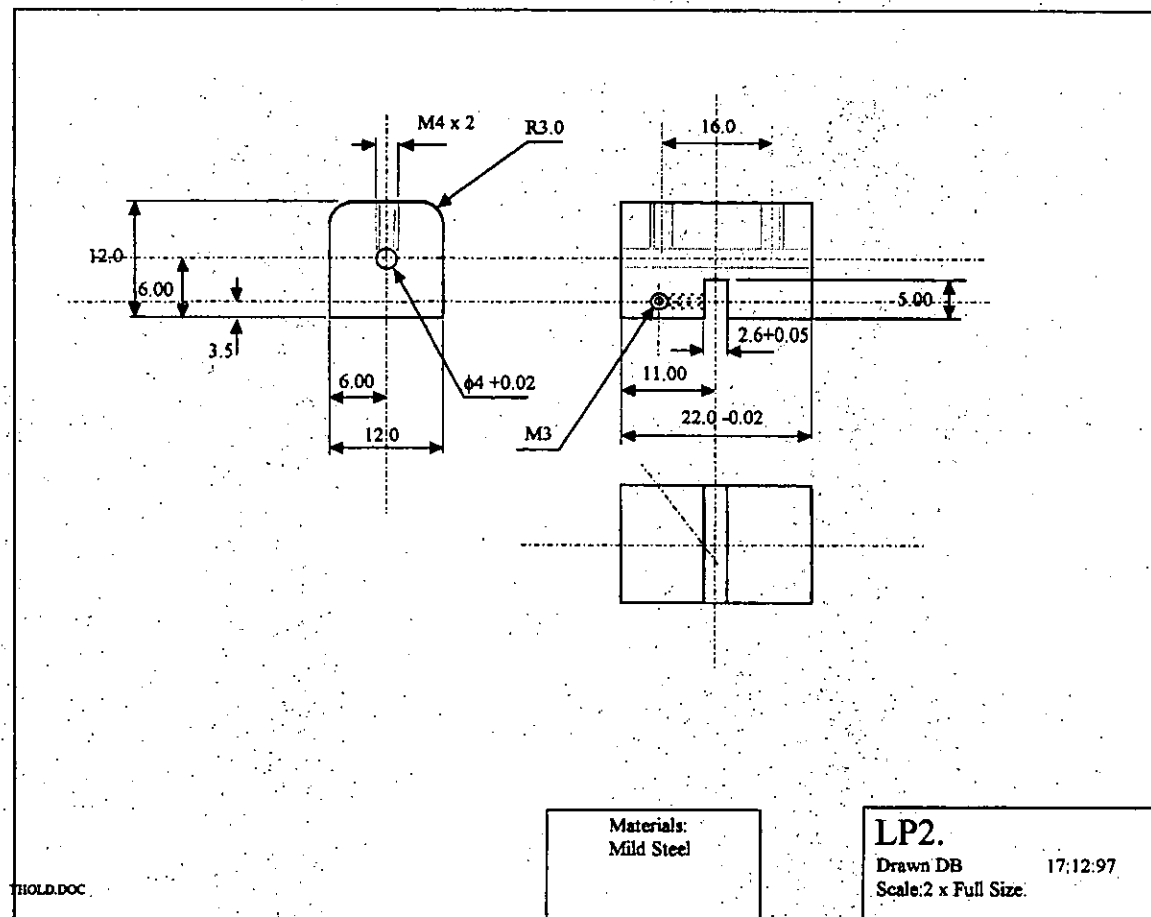
Modifications and work holder for initial test apparatus.

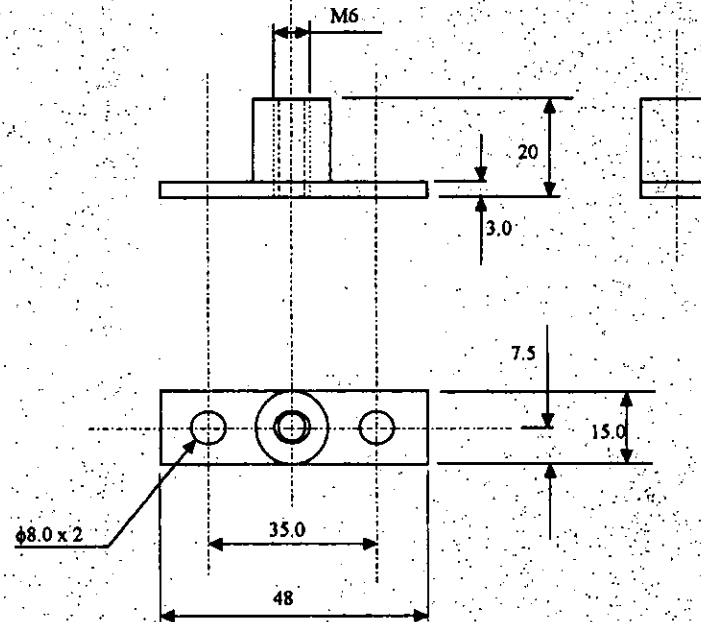


LP1.DOC

Materials:
Main block: Mild steel.
Base: Gauge plate.

LP1.
Drawn DB 17:12:97
Scale: Full Size.





Materials:
Mild Steel

LP3.

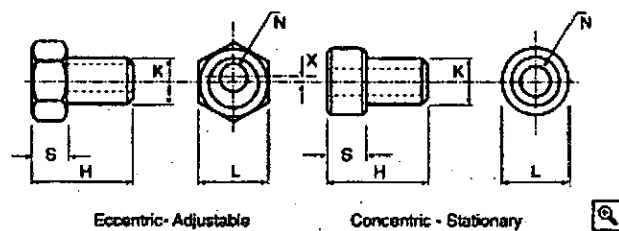
Drawn DB
Scale: Full Size.

17:12:97

JACK.DOC

APPENDIX A2

Linear bearing details for new test facility.



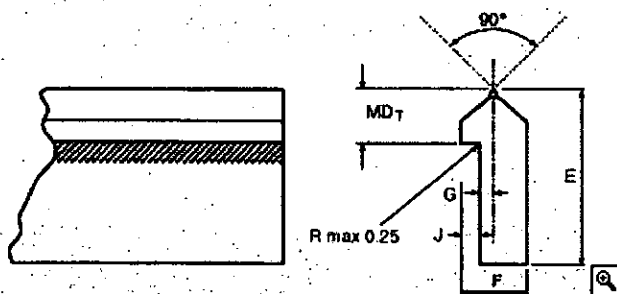
Dimensions

Size	H	K*	L	N	X	S	Wt./g
1	13.97	4.75	11.11	3.60	0.30	6.3	5
2	17.93	9.51	14.28	6.10	0.60	7.13	11
3	25.14	11.99	19.05	8.10	1.06	9.52	26
4	29.9	14.99	22.22	10.10	1.52	11.09	45

* Fits corresponding wheel bore

Wheel mounting adaptors.

(Adapted from RS components)

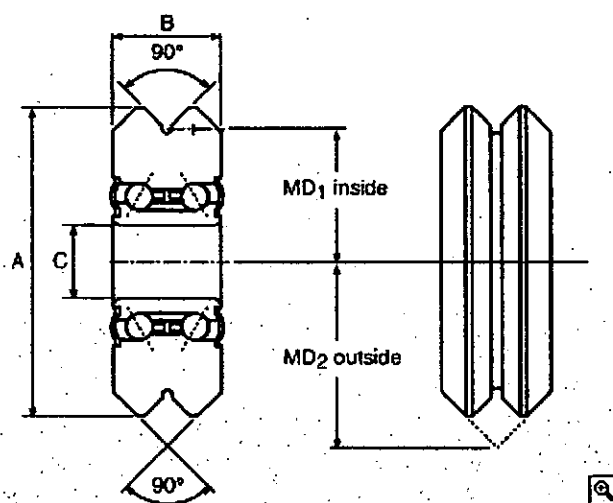


dimensions

Size	E	F	G	H	MD _T	Kg/m
1	11.09	4.74	0.78	1.57	3.17	0.272
2	15.87	6.35	0.78	2.36	4.75	0.509
3	22.22	8.71	1.57	2.76	6.35	1.02
4	26.97	11.09	2.36	3.17	7.92	1.63

Linear Slide Rail.

(Adapted from RS components)



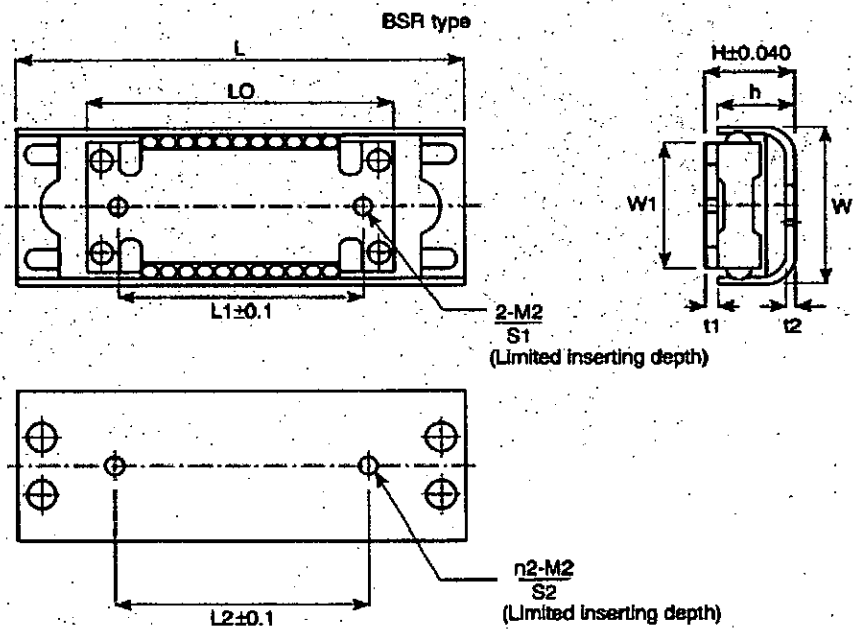
dimensions

Size	A	B	C	MD ₁	MD ₂	Wt./g
1	19.55	7.87	4.76	7.92	11.86	12.0
2	30.73	11.09	9.52	12.7	18.23	40.0
3	45.72	15.87	12.0	19.05	26.97	136.0
4	59.94	19.05	15.01	25.4	34.92	285.0

Linear Slide wheel.

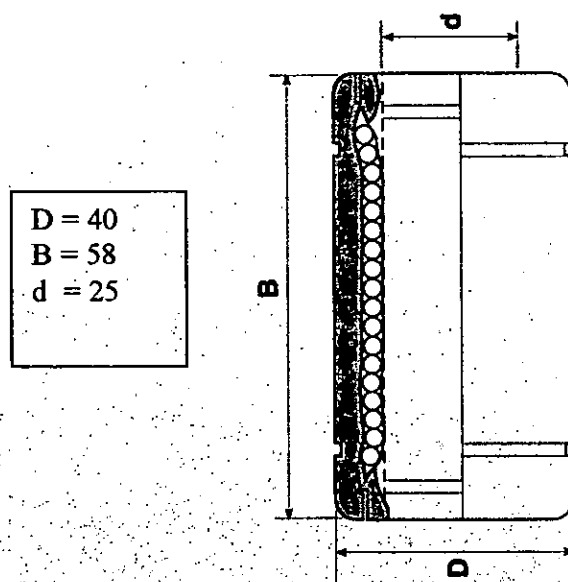
(Adapted from RS components)

	H	L	Stroke max.	W1	L0	L1	M2
20	10	50	22	16.8	40	32	M3



Top plate Precision ball slide type BSR2050SL

(Adapted from RS components)



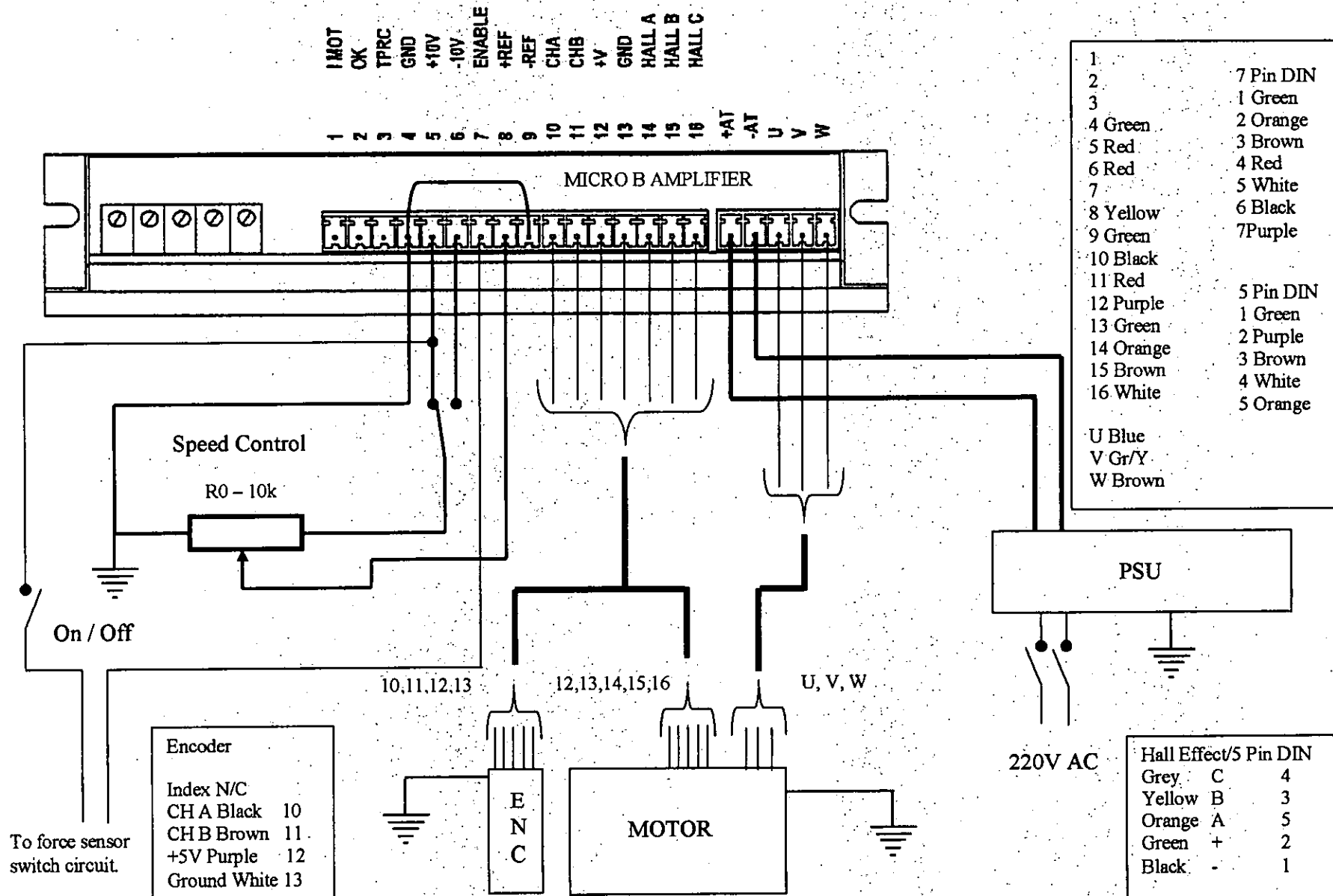
Load application shaft linear bearing type 746-576

(Adapted from RS components)

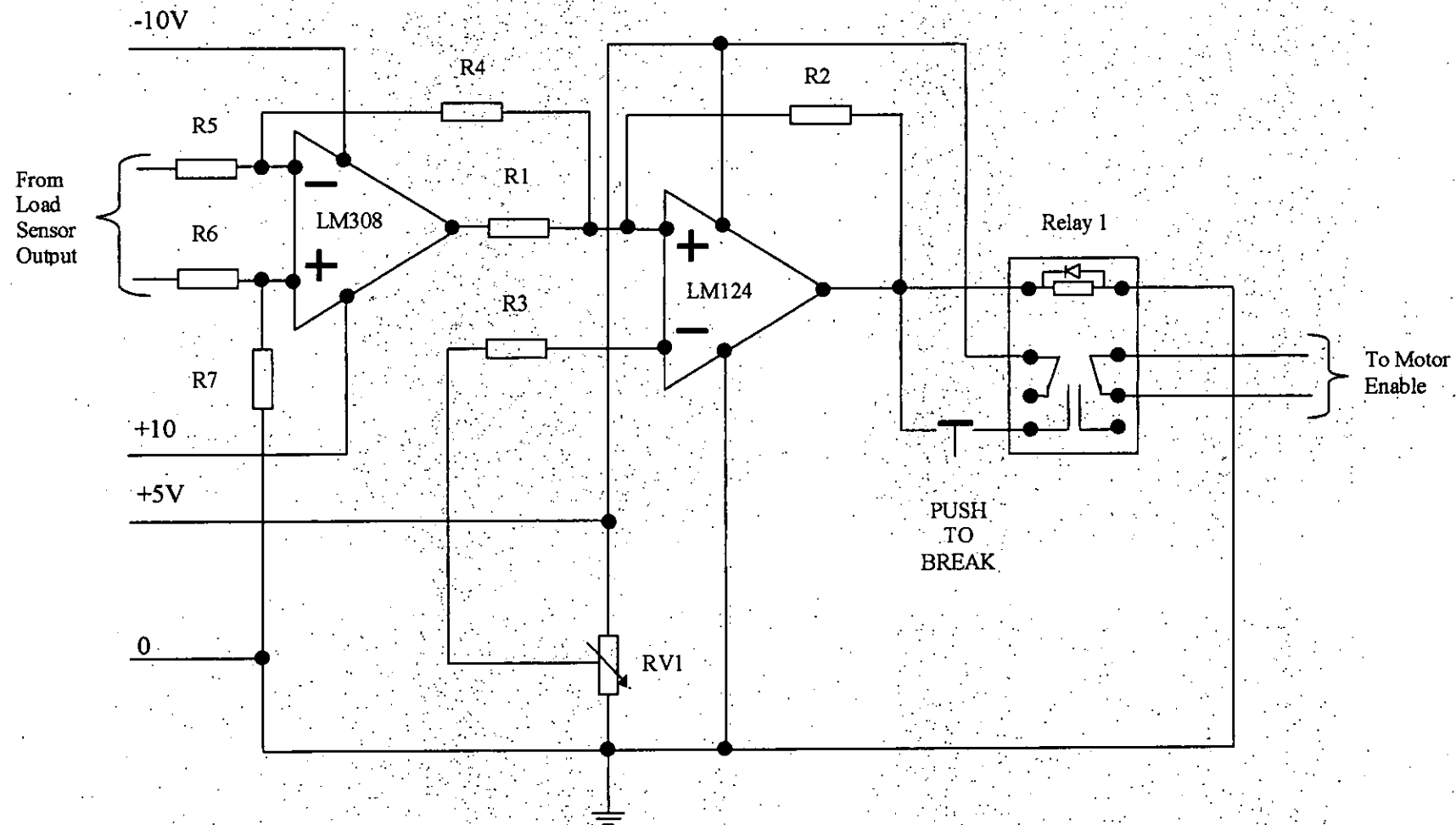
APPENDIX A3

Motor wiring diagram and force switch sensor.

Data collection interface details.



Drive Motor Schematic



Force sensor switch schematic.

Specification	
No. of channels	11 (ADC-11) 22 (ADC-22)
Resolution	10 bit (ADC-11/10 and ADC-22) 12 bit (ADC-11/12)
Input range	0 to 2.5V
Overload protection	$\pm 30V$
Sampling rate	10kHz
Accuracy	$\pm 1\%$ (ADC-11/10 and ADC-22) $\pm 0.5\%$ (ADC-11/12)
Input connector	D25 female
Input impedance	$>1M\Omega$
Output connector	D25 male to PC parallel port
Outputs	1 (digital)
Supplied software (The ADC-11/12 is not supported under DOS)	PicoLog for Windows (3.x, 95/98, NT/2000) PicoScope: DOS and Windows (3.x, 95/98, NT/2000) Drivers & examples: C, pascal, Delphi, Visual Basic, HP VEE and LabVIEW. A macro is also provided to collect data directly into an Excel spreadsheet.



APPENDIX A4

Force sensor details.

ADC terminal block.

MICRO SWITCH Force Sensors

Force Sensor

FS Series

SALES AND SERVICE

Honeywell's MICRO SWITCH Division serves its customers through a worldwide network of sales offices and distributors. For application assistance, current specifications, pricing or name of the nearest Authorized Distributor, contact a nearby sales office. Or call:

1-800-537-6945 USA
1-416-293-8111 Canada
1-815-235-6847 International

INTERNET

<http://www.sensing.honeywell.com>
info@micro.honeywell.com

Specifications may change without notice. The information we supply is believed to be accurate and reliable as of this printing. However, we assume no responsibility for its use.

While we provide application assistance, personally and through our literature, it is up to the customer to determine the suitability of the product in the application.

Honeywell

Sensing & Control
Honeywell Inc.
11 West Spring Street
Freeport, Illinois 61032



Printed with Soy Ink
on 50% Recycled Paper

84-08028-0 796 Printed in USA

Helping You Control Your World

MICRO SWITCH Force Sensors

Force Sensor

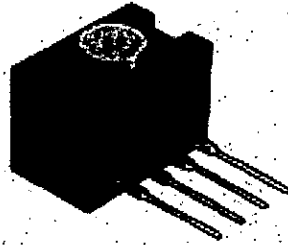
FS Series

FEATURES

- Robust performance characteristics
- Precision force sensing
- Adaptable product design
- Highly reliable
- Signal conditioning available
- Electrically ratiometric output
- Extremely low deflection (30 microns typical @ Full Scale)
- Low repeatability errors ($\pm 0.2\%$ Span)
- Low linearity errors ($\pm 0.5\%$ Span)
- Low off-center loading errors
- Resolution to 1.0 gram force
- Fast response time
- Low power consumption
- High ESD resistance - 10 KV

TYPICAL APPLICATIONS

- Medical infusion pumps
- Kidney dialysis machines
- Robotic end-effectors
- Variable tension control
- Load and compression sensing
- Contact sensing



The FS Series Force Sensor provides precise, reliable force sensing performance in a compact commercial grade package. The sensor features a proven sensing technology that utilizes a specialized piezoresistive micro-machined silicon sensing element. The low power, unamplified, non-compensated Wheatstone bridge circuit design provides inherently stable mV outputs over the 1,500 gram force range.

The force sensor operates on the principle that the resistance of silicon implanted piezoresistors will increase when the resistors flex under an applied force. The sensor concentrates force from the application through the stainless steel plunger directly to the silicon sensing element. The amount of resistance changes in proportion to the amount of force being applied. This change in circuit resistance results in a corresponding mV output level.

The sensor package design incorporates a patented modular construction. The use of innovative elastomeric technology and engineered molded plastics results in load capacities of 5.5 Kg over-force. The stainless steel plunger provides excellent mechanical stability and is adaptable to a variety of applications. Various electrical interconnects can accept pre-wired connectors, printed circuit board mounting, and surface mounting. The unique sensor design also provides a variety of mounting options including mounting brackets, as well as application-specific mounting requirements.

MICRO SWITCH Force Sensors

Force Sensor

FS Series

PERFORMANCE CHARACTERISTICS @ 10 ± 0.01 VDC, 25°C

Preliminary, based on limited test data

Parameter	Min.	Typ.	Max.	Units
Excitation*	—	10	12	VDC
Null shift, 25 to 0°, 25 to 50°C	—	± 0.5	—	mV
Null offset	-30	0	+30	mV
Linearity (BFSL)	—	± 0.5	—	% Span
Sensitivity	—	0.24	—	mV/grf
Sensitivity shift 25 to 0°, 25 to 50°C	—	± 5.0	—	% Span
Repeatability	—	± 0.2	—	% Span
Response time	—	—	1.0	msec
Input resistance	—	5.0 K	—	ohms
Output resistance	—	5.0 K	—	ohms
Plunger deflection	—	30	—	microns
Weight	—	2.0	—	grams
ESD (direct contact - terminals and plunger)	10	—	—	kVolts

* Non-compensated force sensors, excited by constant current (1.5 mA) instead of voltage, exhibit partial temperature compensation of Span.

ENVIRONMENTAL SPECIFICATIONS

Operating temperature	-40 to +85°C (-40 to +185°F)
Storage temperature	-55 to +105°C (-67 to +221°F)
Shock	Qualification tested to 150 g
Vibration	Qualification tested to 0 to 2 kHz, 20 g sine

Note: All force related specifications are established using dead weight or compliant force.

ORDER GUIDE

Catalog Listing	Force Range (grams)	Span, mV			Overforce grams Max.
		Min.	Typ.	Max.	
FSG-15N1A	1,500	290	360	430	5,500

MOUNTING

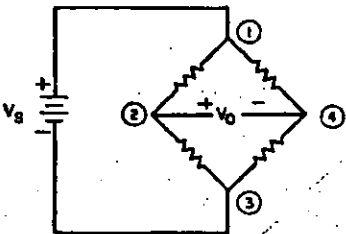
The sensor output characteristics do not change with respect to mounting orientation. Care should be taken not to obstruct the vent hole in the bottom of the sensor housing. Improper venting may result in unstable output.

Mounting bracket mounting torque: 2-5 in. lb. (.21-.56 Nm).

APPLYING FORCE

Evaluation of the sensor is to be performed using dead-weight or compliant force. Application of a rigid, immobile force will result in output drift (decrease) as elastomeric seals relax. Off-center plunger loading has minimal effect on sensor performance and maintains operation within design specifications.

EXCITATION SCHEMATIC



FS SERIES CIRCUIT

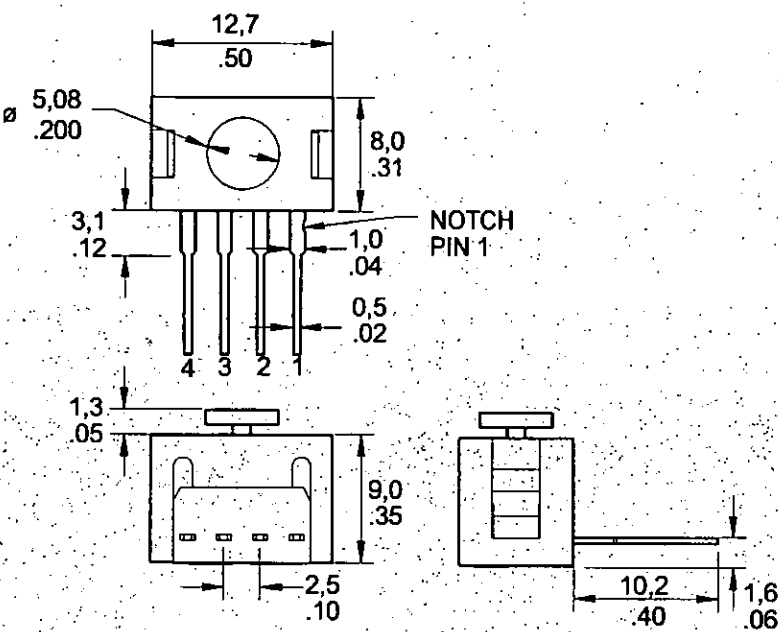
1. Circled numbers refer to sensor terminals (pins). Pin 1 is designated with a notch.
Pin 1 = Supply V_g (+)
Pin 2 = Output, (+)
Pin 3 = Ground, (-)
Pin 4 = Output, (-)
2. The force sensor may be powered by voltage or current. Maximum supply voltage is not to exceed 12 volts. Maximum supply current is not to exceed 1.6 mA. Power is applied across Pin 1 and Pin 3.
3. The sensor output should be measured as a differential voltage across Pin 2 and Pin 4 ($V_o = V_2 - V_4$). The output is ratiometric to the supply voltage. Shifts in supply voltage will cause shifts in output. Neither Pin 2 nor Pin 4 should be tied to ground or voltage supply.

MICRO SWITCH Force Sensors

Force Sensor

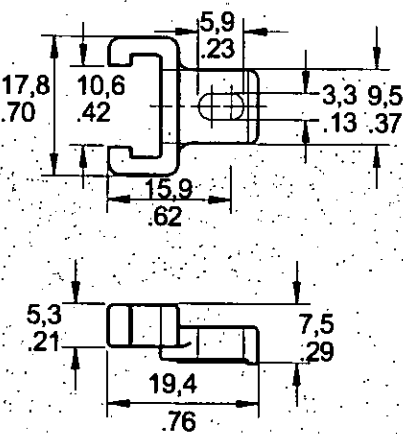
FS Series

MOUNTING DIMENSIONS (for reference only)



ACCESSORY

Catalog Listing	Description
PC15132	Plastic mounting bracket

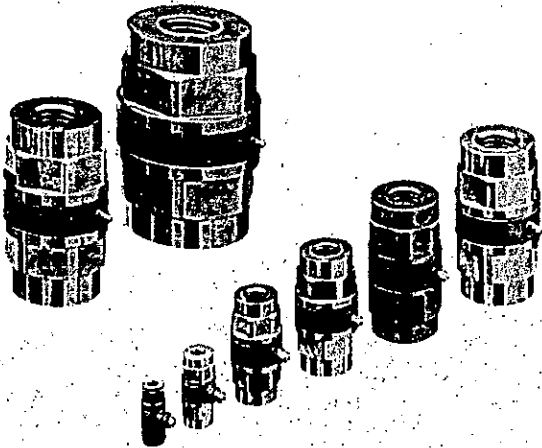


Quarz-Kraftmesselemente
Elements de mesure de force à quartz
Quartz Force Links

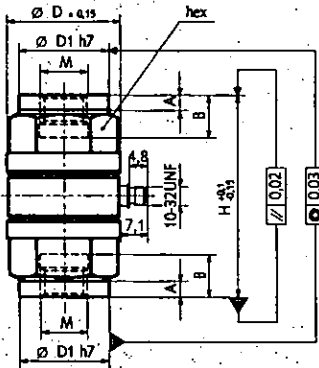
9301B/9371B

Kraftsensoren für das Messen dynamischer und quasistatischer Zug- und Druckkräfte. Capteurs destiné à mesurer des forces dynamiques et quasi-statiques de traction et de compression. Force sensors for measuring dynamic and quasistatic tensile and compression forces.

- Kalibriertes Kraftmesselement
Elément de mesure étalonné
Calibrated force link
- Einfache Montage
Simplicité de montage
Simple Installation
- Zentriersitze für exakten Einbau
Portée de centrage pour montage exact
Centering seats for accurate tilting
- Masseloliert
Isolement par rapport à la masse
Ground-Isolated
- Zubehör für optimale Krafteinleitung
Accessoires pour une transmission optimale des forces
Accessories for optimum force introduction



	Bereich / Gamme / Range Fz		Kalibrierter Teilbereich / Gamme partielle étalonnée / Calibrated partial range		Überlast / Surcharge / Overload		Steifigkeit / Rigidity / Rigidité (N / μm)		Eigenfrequenz / fréquence propre / Natural frequency		Kapazität / Capacité / Capacitance		Drehmoment / couple / torque (max., F _{x,y} , F _z = 0)		Biegemoment / couple de flexion / bending moment (max., F _z = 0)		Schubkraft / force de cisaillement / shear force (max., F _z = 0)		Gewicht / Poids / Weight	
Type	kN	N	kN	N/μm	kHz	pF	Nm	Nm	kN	g	D'	D1	H	A	B	hex	M			
9301B	± 2,5	25	± 2,75	≈ 300	≈90	≈ 8	2	5	0,35	14	11	8,5	25	2	5	9	M5			
9311B	± 5	50	± 5,5	≈ 600	≈70	≈ 23	3	15	0,75	28	15	12,5	30	3	5	13	M6			
9321B	± 10	100	± 11	≈ 900	≈55	≈ 37	14	60	1,5	90	23	18	45	5	10	19	M10			
9331B	± 20	200	± 22	≈1000	≈45	≈ 55	30	120	3	170	29	23	52	5	11	24	M12			
9341B	± 30	300	± 33	≈1800	≈40	≈ 65	50	240	4,5	330	35	31	62	6	14	32	M16			
9351B	± 40	400	± 44	≈2000	≈33	≈ 65	90	370	6	480	41	35	72	7	18	36	M20			
9361B	± 60	600	± 66	≈2800	≈28	≈150	190	830	9	1020	53	45	88	9	22	46	M24			
9371B	±120	1200	±132	≈4000	≈22	≈200	430	2500	18	2500	76	64	108	10	28	65	M30			



Dimensionen / Dimensions / Dimensions / mm						
D	D1	H	A	B	hex	M
11	8,5	25	2	5	9	M5
15	12,5	30	3	5	13	M6
23	18	45	5	10	19	M10
29	23	52	5	11	24	M12
35	31	62	6	14	32	M16
41	35	72	7	18	36	M20
53	45	88	9	22	46	M24
76	64	108	10	28	65	M30

Technische Daten

Données techniques

Technical Data*

Empfindlichkeit	Sensibilité	Sensitivity	pC/N	≈ -4
Ansprechschwelle	Seuil de réponse	Threshold	N	≈0,02
Linearität	Linéarité	Linearity	% FSO	≈±0,5
Hysterese	Hystérésis	Hysteresis	% FSO	≈0,5
Isolationswiderstand	Résistance d'isolement	Isolation resistance	TΩ	≈50
Masselolation	Isolement par rapport à la masse	Ground-isolation	MΩ	≈100
Temperatur-Koeffizient	Coefficient de température	Temperature coefficient	%/°C	-0,02
Betriebstemperatur-Bereich	Gamme de température de service	Operating temperature range	°C	-40 ... 120

* In all Kistler documents, the decimal sign is a comma on the line (ISO 31-0:1992)

Beschreibung

Der Kraftsensor ist unter Vorspannung zwischen zwei Müttern eingebaut und kann daher sowohl Druck- wie auch Zugkräfte messen. Das Quarzelement gibt eine der wirkenden Kraft proportionale elektrische Ladung ab. Diese wird durch eine Elektrode abgenommen und über den Steckeranschluss nach aussen geführt. Das Ladungssignal wird weiter über ein abgeschirmtes Kabel zu einem Ladungsverstärker geführt, welcher dieses in eine proportionale Ausgangsspannung umwandelt. Durch eine entsprechende Auswertelektronik kann der Messwert erfasst und weiterverarbeitet werden.

Der Sensor ist masseisoliert eingebaut. Damit werden Erdschleifenprobleme weitgehend ausgeschaltet.

Anwendung

Das Kraftmesselement eignet sich, dank seiner grossen Steifigkeit, speziell für das Messen von rasch ändernden Zug- und Druckkräften. Das elastische Verhalten des Messobjektes wird dabei praktisch nicht verändert. Quasistatische Messungen sind ebenfalls möglich. **Das Kraftmesselement wird kalibriert geliefert.** Nach einem korrekten Einbau ist es ohne Nachkalibrierung sofort einsatzbereit.

Einsatzbeispiele

Automobilindustrie

- Sicherheitstechnik, Überwachung von Aufprallkräften
- Kraftstösse in Fahrwerken
- Kräfte an Auswuchtmaschinen

Materialprüfung

- Schlagprüfung, Wechselfestigkeit

Werkzeugmaschinen

- Überwachung an Pressen, Stanz-, Präge- und Schweissmaschinen
- Kraftmessungen an Längsführungen

Allgemein Maschinenindustrie

- Überwachung von Abstützkräften (Kraftschwingungen) an Maschinen, welche auf Dämpfungselementen gelagert sind
- Einspannvorgänge, z.B. Kraftsensor kombiniert mit Hydraulikzylinder
- Fügetechnik (Einschleiben, Einpressen von Montageteilen)

Qualitätskontrolle

- Kraftmessungen an Schaltern
- Überwachung von Montageautomaten

Montage

Die Kontaktflächen, welche die Kraft auf das Messelement übertragen, müssen plan, steif und sauber sein. Die Befestigungsschrauben dürfen nicht in den Sackgewinden des Kraftmesselementes aufsteigen. Es ist ein Spiel S (siehe Fig. A, Seite 3) von mindestens 0,5 mm einzuhalten. Die Schrauben sind genügend stark anzuziehen, sodass auch bei der grössten Zugkraft kein Spalt zwischen Kontaktflächen auftritt.

Das Kraftmesselement hat beidseitig Zentriersitze, die den genauen Einbau erleichtern.

Description

Le capteur de force est monté sous précontrainte entre deux écrous et peut donc mesurer des forces de compressions et de traction. L'élément à quartz engendre une charge électrique proportionnelle à la force. Cette charge électrique est captée par une électrode puis acheminée vers l'extérieur par le biais d'un connecteur. Par l'intermédiaire d'un câble blindé, le signal de charge est ensuite acheminé à un amplificateur de charge qui le transforme en une tension de sortie qui lui est proportionnelle. Un système électronique permet alors de saisir et de traiter la valeur mesurée.

Le capteur est moulé avec isolement par rapport à la masse, ce qui permet d'éviter en grande partie les problèmes de circuits de retour par la terre.

Utilisation

Grâce à sa grande rigidité, l'élément de mesure convient parfaitement à mesures de forces de traction et de compression dynamiques. Le comportement élastique de l'objet à mesurer ne se trouve pas modifié de manière notable. Des mesures quasi-statiques sont possibles aussi. **L'élément de mesure est livré étalonné.** Monté correctement, il peut être mis en œuvre immédiatement sans réétalonnage.

Exemples d'utilisation

Industrie automobile

- Technique de sécurité, surveillance des forces de collision
- Etude des impulsions sur les châssis
- Mesure des forces s'exerçant sur les machines à équilibrer les roues

Essais de matériaux

- Essais aux chocs, résistance aux efforts alternés

Machines-outils

- Surveillance des presses, machines à découper, presse à estamper et machines à souder
- Mesures des forces sur les glissières longitudinales

Construction mécanique générale

- Surveillance des forces d'appui (vibrations) s'exerçant sur des machines montées sur des éléments stabilisateurs
- Processus de fixation, p. ex. capteur de force associé à un cylindre hydraulique
- Technique d'assemblage (insertion, encastrement d'éléments de montage)

Contrôles de qualité

- Mesure de forces sur les commutateurs
- Surveillance des robots de montage

Montage

Les surfaces de contact qui transmettent la force aux éléments de mesure doivent être planes, rigides et propres. Les vis de fixation ne doivent pas toucher le fond des alésages filetés de l'élément de mesure. Un jeu S (voir fig. A, page 3) de 0,5 mm au minimum est à respecter. Les vis doivent être serrées suffisamment pour éviter qu'une fente s'ouvrirait entre les surfaces de contact sous la force de tension la plus grande.

L'élément de mesure a des rebords de centrage des deux côtés qui facilitent le montage exact.

Description

The force sensor is mounted under preload between two nuts and, therefore can measure compression and tensile forces. The quartz element yields an electric charge which is proportional to the force. This is picked off by an electrode and transferred via a connector. The charge signal is fed via a screened cable to a charge amplifier, which converts it into a proportional output voltage. An appropriate evaluation circuit can record and further process the measurand.

The sensor is moulded ground-isolated. This largely eliminates ground loop problems.

Application

As a result of its great rigidity, the force link is particularly suitable for measuring rapidly changing tensile and compression forces. The elastic behaviour of the test object is practically not influenced. Quasistatic measurements, are possible, too. **The force link is supplied calibrated.** After correct installation, it is immediately ready for use without recalibration.

Exemples of use

Automobile industry

- Safety technology, monitoring of collision forces
- Mechanical shocks in chassis
- Forces on balancing machines

Material testing

- Impact testing, alternate strength testing

Machine tools

- Monitoring on presses, punching, embossing and welding machines

- Force measurements on longitudinal guideways

General machine building

- Monitoring of supporting forces (force oscillations) on machinery mounted on damping elements
- Clamping processes, e.g. force sensor combined with hydraulic cylinder
- Joining technique (insertion, press fit of components)

Quality control

- Force measurements on switches
- Monitoring of automatic assembly machines

Mounting

The contact faces which transmit the force to the force link must be flat, rigid and clean. The fixing bolts must not touch the bottom of the threaded holes of the force link. A play S (see fig. A, page 3) of at least 0,5 mm must be assured. The bolt must be tightened sufficiently as to avoid that a gap could open between the contact faces under the highest tensile force.

The force link has centering shoulders on both ends which precise mounting easier.

Krafteinleitung

Nach Möglichkeit soll diese konzentrisch zur Achse erfolgen. Exzentrische Krafteinleitung, Biegemomente, Drehmomente sowie Schubkräfte sind nur bis zu einem gewissen Mass zulässig.

Kraftmesselement mit SCS Kalibrierschein

Kistler ist die akkreditierte Kalibrierstelle Nr. 049 des SCS (Swiss Calibration Service) für Kraft. Deshalb können Kraftmesselemente gegen Aufpreis auch mit einem SCS-Kalibrierschein geliefert werden. Sie können dann z. B. als Bezugsnormal im betriebsinternen Kalibrierdienst verwendet werden.

Kalibriert wird dann nur der Druckkraftbereich (100 %FS, 10 %FS und 1 %FS). Wir empfehlen, die Druckkappe und den Flansch (siehe Seite 4) zu verwenden, um reproduzierbare Messungen zu gewährleisten.

Transmission des forces

Dans la mesure du possible, la transmission des forces doit s'effectuer le long de l'axe. L'application excentrique de forces, l'application de moments de flexion, de couples de rotation et d'efforts de cisaillement ne sont admissibles que dans certaines limites.

Elément de mesure de force avec certificat d'étalonnage SCS

Kistler est le laboratoire d'étalonnage no. 049 accrédité par SCS (Swiss Calibration Service) pour la force. Les éléments de mesure peuvent alors être livrés (contre un supplément) avec un certificat d'étalonnage SCS. Ils serviront p. ex. comme étalons de référence dans le service d'étalonnage interne.

Alors seulement la gamme de force en compression (100 %FS, 10 %FS et 1 %FS) sera étalonnée. Nous recommandons d'utiliser la calotte et la bride (voir page 4) pour assurer une bonne reproductibilité des mesures.

Force introduction

As far as possible, this should be concentric to the axis. Eccentric force introduction, bending moments, torques and shear forces are permitted only to a certain extent.

Force link with SCS Calibration Certificate

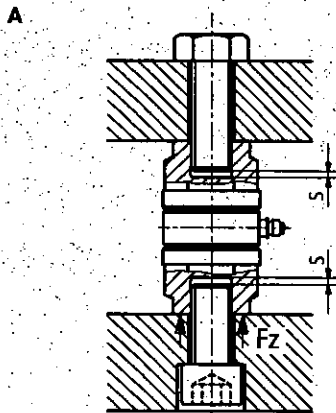
Kistler is the calibration laboratory no. 049 accredited by the SCS (Swiss Calibration Service) for force. Therefore, the force links can be supplied (at an extra charge) with an SCS Calibration Certificate. They can then be used e. g. as reference standards in an internal calibration service.

Only the range for compression force will be calibrated (100 %FS, 10 %FS and 1 %FS). We recommend to use the force distribution cap and the flange (see page 4) to assure a good reproducibility of the measurements.

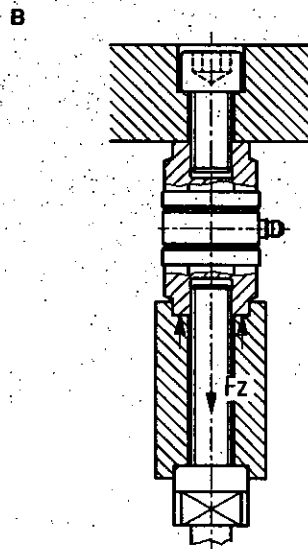
Einbaubeispiele, verschiedene Arten der Krafteinleitung

Exemples de montage - Différents types de transmission des forces

Mounting examples, different types of force introduction



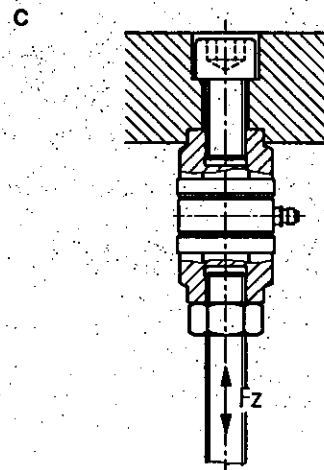
Krafteinleitung von Druckkräften
Transmission des forces de pression
Force introduction of compression forces



Belastung durch Zug- und Druckkräfte über ein Verlängerungsstück. Die Vorspannkraft auf die Hülse darf beim Wirken von Zugkräften einen Minimalwert nicht unterschreiten.

Application de forces de traction et de compression par l'intermédiaire d'une rallonge. La force de précontrainte s'exerçant sur le manchon ne doit pas être inférieure à la valeur minimale en cas d'application de forces de traction.

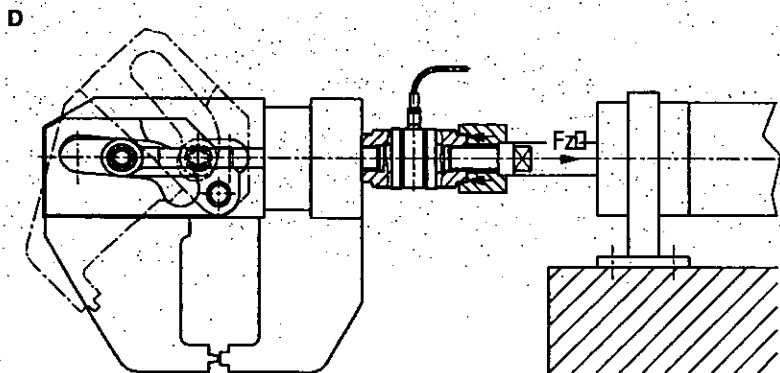
Loading from tensile and compression forces via an extension piece. The preloading force on the sleeve must not be less than a minimum value under the effect of tensile forces.



Krafteinleitung von Zug- und Druckkräften, direkt auf den Gewindeanschluss. In diesem Fall sollte stets eine Gegenmutter verwendet werden.

Transmission des forces de traction et de compression directement sur le raccord fileté. Dans ce cas, un contre-écrou sera systématiquement utilisé.

Force introduction of tensile and compression forces directly onto the threaded connection. In this case, a lock nut should always be used.



Einbaubeispiel eines Kraftmesselementes in einer hydraulischen Spannvorrichtung. Überwachung von Zug- und Druckkräften.

Exemple de montage d'un élément de mesure dans un dispositif de fixation hydraulique. Surveillance des forces de traction et de compression.

Mounting example of a force link in a hydraulic clamping device. Monitoring of tensile and compression forces.

Zubehör

Anschlusskabel

Die verschiedenen Kabelarten passend zum Steckeranschluss 10-32 UNF neg. sind aus dem Kistler Datenblatt Nr. 15.011 ersichtlich.

Druckkappe und Flansch

Für eine optimale Krafteinleitung kann in Kombination zum Kraftmesselement eine Druckkappe und ein Flansch eingesetzt werden. Die Teile sind ebenfalls als Präzisionsteile gefertigt und weisen eine Oberflächenhärte von 400 ... 490 HV (Vickers) auf.

Accessoires

Câbles de connexion

Les différentes variantes de câbles s'adaptant au connecteur 10-32 UNF nég. sont décrites dans la notice technique No 15.011 Kistler.

Calotte distributrice de force et bride

Pour une transmission optimale des forces, il est possible d'utiliser un calotte distributrice de force et une bride en association avec un élément de mesure des forces. Il s'agit de pièces de précision qui présentent une dureté de surface de 400 ... 490 (dureté Vickers).

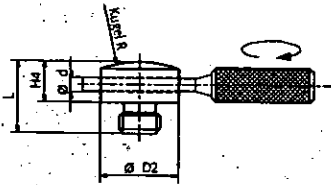
Accessories

Connecting cable

The different cable types suitable for connector Type 10-32 UNF neg. are listed in Kistler data sheet No. 15.011.

Force distributing cap and flange

A force distributing cap and a flange can be used in combination with the force link to provide optimum force introduction. These components are also manufactured as precision parts and have a surface hardness of 400 ... 490 HV (Vickers).

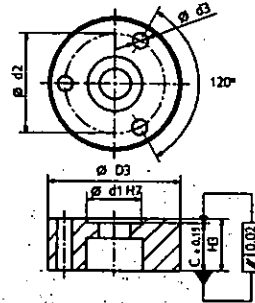


Druckkappe / Calotte distributrice de force / Force distributing cap (Typ 9500A...)

Mit einem zylindrischen Werkzeug kann die Druckkappe eingeschraubt werden.

Le calotte distributrice de force peut être vissé à l'aide d'un outil cylindrique.

The force distributing cap can be screwed in with a cylindrical tool.



Flansch / Bride / Flange (Typ 9501A...)

Eine Zylinderschraube mit Innensechskant gehört zum Lieferumfang des Flansches.

Une vis à tête cylindrique à six pans creux est livrée avec la bride.

A socket head cap screw is supplied with the flange.

Fig. 1

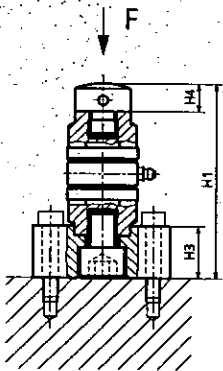


Fig. 1

Kraftmesselement mit Flansch und Druckkappe. Einsatz für Druckkraftbelastungen.

Élément de mesure de forces avec bride et calotte distributrice de force. Utilisation pour les forces de pression.

Force link with flange and pressure distributing cap. Insert for compression force loading.

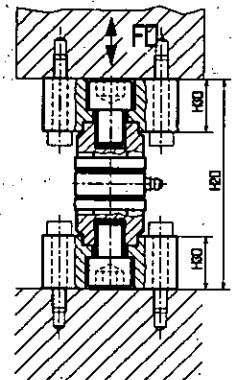
Fig. 2

Kraftmesselement mit beidseitig montierten Flanschen. Einsatz für Zug- und Druckkraftbelastungen.

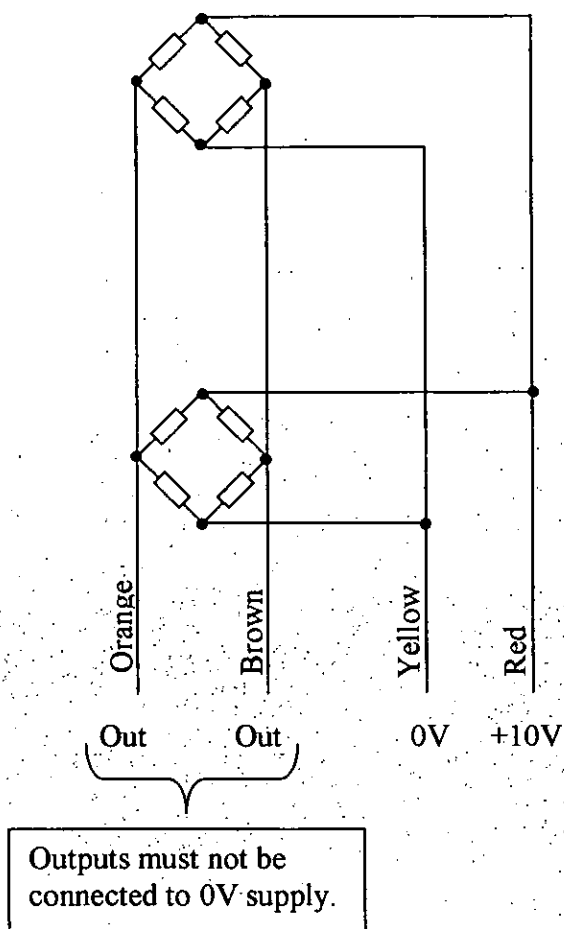
Élément de mesure de forces à brides des deux côtés. Utilisation pour les forces de traction et de pression.

Force link with flanges fitted on both sides. Insert for compression force loading.

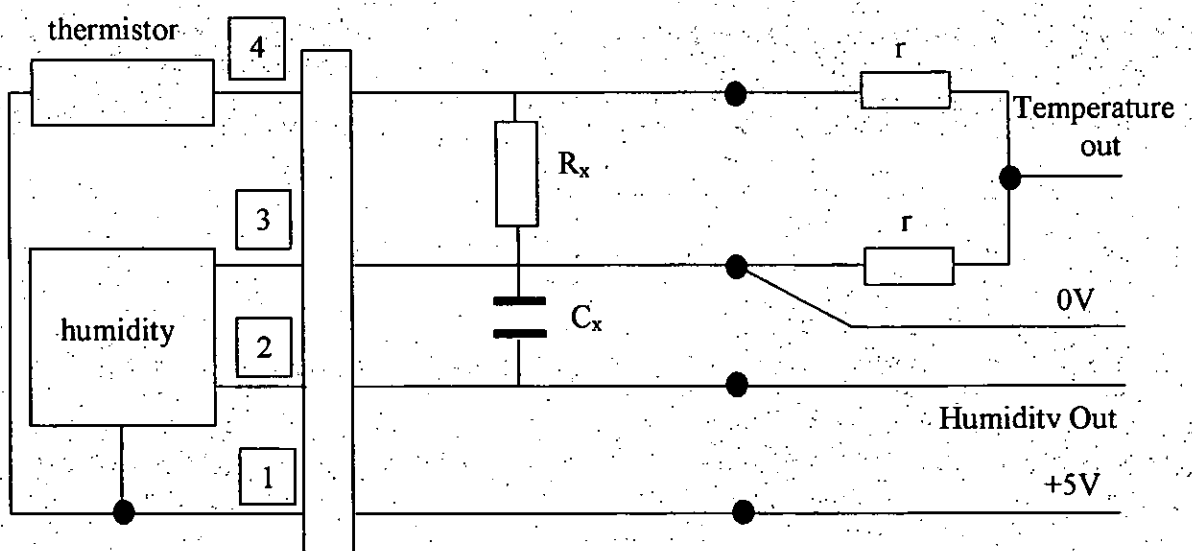
Fig. 2



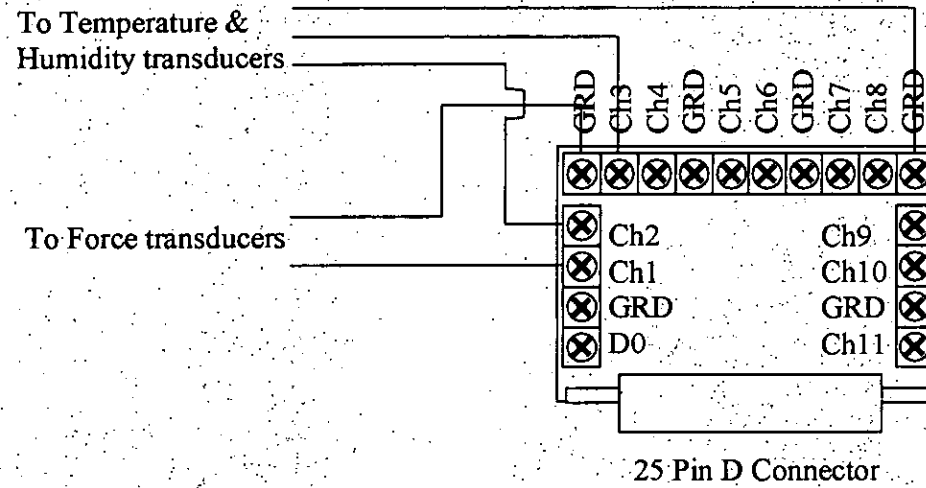
Kraftmesselemente Eléments de mesure de force Quartz force links	Druckkappe Calotte distributrice de force Force distributing cap						Flansch / Bride / Flange							Fig. 1	Fig. 2
Type	Type	D2	L	H4	R	d	Type	D3	H3	d1	d2	d3	C	H1	H2
9301B	9500A0	8,5	8	4	R10	2,2	9501A0	25	9	8,5	18	3,2	8	37	41
9311B	9500A1	12,5	10	6	R15	3,2	9501A1	34	11	12,5	24	4,3	9	45	48
9321B	9500A2	18	17	9	R25	4,3	9501A2	44	18	18	33	5,3	18	70	77
9331B	9500A3	23	21	12	R35	4,3	9501A3	56	22	23	42	6,4	20	84	92
9341B	9500A4	31	28	15	R45	6,4	9501A4	70	29	31	52	8,4	27	104	116
9351B	9500A5	35	33	18	R50	6,4	9501A5	84	37	35	62	10,5	35	125	142
9361B	9500A6	45	41	22	R65	8,4	9501A6	102	44	45	77	13	42	152	172
9371B	9500A7	64	57	32	R90	8,4	9501A7	138	53	64	106	17	51	191	210



Temperature & Humidity transducer schematic.



For R_x and C_x refer to data sheet. The two resistors in the temperature output (voltage divider) is to ensure maximum output does not exceed 2.5V due to limitation imposed by data acquisition system. (max input 2.5V)



ADC11 Connection block showing instrumentation connections.

APPENDIX A5

EVOLUTION OF THE FRICTIONAL CHARACTERISTICS OF COMMERCIALY AVAILABLE BONDED SOLID LUBRICANTS.

Presented at Nordtrib 98.

THE INFLUENCE OF COUNTER-FACE SURFACE FINISH ON THE PERFORMANCE OF BONDED SOLID LUBRICANT FILMS.

Presented at the Second World Tribology Congress. Vienna, September 2001.

EVOLUTION OF THE FRICTIONAL CHARACTERISTICS OF COMMERCIALY AVAILABLE BONDED SOLID LUBRICANTS.

D. Burke¹, and I. Sherrington²

¹ Breed UK Ltd., Carlisle, UK.

² University of Central Lancashire, UK.

Key words: Bonded Solid Lubricants, Static Friction, Dynamic Friction, Lubricant Performance.

Abstract.

This paper examines the performance of a group of commercially available bonded solid lubricants, which contain: Molybdenum Disulphide, Graphite and Polytetrafluoroethylene (PTFE). The products investigated contain these materials as individual lubricants and as mixtures. The paper begins with a brief review of published work which discusses the characteristics of solid lubricants; but its main purpose is to present measurements of dynamic friction coefficients made over the simulated service life of components lubricated by commercial versions of these lubricants. This parameter is acquired by use of a simple reciprocating rig, running in ambient atmosphere and at ambient temperature. Humidity and component surface temperature are recorded, but not controlled. The surface topography and surface preparation of the specimens is the result of a commercial process and no further standardisation is exerted over this aspect of the experiment. The paper discusses the differences in the friction coefficient resulting from the use of each type of coating and examines the effect of increasing the normal load for a smaller group of them. The experimental data is briefly compared with the product manufacturers data. The paper ends by presenting some general conclusions and suggestions for further work.

1. INTRODUCTION.

Solid lubricants are used extensively in industry to provide lubrication for sliding surfaces in contact with each other where oil or grease is not desirable or does not function due to the environmental conditions. For example, in space vehicles where grease would evaporate or nuclear reactors where oil would be decomposed by radiation. They are also used where access for maintenance is not possible or desirable, i.e., in "sealed for life" components. The most commonly available materials in use today are: Molybdenum Disulphide (MoS_2), Graphite, and Polytetrafluoroethylene (PTFE). These materials, normally available in fine powder form, are commonly applied to components by one of several processes. These being: (a) mixing with conventional lubricants such as oil or grease, (b) burnishing the powder into one or both sliding surfaces, (c) mixing with a binding agent and volatile solvent to form a "paint" like liquid which can be applied by brushing, spraying or dipping the components followed by curing to form a solid film, (d) by physical vapour deposition, e.g., sputtering.

(This process forms a very uniform film normally less than $1\mu\text{m}$ thick and is therefore useful for components with a very fine tolerance.)

The laminar structure of graphite and MoS_2 and the contribution of this structure to lubricity is well documented in the literature ^{1,2}. These materials are similar in structure, both have hexagonal layer lattice structures with weak van der Waals bonding between the basal planes. However they have been demonstrated to have totally different frictional properties. Graphite can provide good lubrication in normal atmospheres where water and other condensable vapours are present ^{3,4}, but such conditions can have a detrimental effect on the properties of MoS_2 ⁵. Conversely graphite is a very poor lubricant in vacuum conditions ⁶ while MoS_2 improves as atmospheric pressure decreases ⁷.

The structure of PTFE is also well documented ⁸. It consists of a helical chain of carbon atoms in a zigzag pattern with two fluorine atoms having covalent bonds to each carbon atom. As a consequence of the strong repulsion between the fluorine atoms of each molecule and the lack of polar side groups these molecules can slide easily over each other. Additionally, the compactness of the fluorine atoms renders the material almost completely inert. In general PTFE is accepted to have one of the lowest coefficients of friction of all the solid lubricants in normal atmosphere. A friction coefficient of around 0.04 is often quoted for PTFE sliding against steel in air, and values as low as 0.016 reported for very high loads and low sliding speeds ⁹.

2. MATERIALS AND METHODS.

Today there are many suppliers of bonded solid lubricants, each having a fairly extensive product range utilising either one or more of the above materials, on their own or in combination, bonded using one of several binding agents. To obtain a comparison in performance between some of these commercially available materials twelve were selected for test on a simple reciprocating rig. They are listed in Table 1. These materials were chosen because they had already been tested in a commercial product and had demonstrated variations in performance with extensive data being recorded for each. The components for the tests were produced by a commercial process consisting of: cleaning by a vapour degreasing process followed by a grain refining wash to help produce a fine uniform phosphate layer, then deposition of manganese iron phosphate by immersion in a phosphating bath for a set period of time to provide a "key" for the final coating of bonded lubricant, which was applied by spraying. The component was then heated to remove the bulk of the solvent and the coating cured at elevated temperature. The sample counterfaces were selected from production batches of an actual product and due to the method being a standard process no further constraints were exercised. The base material of the component is CS40 steel which is heat treated to 35-45HRC then "barrelled" with an abrasive media to remove any burrs and oxide layer. The material specification for both counterfaces is given in Table 2. The material sliding against the bonded lubricant was again obtained from a commercial product, test pieces being cut from a specific area of the product to provide suitably sized specimens. The donor product was produced from CS60 steel heat treated to 45-48HRC followed by barrelling then electroplating; first with copper then by nickel and then chromium to provide a decorative finish. The thickness of the plated layers is given in Table 3.

A reciprocating rig was employed in specimen testing as its operational action matched that of the product. It consisted of a simple beam carrying a strain gauge bridge for measuring friction force. The lower specimen reciprocated and the counterface was mounted

Table 1.
Coating Material.

Sample	Material	Binder	μ *	Sample	Material	Binder	μ *
1 (I)	MoS ₂ + Graphite+ ZnPh.	Polyamide- imide.	-	7 (VII)	Graphite 21.6 μ m	Epoxy	-
2 (II)	Graphite+ MoS ₂ + ZnPh.	"	-	8 (VIII)	PTFE+ Graphite 16 μ m	Polyamide- imide	-
3 (III)	PTFE	"	-	9 (IX)	PTFE+ Graphite 20 μ m	"	-
4 (IV)	PTFE	"	0.06	10 (X)	MoS ₂	Epoxy / Phenolic	-
5 (V)	PTFE	Epoxy	0.06	11 (XI)	MoS ₂ + Graphite	Epoxy	0.03 to 0.08
6 (VI)	Graphite 12 μ m	"	0.06	12 (XII)	MoS ₂ + Graphite	"	0.03 to 0.08

* μ given by manufacturers

Table 2.
Sample Materials. (% of element content in steel.)

	C	Mn	Si	Cr	Ph	S
CS 40	0.4 - 0.45	0.7 - 0.9	0.15 - 0.35	-	0.02 max	0.01 max
CS 60	0.6 - 0.65	0.7 - 0.9	0.15 - 0.35	0.20 - 0.30	0.015 max	0.01 max

Table 3.
Electroplating thickness.

Material	Copper	Nickel	Chromium
Thickness μ m.	0.5 minimum	8.0 minimum	0.13 minimum

in a "loading beam". Both specimens were electrically insulated to permit measurements of contact resistance. Specimen temperature, ambient temperature and ambient humidity were also measured. The specimen configuration is illustrated in fig. 1. Tests were conducted with 10N & 100N normal loads at a cycling speed of 48 cycles per minute for a duration of 50,000 cycles. Measurements were taken of: friction force, electrical resistance, ambient temperature, ambient humidity and specimen bulk temperature, every 10th cycle for the first 200 cycles, then every 200th cycle. Before each test the applied load was checked with a calibrated digital force meter at a location in line with the geometric centre of the specimen and found to be:

9.8N for the nominal 10N test and 99.85N for the nominal 100N test. (For ease and simplicity nominal load values were used to estimate the friction coefficients quoted in the paper.)

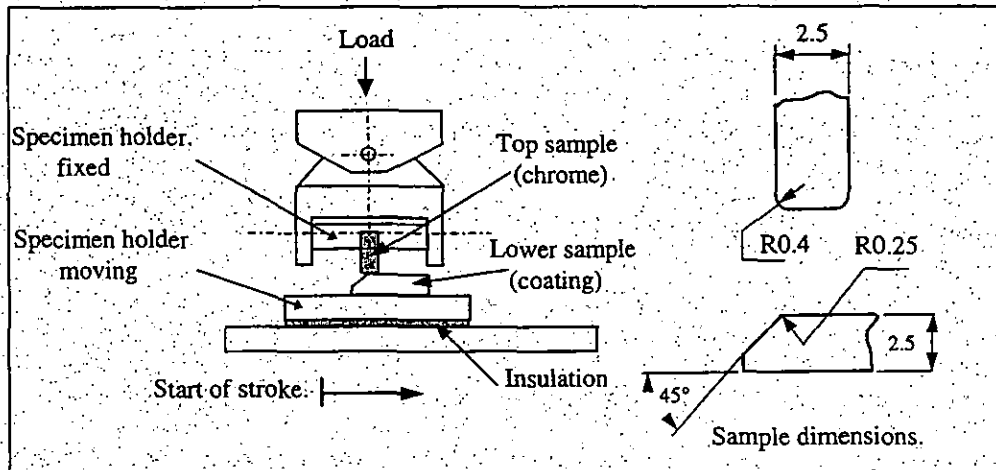


Fig 1. Schematic of reciprocating rig and test samples.

3. RESULTS.

A summary of the friction force measurements obtained using the 10N nominal test load are illustrated in figs. 2 and 3. They record the maximum dynamic friction force in the stroke as a function of the number of cycles. (Note, the location of the friction measurement is not necessarily at a fixed point in the stroke.) Figs. 4 and 5 illustrate average electrical resistance between the counterface as a function of the number of cycles. This measurement is made over a variable length of stroke towards the zero velocity end where the stress at the contact is lower: (i.e., in a zone where the contact zones of the specimens largely overlap.) Similar data is plotted for the 100N nominal load tests in figs. 6 and 7. (Note that all output data is filtered the friction data is processed by a low pass Butterworth filter with a cut off of 30 Hz and the electrical resistance data is obtained by averaging resistance readings from areas where the film appears to be worn but not completely removed.) Fig 8 contains the typical ambient temperature, specimen temperature and atmospheric humidity curves, vs. number of cycles, for the series of tests. No significant temperature rise was observed in the specimens during each of the tests. Due to the nature of the test apparatus, it was not possible to determine the static friction force reliably as the stiffness/damping of the load beam was insufficient to prevent uncontrolled oscillation of the specimen.

4. DISCUSSION.

All the specimens were examined under a microscope and a digitised record produced of the surfaces before and after cycling. Appendix 1 shows images of (a) the worn coatings, (b) the unworn coatings, (c) the worn counterfaces. These images show that before cycling the coatings have asperities of differing size and texture, some appear "granular" while others

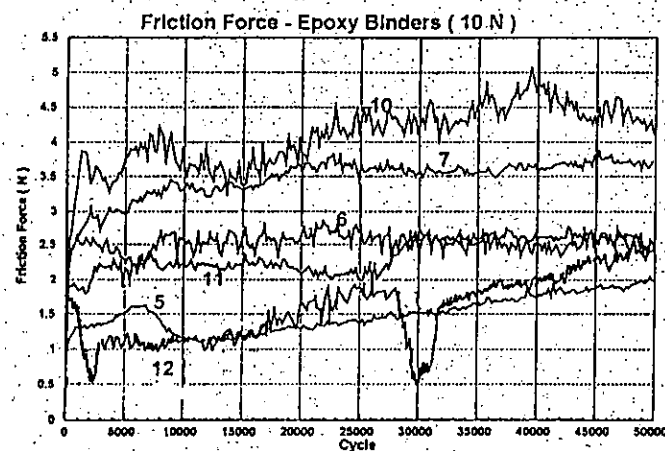


Fig. 2.

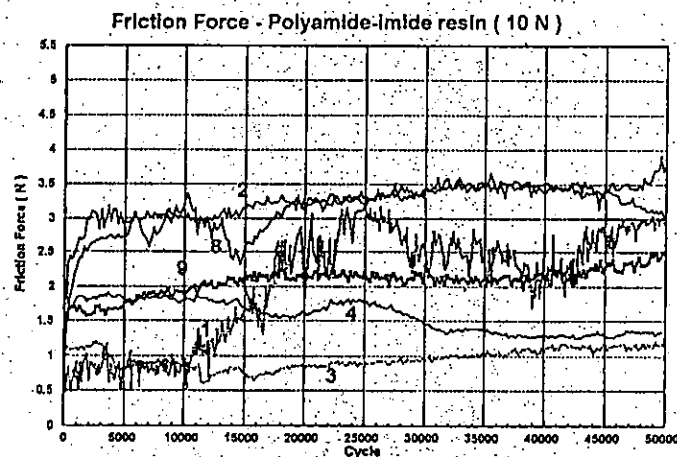


Fig. 3.

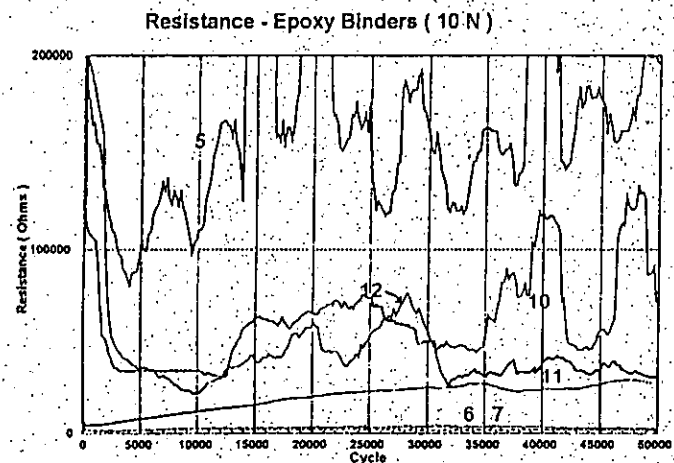


Fig. 4.

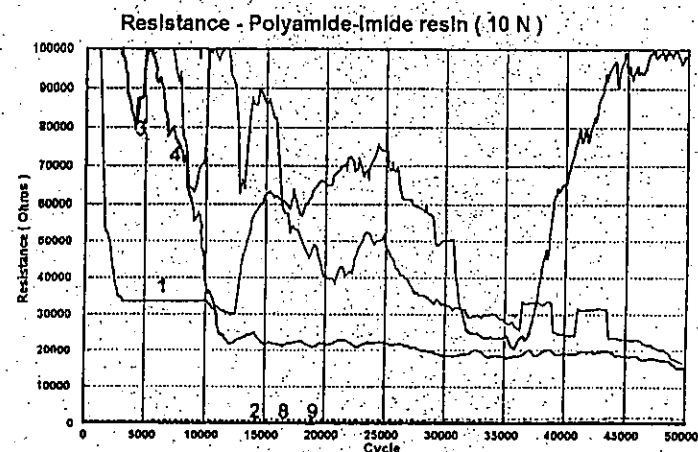


Fig. 5.

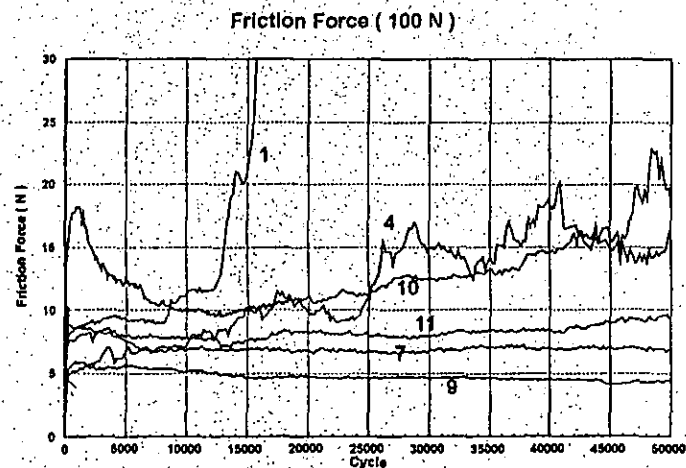


Fig. 6.

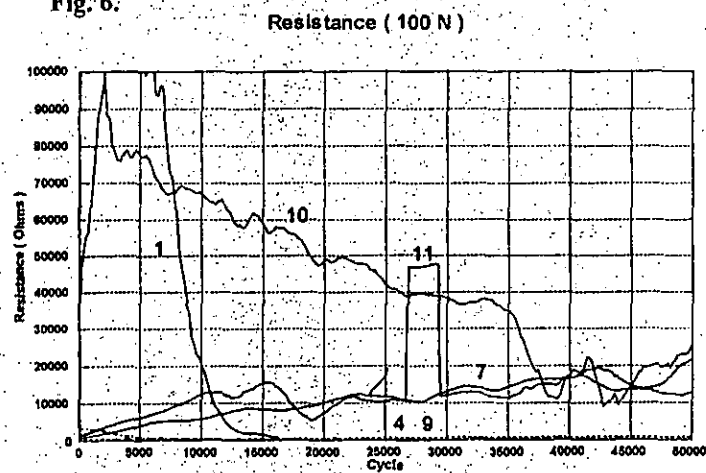


Fig. 7.

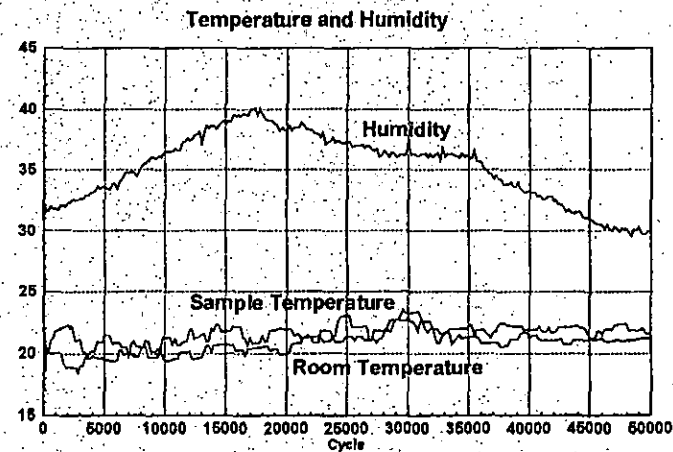


Fig. 8.

Sample	Material
1	MoS ₂ +Graphite+ZnPh
2	Graphite+ MoS ₂ +ZnPh
3	PTFE
4	PTFE
5	PTFE
6	Graphite 12μm
7	Graphite 21.6μm
8	PTFE+Graphite 16μm
9	PTFE+Graphite 20μm
10	MoS ₂
11	MoS ₂ +Graphite
12	MoS ₂ +Graphite

appear to have "flowed" and have a "splattered" appearance. Also apparent are defects such as small cracks, probably due to the curing process. After cycling the topography of the counterface is such that it contains unidirectional scratches. Some scratching appears to be more aggressive on certain samples and some samples appear to contain craters in which wear particles accumulate. The chrome plated specimen is displayed as the right hand most illustration with the leading edge to the right. In all cases they appeared to acquire a "transfer film" which rubbed off easily on samples 3 and 4 and on samples 8 and 9 appeared to be mechanically or chemically attached.

In the 10N load tests samples 3 & 4 (PTFE/Polyamide-imide binder) exhibited the lowest coefficient of friction over the test duration. Sample 5 (PTFE/Epoxy binder) was in the same range with the epoxy binder apparently having little effect on performance. Samples 8 & 9 (Graphite/PTFE polyamide-imide binder) start with a coefficient of 0.06. These increase to 0.24 and 0.17 over the first 500 cycles then, for sample 8, to 0.3 over the next 2000 cycles with sample 9 showing a gradual increase to 0.22 over some 20,000 cycles. It should be noted that samples 8 and 9 are the same material the only difference being the initial coating thickness, of which the thicker sample exhibits the lower friction coefficient and more stable performance. Samples 1, 2, & 11 start at $\mu = 0.05 - 0.08$ and rise to their limiting friction coefficient. Samples 2 and 11 over 200 cycles and sample 1 over 12000 cycles. Sample 12 "beds in" over 2000 - 3000 cycles then ramps up to its limiting friction coefficient. This test was stopped for a period of one hour at about 25,000 cycles and on restart appeared to repeat this phenomena. This could be due to water vapour from the atmosphere having an effect while the components were at rest¹⁰. Sample 10 was the only sample of MoS₂ on its own and there is nothing very similar to compare its performance directly with, but against samples 1, 2, 11 & 12 it has a higher friction coefficient after 2000 cycles and it is similar to sample 2. Samples 6 and 7 have similar trends but again like samples 8 and 9 the friction coefficient varies with initial film thickness, only this time the lower coefficient belonging to the thinner of the two.

Six of the materials were tested with a 100N normal load, sample 1 "bedding in" over 7000 cycles then rapidly ramping up to a friction coefficient over 0.3, at which point the test was stopped. Samples 7, 9, and 11 gave the best performance with friction coefficient ranging from 0.05 to 0.08 with little deterioration over the cycling period. Samples 4 and 10 started with a friction coefficients of 0.08 and 0.05 and gradually deteriorated to 0.2 and 0.15

Electrical resistance curves for samples 2, 6, 7, 8, 9 and 11 showed very low resistance throughout the test and this is probably indicative of the high amount of graphite present. Sample 1 and 12 start high, but rapidly drop over 2500 cycles to a fairly stable level. Sample 10 is similar to 1 and 12, but its performance is more erratic towards the end of the cycling. Samples 3 and 5 showed high resistance at the start then fluctuated between high and low resistance possibly as small areas of the coating were broken through and repeatedly recovered. Sample 4 starts with a high resistance and then after 15000 cycles gradually reduces.

It can be seen that in the low load tests none of the friction coefficients measured matched those claimed by the manufacturers, although sample 3 was very close for a period with a coefficient of 0.075. In general, the authors believe that the friction coefficients differ from those quoted because the test conditions employed by manufacturers differ radically from those described here. (Only samples 11 and 12 have clearly defined test conditions published by the manufacturer² to the authors knowledge.) In the high load tests samples 7 and 9 had friction coefficients fairly close to those quoted by the manufacturer.

5. CONCLUSIONS.

It should be noted that the data presented was obtained from only one test on each material. Consequently, it may not be fully representative of their performance. Measurements will be subject to statistical variation, the influence of changes in ambient humidity, vibration and other variables associated with sample preparation which are not detailed in the paper.

In general, friction coefficients measured in the experiments described here tended to be higher than those quoted by manufacturers, the authors presume this to arise as a consequence of differences in the test methods.

It has been reported that the friction coefficients for solid lubricants containing PTFE and MoS₂ reduce as load increases⁹. This result is observed in the tests completed here. Although, somewhat surprisingly, the same result is also observed for graphite. (Sample 7.)

The test for sample 12 (MoS₂ + graphite.) was suspended at about 28000 cycles to allow data transfer to take place. The behaviour of the friction coefficient following this pause was somewhat surprising, friction briefly reduced instead of following the monotonic increase which had developed up to that point in the test. Clearly this warrants further investigation.

The observations made during these experiments will be used to guide the selection of a solid lubricant for a commercial application. They will also inform the specification of a new, improved test machine which is planned for use in more detailed testing of a similar nature on a smaller group of materials.

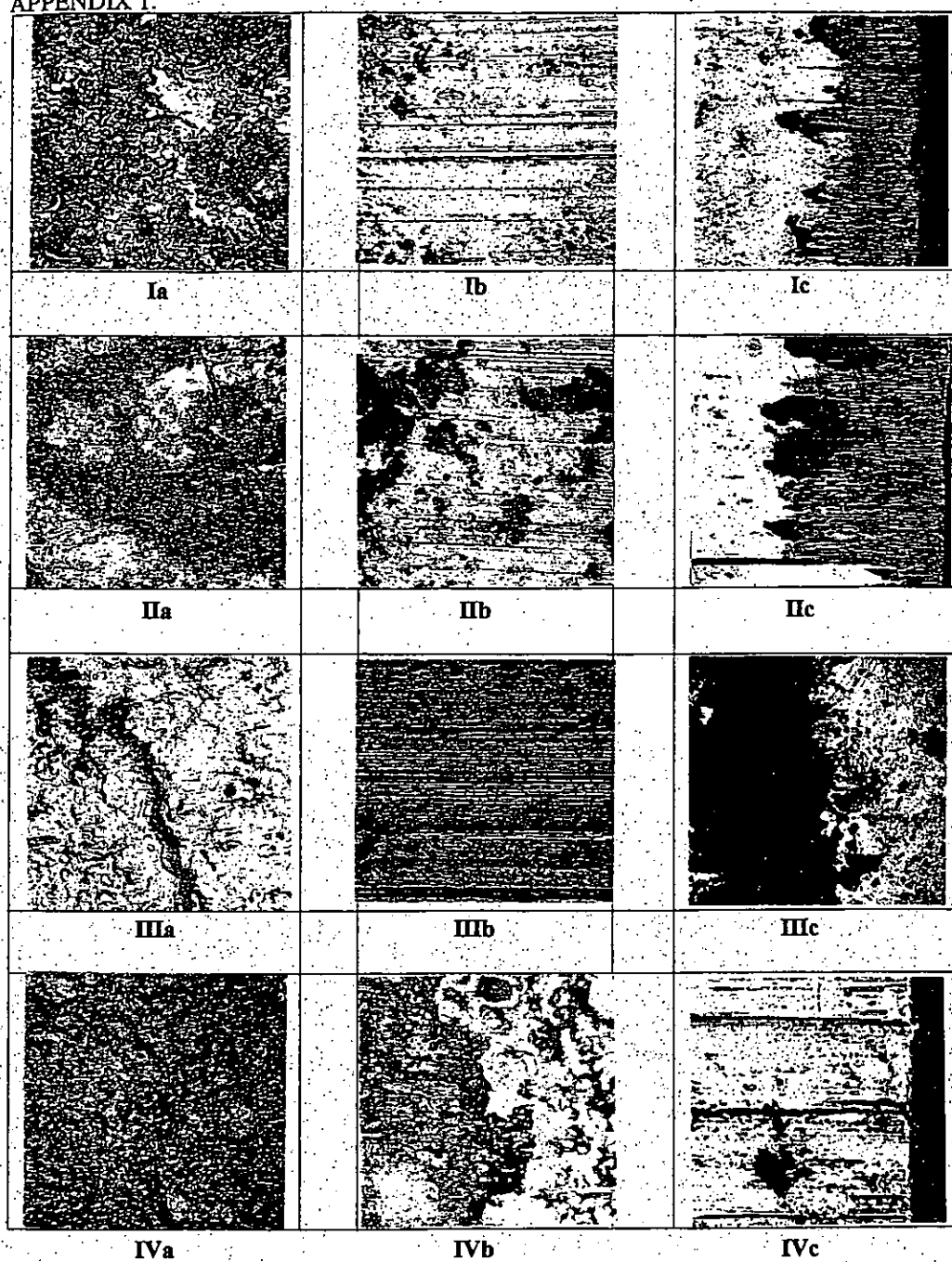
6. ACKNOWLEDGEMENTS.

The authors wish to express their indebtedness to all those who assisted and advised during the project and especially: Breed UK for their sponsorship and Paul Bowman for his assistance with the test programme and his expertise in data processing.

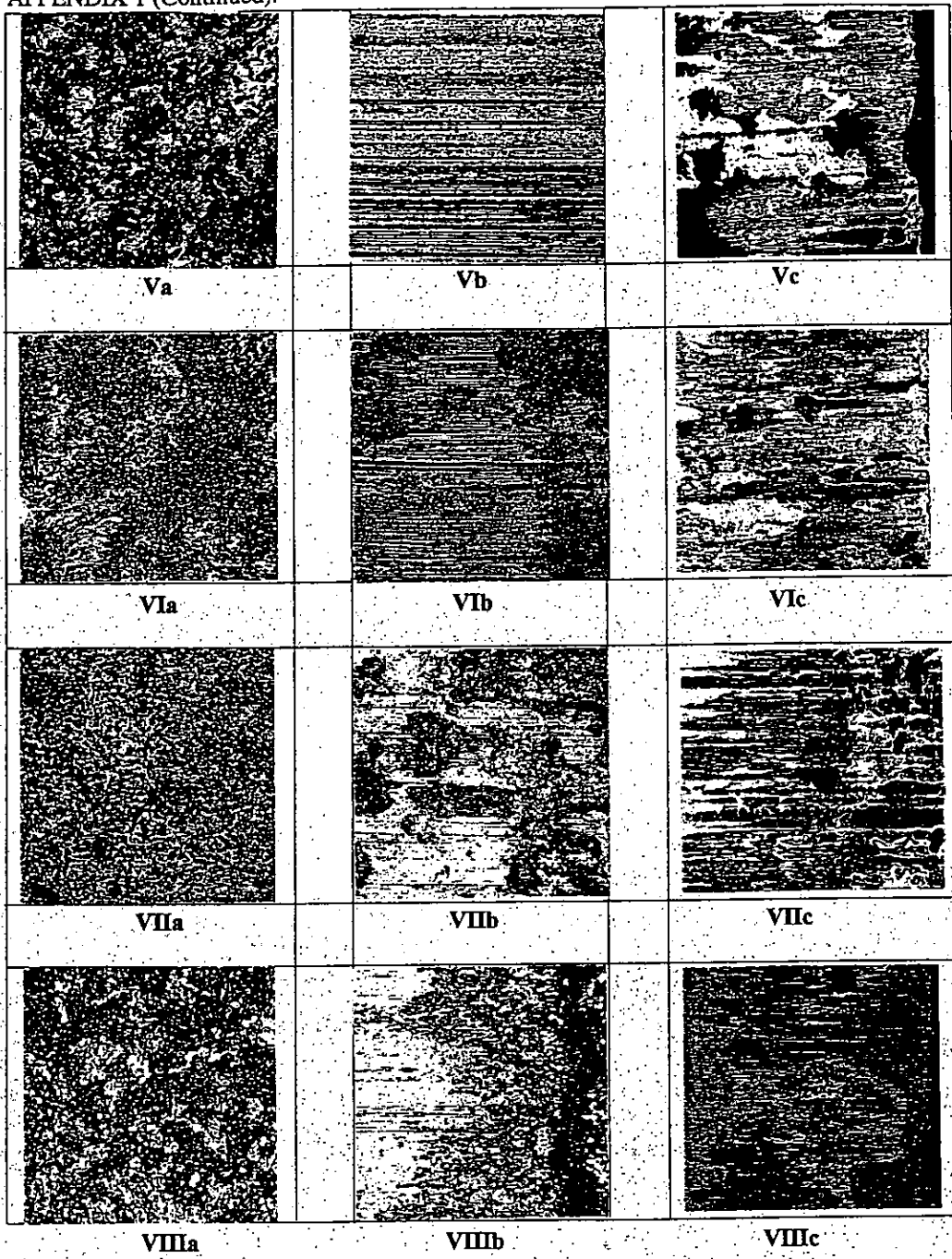
7. REFERENCES.

- [1] Wilson, B. (Ed.) Product review. - Solid Lubricants. *Industrial Lubrication and Tribology*. 47(6) (1995) pp-18.
- [2] Zechel, R., Lonsky, P., Trautmann, H., Ebenslander, H., Holinski, R., Lapple, W., Meixner, R. *Molykote*. Dow Corning, (1991).
- [3] Savage R. H. and Schaeffer D. L., Vapour lubrication of graphite sliding contacts. *J. Appl. Phys. D.* 27, pp136-138.
- [4] Lancaster J. K. and Pritchard J. R., The influence of environment and pressure on the transition to dusting wear of graphite. *J. Appl. Phys. D.* 14, (1981), pp 747-762.
- [5] Kay E., Tech report No 65219. Royal Aircraft Establishment. (Oct., 1965).
- [6] Roselman I. C. and Tabor D., The friction of carbon fibres. *J. Appl. Phys. D.* 2, (1976), pp. 2517-32.
- [7] Buckley D. H., *Surface effects in adhesion, friction, wear and lubrication*. Elsevier, (1981).
- [8] Banks R. E., *Fluorocarbons and their derivatives*. Oldbourne Press, London: (1964).
- [9] Clauss F. J., *Solid lubricants and self lubricating solids*. Academic Press. (1972).
- [10] Saloman G., De Gee A. W. J., Zaat J. H., Mechano-chemical factors in MoS₂ lubrication. *Wear* 7, (1964), pp. 87-101.


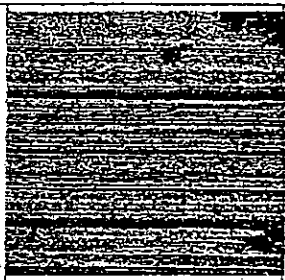

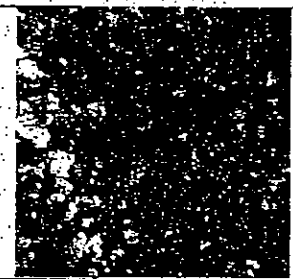
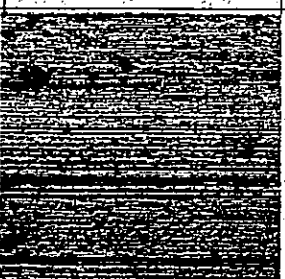



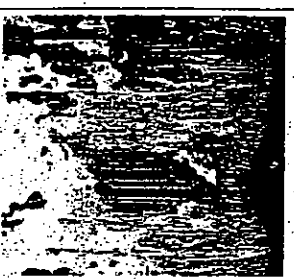
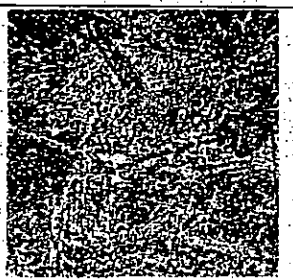


APPENDIX 1.



APPENDIX 1 (Continued).



APPENDIX 1 (Continued).

		
IXa	IXb	IXc
		
Xa	Xb	Xc
		
XIa	XIb	XIc
		
XIIa	XIIb	XIIc

THE INFLUENCE OF COUNTER-FACE SURFACE FINISH ON THE PERFORMANCE OF BONDED SOLID LUBRICANT FILMS.

D. BURKE

Technology Innovation Centre, University of Central England in Birmingham, Perry Barr, Birmingham B42 2SU, UK

I. SHERRINGTON

Department of Engineering and Product Design, University of Central Lancashire, Preston PR1 2HE, Lancashire, UK.

E. W. ROBERTS

AEA Technology, Birchwood Technology Park, Risley, Warrington, Cheshire, WA3 6AT

SUMMARY

The effect of the surface finish of a hardened AISI chrome steel ball sliding against a hardened 080M40 steel surface lubricated with a thin bonded solid lubricant BSL film is described in this paper. Four surface finishes were used for the balls. It was found that with high applied loads the life of the BSL film increased with an increase in roughness. With low applied loads it was found that the smoother finish produced a longer life (The as supplied, smooth finish continued for 500Km without failure.) It was also found that at high loads an increase in velocity lead to an increase in lubricated contact life. (Failure being deemed as the point where the friction coefficient becomes erratic and reaches a value of 0.3) The results of the investigation demonstrate three distinct phases of performance and an empirical equation is presented for the behaviour of the friction coefficient for the initial phase. This investigation is the initial stage of a much larger study and proposals are presented for the continuation of this work.

Keywords: Bonded solid lubricants, Surface Topography, Wear, Friction

1 INTRODUCTION.

Bonded solid lubricants (BSLs), sometimes known as anti-friction (AF) coatings, consist of a fine, powdered solid lubricant mixed with a resin matrix. Typically, up to 80% of the mixture may be lubricant with the remainder being the resin matrix, stabilisers, pigments and fillers. The resin matrix serves to bind the lubricant to the surface of the component that it lubricates and it is this element which largely separates BSLs from other classes of solid lubricants.

BSLs are very widely used to lubricate components in both domestic and industrial products. They are employed to give components a maintenance free service life, and reduce friction and wear. Components lubricated with BSLs are commonly quite small, normally only a few millimetres in scale and lightly loaded. However, BSLs can be used on much larger components. (E.g. the ten metre diameter ball joints used in the giant storm surge barrier near the Hook of Holland.) [1].

The function of a BSL is similar to that of a conventional liquid lubricant in that it forms a low shear film between the sliding surfaces to separate them reducing friction and wear. At the onset of movement the lubricant component of the BSL forms a transfer film on the sliding counterface, further sliding occurs between this transfer film and the bulk of the BSL, this mechanism

effectively prevents adhesive wear of the surfaces of the principle components [2].

The development of the transfer film and wear of the remaining BSL coating has been studied in some depth over the past 50 years. The effect of substrate surface roughness on the wear life and friction coefficient is also well documented [3,4,5]. In 1942 Bowden and Tabor demonstrated the effect of film thickness of thin metallic films on the friction and wear properties of a sliding couple [6]. Several authors expanded on this work, including Rabinowicz who proposed a method for predicting the wear life of a solid lubricant (including metallic and bonded films), based on the characteristic junction size and wear particle size [7]. Later Bahun and Jones proposed that the wear life of a BSL was directly proportional to the square root of the coating thickness and inversely related to the applied load [8].

Some work has been published on the effect of the surface topography of the counterface on the wear of polymers e.g. Jain and Bahadur [9]. However little work has apparently been published on the effect of the counterface surface finish on the performance of BSLs. The objective of the investigation described in this paper is to examine the effect of the counterface surface topography on a particular BSL under a variety of conditions. This paper describes the first stage in a more extensive programme to establish the performance of a

number of bonded solid lubricant combinations in an effort to generate a selection database and guidelines on frictional performance for engineers and designers.

2 EXPERIMENTAL.

A test machine was designed to allow conventional pin on disk as well as linear reciprocating experiments to be performed, this being achieved by a removable reciprocating platform and use of a disk adapter. The drive to this platform or adapter is by flat belt from a variable speed brushless DC motor which provides a low noise and low vibration test platform. A vertical spindle mounted in a carriage which is carried on linear bearings allows the application of a load to the counterface and disk. Piezo resistive force transducers are attached to this carriage to allow measurement of the friction force during operation. During the design of this machine special consideration was given to the stiffness of the supporting members and drive mechanism. Test machine stiffness is known to have a significant effect in tribotesting [10].

2.1 Test Specimens.

The test specimens consisted of 12mm diameter hardened AISI chrome steel balls and ground disks. The balls were prepared by grit blasting with 3 different grades of carbonundum abrasive to achieve 4 surface finishes as shown in table 1.

Description	Grit Grade	Roughness $\mu\text{m } R_a$
As Rec'd	None	0.297
Fine (F)	60/80EB	3.01
Medium (M)	24/30EB	4.07
Course (C)	16E	4.87

Table 1: Surface finish preparation of steel balls

Disks of 75mm diameter, hardened 080M40 steel were prepared by radial grinding with the dominant lay direction as illustrated in Figure 1. They were then grit blasted and manganese iron phosphated prior to coating with the BSL. The disk was coated with a commercial BSL containing PTFE and Graphite in a Polyamide-imide binder. The thickness of this coating being $20\mu\text{m} \pm 5\mu\text{m}$.

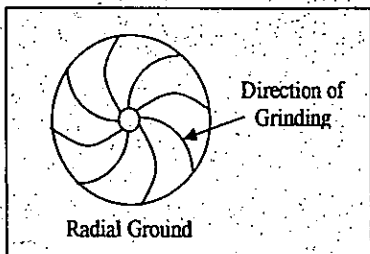


Figure 1: Disk grinding Pattern.

2.1 Test Conditions.

The pin on disk test configuration was employed for the tests described in this paper. The test conditions are presented in figure 2 and table 2. Figure 2 illustrates the test hierarchy in a tree format. For each test speed a test is performed for all four ball roughnesses at low and high load. (10N and 100N respectively.) Only one repetition is made of each test as the principal aim is to investigate changes in performance over a range of operating conditions. Operating conditions have been deliberately set an order of magnitude apart to emphasise effects. Table 2 presents details of the operating conditions for each test.

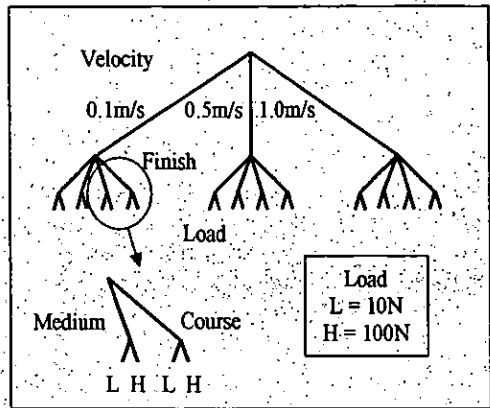


Figure 2 Test programme Diagram.

Test No.	V ms^{-1}	Track ↓ m	Finish	Load H L
1 & 13	0.1	0.03	As rec'd	1 13
2 & 14	0.1	0.03	F	2 14
3 & 15	0.1	0.03	M	3 15
4 & 16	0.1	0.03	C	4 16
5 & 17	0.5	0.04	As rec'd	5 17
6 & 18	0.5	0.04	F	6 18
7 & 19	0.5	0.04	M	7 19
8 & 20	0.5	0.04	C	8 20
9 & 21	1.0	0.05	As rec'd	9 21
10 & 22	1.0	0.05	F	10 22
11 & 23	1.0	0.05	M	11 23
12 & 24	1.0	0.05	C	12 24

Table 2: Matrix of test conditions.

The tests were conducted in ambient temperature and atmosphere in an engineering laboratory. Although temperature and humidity were recorded no attempt was made to further control these parameters. Calibration of the force transducers was performed prior to the tests.

3 RESULTS

Figures 3 to 5 present the friction coefficients measured for the 100N applied load tests. Figure 6 presents the results of the 10N load tests conducted to date. Figure 7 summarises all the friction coefficient curves measured over the first 700m of sliding.

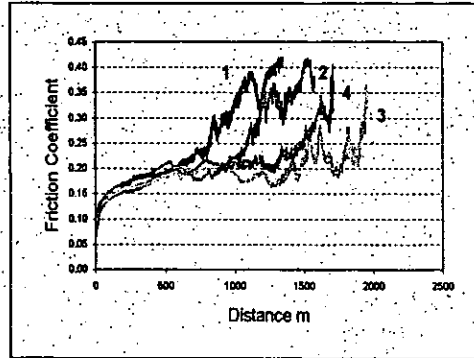


Figure 3: Friction coefficient as a function of sliding distance, test 1 - 4. 100N 0.1ms⁻¹

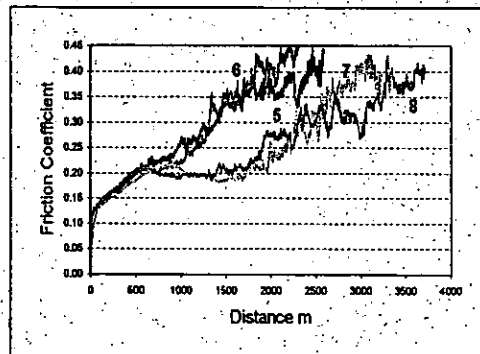


Figure 4: Friction coefficient as a function of sliding distance, test 5 - 8. 100N 0.5ms⁻¹

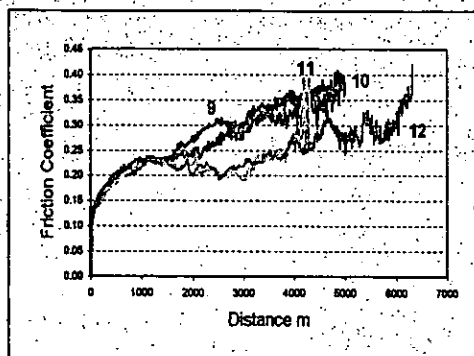


Figure 5: Friction coefficient as a function of sliding distance, test 9 - 12. 100N 1.0ms⁻¹

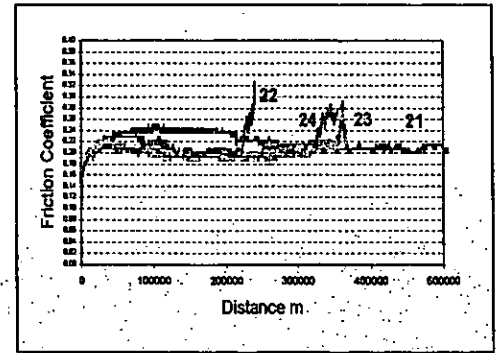


Figure 6: Friction coefficient as a function of sliding distance, test 21 - 24. 10N 1.0ms⁻¹

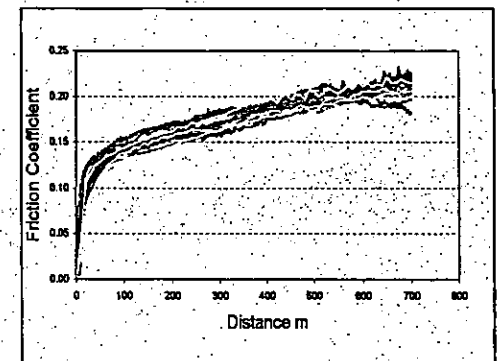


Figure 7: Friction coefficient as a function of sliding distance, test 1 - 12 first 700m

4 DISCUSSION

The results obtained demonstrate three distinct regions of performance:

- an initial phase where the friction coefficient increases rapidly over a short distance then more gradually against distance travelled.
- a steady state region where the friction coefficient remains approximately constant.
- a final stage where there is a chaotic, rather than incremental rise in the friction coefficient.

The results for the 100N tests also suggest:

- sliding life decreases with decrease in velocity.
- the counterface roughness has little effect on performance in the initial stage.
- the counterface roughness has a marked effect on sliding life in the second and third stages of operation indicating that the smoother finishes have a shorter life. i.e. lower sliding time or distance covered prior to reaching a friction coefficient of 0.3.

Similarly the results for the 10N tests suggest:

- friction in the initial stages is not affected by counterface roughness.
- the counterface roughness has a marked effect on sliding life in the second and third stages of performance, but, while the grit blasted samples

follow a similar trend to the high load tests, the smooth finish (as rec'd) continued to 500km without failure.

- At the time of writing it is not possible to comment on the effect of velocity as the test programme is incomplete.
- The coefficient of friction for all parameters at the onset of the steady state phase lie within a tight band of 0.18 – 0.25. Coefficients of friction as low as 0.05 were recorded at the onset of sliding but rapidly reach a value of 0.15 within the first 150 metres.

The collection of the friction curves in Fig 8 demonstrate the relatively repeatable results over the 12 tests. This initial stage of performance follows the function:

$$y = a \ln x + b$$

An empirical equation for the change in friction coefficient over this range is thus:

$$\text{Friction coefficient} = 0.035 \times \ln \text{sliding distance} + 0.025$$

Where the constants are the averages from the 12 tests and the expression is reliable irrespective of load, speed or counterface surface finish.

5 CONCLUSIONS

Three distinct regions of performance have been demonstrated for a particular type of bonded solid lubricant at various counterface finishes, loads and velocities.

It was found that with high applied loads the contact life increased with velocity and counterface surface finish had a marked effect on performance. In general the smoother the finish (lower the R_a value) the shorter the lifetime. The opposite was found for the low load tests where the smooth, as received, finish gave a good performance sliding over 500km sliding distance without failure.

It was found to be possible to form an empirical equation to describe the friction coefficient for the first few hundred metres of sliding which was independent of load, speed and surface finish.

6 FURTHER WORK

It is proposed that the following work will form the basis of a further study:

- A study of the contact evolution during the initial and second stages of performance. This will involve measurement of the contact spot size and track geometry to determine if Hertzian contact analysis correctly predicts the friction coefficients in these phases.
- An investigation into the effect of using different types of lubricant and matrix mixture proportions.

- A study to determine if different sliding conditions have an effect. A comparison of reciprocating/continuous motion will be undertaken.

ACKNOWLEDGEMENTS.

The Authors are grateful to Armourcote Surface Treatments Ltd. Long Causeway Leeds LS9 0NY UK for their help in the preparation and coating of the sample disks.

REFERENCES.

- [1] Glusing, H. The lubricant carries the complete load. NORDTRIB '98 Proceedings of the 8th International conference on Tribology. 7-10 June 1998 Denmark: 27-35.
- [2] Fusaro, R. L. Effect of load, area of contact and contact stress on the tribological properties of polyimide bonded graphite fluoride films. ASME. Conference on wear of materials. 1981: 625-636.
- [3] Fusaro, R. L. Effects of substrate chemical pretreatment on Tribological properties of Graphite films. ASLE 3rd International on solid lubrication. 1-11.
- [4] Lin, J. F. and Guu, Y.Y. Factors affecting the tribological performance of three resin bonded solid lubricants. Tribology transactions. 42. (1999) 3. 601-609.
- [5] Kawamura, M. Aoki, I. And Yoshida, K. Practical applications of bonded solid film lubricants in the commercial field. ASLE SP 14. (1984) 114-122.
- [6] Bowden, F. P. Tabor, D. The lubrication of thin metallic films and the action of bearing materials. Applied Physics. 14. (1943) 141-151.
- [7] Rabinowicz, E. Variation of friction and wear of solid lubricant films with film thickness. ASLE/ASME Lubrication conference. Minneapolis. 1966.
- [8] Buhari, C. J. Jones, J. R. Influence of load, speed and coating thickness on the wear life of a bonded solid lubricant. Lubrication Engineering 25 (1969) 9. 351-355.
- [9] Jain, V. K. Bahadur, S. Surface topography changes in polymer-metal sliding – I. Transactions of the ASME Vol 102 (1980) 520-525.
- [10] Gee, M. G. Effect of test machine dynamics on the sliding wear of alumina. Wear testing of advanced materials. Divaker, R. and Blau, P. J. Eds. ASTM STP 1167 Philadelphia (1992) 24-44.